The Astbury Centre for
Structural Molecular Biology

UNIVERSITY OF LEEDS

ANNUAL REPORT 2020

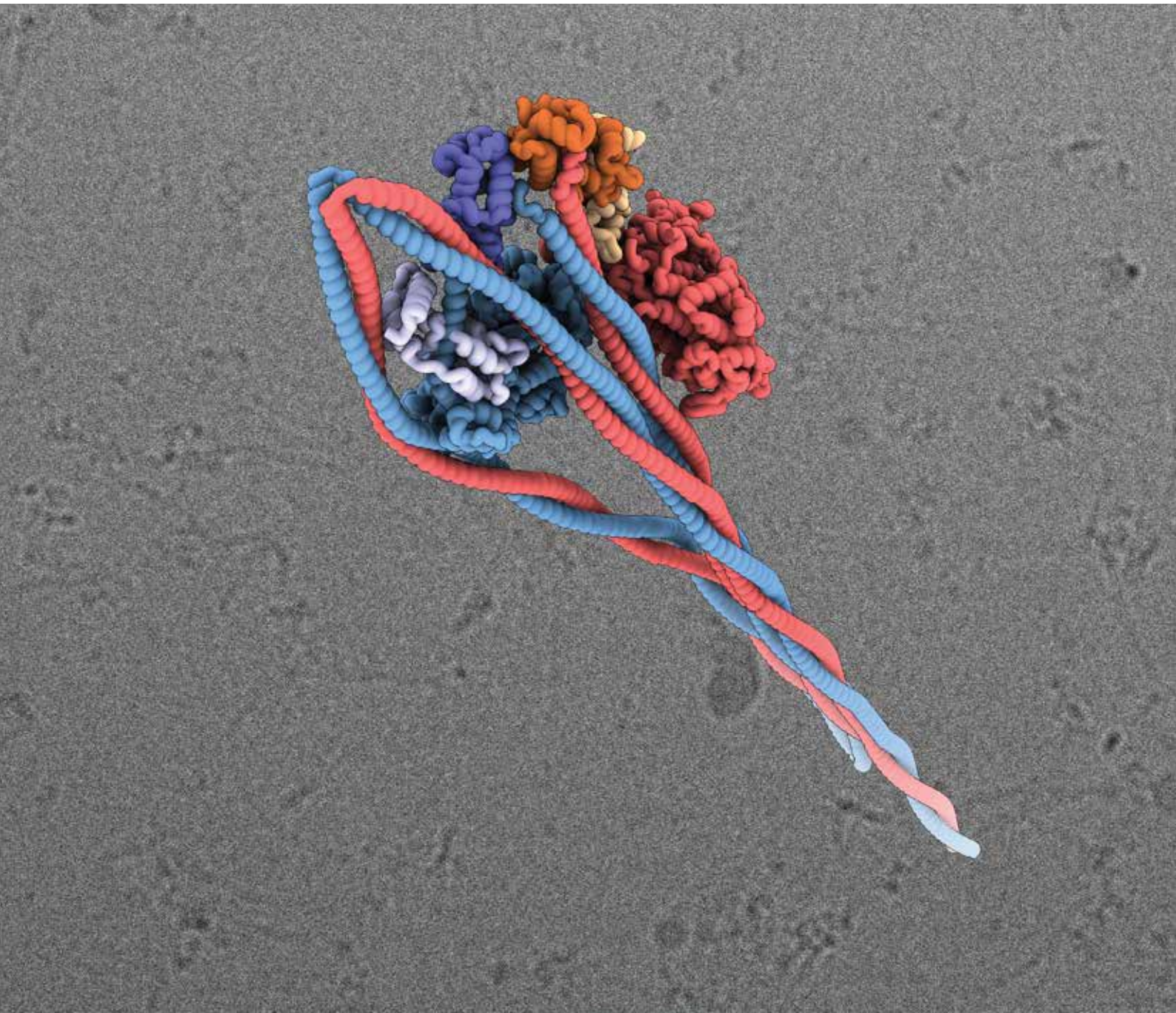

Front cover illustration

This structure, published in Nature, was the result of a collaboration between Professors Michelle Peckham and Neil Ranson of the Asbury Centre and is described on p67 of this report.

Mission Statement

The Astbury Centre for Structural Molecular Biology will promote world-class interdisciplinary research to understand macromolecular behaviour in health and disease.

Introduction

Welcome to the Annual Report of the Astbury Centre for Structural Molecular Biology for 2020. The past year has been a different and difficult one for all, both personally and professionally, due to the impact of COVID-19 and I want to start by saying that I hope you and your loved ones are all well and staying safe as we continue into 2021. I am extremely proud of the way our colleagues in the Astbury Centre have continued to work hard and adapted to the changes around them and would like to thank every member of the Centre: our Support staff, Technicians, Facility Managers, Staff Scientists, Students, Post-docs, Fellows, the Academic staff and our Astbury Administrator Lucy Gray for their efforts in helping to maintain the successes of the Centre and continue their exciting interdisciplinary research. Thank you all.

As we all worked from home and got to grips with virtual meetings we were able to continue our Astbury seminar series and welcomed speakers from the UK and EU via Zoom. A huge thanks to all those that gave talks and we look forward to welcoming speakers to the Centre in person as soon as possible!

We also made good use of our time during lockdown, and I am delighted to inform you that we have now a new Astbury Centre website https://astbury.leeds.ac.uk/ where you will find out about our latest news, Centre members, Facilities and more. Thank you to Lucy Gray for helping to put the new website together and to Alan Berry for his enormous contributions in constructing and running our web site for the last decades!

The 2020 VC Jordan/PR Radford Prize for the best PhD thesis in the Astbury Centre (https://astbury.leeds.ac.uk/about/the-vc-jordan-pr-radford-prize/) was awarded to Rachel Johnson. Rachel received the prize for her work on *Investigating the role of cryo-EM as a tool for structure-based drug design* and gave a superb talk about her PhD and latest research at the Astbury virtual Away Day. The meeting was a great success with over 200 members joining from across the Centre to listen to talks from our PhD students, Post-docs and PIs.

The Centre welcomed two new PI members in 2020: Anton Calabrese (University Academic Fellow and Sir Henry Dale Fellow, School of Molecular and Cellular Biology) and George Heath (University Academic Fellow, School of Biomedical Sciences and Physics and Astronomy). They bring expertise and research programmes in biological mass spectrometry and high speed AFM of proteins and their complexes. We were also delighted to welcome our new PhD students and postdocs to the Centre this year, bringing our total number of researchers to >300, including 68 academic staff, 184 PhD students, >100 postdoctoral researchers and 13 Research Fellows.

Astbury Centre members continued to publish their research in a wide range of journals in 2020 with highlights in all major journal spanning the disciplines. A full list can be found at the end of this report. We also enjoyed many successes in 2020 in terms of grant income. £13.5M of new project and programme grants brings the Astbury grant portfolio to a highly impressive £62M share of a total of £89M of grants: a testament to the hard work and successes of our members especially during these difficult times. We are grateful to the funding agencies who support our science, including BBSRC, EPSRC, MRC, Wellcome, CRUK, other charities, EU and Industry. We also acknowledge, with thanks, the support of the University of Leeds and the Faculties of Biological Sciences, Engineering and Physical Sciences and Medicine and Health, and the Schools of Chemistry, Molecular and Cellular Biology, Biomedical Sciences, Biology and Physics and Astronomy for their support of the Centre and our research.

Congratulations also go to Alex O'Neill, David Brockwell, Andrew Macdonald and Lars Jeuken who were promoted to Professor and Peter Adams and Robin Bon for their promotion to Associate Professor. Well done all on your much-deserved achievements. Also notable this year was the exciting news that I was awarded OBE for services to molecular biology: it would never have happened without the Astbury Centre which has been my pleasure to direct for the last 9 years.

The Astbury Early Careers Researcher Forum, led by a team of Post-docs, held several well attended virtual events including CV surgery sessions and talks on careers in industry and academia. See more on the Astbury website https://astbury.leeds.ac.uk/about/astbury-early-careers-research-forum/.

The Astbury Society, led by the presidents Romany McLure and Frank Charlton, hosted a fantastic virtual Christmas quiz night and continued their fundraising efforts. The Society has raised over £6,500.00 to date for the Leeds Children's Charity. See more about the Astbury Society on the Astbury website https://astbury.leeds.ac.uk/about/astbury-society/.

I hope that you enjoy reading this Annual Report. Thank you to David Brockwell and Lucy Gray for editing this report, Ralf Richter, Glyn Hemsworth and Peter Adams for proofreading it, everyone who contributed reports, and all who participated in the Astbury Centre's activities in 2020.

Finally, ending on a personal note, this will be my last Annual Report, as my third term of office ends in March 2021. After 9 years at the helm, an additional 3 years as Deputy Director and a non-stop 22 years on the Executive Group, I can look back with enormous pride at all we have achieved together. I am delighted to announce that our next, the fifth Director of the Astbury Centre will be Neil Ranson. I know Neil will do an excellent job leading the centre into the future, with lots more excitement and great science in the years to come.

With best wishes to you all,

Sheena E. Radford, OBE, FMedSci, FRS

Director, Astbury Centre for Structural Molecular Biology,
Leeds, March 2020

Please note that this report (as well as those from previous years) is also available as a PDF document which can be downloaded from our website (www.astbury.leeds.ac.uk).

CONTENTS

	Pages
Model lipid membranes assembled from natural plant thylakoids into 2-D microarray patterns as a platform to assess light-harvesting proteins *Sophie Meredith, Ashley Hancock, Simon Connell, Stephen Evans and Peter Adams*	1-2
Photosynthetic organisms for phosphate recovery from waste water *Miller Alonso Camargo-Valero, Jaimie Paterson, Johan Pasos-Panqueva, Tatiana Zúñiga-Burgos, Stephen Slocombe and Alison Baker*	3-4
Nek7 conformational flexibility and inhibitor binding probed through protein engineering of the R-spine *Sharon Yeoh and Richard Bayliss*	5-6
ESCRT-II/-III remodelling of phase separated membranes is dependent on the phase localisation of phosphatidylserine lipids *Andrew Booth and Paul Beales*	7-8
Structural insights into non-ribosomal peptide synthetases *Daniel Van and Alan Berry*	9
Understanding the modulation of TRPC1/4/5 cation channels through photoaffinity labelling and cryo-electron microscopy *Claudia Bauer, Isabelle Pickles, David Wright, Aisling Minard, Katie Simmons, Eulashini Chuntharpursat-Bon, Rachel Johnson, Nik Kapur, Megan Wright, Stuart Warriner, David Beech, Stephen Muench and Robin Bon*	10-11
Assessing the developability and manufacturability of biopharmaceuticals in vitro and in vivo *Jessica Ebo, Romany McLure, Leon Willis, Ioanna Panagi, Samantha Lawrence, Alex Page, Frank Sobott, Nikil Kapur, Sheena Radford and David Brockwell*	14-15
Inter-domain dynamics of the periplasmic chaperone SurA and multi-site binding to its outer membrane protein clients *Bob Schiffrin, Matthew Watson, Theodoros Karamanos, Martin Walko, Paul White, Andrew Wilson, Antreas Kalli, Roman Tuma, David Brockwell, Sheena Radford and Antonio Calabrese*	16-17
Structure and function of 50 nm extracellular filaments in reproduction *Mehrnaz Montazeri, John Trinick, Elwyn Isaac and Joe Cockburn*	18
A multiscale understanding of protein hydrogels with insight from theory and experimentation *Matthew D.G. Hughes, Benjamin S. Hanson, Christa Brown, Kalila Cook, Alex Wright, Sophie Cussons, David J. Brockwell and Lorna Dougan*	19-20
The role of water in extreme environments: solute specific perturbations to water structure and dynamics *Harrison Laurent and Lorna Dougan*	21-22
From single “live” cells to tissue: biophysical approaches for cancer progression, patient stratification and understanding drug activity *Julia Gala de Pablo, Chloe Kirkby, Fern Armistead and Stephen Evans*	23-24
Theranostics for the treatment on cancer and biofilms *Leeds Microbubble Consortium and Stephen Evans*	25-26
Fibrinogen interaction with complement C3: a potential therapeutic target to reduce thrombosis risk *Rhodri J. King, Katharina Schuett, Christian Tiede, Vera Jankowski, Vicky John, Abhi Trehan, Katie Simmons, Sreenivasan Ponnambalam, Robert F. Storey, Michael J. McPherson, Darren C. Tomlinson, Ramzi A. Ajjan and Colin W.G. Fishwick*	27-28
The structure of a native orthobunyavirus ribonucleoprotein reveals a key role for viral RNA in defining its helical architecture	29

Francis R. Hopkins, Beatriz Álvarez-Rodríguez, Samantha Hover, Koulla Panayi, George Heath, Thomas A. Edwards, John N. Barr and Juan Fontana
Drug repurposing targeting the SARS-CoV2 envelope (E) protein ion channel 30-31
Gemma Swinscoe, Sonia Abas Prades, Richard Foster and Stephen Griffin
Glycan-gold nanoparticles as multifunctional probes for multivalent lectin-carbohydrate binding: implications for blocking virus infection and nanoparticle assembly 32-33
Darshita Budhadev, Emma Poole, Inga Nehlmeier, Yuanyuan Liu, James Hooper, Elizabeth Kalverda, Uchangi Satyaprasad Akshath, Bruce Turnbull, Dejian Zhou and Yuan Guo
Modelling the active SARS-Cov-2 helicase complex as a basis for structure-based inhibitor design 34-35
Sarah Harris
Millisecond dynamics of an unlabelled amino acid transporter 36-37
George Heath
Targeting enzymes for improved plastic break down 38-39
Badri S. Rajagopal, Anna Ah-San Tan, Darren Tomlinson and Glyn R. Hemsworth
Investigating the Structure and Function of Murine Norovirus (MNV) VP1 Capsid Protein 40-42
Jake Mills, Joseph Snowden, Oluwapelumi Adeyemi, Nicola Stonehouse and Morgan Herod
Macromolecular crowding enhances the detection of DNA and proteins by a nanopore 43-44
Chalmers Chau, Sheena Radford, Paolo Actis and Eric Hewitt
Understanding the mechanism of antimicrobials that target electron-transport chain enzymes 45-46
Debajyoti Dutta, Stephen P. Muench and Lars Jeuken
Understanding the structure, dynamics and lipid interactions of the complete T cell receptor using multi-scale simulations 47-48
Dheeraj Prakaash, Graham Cook and Antreas Kalli
Insights into Hsp40 mediated proteostasis and anti-aggregation by nuclear magnetic resonance spectroscopy 49-50
Theodoros K. Karamanos
Non-parametric analysis of non-equilibrium simulations 51
Sergei Krivov
Receptor tyrosine kinase signalling in the absence of growth factor stimulation: response to cellular stress 52-53
Eleanor Cawthorne, Christopher Jones, Sophie Ketchen, Chi-Chuan Lin, Dovile Milonaityte, Kin Man Suen and John Ladbury
Cellular re-wiring: Understanding how oncogenic viruses transform their host cells 54-55
Molly Patterson, James Scarth, Ethan Morgan, Diego Barba-Moreno, Yigen Li, Corinna Brockhaus, Eleni-Anna Loundras, Miao Wang and Andrew Macdonald
TMEM16A/ANO1 calcium-activated chloride channel as a novel target for the treatment of human respiratory syncytial virus infection 56-57
Hayley Pearson, Eleanor Todd, Samantha Hover, Martin Stacey, Jonathan Lippiat, Adrian Whitehouse, John Barr and Jamel Mankouri
Electron microscopy of membrane proteins to underpin structure guided inhibitor design 58-59
David Klebl, Rebecca Thompson, Frank Sobott and Stephen Muench
Activity-Directed Synthesis of Bioactive Small Molecules 60-62
Shiao Chow, Justin Clarke, Adam Green, Fruzsina Hobor, Abbie Leggott, Alex O'Neill, Stuart Warriner, Andrew Wilson and Adam Nelson

Breaking symmetry of the centriole 63-64

Takashi Ochi
Tissue-specific tools to identify regulators of transcellular chaperone signalling 65-66
Jay Miles, David Westhead and Patricija van Oosten-Hawle
The Shutdown State of Smooth Muscle Myosin and other stories 67-68
Charlotte Scarff, Glenn Carrington, David Casas-Mao, Neil Ranson, Peter Knight, Alistair Curd, Brendan Rogers, Ruth Hughes, Christian Tiede, Chi Trinh and Michelle Peckham
Interrogating structural dynamics of mechanosensitive membrane proteins by pulsed EPR spectroscopy 69-70
Benjamin J. Lane, Yue Ma, Andrew M. Hartley, Bolin Wang, James Ault, Frank Sobott, Antonio N. Calabrese, Antreas Kalli and Christos Pliotas
A Master Regulator for Function and Toxicity in Alpha-Synuclein 71-72
Sabine Ulamec, Ciaran Doherty, Roberto Maya-Martinez, Sarah Good, Patricija van Oosten-Hawle, Nasir Khan, David Brockwell and Sheena Radford
Investigating the mechanism of SusCD-like TonB-dependent transporters using cryo-electron microscopy 73-74
Joshua White, Shaun Rawson and Neil Ranson
Basis for surface-templated amyloid growth revealed by the structures of Type-2 Diabetes amyloid IAPP and its early-onset variant S20G 75-76
Rodrigo Gallardo, Matthew Iadanza, Yong Xu, George Heath, Richard Foster, Sheena Radford and Neil Ranson
A Method to Quantify Molecular Diffusion within Thin Solvated Polymer Films 77-78
Rickard Frost, Saikat Jana, Fouzia Bano and Ralf Richter
Regulation of antimycin biosynthesis is controlled by the ClpXP protease 79-80
Bohdan Bilyk, Asif Fazal and Ryan Seipke
Aptamer-ligand recognition studied by native ion mobility-mass spectrometry 81-82
Elise Daems, Debbie Dewaele, Konstantin Barylyuk, Karolien De Wael and Frank Sobott
Structural insight into Pichia pastoris fatty acid synthase 83-84
Joseph Snowden, Jehad Alzahrani, Lee Sherry, Martin Stacey, David Rowlands, Neil Ranson and Nicola Stonehouse
A Case Study of Eukaryogenesis: the Evolution of Photoreception by Photolyase / Cryptochrome Proteins 85-86
Jennifer Miles and Paul Taylor
DNA origami nanostructures for biological and biomedical applications 87-88
Ashley Stammers and Neil Thomson
Lamellar structure of bacterial photosynthetic antennae 89
Rebecca Thompson, Neil Ranson and Roman Tuma
Arbovirus replication and host cell interactions 90
Andrew Tuplin
Investigating the limits of sortase-catalysed protein labelling 91-92
Holly Morgan, Zoe Arnott, Kristian Hollingsworth, Yixin Li, Jonathan Dolan, Tomasz Kaminski, Charlie Stevenson, Bruce Turnbull and Michael Webb
Virus-host cell interactions required for oncogenic virus replication and transformation 93-94
Oliver Manners, James Murphy, Sam Dobson, Sophie Schumann, Tim Mottram, Amy Barker, Becky Foster, Zoe Jackson, Holli Carden, Katie Harper, Ellie Harrington, Freddy Weaver and Ade Whitehouse
Modulation of Protein-Protein Interactions Using Chemical Biology Approaches 95-96
Emma E. Cawood, Sergi Celis, Jessica S. Ebo, Nicholas Guthertz, Zsófia Hegedüs, Kristina Hetherington, Fruzsina Hóbor, Sonja Srdanovic, Martin Walko, Chi Trinh, Thomas. A. Edwards, Theo K. Karamanos, Adam Nelson, Sheena E. Radford and Andrew J. Wilson
Defining the structural mechanisms for human DNA damage response and repair in cancer cells 97-98

William Wilson and Qian Wu
Assembly, activation and function of BRCC36 deubiquitylating complexes 99-100
Lisa Campbell, Francesca Chandler, Martina Foglizzo, Linda Makhlouf, Laura Marr, Miriam Walden and Elton Zeqiraj
Photon induced quantum yield regeneration of cap-exchanged CdSe/CdS quantum rods for ratiometric biosensing and cellular imaging 101-102
Weili Wang, Yifei Kong, U.S. Akshath, Christian Tiede, Yuan Guo and Dejian Zhou

Model lipid membranes assembled from natural plant thylakoids into 2-D microarray patterns as a platform to assess light-harvesting proteins

Sophie Meredith, Ashley Hancock, Simon Connell, Stephen Evans and Peter Adams

Introduction

The photosynthetic membranes of plants, found within chloroplasts, are termed “thylakoid membranes”. These membranes contain a large network of light-harvesting (LH) protein complexes, each containing a high density of pigments. Determining the concentration and relative positions of LH and photosystem proteins is crucial for the understanding of both excitation energy migration and subsequent electron transport across membranes. Previous studies have measured the structure and function of either single proteins or fragmented natural membranes, however, these are not an ideal platform to test system functionality because of their heterogeneous composition and unstable nature. There is a compelling need for a model of thylakoids that has an intermediate level of complexity: consisting of the full range of proteins found in the native thylakoid membrane, but with control over membrane composition and amenability to high-resolution microscopy. An ideal model system would consist of a stable lipid membrane on a solid support which contains the complete network of photosynthetic proteins embedded within a bilayer comprised of a native-like mixture of lipids. Recently, Morigaki and co-workers presented a new type of "hybrid membranes" by incorporating thylakoid components into supported lipid bilayers (SLBs) within an array-patterned template. The empty templates were formed from photo-polymerized diacetylene-phosphocholine (Diyne-PC) lipids which promote the formation of “hybrid membranes” from a combination of synthetic lipid vesicles and natural thylakoid membranes. The result is an array of discrete, high-quality SLBs that are patterned into easily recognizable microarrays to allow for more accurate analysis. Here, we apply this model for the first time to interrogate the behaviour of LH proteins at the micro- and nanoscale, and assess the efficacy of this model.

Results and Discussion

A combination of fluorescence lifetime imaging microscopy (FLIM) and atomic force microscopy (AFM) were used to reveal the differences in photophysical state and lateral organization between native thylakoid and hybrid membranes. A quantitative analysis of the fluorescence intensity, fluorescence lifetime and nanoscale protrusions within hybrid membranes reveals they contain lower concentrations of LH proteins and fewer protein-protein interactions than thylakoids. Specifically, FLIM showed that hybrid membranes had a

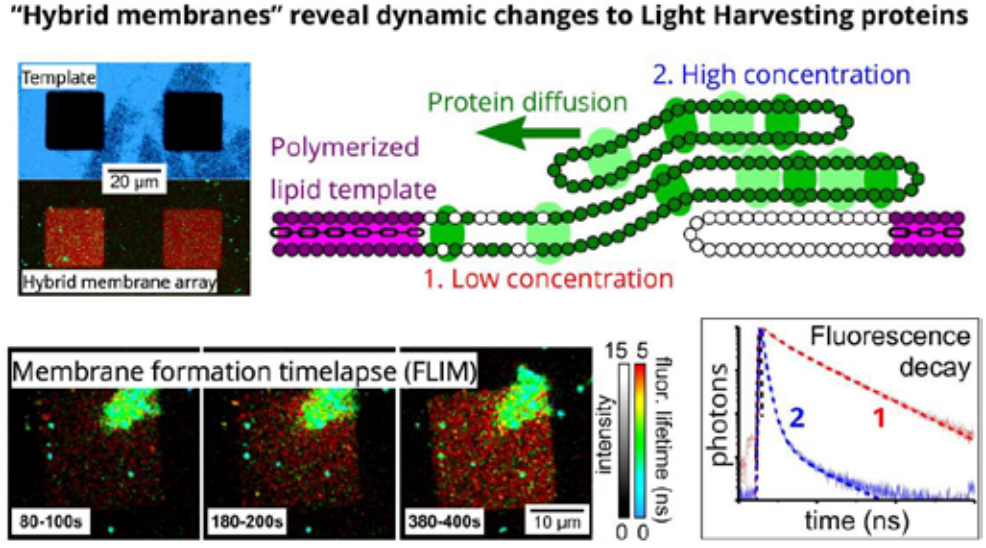

Figure 1: A polymerized lipid bilayer (*purple*) templates the self-assembly of “hybrid membranes” from natural photosynthetic membranes (*green*) and synthetic lipids (*colourless*). During membrane formation, transmembrane proteins migrate from natural membranes into underlying lipid bilayers, decreasing the protein concentration and uncoupling protein-protein interactions (manifested as an increased fluorescent lifetime). Graphical abstract from the paper cited below.

longer fluorescence lifetime (~4 ns) compared to native membranes (~0.5 ns), which indicates that the protein density is reduced due to a reduction in “self-quenching” which is known to occur if LH complexes are tightly clustered. AFM revealed the nanoscale structure of the membranes, including observing the height of the lipid bilayers, the protein density and the structure of the polymerized template. Furthermore, the assembly process was observed in real time and the migration of LH proteins from thylakoid membranes into putative hybrid membranes was monitored (Figure 1), and the kinetics of membrane assembly were deduced. The resulting model system within each corral is a high-quality supported lipid bilayer that incorporates laterally-mobile LH proteins. Finally, a comparison of hybrid membranes versus proteoliposomes revealed that photochemical assays commonly used in the photosynthesis community to test the electron transfer activity of Photosystem II may actually produce false-positive results.

In other work in our group, we have been assessing the ultrafast timescale of energy transfer between synthetic “Texas Red” chromophores and plant LH proteins. To generate a system of single membrane proteins, each within their own portion of lipid bilayer, we used lipid nanodiscs with the incorporation of both the LH protein and the Texas Red chromophore. Transient absorption spectroscopy and theoretical modelling of excitation energy transfer have quantified the picosecond dynamics. This work has been submitted for publication.

Funding
The collaboration between Leeds and Kobe was supported by an International Exchanges Cost Share award from The Royal Society UK. Funding was provided by BBSRC and EPSRC.

Collaborators
University of Leeds: Lars Jeuken.
External: Kenichi Morigaki and Takuro Yoneda (University of Kobe).

Photosynthetic organisms for phosphate recovery from waste water

Miller Alonso Camargo-Valero, Jaimie Paterson, Johan Pasos-Panqueva, Tatiana Zúñiga-Burgos, Stephen Slocombe and Alison Baker

Introduction

Phophorus (P) is an essential element for life but is simultaneously both scarce and overabundant. Over 50% of agricultural land is deficient in P and so supplementation via the use of fertiliser is necessary for optimal crop yields. At the same time, nutrient rich waste waters arising from human activities pose a threat to environmental ecosystems if discharged untreated. Current treatment requires building and maintaining expensive infrastructure. In industrialised countries this imposes a major cost on water companies and consumers, whilst in many countries of the global south it is simply unaffordable or unsustainable. Even when wastewaters are treated, most of the P is not recovered in an agriculturally usable form. This matters because there is a finite quantity of P on earth and human activity is converting limited reserves of high quality P-rich rock into fertiliser at an unsustainable rate, since replenishment of these reserves will take millions of years. Hence, there is an urgent necessity to recover and recycle P from waste streams and photosynthetic organisms could hold the key. We are exploring the potential for using and developing microalgae and duckweeds for P capture and recycling. These organisms take up nutrients including P from waste water using solar energy and convert it into biomass, thereby cleaning the water and producing a product with potential for use as feed, fertiliser or energy production.

Results and Discussion

Duckweeds are a group of small floating macrophytes that grow in a wide range of climatic conditions (Figure 1).

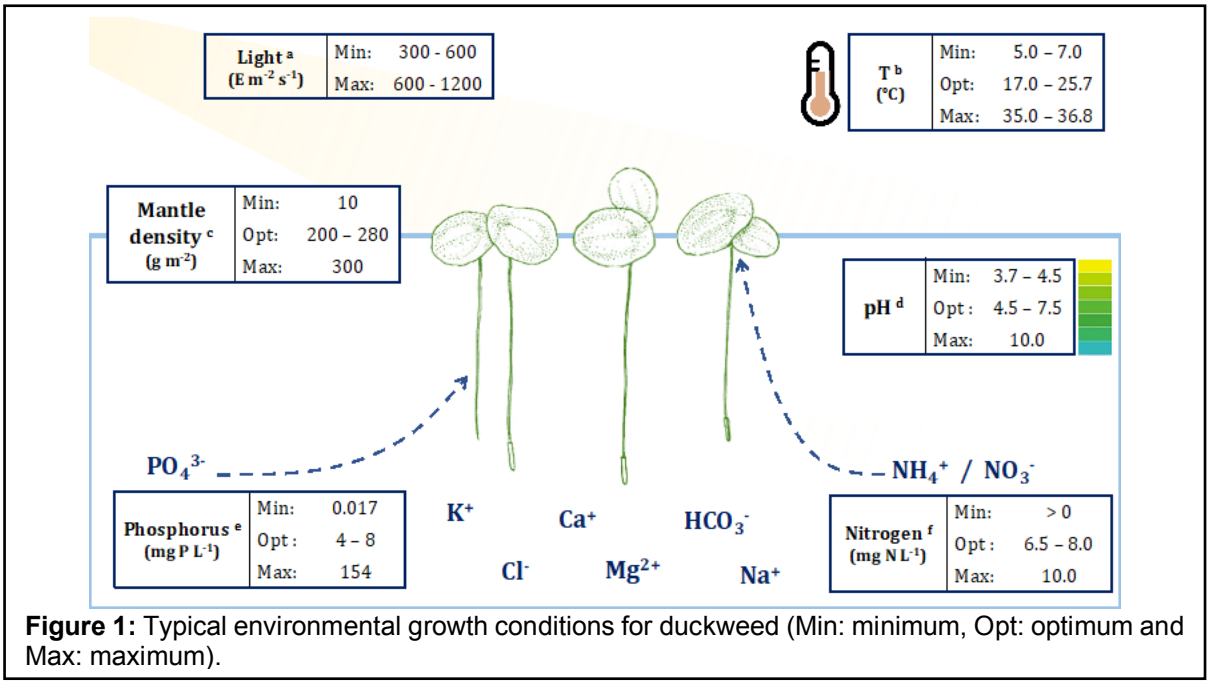

Figure 1: Typical environmental growth conditions for duckweed (Min: minimum, Opt: optimum and Max: maximum).

They have been used for nutrient recovery from a range of waste waters, and the resultant biomass has been used for feed and biofuel production (e.g., biomethane, bioethanol), but most reported experiments have been done under 'optimal' conditions of temperature and photoperiod in the laboratory, or in the field under tropical conditions. Although it was generally assumed that a temperate climate would not be suitable, we showed that even under cool short day conditions where growth was slow duckweed continued to remove P from the surrounding media. This led to additional findings uncoupling biomass growth from P uptake from P-rich waste waters (Paterson et al., 2020). This opens the door to explore duckweed based systems for nutrient recovery at small wastewater treatment works (even in temperate climate countries), with a novel approach in which operational conditions are optimised for P

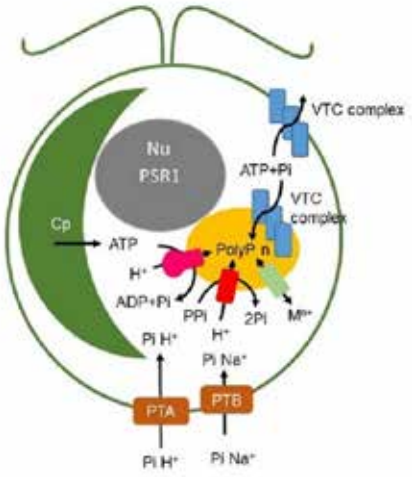

Figure 2. Schematic of polyphosphate synthesis in *Chlamydomonas*.

uptake and recovery. Microalgae represent an alternative route to sustainable nutrient recovery. They exhibit a phenomenon known as luxury P uptake where they can accumulate P over and above the level needed for immediate growth. The mechanisms of sensing and signalling P status are only partially known (Slocombe et al., 2020). We are manipulating genes involved in the P response in the model alga *Chlamydomonas reinhardtii* (Figure 2) in order to dissect their roles in luxury P uptake. In a parallel approach we have been carrying out forward genetic screens for hyper accumulating strains which has generated two distinct classes of mutants that are currently under investigation. Potential applications include the use of microalgae to simultaneously control and recover nitrogen and phosphorus from waste streams in a form that can contribute to nutrient recycling into agriculture (i.e., nutrient rich algal biomass as a slow release fertiliser).

Publications

Paterson J.B., Camargo-Valero M.A. and Baker A. (2020) Uncoupling growth from phosphorus uptake in Lemna: Implications for use of duckweed in wastewater remediation and P recovery in temperate climates. *Food Energy Secur.* **9:**e244.

Slocombe S.P., Zuniga-Burgos T., Chu L.L., Wood N.J., Camargo-Valero M.A.*, et al.* (2020) Fixing the broken phosphorus cycle: wastewater remediation by microalgal polyphosphates. *Front. Plant. Sci.* **11**:982.

Wood N.J., Baker A., Quinnell R.J. and Camargo-Valero M.A. (2020) A simple and nondestructive method for chlorophyll quantification of chlamydomonas cultures using digital image analysis. *Front. Bioeng. Biotechnol.* **8**:746.

Funding

BBSRC, EPSRC and GCRF.

Collaborators

University of Leeds: Dr Miller Alonso Camargo-Valero (School of Civil Engineering), Dr Iain Manfield (Biomolecular Interactions Facility).
External: Professor Alison Smith (Department of Plant Sciences, University of Cambridge) Professor Miguel Pena-Varon (Universidad del Valle, Cali, Colombia), Professor Azmi Bin Aris Tncpi (Universiti Teknologi Malaysia, Malaysia).

Nek7 conformational flexibility and inhibitor binding probed through protein engineering of the R-spine

Sharon Yeoh and Richard Bayliss

Introduction

Nek7 is a serine/threonine-protein kinase required for proper spindle formation and cytokinesis. Nek7 is 1 of 11 Neks (NIMA-related kinases) found in humans, and contributes to the assembly of a robust mitotic spindle apparatus. Elevated Nek7 levels have been observed in several cancers, and inhibition of Nek7 might provide a route to the development of cancer therapeutics. To date, no selective and potent Nek7 inhibitors have been identified. The crystal structure of unphosphorylated, inactive Nek7 revealed an autoinhibited conformation with the side chain of Tyr97 pointing down into the active site. Protein kinases have two 'hydrophobic spines', the regulatory (R-spine) and catalytic (C-spine), which traverse the N and C-lobes. The proper stacking of the residues within the R- and C-spines is a hallmark of an active kinase conformation, and is typically triggered by phosphorylation within the activation loop and binding of the ATP, for the R- and C-spines, respectively. Tyr97 is one of Nek7's four R-spine residues, and therefore Nek7 crystal structures exhibit an improperly formed R-spine, characteristic of an inactive kinase. We reasoned that the preference of Nek7 to crystallise in this inactive conformation might hinder attempts to capture Nek7 in complex with Type I inhibitors.

Results and Discussion

Nek7 adopts an inactive conformation in all published structures, and we reasoned that Nek7 trapped in an active conformation would crystallise in a different form. Here, we have introduced aromatic residues into the R-spine of Nek7 mimic the R-spine of Plk1, with the aim of stabilising the active conformation of the kinase through R-spine stacking. The all-aromatic, strong R-spine mutant Nek7^{SRS} (L86H Y97F L180F) retained catalytic activity and was crystallised in complex with compound **51**, an ATP-competitive inhibitor of Nek2 and Nek7 (Figure 1). Subsequently, we obtained the same crystal form for wild-type Nek7^{WT} in apo form and bound to compound **51**. The R-spines of the three well-ordered Nek7^{WT} molecules exhibit variable conformations while the R-spines of the Nek7^{SRS} molecules all have the same, partially stacked configuration.

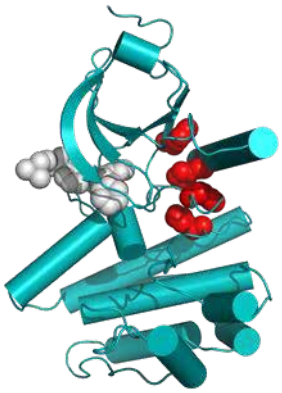

Figure 1: Crystal structure of Nek7^{SRS} mutant (teal) in complex with compound **51** (white). The side chains of the R-spine residues (red) form a stacked configuration, but it is not perfectly aligned as would be expected for an active kinase.

Compound **51** bound to Nek2 and Nek7 in similar modes, but differences in the precise orientation of a substituent highlights features that could be exploited in designing inhibitors that are selective for particular Nek family members. Although the SRS mutations are not required to obtain a Nek7–inhibitor structure, we conclude that it is a useful strategy for restraining the conformation of a kinase in order to promote crystallogenesis.

Publications

Byrne M.J., Nasir N., Basmadjian C., Bhatia C., Cunnison R.F.*, et al.* (2020) Nek7 conformational flexibility and inhibitor binding probed through protein engineering of the R-spine. *Biochem. J.* **477**:1525-1539.

Funding

This work was funded by the MRC and CRUK.

Collaborators

External: Christine Basmadjian and Céline Cano (Newcastle University Centre for Cancer, School of Natural and Environmental Sciences, Newcastle University, Newcastle Upon Tyne), Chitra Bhatia, Rory F. Cunnison and Katherine H. Carr (Department of Molecular and Cell Biology, University of Leicester, Leicester),
Corine Mas-Droux (Section of Structural Biology, The Institute of Cancer Research, London).

ESCRT-II/-III remodelling of phase separated membranes is dependent on the phase localisation of phosphatidylserine lipids

Andrew Booth and Paul Beales

Introduction

The endosomal sorting complex required for transport (ESCRT) is a membrane remodelling complex conserved across all higher organisms. It is involved in a wide range of membrane-related mechanisms, including multivesicular body formation, viral budding, cellular abscission and membrane repair. Its activity can be reconstituted in minimal model membranes, such as giant unilamellar vesicles (GUVs), where its biophysical mechanisms can be investigated. The ESCRT proteins bind to the GUV membrane and assemble into supramolecular spiral filaments that drive membrane invagination and scission, generating intralumenal vesicles (ILVs) that can encapsulate cargo from the extravesicular environment. The resulting multicompartment structure of a GUV containing multiple ILVs is analogous to the compartmentalisation in eukaryotic cells, hence ESCRTs are also of significant interest in bottom-up synthetic biology for controlled compartmentalisation in artificial cells.

ESCRT components bind electrostatically to anionic phospholipids and their membrane remodelling activity is known to be dependent on the local mechanical properties of the membrane. Natural biomembranes have spatial heterogeneity in both lipid composition and mechanics due to, for example, the formation of lipid rafts. The local chemical and mechanical properties of the lipid bilayer could therefore provide control over ESCRT activity. We investigated this hypothesis using phase separated GUVs with coexisting liquid ordered (L_o) and liquid disordered (L_d) domains. The location of anionic phosphatidylserine (PS) lipids in these phase separated GUVs was controlled by the degree of unsaturation of their acyl tails. Unsaturated DOPS lipids are expected to favour the L_d phase and saturated DPPS lipids are expected to favour the L_o phase. Fluorescence confocal microscopy was then applied to study the effect of the ESCRT-II and ESCRT-III complex on GUVs with PS lipids in either one or both of the L_o and L_d phases.

Results and Discussion

The localisation of PS lipids in the GUVs was confirmed using a fluorescent Annexin-V that binds specifically to PS lipids on the membrane. The activity of the ESCRTs, assayed by the formation of ILVs that encapsulate a fluorscent cargo from the external solution, was shown to be highest when PS lipids were localised to L_d domains and lowest when PS lipids were only present in L_o domains. However, surprisingly, the membranes of the ILVs were found to be rich in L_o lipids. The parent GUV membranes also become depleted in the L_d phase. Clues to this surprising behaviour were found in the observation of stalled ILV buds at the GUV membrane, where the membrane bud is formed from L_o membrane, but L_d lipids are participating at the neck of the invagination.

We interpret our observations as follows: the individual ESCRT components electrostatically bind to the L_d phase by binding to DOPS, where they then self-assemble into ESCRT complex spiral filaments. These spiral complexes form rigid patches on the membrane surface that thermodynamically favour the localisation of more rigid L_o domains beneath them. The ESCRT complex induces invagination of the L_o membrane patches where the less rigid L_d membrane forms the high curvature neck of the invagination. Upon scission of the L_o-rich ILV, L_d phase lipids are excised from the parent membrane, increasing its relative L_o composition. This demonstrates a mechanism of chemical and mechanical control of ESCRT activity by the local lipid composition of the target membrane. These mechanisms are schematically summarised in Figure 1.

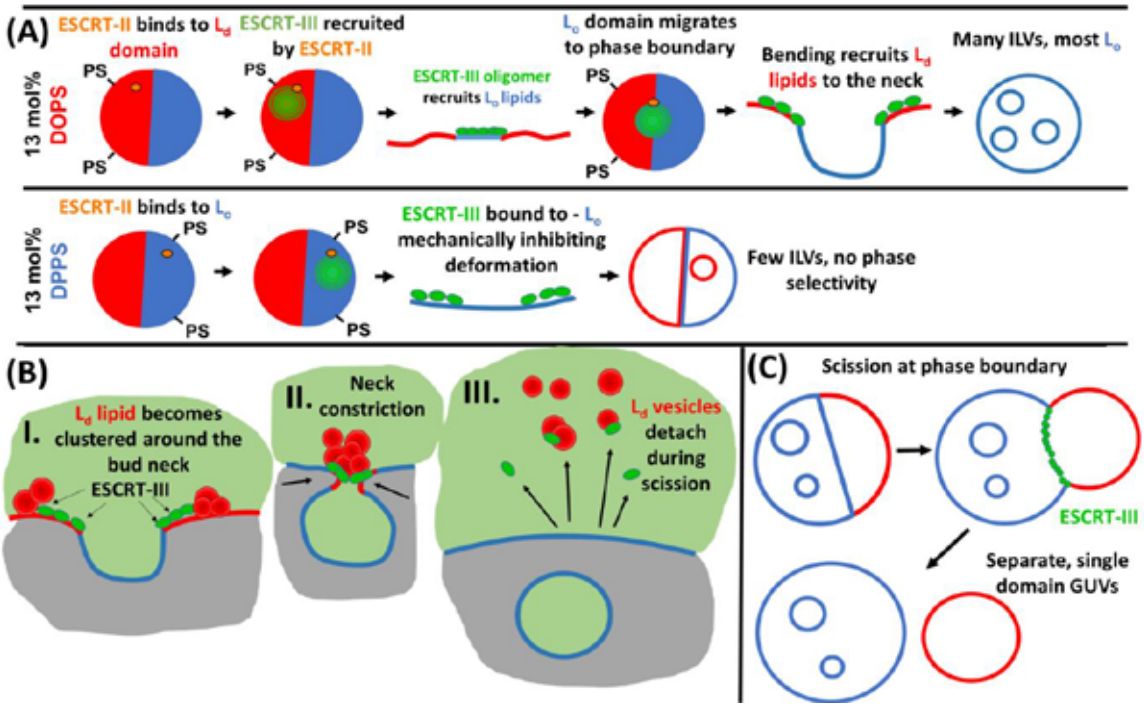

Figure 1: Proposed mechanistic models of the phase behaviour observed in ESCRT-induced ILV formation in phase separated GUVs. **A:** Model of ESCRT assembly and membrane remodelling activity in GUVs with PS lipids concentrated in L_d (13 mol% DOPS) or L_o (13 mol% DPPS) domains. **B:** Depletion of GUV membrane L_d domain by ejection of clustered L_d vesicles from the ILV bud neck during scission. **C:** Possible ESCRT-driven scission at GUV phase boundaries leading to distinct enriched or single domain GUVs as observed.

Interestingly, enrichment of L_o-favouring lipids in endosomes and exosomes (generated by ESCRT activity) compared to the parent plasma membrane have been reported in lipidomics studies. This suggests that similar biophysical mechanics may persist *in vivo*. This has implications for the validity of results using recently reported fluorescent membrane tension probes that indirectly report tension through changes in membrane phase composition, that assume a constant lipid composition of cellular organelles during the timescale of observed remodelling events. Additional controls may therefore be required to confirm the interpretations from experiments that utilise these novel mechanobiological probes. Our results reveal complex coupling between mechanics, composition and phase separation in the function of biomolecular systems relevant to cellular processes and with potential applications in novel chemical technologies utilising artificial cells.

Funding
This work was funded by the EPSRC.

Collaborators
External: Christopher J. Marklew and Barbara Ciani (University of Sheffield).

Structural insights into non-ribosomal peptide synthetases

Daniel Van and Alan Berry

Non-ribosomal peptide synthetases (NRPSs) are large, modular enzymes that are responsible for the biosynthesis of secondary metabolites (non-ribosomal peptides) mainly in bacteria. As the name reveals, they use amino acid building blocks to form a peptide backbone, which can be further modified by tailoring enzymes encoded within the biosynthetic gene cluster. Due to their modular nature and relatively simple chemistries, the potential to generate novel non-ribosomal peptides through recombinatorial biosynthesis has been an exciting prospect in antimicrobial compound discovery (Figure 1). Unfortunately, progress in this area has been hindered due to an over-simplification of the assembly line-like systems and attempts have been made to understand the structure-function relationship of NRPS systems. Currently, a handful of module structures have been published, allowing the first insights into how these large proteins interact and what key interactions are required for successful chain elongation. They have shown the large NRPS structures to be very dynamic, undergoing large conformational changes, in order to grow the peptide backbone; however they reveal little about inter-module interactions, which are crucial for function.

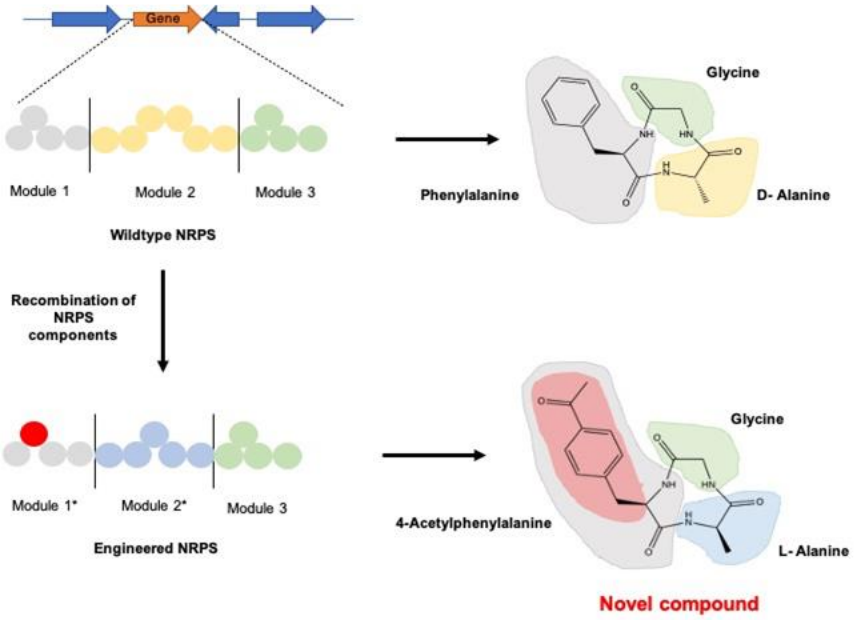

Figure 1: Schematic of recombinatorial biosynthesis potential of non-ribosomal peptide synthetase systems.

In the lab, we aim to understand this in greater detail. We recombinantly identify, express, purify and characterise NRPS modules using a combination of bioinformatics, biochemical assays and structural techniques (X-ray crystallography and electron microscopy) to probe the necessary interactions within NRPSs. We are also interested in understanding intra-module interactions. We study linker regions between domains using bioinformatics to identify conserved regions, introduce mutations, and use a combination of *in vitro* and *in vivo* techniques to probe dynamics. We hope to use information from these studies to guide novel NRPS system assembly methods to generate novel antimicrobical compounds in the fight against antimicrobial resistance.

Funding
This work was funded by The Wellcome Trust.

Collaborators
University of Leeds: Ryan Seipke

Understanding the modulation of TRPC1/4/5 cation channels through photoaffinity labelling and cryo-electron microscopy

Claudia Bauer, Isabelle Pickles, David Wright, Aisling Minard, Katie Simmons, Eulashini Chuntharpursat-Bon, Rachel Johnson, Nik Kapur, Megan Wright, Stuart Warriner, David Beech, Stephen Muench and Robin Bon

Introduction

Transient Receptor Potential Canonical (TRPC) proteins form tetrameric, non-selective cation channels permeable by Na^+ and Ca^{2+}. TRPC channels may consist of homo- or heterotetramers of subunits, which can have distinct function and biophysical/pharmacological properties. Our research focuses on channels formed by TRPC1, TRPC4 and TRPC5, which are rapidly emerging as potential drug targets for the treatment of (amongst others) CNS disorders, kidney disease, and cardiometabolic disease. Until recently, structural insight into the modulation of TRPC1/4/5 channels and tools to probe ligand engagement by TRPC1/4/5 channels in cells were lacking, thereby hindering fundamental and translational studies of TRPC1/4/5 pharmacology.

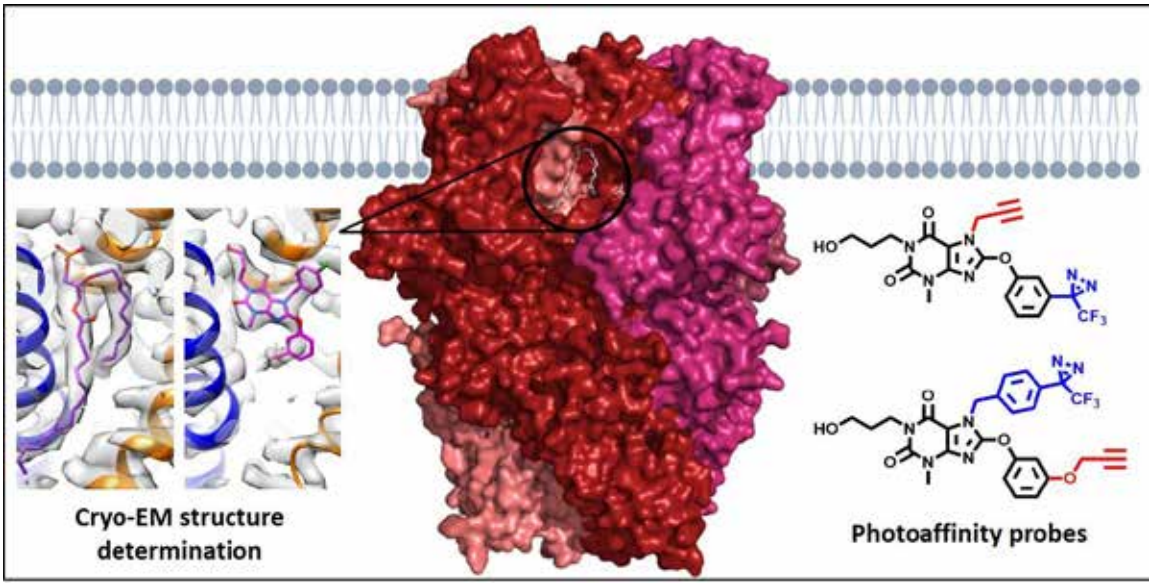

Figure 1: The cryo-EM structure of a human TRPC5 channel (middle), with detailed views of one of its four xanthine/phospholipid binding sites in the *apo* and Pico145-bound structures (left). Xanthine-based photoaffinity probes (right) incorporating a diazirine-based photocrosslinker (blue) and an alkyne handle for bioorthogonal ligation (red) were developed to probe ligand engagement by TRPC5 channels in human cells.

Results and Discussion

We developed a set of xanthine-based photoaffinity probes (Figure 1) that closely mimic the most potent TRPC1/4/5 inhibitor, Pico145. Using these compounds, we developed a photoaffinity labelling protocol to detect and quantify molecular interactions of xanthine-based TRPC1/4/5 modulators in human cells. We found that IC_{50} values in competition binding assays closely mimicked IC_{50} values obtained in functional assays of TRPC channel activity, suggesting that xanthines such as Pico145 modulate TRPC1/4/5 channels through a direct binding interaction. Using single-particle cryo-electron microscopy, we determined structures of a homomeric human TRPC5 channel in the presence and absence of Pico145, to resolutions of 2.8-3.0 Å (Figure 1). These structures revealed that Pico145 binds to a conserved lipid binding site of TRPC5, where it displaces a bound, endogenous phospholipid (Figure 1). The structural analysis was consistent with results from docking simulations and site-directed mutagenesis experiments. In addition, our TRPC5 cryo-EM structures revealed a putative, conserved intracellular zinc-binding site formed by residues previously implicated

in post-translational modifications, channel gating and/or trafficking, suggesting that this small domain may be an important regulatory node of TRPC channels. Overall, our data provided the first detailed insight into the mode of action of a class of small-molecule TRPC1/4/5 modulators, which may support future structure-guided TRPC drug discovery efforts.

Publications

Wright D.J., Simmons K.J., Johnson R.M., Beech D.J., Muench S.P.*, et al.* (2020) Human TRPC5 structures reveal interaction of a xanthine-based TRPC1/4/5 inhibitor with a conserved lipid binding site. *Commun. Biol.* **3**:704.

Bauer C.C, Minard A.M., Pickles I.B., Simmons K.J., Chuntharpursat-Bon E., Burnham M.P., Kapur N., Beech D.J., Muench S.P., Wright M.H., Warriner S.L. and Bon R.S. (2020) Xanthine-based photoaffinity probes allow assessment of ligand engagement by TRPC5 channels. *RSC Chem. Biol.* **1:** 436-448.

Funding

This work was funded by the BBSRC, the BHF and the Wellcome Trust.

Collaborators

External: Matthew P. Burnham (formerly AstraZeneca).

Novel allosteric inhibitors of Ras activation

Marie Anderson, Roberto Maya Martinez, Sebastien Cardon and Alex Breeze

Introduction

Upregulation of (K, H and N)-Ras-mediated signalling via mutations or hyperactivation is one of the most prevalent, yet intractable oncogenic mechanisms in human cancers. Efforts to directly target Ras and its constitutively-activated mutated forms have met with limited success, while inhibition of downstream effectors including kinases of the Raf-MEK-Erk and PI3 kinase pathways fall foul of rapid mutational escape and signalling network rewiring. Other approaches are thus sorely needed. Blocking Ras activation through inhibition of its upstream guanine nucleotide exchange factor, SOS, is currently being investigated and our work aims to exploit a novel small-molecule mechanism discovered in our lab.

Results and Discussion

Using a biophysical screen (thermofluor / T_m shift), we identified a novel small-molecule series that binds competitively with active Ras at the allosteric activation site in SOS. This unique binding mechanism was identified and confirmed both by amide chemical shift perturbations in ^{1}H-^{15}N TROSY-HSQC NMR spectra of SOScat (the catalytic domain of SOS, comprising Ras Exchanger Motif and Cdc25 domains), and by soaking into crystals of a SOS:H-Ras binary complex (Ras bound at the 'catalytic' site) followed by X-ray structure solution (2.4 Å resolution), with compound density present in the novel site (Figure 1A). Since hyperactivation of SOS by constitutive allosteric site Ras binding is a major mechanism of mutant Ras-mediated tumorigenesis, our compounds hold the potential to inhibit signalling by all forms of mutant Ras – previously viewed as an intractable challenge. Furthermore, our compounds are distinct in mechanism from series published by other groups (e.g. Bayer AG; Figure 1A). Importantly, they bind in a site that is identical between SOS1 and SOS2, the two major isoforms of SOS in human cells, while key residue differences in the catalytic Ras-proximal site targeted by the Bayer compound cause a drop-off in binding potency between SOS1 and SOS2.

Our current focus is to improve the potency and physical properties of our allosteric SOS inhibitors. Alongside structure-driven medicinal chemistry improvements to our current series, we are conducting NMR and XChem (Diamond Light Source) crystallographic fragment screens to identify new scaffolds that we can merge / hop into the existing series. Progress

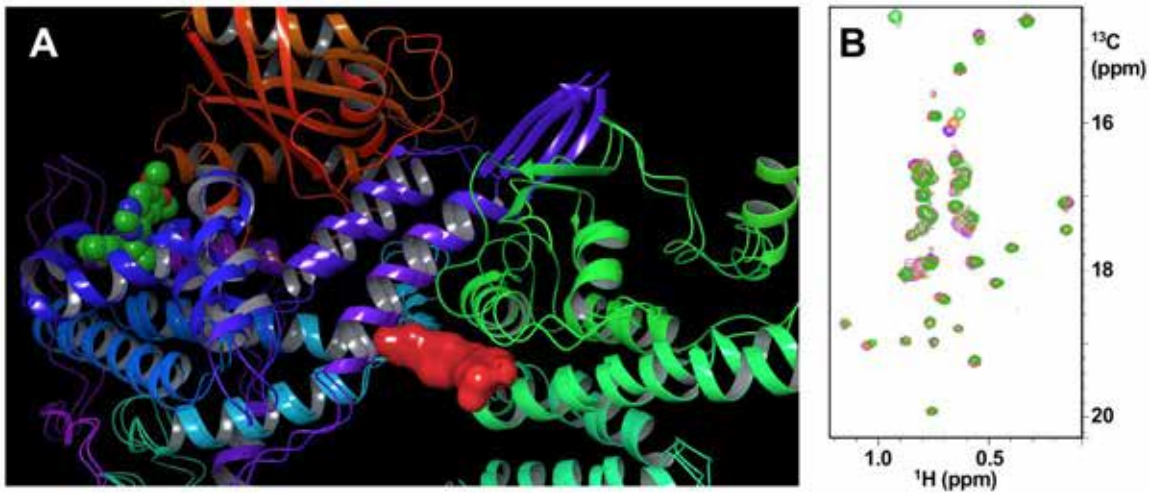

Figure 1: (**A**) X-ray crystal structures of SOScat and SOScat:H-Ras (catalytic site; Ras in orange ribbon) complex, showing locations of the Bayer inhibitor binding site (CPK spheres, green carbons) and the novel allosteric Ras-site inhibitor (red surface) identified in our work. (**B**) ^{1}H-^{13}C methyl-TROSY HMQC NMR spectrum of SOScat (Ile δ1-methyl-^{13}C labelled) showing residue-specific chemical shift changes characteristic of binding with increasing concentrations (purple > orange > green) of allosteric-site inhibitor.

will be monitored through biophysical, biochemical and cell-based assays of SOS binding, Ras activation inhibition, and Ras pathway blockade. In order to discriminate between fragments that bind at the 'Bayer' site and those binding in our novel allosteric site, we have developed an NMR-based assay that exploits the unique and distinct chemical shift signatures induced by the Bayer and by our reference allosteric-site inhibitors in ^{1}H-^{13}C methyl-TROSY HMQC NMR spectra acquired on selectively Ile-δ1-methyl labelled SOScat (Figure 1B). For those fragments showing chemical shift patterns consistent with allosteric-site binding, we will co-crystallise and/or soak into SOS1 and SOS2 crystals to obtain high-resolution structural information that can guide medicinal chemistry design-based elaboration and drive development of higher potency inhibitors.

In conclusion, we have identified compounds that bind in an allosteric Ras activator site on SOS, with the potential to disrupt hyperactive Ras cellular signalling from mutant K-Ras. We demonstrate an example of the structural and biophysical assay cascade that we are using to improve compound affinity and physical properties via fragment-based scaffold hopping.

Funding
This work is funded by Cancer Research UK (to Breeze and Tomlinson), and previously by Pancreatic Cancer Research Fund (to Breeze and Waring).

Collaborators
University of Leeds: Darren Tomlinson.
External: Mike Waring (CRUK Newcastle Drug Discovery Unit, University of Newcastle).

Assessing the developability and manufacturability of biopharmaceuticals *in vitro* and *in vivo*

Jessica Ebo, Romany McLure, Leon Willis, Ioanna Panagi, Samantha Lawrence, Alex Page, Frank Sobott, Nikil Kapur, Sheena Radford and David Brockwell

Introduction

Monoclonal antibodies (mAbs) have emerged as highly effective therapeutics and now comprise over half of first-time approvals. Despite their success the inherent metastability of proteins can result in local or global unfolding that can lead to protein aggregation. These aggregates can jeopardise development through loss of function and/or eliciting unwanted immune response in patients. Understanding why mAbs aggregate and predicting which molecules are least aggregation-prone, is of great interest to both industry and academia. To address this, we have developed two novel techniques to identify aggregation-prone proteins.

Results and Discussion

Tripartite β-lactamase platform for studying protein aggregation

An *in vivo* assay has been developed for the selection and evolution of aggregation-resistant proteins that circumvents the need for protein purification. In this assay, the test protein is fused in frame between the two domains of the *E. coli* periplasmic enzyme β-lactamase. If the test protein aggregates, the β-lactamase enzyme is unable to function and *E. coli* lose their resistance to β-lactam antibiotics (Figure 1a). This tripartite β-lactamase (TPBLA) is able to assess the aggregation propensity of a variety of therapeutically relevant scaffolds, including single-chain variable fragments (scFv) of the V_H and V_L domains of an IgG fused together by a linker. In this study, we took a previously characterised IgG with known developability issues (IgG-WFL) and the aggregation resistant counterpart (IgG-STT) that differ by three residues on the V_H domain (W35S, F36T and L64T) and assessed their aggregation-propensity as a scFv in the TPBLA. The results showed a striking difference between WFL and STT in the TPBLA (Figure 1b), recapitulating the known differences in the aggregation behaviour of the IgGs previously characterised *in vitro*.

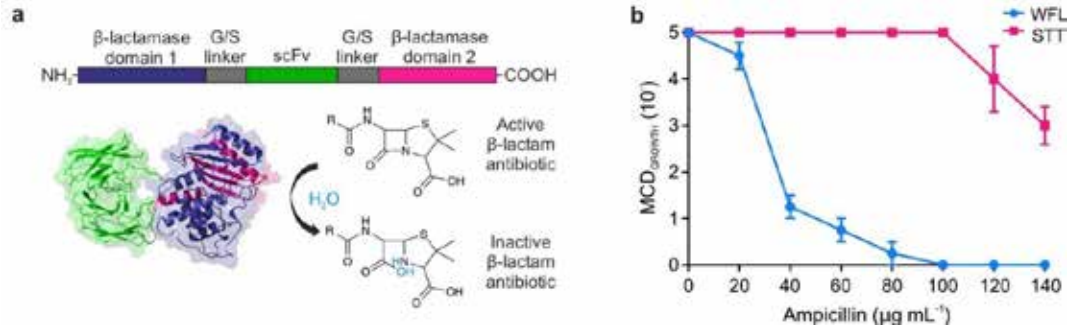

Figure 1: Tripartite β-lactamase assay. (a) The test protein (green) is inserted into a 28-residue glycine/serine-rich linker (grey) separating the two domains of the *E. coli* enzyme TEM-1 β-lactamase (purple and pink). Correct folding of the test protein in the *E. coli* periplasm enables the two halves of β-lactamase to be brought into close proximity to form the functional enzyme active site that hydrolyses β-lactam antibiotics. (b) Antibiotic survival curve of the maximal cell dilution allowing growth (MCD_{GROWTH}) on solid medium over a range of ampicillin concentrations for bacteria expressing the aggregation-prone WFL within β-lactamase (blue) or the aggregation-resistant sequence STT (pink).

In combination with directed evolution, the TPBLA can identify mutational hotspots that limit the developability of candidate therapeutic mAbs. The evolution of WFL highlighted 12 hotspot residues, six in the V_H and three in the V_L regions that contributed to aggregation. Importantly, the TPBLA does not require any structural knowledge or prior biophysical information about the protein of interest and can be used to reveal residues that modulate aggregation that could not be predicted *a priori* using currently available algorithms.

Extensional Flow Device (EFD) to identify manufacturable antibodies

Biopharmaceuticals can also aggregate *in vitro*, especially during their long and complex manufacturing process. Throughout bioprocessing, mAbs encounter harsh hydrodynamic forces, namely shear and extensional flows, in addition to interfacial effects. We have developed a low-volume extensional flow device (EFD) which subjects mAbs to defined flow

fields akin to those found in processing steps (Figure 2a). Previously, we have used the model mAbs WFL and STT (above) to establish which factors account for a protein's aggregation propensity under flow. STT was found to be much more resistant to flow than WFL. However, these model proteins represent a minute subset of the antibody sequences currently in development. Do all IgGs exhibit such contrasting aggregation behaviour under flow? How does behaviour of a mAb in the EFD compare with that in other assays?

To address these questions, we took a subset of 33 IgG1 mAbs (dubbed the $(Clinical)_{33}$ herein) whose V_H and V_L domains were derived from clinically relevant molecules. These mAbs formed part of a larger pool of mAbs (137), whose biophysical properties were previously interrogated using 12 different biophysical assays by our collaborators (Adimab). The $(Clinical)_{33}$ were stressed for 200 passes in the EFD under identical buffer conditions. The samples were then clarified by centrifugation, before the amount of insoluble protein was quantified by UV-Vis spectroscopy. A broad aggregation response was exhibited by the $(Clinical)_{33}$ in response to stress in the EFD, with the amount of aggregate ranging from ~10–80% in pellet (Figure 2b). Notably, this did not correlate with the basal aggregate level of the quiescent samples. The % in pellet for each mAb in the $(Clinical)_{33}$ was statistically correlated with the historic data from the original 12 assay dataset. This analysis showed that whilst the EFD is closely related to assays which probe the thermodynamic stability and 'stickiness' of a mAb, it has a unique branch in the 'family tree' of assays (Figure 2c, red box). *In* silico algorithms could not rationalise or predict the response to flow. Together, this suggests flow and the EFD probe unique features of a mAb, which may help distinguish manufacturable candidates from sensitive ones.

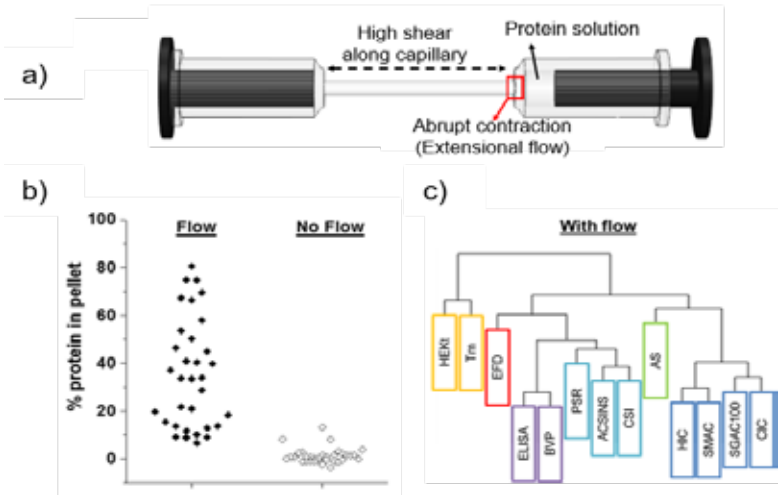

Figure 2. Extensional flow device to screen mAb aggregation *in vitro*. (a) The EFD comprises two syringes connected *via* a glass capillary. Protein solution is shuttled between the two syringes, with the abrupt contraction generating a harsh extensional flow field (strain = 11,750 s^{-1}), followed by shear along the capillary (shear = 52,000 s^{-1}). Each pass takes ~ 6 s, with exposure to the above forces taking < 50 ms. (b) Aggregation for the $(Clinical)_{33}$ following stress in the EFD. The control samples (white circles) did not significantly aggregate. **c)** Hierarchical clustering was used to compare the EFD data for the $(Clinical)_{33}$ with those from other assays. The coloured boxes indicate assays which probe similar

Publications

Ebo J.S., Saunders J.C., Devine P.W.A., Gordon A.M., Warwick A.S., *et al.* (2020) An *in vivo* platform to select and evolve aggregation-resistant proteins. *Nat. Commun.* **11**:1816.

Willis L.F., Kumar A., Jain T., Caffry I., Xu Y., Radford S.E., Kapur N., Vásquez M., and Brockwell D.J. (2020) The uniqueness of flow in probing the aggregation behavior of clinically relevant antibodies. *Engin. Rep.* **2**:e12147.

Funding

This work was funded by the BBSRC.

Collaborators

External: Janet Saunders, Paul Devine, Nicholas Bond, Richard Turner and David Lowe (AstraZeneca PLC); Tushar Jain, Isabelle Caffry, Yingda Xu and Max Vásquez (Adimab LLC).

Inter-domain dynamics of the periplasmic chaperone SurA and multi-site binding to its outer membrane protein clients

Bob Schiffrin, Matthew Watson, Theodoros Karamanos, Martin Walko, Paul White, Andrew Wilson, Antreas Kalli, Roman Tuma, David Brockwell, Sheena Radford and Antonio Calabrese

Introduction

The outer membrane (OM) of gram-negative bacteria is packed with outer membrane proteins (OMPs) that perform a range of functions that are essential for bacterial survival. A multicomponent assembly pathway is responsible for OMP biogenesis, which begins with their synthesis on cytosolic ribosomes. The unfolded, aggregation-prone OMPs must then be translocated across the inner membrane and escorted across the periplasm to the OM for insertion by the β-barrel assembly machinery (BAM). SurA is the major conserved OMP chaperone in the periplasm responsible for preventing aggregation and delivering OMPs to BAM. *E. coli* SurA comprises three domains: a core domain (made of N and C terminal regions), and two parvulin-like peptidylprolyl isomerase (PPIase) domains (P1 and P2) (Figure 1a). Despite available structural data, how SurA binds and chaperones its unfolded OMP clients remains unknown. Our work aims to (i) elucidate the molecular mechanism(s) by which SurA binds its client proteins, (ii) determine how SurA delivers its unfolded OMPs to BAM, and (iii) reveal how SurA-delivered OMPs are folded by the BAM complex. Here, we have used a range of biochemical and biophysical techniques to investigate the molecular mechanism(s) of *E. coli* SurA, and demonstrate key roles for inter-domain conformational dynamics and multiple substrate interaction sites in SurA activity.

Results and Discussion

We first set out to investigate if the elongated architecture of SurA determined by X-ray crystallography was representative of the conformation of SurA in solution. We employed chemical crosslinking-mass spectrometry (XL-MS), to covalently link residues that are within 35 Å (Cα-Cα solvent accessible surface distance) (Figure 1b), and single-molecule FRET (smFRET), to measure the distances between SurA domains (Figure 1c). The results indicate that in solution the P2 domain resides much closer to the core/P1 domains than suggested by the crystal structure, and show that there are multiple co-existing populations; including states wherein P1 is open and closed with respect to the core domain.

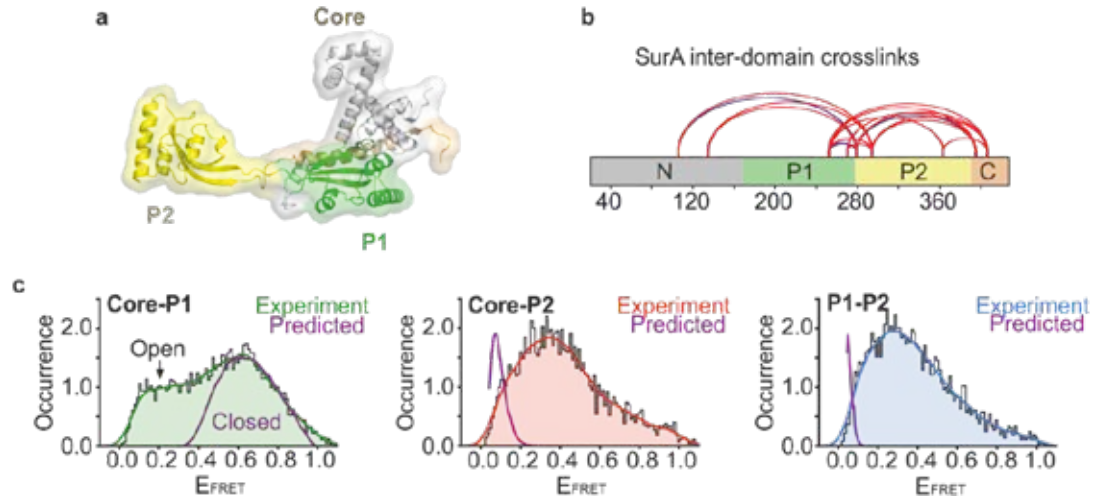

Figure 1. Solution structure of SurA. (a) Crystal structure of *E. coli* SurA. (b) Detected inter-domain crosslinks. Crosslinks consistent/inconsistent with the crystal structure are shown in blue/red, respectively. (c) E_{FRET} distributions for pairwise inter-domain distance measurements. The experimental data differ from the E_{FRET} values predicted from the crystal structure. The data indicate that both open and closed states of P1 exist, and that the P2 domain populates conformations closer to core/P1 than the crystal structure suggests.

Next we studied how SurA binds OMPs and how this affects conformations adopted by the chaperone. Using hydrogen-deuterium exchange-mass spectrometry (HDX-MS) we determined that in the presence of the client OmpX regions in the core domain became protected from exchange, suggesting that these regions form the primary binding site for OMPs (Figure 2a). This observation is consistent with data from XL-MS (Figure 2b). Notably, the interface between the core and P1 domains (Figure 2a) becomes deprotected in the HDX-MS experiments, consistent with a structural reorganisation of this interface upon client binding. This structural reorganisation between the core and P1 domains was confirmed using smFRET measurements in the absence/presence of OmpX (Figure 2c).

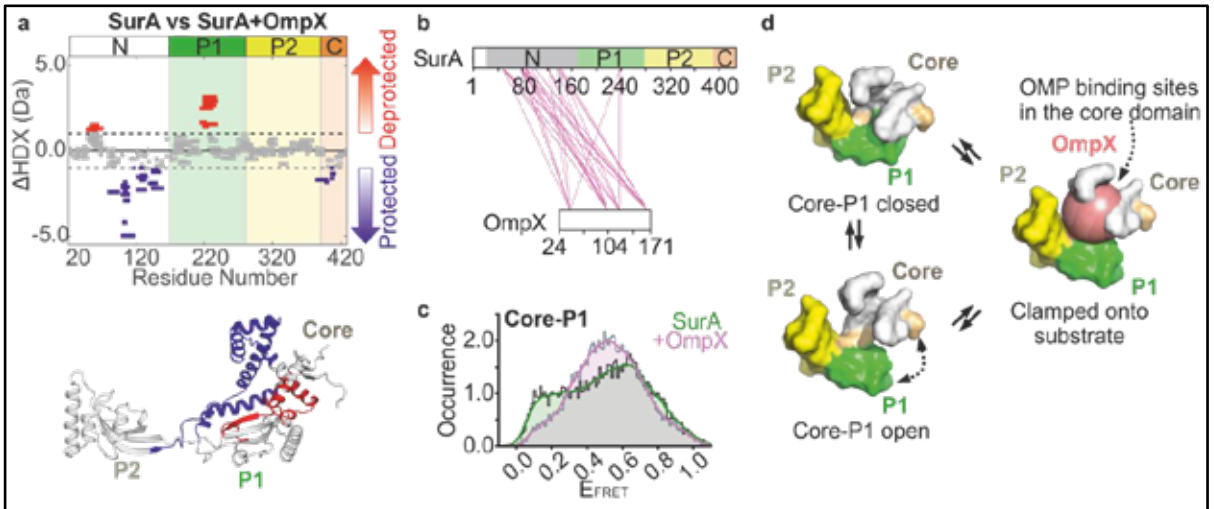

Figure 2. SurA binding to OMP clients. (a) HDX-MS data showing that in the presence of OmpX regions of protection and deprotection in SurA cluster to the core domain and the core/P1 interface, respectively. (b) Detected interprotein crosslinks (using tag-transfer crosslinkers) between SurA and OmpX. Crosslinks were primarily detected to the N-terminal region of the core domain. (c) E_{FRET} distributions for the interdomain distance between the core and P1 domains in the absence or presence of OmpX. (d) Summary of SurA conformational dynamics and a proposed mechanism of substrate binding. The P1 domain can adopt closed and open states and substrate binding results in the P1 domain adopting a structure intermediate between the open and closed conformations.

Overall, the results obtained suggest that in solution SurA adopts compact conformations dissimilar to the reported crystal structure, including states where the P1 domain is open with respect to the core domain (Figure 2d). Client binding occurs in a cradle formed between the three domains of SurA, with the primary OMP binding sites located in the core domain (Figure 2d). Ongoing work now aims to understand the mechanism by which SurA delivers OMP clients to BAM for folding. This information may inform new strategies to control bacterial infections as the OMP assembly pathway is essential and widely conserved across gram-negative pathogens, and therefore an excellent potential antibiotic target.

Publications

Calabrese A.N., Schiffrin B., Watson M., Karamanos T.K., Walko M.*, et al.* (2020) Inter-domain dynamics in the chaperone SurA and multi-site binding to its outer membrane protein clients. *Nat. Commun.* **11**:2155.

Funding

This work was funded by the BBSRC, EPSRC and MRC.

Structure and function of 50 nm extracellular filaments in reproduction

Mehrnaz Montazeri, John Trinick, Elwyn Isaac and Joe Cockburn

Introduction

Drosophila melanogaster is a widely used model animal and many of its cellular mechanisms are similar in diverse species, including humans. A striking feature of Drosophila reproduction, reported 50 years ago but not explored further, concerns large numbers of extracellular filaments found in the male accessory gland (MAG), which is the equivalent of the human prostate. The accessory gland generates most of the components of the seminal fluid that bathes and protects sperm during and after copulation, and its contents are transferred to the female. These MAG products include a plethora of proteins as well as vesicles (40-100 nm in diameter) known as exosomes. Early reports also showed the seminal fluid also contains large numbers of very distinctive filaments 50 nm wide and up to 30 microns long, which are released from the MAG secondary cells. The most detailed micrographs showed that the filaments are a tube of 10 peripheral protofilaments that connect to a central structure. The filaments are also seen alongside sperm in the female seminal receptacle and are presumed important for sperm maintenance.

Drosophila, like many animals, can store sperm for considerable periods in the female. This is an important but poorly understood phenomenon that obviously offers great advantages to the animal. Storage allows the female to produce hundreds of progeny over several weeks from a single mating. The 50 nm filaments do not appear to be present in humans, but there are reports with electron micrographs showing similar filaments in male reproductive glands of crustaceans, house flies and snakes. Sperm can sometimes be stored in post-mated female snakes for more than 5 years before an egg is fertilised.

There were a few papers concerning the 50 nm filaments in the 1960s and 70s, but we can find no recent work, and their structure, composition and function(s) remain unknown. There is considerable interest in the function of exosomes (also known as prostasomes in mammals) present in seminal fluid of animals from diverse taxa, since they are thought to be important for protecting sperm, regulating capacitation and sperm-egg fusion. By inference, the extracellular filaments may also function in sperm protection, maintenance and activation in the female. In the past decade *Drosophila* studies have made major contributions to understanding of the structure and physiological roles of seminal fluid components. In this Leverhulme funded project, we aim to use *Drosophila* to discover the structure and functions of 50 nm filaments.

Funding

This work was funded by the Leverhulme Trust.

A multiscale understanding of protein hydrogels with insight from theory and experimentation

Matthew D.G. Hughes, Benjamin S. Hanson, Christa Brown, Kalila Cook, Alex Wright, Sophie Cussons, David J. Brockwell and Lorna Dougan

Introduction

Globular protein hydrogels are a class of hierarchical viscoelastic network in which folded proteins are the smallest structural subunit. When a solution of protein subunits are exposed to light in solution, photo-activated covalent cross-links form between tyrosine residues. These residues may exist naturally, or be specifically added using protein engineering techniques. In either case, continuous formation of these cross-links, together with diffusion, leads to the formation of a fractal network of connected protein material. Subsequent interactions with the surrounding solution leads to absorption of water into the network, swelling the system to an eventual equilibrium, a hydrogel. Our research interests span the full range of behaviour in protein hydrogel systems, from experimental investigations of specific systems, to more abstract theoretical investigations of the formation of the gel networks, and even combining protein hydrogels with microbubbles. Our report will give a flavour of how our understanding has progressed over the past year, and our plans going forward.

Results and Discussion

Maltose binding protein (MBP) is an interesting protein for us, as the binding of maltose into the active site stabilises the MBP thermodynamically, and can also stabilise it mechanically depending on the direction of applied force. We have investigated how stabilisation of the protein subunit affects the mechanical response of the overall hydrogel (Hughes et al. 2020).

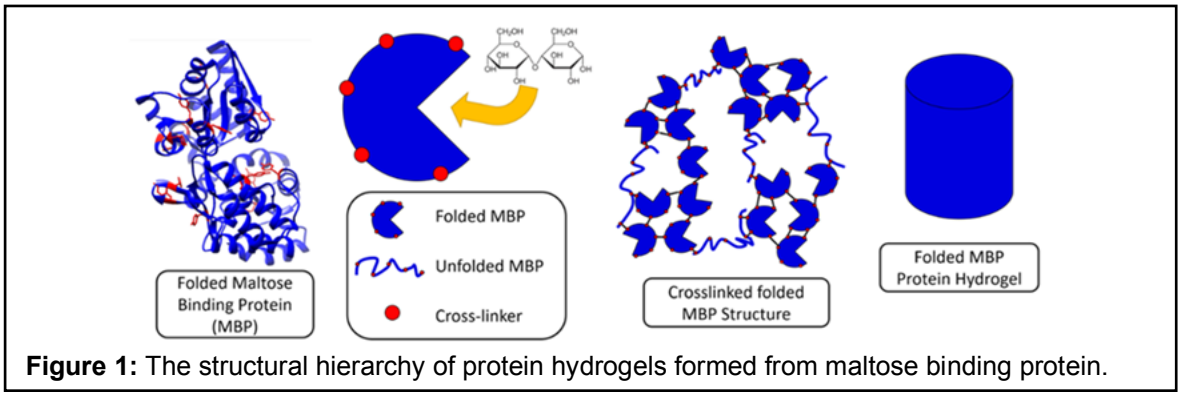

Figure 1: The structural hierarchy of protein hydrogels formed from maltose binding protein.

Using circular dichroism, we observed that while unfolded protein is present in the gel network, the addition of maltose had very little effect on the overall amount of unfolding upon gelation. While counter-intuitive, small-angle X-ray scattering (SAXS) and small-angle neutron scattering (SANS) experiments nevertheless also showed that the presence of maltose does not significantly affect the gel structure at the mesoscale. However, rheological measurements show that the addition of maltose does result in an increase in the shear modulus of the gel, indicating that a hierarchical translation of nanoscale mechanical properties to the macroscale is still possible. With detailed analysis of the SAS data, we were able to postulate a structural explanation to reconcile these observations (Hughes et al. 2020).

The structural complexity of the individual protein subunit means that some form of coarse-graining is required for simulations at the network scale. We have been approaching this in two different ways. One approach uses a fully dynamic simulation framework called “BioNet”, a pseudo-colloidal simulation in which proteins are modelled as spheres with steric repulsion. Importantly, however, these spheres have specific binding sites (i.e. residues) explicitly defined on the surface of the spheres, leading to novel emergent behaviour. We observed that the volume fraction of a protein solution is the dominant parameter in determining the resultant structural characteristics of the system, but that protein binding site topology can be used to slightly modulate this (Hanson and Dougan 2020). In an alternate approach we designed a coarse-grained system in which space itself is discretised, accelerating the simulation speed. From this, we investigate the effect of reducing the reaction rate in our network systems. A

preliminary result shows that we can distinguish between reaction- and diffusion-limited systems with this model, indicating that different structures ought to emerge if the cross-linking rate is reduced. We have recently published experimental evidence for this in protein hydrogels formed from bovine serum albumin (BSA), where the reaction rate was reduced by lowering the light intensity (Aufderhorst-Roberts et al. 2020).

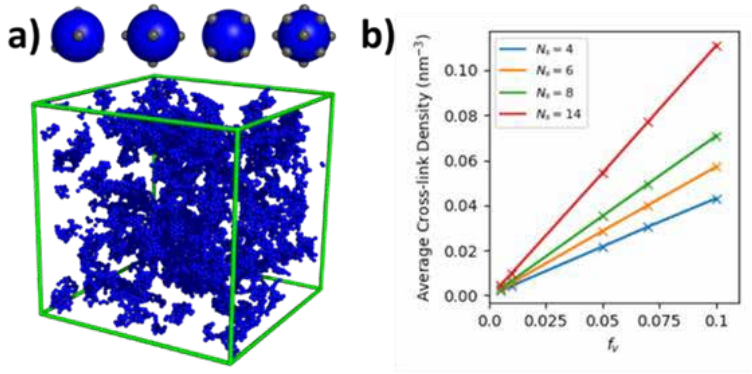

Figure 2: BioNet, a bespoke, dynamic mesoscale modelling technique used in our group a) The subunits used in (top) and a representative network formed (bottom) via BioNet simulation. b) We observe that volume fraction and protein topology both affect the cross-linking density throughout the network.

We are exploring BSA protein hydrogels as a controllable drug delivery system, by encompassing drug loaded microbubbles. The microbubbles are composed of a gas core stabilised by a lipid monolayer shell, and the application of ultrasound causes cavitation, violently disrupting the lipid shell and resulting in the release of drugs on-demand. Initial work suggests that network formation in the presence of microbubbles produces a weaker hydrogel.

Continuous collaboration is our goal, and we are aiming to use our simulation results to inform experimentation and vice versa. Indeed, the fractal dimension is a structural parameter which can be calibrated across all of our projects, and in principle, so can mechanical responses. The key to fully reconciling our modelling and experiments will be the inclusion of protein unfolding. This is currently being integrated into BioNet using novel statistical mechanical methods, and will potentially be explicitly investigated experimentally in the near future.

Publications

Aufderhorst-Roberts A., Hughes M.D.G., Hare A., Head D.A., Kapur N., *et al.* (2020) Reaction rate governs the viscoelasticity and nanostructure of folded protein hydrogels. *Biomacromolecules* **21**:4253.

Hanson B.S. and Dougan L. (2020) Network growth and structural characteristics of globular protein hydrogels. *Macromolecules* **53**:7335.

Hughes M.D.G., Cussons S., Mahmoudi N., Brockwell D.J. and Dougan L. (2020) Single molecule protein stabilisation translates to macromolecular mechanics of a protein network. *Soft Matter* **16**:6389.

Funding

These projects are supported by EPSRC and the White Rose Industrial Biotechnology studentship network. We also acknowledge the ISIS Neutron and Muon spallation source.

Collaborators

University of Leeds: Dr David Head
External: Dr Najet Mahmoudi (ISIS spallation source).

The role of water in extreme environments: solute specific perturbations to water structure and dynamics

Harrison Laurent and Lorna Dougan

Introduction

Liquid water is fundamental to life as we know it, acting as solvent, catalyst, reactant, chaperone, controller, and provides the major driving force for biomolecular self-assembly, dynamics, and function in living systems. When considering water in biological systems it becomes abundantly clear that a simple structural or dynamic picture is insufficient, particularly when considering aqueous systems containing multiple solute species. An approach considering both structural and dynamic perturbations to water is therefore required if one is to draw meaningful conclusions. Neutron diffraction and subsequent computational modelling provides a powerful tool to resolve atomistic detail of the structural perturbations in aqueous systems, and nuclear magnetic resonance (NMR) is well equipped to reveal details of dynamic perturbations. We combine these two experimental techniques to investigate structural and dynamic perturbations to water in tertiary aqueous solutions of $Mg(ClO_4)_2$ and trimethylamine N-oxide (TMAO). $Mg(ClO_4)_2$ has previously been shown to perturb water structure in a manner similar to that of a large external pressure, whereas TMAO has previously been shown to protect proteins against pressure induced denaturation, hence this tertiary solution was chosen to investigate the potentially competing effects of these two solutes.

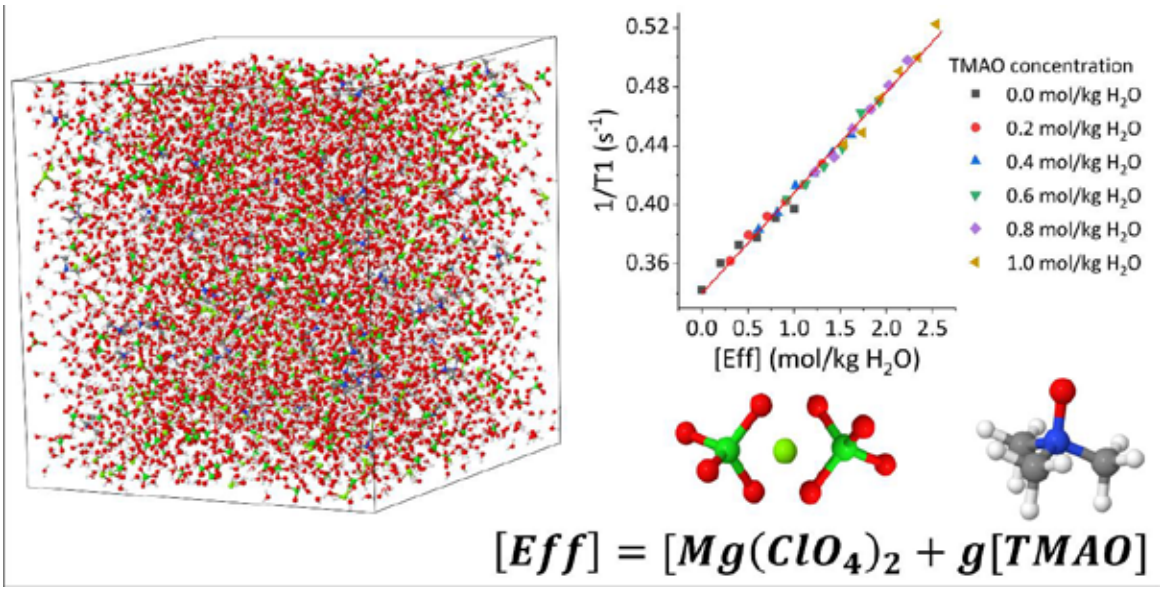

Figure 1: Structural and dynamic perturbations to water by magnesium perchlorate and trimethylamine N-oxide can be examined by combining neutron scattering and nuclear magnetic resonance. The total effective solute concentration can be expressed as a weighted sum of each individual solute concentration. This shows that TMAO is 1.54 times more effective at perturbing water structure and dynamics.

Results and Discussion

Neutron diffraction data were taken using the NIMROD instrument at the ISIS Facility, Rutherford Appleton Laboratories. This was done at 25°C for pure water, 1.0 M TMAO, 0.2 M $Mg(ClO_4)_2$, 1.0 M TMAO + 0.2 M $Mg(ClO_4)_2$, 2.7 M $Mg(ClO_4)_2$, and 1.0 M TMAO + 2.7 M $Mg(ClO_4)_2$. Hydrogen/deuterium isotopic substitution was used to exploit the large difference in the coherent neutron scattering length between hydrogen and deuterium. The raw scattering data were then corrected for multiple scattering, inelasticity effects, etc. using Gudrun, and then used to produce simulated boxes of molecules whose scattering patterns are consistent with the corrected data through empirical potential structure refinement (EPSR), and calculations are completed for hydrogen bond interaction energies, bond angles, and the relative abundance of various hydrogen bonded conformations of water molecules, such as

bifurcated hydrogens. NMR measurements were performed at 27°C in a range of 0 - 1.0 M TMAO and $Mg(ClO_4)_2$ in 0.2 M steps, resulting in 36 total samples.

The average interaction energy between two hydrogen bonded water molecules in the bulk, that are directly hydrating a solute molecule, shows that hydrogen bonds between water molecules are weakened in $Mg(ClO_4)_2$ solutions, but strengthened upon subsequent addition of TMAO. This is supported by monitoring the position of the ^1H peak associated with water in NMR. A shift to lower values is consistent with weakened hydrogen bonding between water molecules and vice versa. Here we observe a peak shift to lower values with increasing $Mg(ClO_4)_2$ concentration, but a shift to higher values with increasing TMAO concentration. Therefore, when one considers the *structural* perturbation to the water network in these tertiary solutions, the two solutes effectively cancel each other out.

NMR measured changes to the rotational correlation time of the water molecules by monitoring the T_1 decay time, and measure the diffusion coefficient for water molecules. This provides us with measures of *dynamic* perturbations to the system. Here we observe that both TMAO and $Mg(ClO_4)_2$ act to slow the dynamics of the water molecules and that these effects appear to be additive. This result is supported by EPSR by monitoring the relative abundance of water molecules in a bifurcated hydrogen conformation. This conformation is an intermediate step that occurs as a water molecule switches hydrogen bonding partners, and therefore its relative abundance is an indication of how frequently hydrogen bond switching events are occurring and serves as a measure of dynamics. Here we observe a reduction in the abundance of bifurcated hydrogens with increasing $Mg(ClO_4)_2$, and a further reduction upon subsequent TMAO addition, consistent with slowed dynamics observed with EPSR.

We have therefore observed that TMAO and $Mg(ClO_4)_2$ perturb water *structure* in an opposite manner, but perturb water *dynamics* in an additive manner. We can then quantify one solutes perturbing ability relative to the other by plotting each of the 5 discussed datasets as a function of "effective total solute concentration", as described by $[Eff] = [Mg(ClO_4)_2] + g[TMAO]$, where g is a weighting parameter that describes the perturbing ability of TMAO relative to $Mg(ClO_4)_2$. We show that TMAO is 1.54 times more effective at perturbing water structure and dynamics than $Mg(ClO_4)_2$. This technique can be applied to any number of tertiary aqueous solutions and provide a way of meaningfully investigating complex aqueous environments.

Publications

Laurent H., Baker D.L., Soper A.K., Ries M.E. and Dougan L. (2020) Solute specific perturbations to water structure and dynamics in tertiary aqueous solution. *J. Phys. Chem. B* **124**:10983.

Laurent H., Soper A.K. and Dougan L. (2020) Trimethylamine N-oxide (TMAO) resists the compression of water structure by magnesium perchlorate: terrestrial kosmotrope vs. Martian chaotrope. *Phys. Chem. Chem. Phys.* **22**:4924.

Funding

This project was supported by EPSRC and the ISIS Facility.

Collaborators

University of Leeds: Internal: Michael Ries, Daniel Baker
External: Alan Soper, ISIS Facility, Rutherford Appleton Laboratories.

From single “live” cells to tissue: biophysical approaches for cancer progression, patient stratification and understanding drug activity

Julia Gala de Pablo, Chloe Kirkby, Fern Armistead and Stephen Evans

Introduction

Raman spectroscopy provides a label free approach for the analysis of molecular signals with sub-cellular resolution. We have shown that correlating Raman measurements with fluorescence microscopy allows us to follow drug uptake within cells and understand why the drug behaves differently in different cell types. Further, we have shown that Raman coupled with machine learning approaches can be used to study biopsy tissue and to be able to predict whether a patient is likely to respond to radiotherapy or not. Finally, we have continued our mechanical deformation studies on single cells to understand how the mechanical properties of cells change during cancer progression.

Results and Discussion

Raman spectroscopy has been used to observe uptake, metabolism and response of single-cells to drugs. Photodynamic therapy is based on the use of light, a photosensitiser and oxygen to destroy tumour tissue. We used single-cell Raman spectroscopy to study the uptake and intracellular degradation of a novel photosensitiser with a diphenylacetylene structure, DC473 (Figure 1), in live single-cells from colorectal adenocarcinoma cell lines SW480, HT29 and SW620. DC473 was seen to predominantly accumulate in lipid droplets, showing higher accumulation in HT29 and SW620 cells than in SW480 cells, with a broader DC473 peak shifted to higher wavenumbers. DC473 activation and effects were tracked on live single cells for 5 min. Upon exposure to UV light, the DC473 signal intensity dropped, with remaining DC473 shifting towards higher wavenumbers and widening, with a lifetime of approximately 50 s. Morphologically, SW480 and SW620 cells showed changes upon photodynamic therapy, whereas HT29 cells showed no changes. Morphological changes correlated with higher remaining DC473 signal after UV exposure. Our research suggests that DC473 forms aggregates within the cells that disaggregate following activation, showing the potential of Raman spectroscopy for the study of time-dependent single-cell pharmacodynamics (de Pablo et al. 2020).

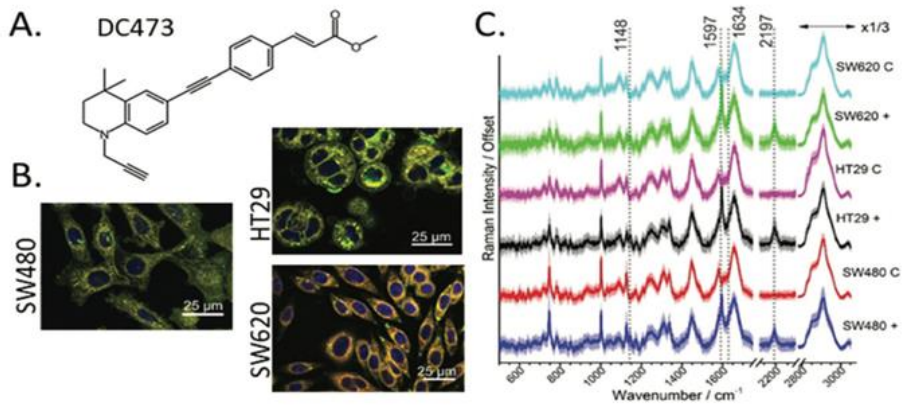

Figure 1: A. Chemical structure of DC473. B. Confocal fluorescence images of cells for each cell line, where blue is DNA, and green and red are two emission channels for Nile Red: triglycerides (green) and phospholipids (red). C. Average spectra of live single cells of the different cell lines, where + indicates cells following incubation with 4 µ M of DC473 and C indicates cells with an equivalent volume of DMSO.

Rectal cancer patients frequently receive pre-operative radiotherapy (RT), prior to surgical resection. However, colorectal cancer is heterogeneous and the degree of tumour response to pre-operative RT is highly variable. There are currently no clinically approved methods of predicting response to RT, and a significant proportion of patients will show no clinical benefit, despite enduring the side-effects. We evaluated the use of Raman spectroscopy (RS), a non-destructive technique able to provide the unique chemical fingerprint of tissues, as a potential tool to stratify patient response to pre-operative RT. Raman measurements were obtained

from the formalin-fixed, paraffin-embedded (FFPE) pre-treatment biopsy specimens of 20 rectal cancer patients who received pre-operative RT. A principal component analysis and linear discriminant analysis algorithm was able to classify patient response to pre-operative RT as good or poor, with an accuracy of 86.04 ± 0.14% (standard error). Patients with a good response to RT showed greater contributions from protein-associated peaks, whereas patients who responded poorly showed greater lipid contributions. These results demonstrate that RS is able to reliably classify tumour response to pre-operative RT from FFPE biopsies and highlights its potential to guide personalised cancer patient treatment.

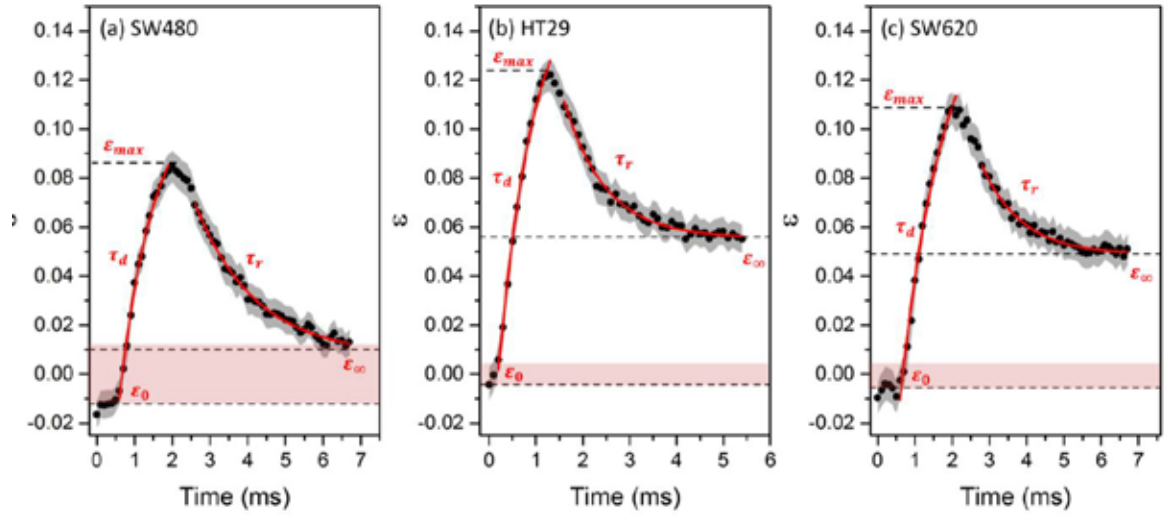

Figure 2: High speed imaging and shape analysis provides strain, ε, tracking for three colorectal cancer cell types as a function of time, showing changes in viscoelastic response as a function of disease progression (Armistead et al. 2020).

We presented the first example of using microfluidic deformation to distinguish between non-metastatic and metastatic colorectal cells (CRCs) and support the expectation that metastatic cells are more deformable than non-metastatic cells due to cytoskeletal changes (Figure 2). Further, we found that multiple parameters were needed to be able to distinguish the four cell types from each other. We observed that SW620 and HT29 are more deformable and softer than SW480 and do not recover their original strain suggesting that they undergo an additional slower relaxation process, occurring over a long time period. Single cell and multiple parameter analysis showed changes in the mechanical properties of CRC cells attributed to specific sub-structural changes, and that these can also be used to classify different cell types. Results show that a single-cell high-throughput technique combined with multiparameter analysis will allow us to advance our understanding of cancer progression, and to accurately classify heterogeneous samples of disease states.

Publications

de Pablo J.G., Chisholm D.R., Ambler C.A., Peyman S.A., Whiting A., *et al.* (2020) Detection and time-tracking activation of a photosensitiser on live single colorectal cancer cells using Raman spectroscopy. *Analyst* **145**:5878.

Armistead F.J., De Pablo J.G., Gadelha H., Peyman S.A. and Evans S.D. (2020) Physical biomarkers of disease progression: on-chip monitoring of changes in mechanobiology of colorectal cancer cells. *Sci Rep* **10**:3254.

Funding

This work was supported by an EPSRC DTP studentship, and a University of Leeds Scholarship.

Collaborators

University of Leeds: Dr N. West, Dr H. Wood, Dr S Peyman.
External: Prof A. Whiting & Prof C. A. Ambler (Durham University).

Theranostics for the treatment on cancer and biofilms

Leeds Microbubble Consortium and Stephen Evans

Introduction

Theranostics are materials that combine therapeutic and diagnostic properties for the identification and treatment of disease. In particular, our work has focused on developing two classes of materials, those based on therapeutic microbubbles and those on gold nanomaterials. We have developed these for the treatment of cancer and biofilms.

Results and Discussion

We developed a microfluidic platform for the formulation of complex microbubble architectures consisting of a lipid shelled microbubble, with attached liposomal payload, and antibody targeting (Figure 1, *left*). These therapeutic agents are targeted to newly formed vasculature associated with tumour growth. Ultrasound was used to image the bubbles and burst them at the tumour creating a localised release of therapeutic agent. The localised delivery and drug uptake allowed more toxic agents to be used whilst reducing the potential of offsite toxicity (Ingram et al. 2020). The approach has led to improved therapeutic index in pre-clinical models (Figure 1, *right*) and we are currently planning for our first in human test.

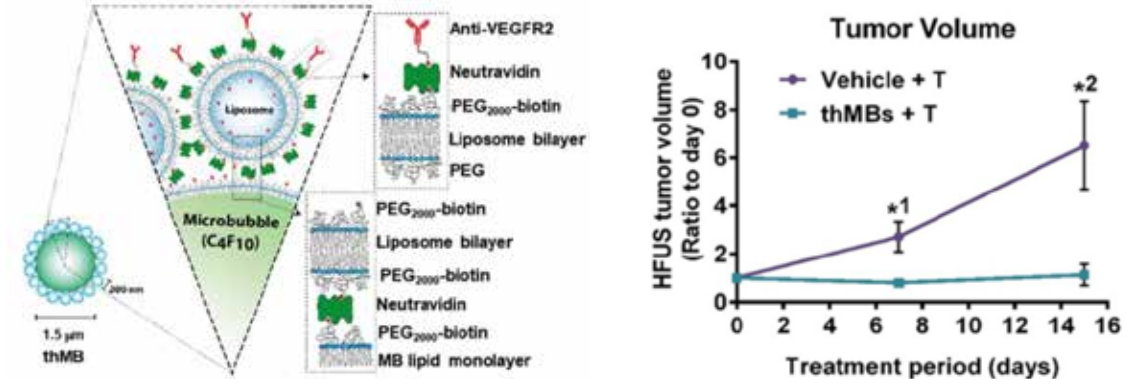

Figure 1. (*Left*) *S*chematic of therapeutic microbubble (thMB) structure, with antibody targeting, liposomal drug loading and lipid coated bubble. (*Right*) Tumour size as determined using ultrasound as a function of time for different treatments (Ingram et al. 2020).

We also demonstrated that such structures can be freeze-dried, stored for many months and reconstituted as required. This removes the necessity of producing them at the point of application. Further, our approach allows the exchange the gas core to create oxygen, or other gases in the bubble, which might improve drug efficacy (Abou-Saleh et al. 2020). In a separate piece of work we demonstrated that microfluidics provides a good platform for studying thMB/spheroid interactions (Bourn et al. 2020). Finally, we have also developed a novel 'nested nanobubble' architecture in which nanobubbles, and encapsulated within drug loaded liposomes, allow ultrasound triggered release from liposomes (Batchelor et al. 2020). Our work on the development of gold nanomaterials for photoacoustic imaging and photothermal therapy has led to the production of gold with different architectures such as nano-plates, -prisms, and -pinecones (Ye, Azad et al. 2020). These have both catalytic and nanoenzyme properties and have potentials for early detection (including amplified lateral flow and ELISAs) as well for therapy.

One form of material produced was an 'open ended hollow gold nanotube' (Figure 2, *left*). Such nanotubes penetrate the cell membrane and are rapidly trafficked to the nucleus (Figure 2, *right*) avoiding normal endocytotic pathways and are of potential interest for infrared based photothermal therapy and drug delivery (Ye, Connell et al. 2020). Embedding gold nanoparticles into gels together with antimicrobial peptide loaded liposomes allowed us to demonstrate the photo-triggered release of antimicrobial peptides and killing of bacteria. This on-demand release of antimicrobial and effective repeated release profiles has potential for use in dressings (Moorcroft et al. 2020).

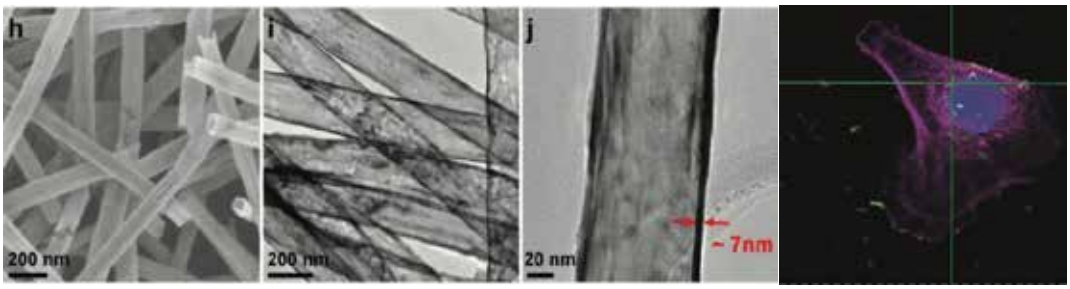

Figure 2. (*Left*) Hollow gold nanotube. (*Right*) Nanotube (green) uptake into cells and transport to nucleus (Ye et al. 2020).

Publications

Ingram N., McVeigh L.E., Abou-Saleh R.H., Maynard J., Peyman S.A.*, et al.* (2020) Ultrasound-triggered therapeutic microbubbles enhance the efficacy of cytotoxic drugs by increasing circulation and tumor drug accumulation and limiting bioavailability and toxicity in normal tissues. *Theranostics* **10**:10973.

Abou-Saleh R.H., Delaney A., Ingram N., Batchelor D.V.B., Johnson B.R.G.*, et al.* (2020) Freeze-dried therapeutic microbubbles: stability and gas exchange. *ACS Appl. Bio. Mater.* **3**:7840.

Bourn M.D., Batchelor D.V.B., Ingram N., McLaughlan J.R., Coletta P.L.*, et al.* (2020) High-throughput microfluidics for evaluating microbubble enhanced delivery of cancer therapeutics in spheroid cultures. *J. Control. Release* **326**:13.

Batchelor D.V.B., Abou-Saleh R.H., Coletta P.L., McLaughlan J.R., Peyman S.A.*, et al.* (2020) Nested nanobubbles for ultrasound-triggered drug release. *ACS Appl. Mater. Interfaces* **12**:29085.

Ye S.J., Azad A.A., Chambers J.E., Beckett A.J., Roach L.*, et al.* (2020) Exploring high aspect ratio gold nanotubes as cytosolic agents: structural engineering and uptake into mesothelioma cells. *Small* **16**:2003793.

Ye S.J., Connell S.D., McLaughlan J.R., Roach L., Aslam Z.*, et al.* (2020) One-step preparation of biocompatible gold nanoplates with controlled thickness and adjustable optical properties for plasmon-based applications. *Adv. Funct. Mater.* **30:**2003512.

Moorcroft S.C.T., Roach L., Jayne D.G., Ong Z.Y. and Evans S.D. (2020) Nanoparticle-loaded hydrogel for the light-activated release and photothermal enhancement of antimicrobial peptides. *ACS Appl. Mater. Interfaces* **12**:24544.

Funding

This work was funded by the EPSRC, the British Lung Foundation, and NIHR.

Collaborators

University of Leeds: Microbubble Consortium
External: Prof. Stefan Marciniak (U. Cambridge), Papworth Hospital (Medicines Discovery Catapult).

Fibrinogen interaction with complement C3: a potential therapeutic target to reduce thrombosis risk

Rhodri J. King, Katharina Schuett, Christian Tiede, Vera Jankowski, Vicky John, Abhi Trehan Katie Simmons, Sreenivasan Ponnambalam, Robert F. Storey, Michael J. McPherson, Darren C. Tomlinson, Ramzi A. Ajjan and Colin W.G. Fishwick

Introduction

Hypofibrinolysis is associated with increased risk of atherothrombotic events. Although most studies have only shown an association between hypofibrinolysis and cardiovascular (CV) disease, a more recent longitudinal study in a large population of patients with acute coronary syndrome has demonstrated that prolonged fibrin clot lysis is an independent predictor of CV mortality. Therefore, it was proposed that reducing residual thrombosis risk in patients with coronary artery disease requires targeting the fibrinolytic system in addition to anti-platelet therapies. Indeed, the combination of anti-coagulant and anti-platelet therapy agents reduces vascular thrombotic events but at the expense of increased risk of bleeding. Therefore, a more targeted approach is required that improves hypofibrinolysis and reduces the risk of vascular thrombosis without increasing bleeding events. Complement C3, which is incorporated into fibrin clots, has been shown to modulate fibrin clot lysis, an effect that may be exaggerated in higher vascular risk patients. C3 plasma levels have shown correlations with ex-vivo plasma clot lysis in individuals with diabetes as well as healthy controls. Moreover, plasma levels of this protein were independent predictors of resistance to fibrinolysis in 875 high vascular risk patients with type 2 diabetes. These data suggest that C3 represents a credible therapeutic target to shorten fibrin clot lysis and ultimately reduce thrombosis risk. However, these functional studies have been conducted using pooled C3 and studies assessing consistency of the response in different individuals, crucial to establish the therapeutic potential of C3, are lacking. We have recently demonstrated that fibrin clot lysis can be modulated to stabilise the clot with the use of small conformational proteins, termed Affimers. This Affimer technology showed restoration of abnormal lysis of clots made from plasma samples of individuals with haemophilia, indicating a potential therapeutic role for these proteins. However, it remains unknown whether Affimers can be used to enhance clot lysis, particularly in individuals at high vascular risk. The aim of this work was to establish the role of C3 as a therapeutic target for enhancing fibrinolysis and reducing thrombosis risk.

Results and Discussion

There are a number of novel findings in this work that can be summarised as follows: i) C3 purified from individual patients consistently prolongs clot lysis, ii) the β-chain of fibrinogen in the area of Cys424-Arg445 represents one region of interaction with complement C3, iii) Affimer proteins provide a tool for targeted modulating of fibrin clot lysis by interfering with fibrinogen-C3 interactions. While C3 protein purified from individual plasma samples consistently prolonged clot lysis, an inter-individual variability in the response was noted, which may be related to the degree of incorporation of C3 into the clot. This was particularly pronounced in C3 purified from diabetes samples, which may be related to alternative post-translational modifications in the protein. We identified six lysine residues that were glycated in T1DM samples, but not controls. The variability in glycation sites comparing individuals with T1DM suggests that the ability of lysine residues on C3 to undergo glycation has a large inter-individual variability, which may modulate the anti-fibrinolytic effects of the protein. Interestingly, in vitro glycation of C3 showed largely similar patterns, favouring glycation of certain lysine residues, suggesting this consistency is related to a steric effect. Previous work has shown that glycation of proteins involved in coagulation and lysis alters clot structure and/or the efficiency of fibrinolysis. For example, fibrinogen glycation alters fibrin network characteristics, and the degree of protein glycation correlates with glycaemic control measured as HbA1c. Proteins in the fibrinolytic system are also affected as plasminogen glycation in diabetes compromises conversion to plasmin and modulates enzyme activity. There was no clear correlation between number of lysine residues glycated and the antifibrinolytic effects of C3, but this may be due to the small number of samples analysed or it may simply indicate that some lysine residues are more important than others and extensive glycation of multiple residues is not required to observe an effect. Overall, however, our data

suggest that glycation of C3 increases its antifibrinolytic effect, although it remains unclear which lysine residues are important for the observed effect. Our binding studies indicate that three areas on the β-chain of fibrinogen play a role in C3-fibrinogen interactions. In particular, two of these areas, located on the N terminus, were in close proximity and separated by a single amino acid. We should acknowledge that the microarray technique only identifies linear interactions, and it is possible that additional conformational interactions take place between the two proteins. However, we should not underestimate the importance of linear binding between proteins with previous work demonstrating the importance of such interactions between fibrinogen and FXIII. A key finding of our work is a proof of concept for a novel methodology to modulate fibrin clot lysis, and hence thrombosis risk, in individuals with diabetes. We describe a new technique that identified a small binding protein with two variable loops (Affimer A6), with one of the loops sharing sequence identity with an exposed portion of C3, likely to be involved in protein-protein interactions. Interestingly, Affimer A6 was able to abolish C3-induced prolongation of lysis with high specificity, regardless as to whether C3 was purified from control or diabetes samples. Moreover, Affimer A6 was capable of reducing plasma clot lysis from both healthy controls and patients with diabetes. We and others have shown that changes in clot lysis by 6-18% are clinically significant and therefore the observed 7-11% reduction in clot lysis by Affimer A6 is likely to be clinically meaningful. Although speculative, this targeted enhancement of clot lysis is unlikely to significantly increase bleeding risk, making this approach clinically promising. The predicted binding sites of both loops of Affimer A6 were in close proximity within the β-chain of fibrinogen and close to the region of fibrinogen that interacts with C3 using microarray screening. Taken together, the N terminus of the β chain of fibrinogen represents a binding site for complement C3, which may be important for the development of agents that improve efficiency of fibrinolysis, particularly in high-risk vascular patients. These findings open a new avenue for the identification of therapeutic targets to modulate the hypofibrinolytic environment in high-risk patients, which may have future clinical implications.

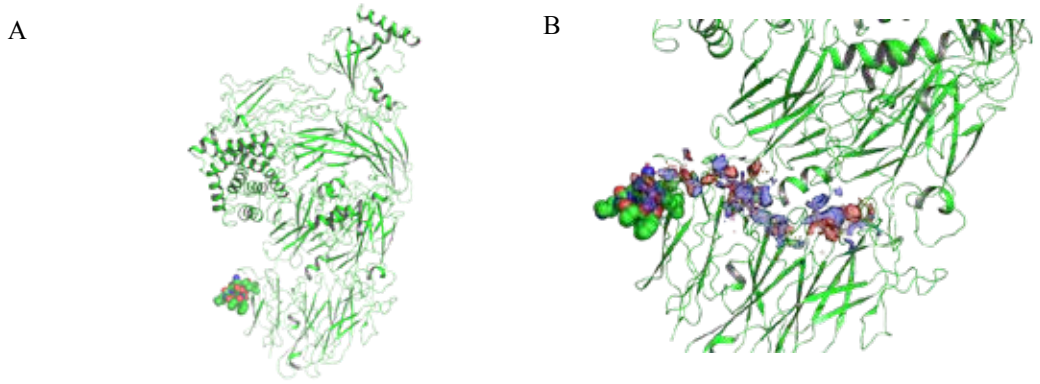

Figure 1. Affimer A6 sequence identity with C3 and potential protein-protein interaction sites on C3. A) Loop 2 of Affimer A6 showing sequence identity with the area labelled in red spheres on the C3 molecule. B) Enlarged area of potential protein-protein interaction sites on complement C3 (labelled in different colours) identified as the best scoring site using the SiteMap module of Glide (Schrodinger Inc).

Funding
PhD Fellowship from Sir Jules Thorn Charitable Trust. Diabetes UK funded part of this work.

Collaborators
External: Schuett, K (University Hospital Aachen, Germany); Jankowski, V (Aachen University, Germany); Storey, RS (University of Sheffield).

The structure of a native orthobunyavirus ribonucleoprotein reveals a key role for viral RNA in defining its helical architecture

Francis R. Hopkins, Beatriz Álvarez-Rodríguez, Samantha Hover, Koulla Panayi, George Heath, Thomas A. Edwards, John N. Barr and Juan Fontana

Introduction

The *Bunyavirales* order of segmented, negative-sense RNA viruses contains over 500 named isolates, several of which cause fatal human disease, for which FDA-approved vaccines or therapies are not available. As with all negative sense RNA viruses, the bunyavirus genome is not naked; instead the RNA is associated with the nucleocapsid protein (NP) to form an ordered assembly known as the ribonucleoprotein (RNP). As formation of the RNP is essential for multiple viral activities, a detailed understanding of its structure will reveal both fundamental details of bunyavirus processes, and targets for future anti-viral therapies. However, no high-resolution structures of bunyavirus RNPs in their native state currently exist. Structural information of the RNPs is limited to X-ray and cryo-electron microscopy (cryo-EM) structures of recombinant NP.

Results

We have structurally characterised native RNPs purified from infectious Bunyamwera virus (BUNV), one of the model viruses for the *Bunyavirales* order. While highly flexible, a combination of EM techniques allowed us to obtain a 13 Å structure of the BUNV RNP. Atomic force microscopy further allowed us to determine the handedness of the helix. Taking advantage of the existing X-ray crystallography structure of NP, we then performed molecular dynamics to generate a pseudo-atomic BUNV RNP model. Our model shows the native BUNV RNP to be a flexible helix with RNA sequestered on its inner face. The model revealed novel residues involved in helix-building NP-NP interactions that were not identified by previous crystallography studies, and functional analysis by mini-genome assay confirmed their importance for RNP function. Our model showed NP monomers within the RNP helix only interact laterally, as the successive turns of the helix are too far from each other to allow longitudinal interactions. Instead, RNAse analysis showed that the RNA plays a key role in maintaining overall helical RNP architecture. Taken together, our findings reveal the molecular basis for the inherent flexibility of bunyavirus RNPs, which is of critical importance for several aspects of the replication cycle, from genome packaging to segment circularization.

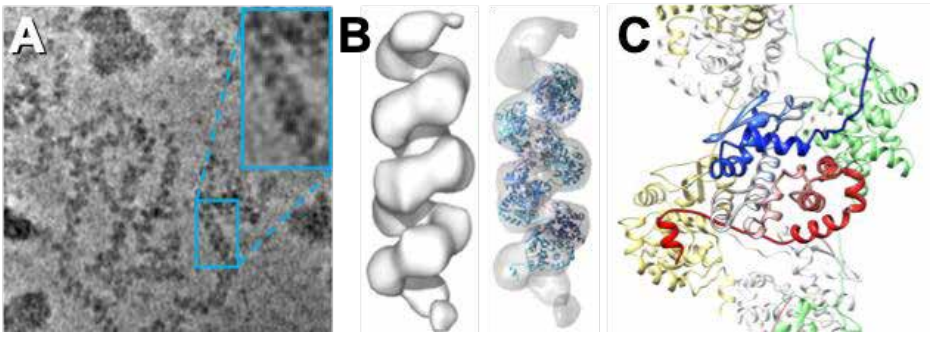

Figure. Structure of a native BUNV RNP. (A) Cryo-EM of purified BUNV RNP. Inset shows a section with a helical NP arrangement. (B) Cryo-EM average of a native RNP (left), with pseudoatomic model fitted into it (right). (C) RNP model. A monomer, coloured N-terminus (blue) to C-terminus (red), interacts with the adjacent monomers by the N- and C-terminal arms, but there are no longitudinal interaction.

Funding

All Electron Microscopy was performed at ABSL which was funded by the University of Leeds and the Wellcome Trust. This work was supported by the BBSRC White Rose Mechanistic Biology DTP, a EU Marie Sklodowska-Curie Actions (MSCA) Innovative Training Network (ITN), the University of Leeds University Academic Fellow scheme and the MRC.

Drug repurposing targeting the SARS-CoV2 envelope (E) protein ion channel

Gemma Swinscoe, Sonia Abas Prades, Richard Foster and Stephen Griffin

Introduction

Ion channels have become some of the most successful drug targets in medicine, although within this area of drug development, virus-encoded ion channels are poorly represented. Virus-encoded ion channels, identified in many different viruses, are referred to as viroporins. Viroporins function in multiple stages of viral lifecycles, from entry to egress to pathogenesis. We have previously demonstrated the effectiveness of both repurposing and developing drugs against viroporins, in hepatitis C virus (HCV) and Zika virus (ZIKV), using our highly validated *in vitro* dye-release system, showing that viroporins are creditable targets for the development of antiviral agents.

Zoonotic transmission of coronaviruses (CoV) has already given rise to several outbreaks in the 21st century, with severe acute respiratory syndrome associated coronavirus 2 (SARS-CoV2) resulting in >95 million confirmed cases of COVID worldwide. The rapid spread of SARS-CoV2 in early-2020 caught many countries unprepared, causing catastrophic strain on their economies and health care services, which continue to struggle as the pandemic lingers. The ongoing COVID19 pandemic highlights the necessity for high-throughput antiviral discovery, to rapidly combat emerging viral infections. The repurposing of licenced drugs has become an appealing proposition to tackle COVID19, as promising candidates could be deployed quickly. Many studies across the global scientific community have turned to screening licenced drugs and therapeutics against SARS-CoV2, although there have been cases where the urgency and insufficient consideration of coronavirus biology has resulted in the inappropriate repurposing of some drugs. This demonstrates an importance in understanding the biological mechanisms behind these repurposed drugs, as it prevents futile trails from taking place and enables effective monitoring of resistance should it arise.

The envelope (E) protein of coronaviruses is a small (8-10 kDa) hydrophobic structural protein, which is found incorporated into the viral membrane. SARS-CoV1 E protein was shown to possess channel-forming activity, as well as having multiple protein-protein interactions associated with further functions. High conservation between SARS-CoV1 and SARS-CoV2 suggested shared functionality, which has now been confirmed in several studies. Using our high-throughput dye release system for testing the function of viroporins, we have screened over ~1000 drug compounds from commercially available FDA-approved and drug-repurposing libraries against SARS-CoV2 E protein. We are now moving these compounds into virus culture to test their efficacy and to validate their mode of action.

Results and Discussion

SARS-CoV2 E proteins are comprised of multiple α-helical domains, one of which traverses the membrane. For the purpose of high-throughput screening, a synthetic peptide was

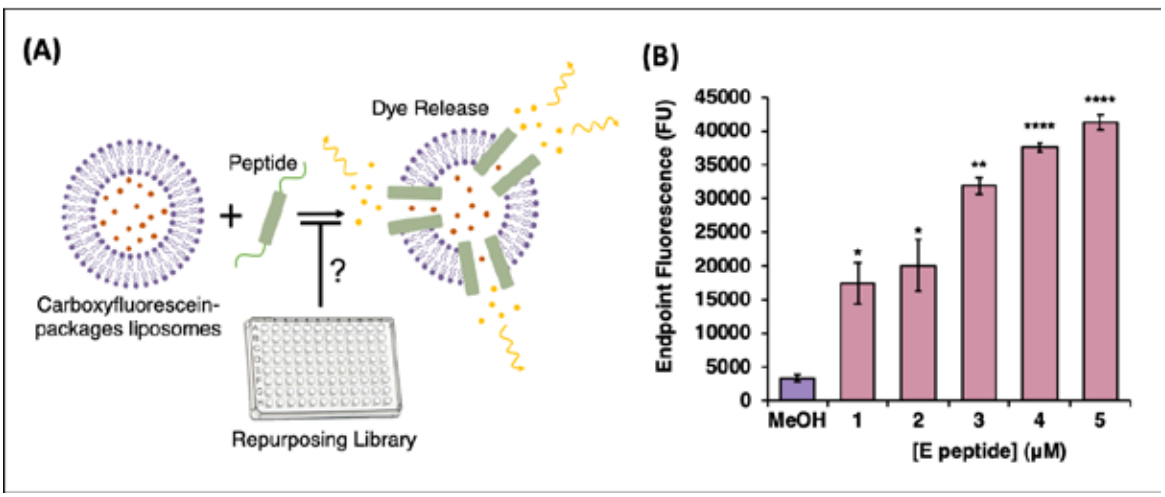

Figure 1: (A) Schematic of *in vitro* dye release system and high-throughput screening method. (B) Dose-dependent dye release, in terms of fluorescence emitted, for SARS-CoV2 E peptide.

designed that encompasses this transmembrane helix. This E peptide was shown to display a dose-dependent channel activity in our dye release system. Furthermore, we validated our screening system by confirming that SARS-CoV2 E peptide channel is sensitive to adamantane compounds. SARS-CoV1 E protein has previously been described to be sensitive to amantadine, through an N-terminal binding site, so this gives us the confidence that our system is suitable for identifying inhibitory compounds. We commenced screening with a small FDA-approved library of ~200 licenced drug compounds. This small library enabled us to optimise compound screening concentration and set a suitable inhibition threshold for identifying hits. From this screen, we identified eight compounds, which reduce E peptide channel activity to ≤ 65% at 400 nM.

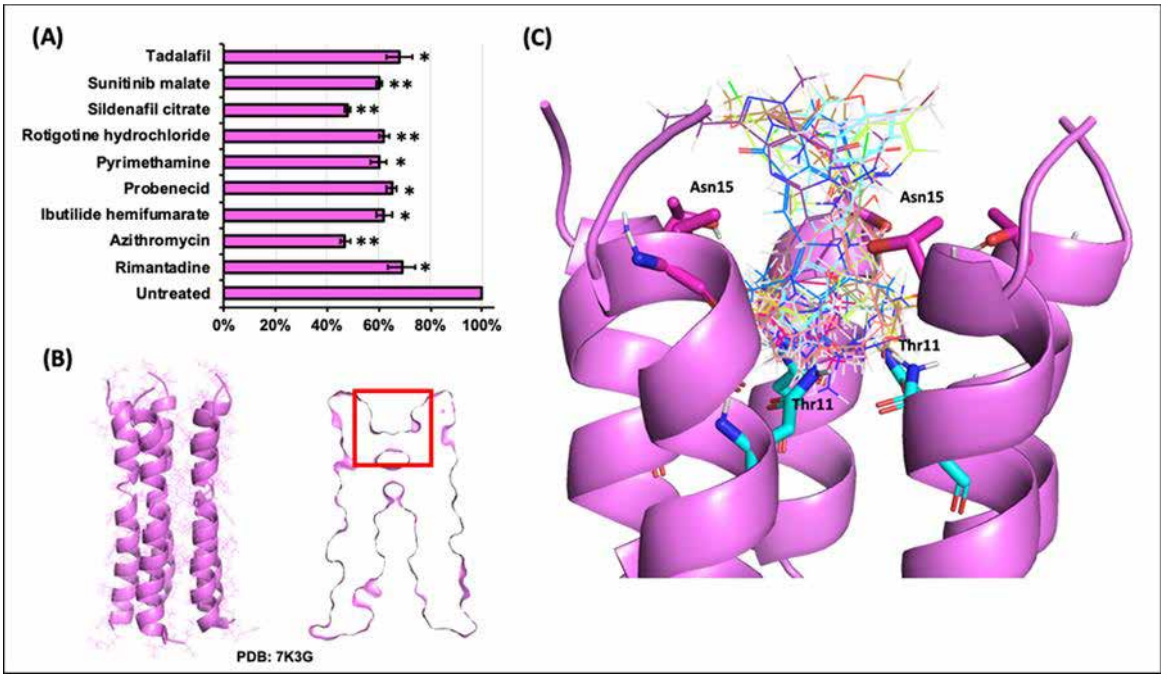

Figure 2: (A) Hit compounds from FDA-approved library of compounds. (B) Ribbon diagram of PDB:7K3G alongside pore cavity with N-terminal binding site highlighted. (C) Overlay of provisional hit compounds, docked against the N-terminal binding site.

Investigating these hit compounds further, provisional docking was performed with a SARS-CoV2 E-TM structure (PDB:7K3G) against the N-terminal binding site. All of our hit compounds, except for Azithromycin, displayed a convincing binding position. Thus, we intend to test each of these compounds in virus culture against SARS-CoV2 to validate their antiviral activity, whilst continuing to use our *in vitro* dye release system to screen further repurposing libraries.

Publications

Shaw J, Gosain R, Kalita M.M, Foster T.L, Kankanala J, Mahato D.R, Abas S, King B.J, Scott C, Brown E, Bentham M.J, et al. (2020) Rationally derived inhibitors of hepatitis C virus (HCV) p7 channel activity reveal prospect for bimodal antiviral therapy. *eLife* **9**:e52555.

Scott C, Kankanala J, Foster TL, Goldhill DH, Bao P, Simmons K, Pingen M, Bentham M, Atkins E, Loundras E, Elderfield R, Claridge J.K, Thompson J, Stilwell P.R, Tathineni R, McKinnie C.S, Targett-Adams P, Schnell J. R, Cook G.P, et al. (2020) Site-directed M2 proton channel inhibitors enable synergistic combination therapy for rimantadine-resistant pandemic influenza. *PLOS Pathogens* **16**:e1008716.

Funding

This work was funded by a UoL MRC CiC COVID-19 funding call.

Collaborators

External: Andrew Davidson and Dek Woolfson (University of Bristol).

Glycan-gold nanoparticles as multifunctional probes for multivalent lectin-carbohydrate binding: implications for blocking virus infection and nanoparticle assembly

Darshita Budhadev, Emma Poole, Inga Nehlmeier, Yuanyuan Liu, James Hooper, Elizabeth Kalverda, Uchangi Satyaprasad Akshath, Bruce Turnbull, Dejian Zhou and Yuan Guo

Introduction

Multivalent lectin-glycan interactions are widespread and mediate many important biological functions which include cell-cell communication, pathogen-host cell recognition, attachment and infection, and modulation of immune responses. As most monovalent lectin-glycan binding events are often too weak to be biofunctional, many lectins form multimeric structures to cluster their carbohydrate-binding-domains for efficient binding with spatially matched multivalent glycans to enhance binding affinity and specificity. The overall multivalent affinity is not only directly linked to the monovalent affinity, but also the glycan valency and the mode of binding. In general, a pair of spatially matched multivalent binding partners can bind simultaneously with each other and form a single entity. This gives the highest affinity enhancement and selectivity due to the most favorable enthalpy and entropy terms. While those without such spatial and orientation matches may intercross-link with each other to maximize binding enthalpy and form large scale assemblies, but this typically gives lower affinity enhancement and binding specificity due to an unfavorable entropy penalty. Therefore, understanding the structural mechanism underlying the affinity enhancement in multivalent protein-ligand binding is key to the design of potent, specific multivalent inhibitors against a target multivalent receptor. Here we have developed a novel gold nanoparticle (GNP) based technique and employed two closely related viral receptors, tetrameric DC-SIGN and DC-SIGNR to address this to guide receptor specific inhibitor design.

Results and Discussion

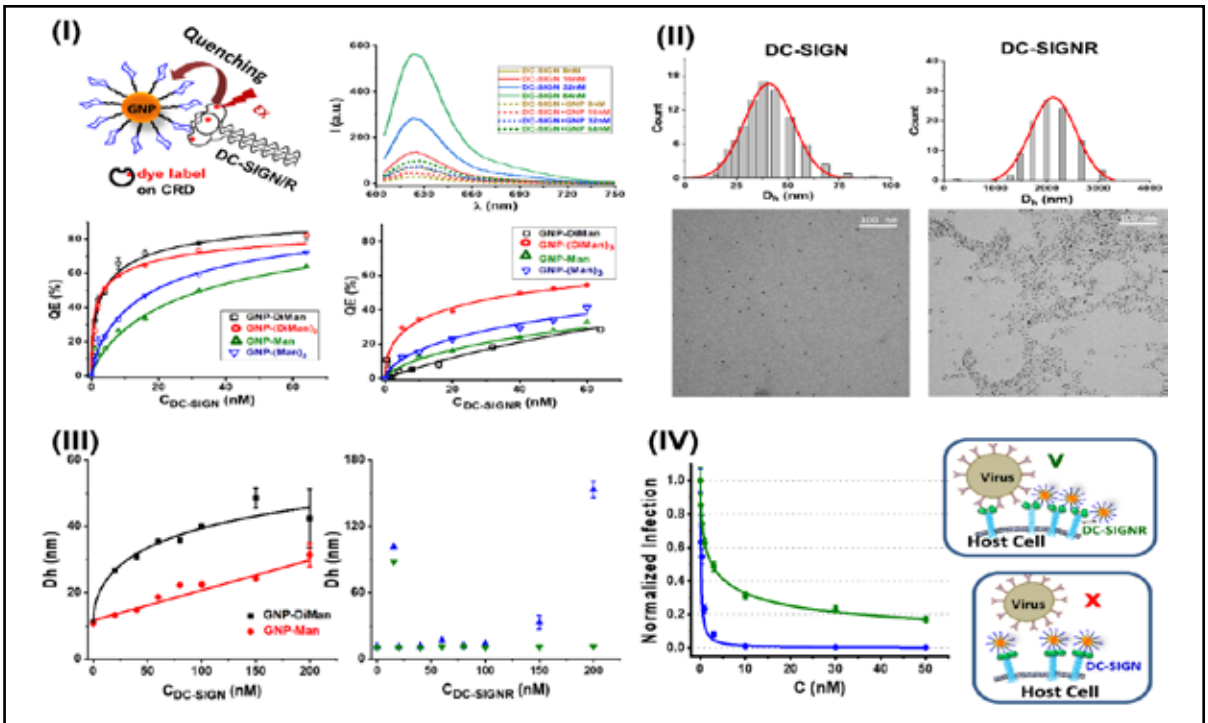

Figure 1: (I) Fluorescence quenching study shows that DC-SIGN binds to GNP-glycan with higher affinity than DC-SIGNR; (II) DC-SIGN simultaneously binds to GNP-Man (A2, B2) but DC-SIGNR cross-links GNP-Mans (A3, B3); (III) DC-SIGN-GNP assembly can be readily formed (A) but DC-SIGNR-GNP assembly can only be formed when protein concentration is above a threshold (B); (IV) GNP-glycan efficiently and effectively inhibits cell surface DC-SIGN mediated viral cell entry but only partially inhibits DC-SIGNR mediated viral cell entry.

GNP-glycan	Receptor	K_d (nM)	IC/EC_{50} (nM)
GNP-Man	DC-SIGN	33.1 ± 2.1	0.26±0.08
GNP-DiMan	DC-SIGN	3.9 ± 0.3	0.095±0.017
GNP-Man	DC-SIGNR	214 ± 68	7.3±1.2*
GNP-DiMan	DC-SIGNR	152 ± 37	0.63±0.09*

Table Summary of binding affinity of DC-SIGN/R binding to various GNP-glycans derived from Figure and inhibition data for GNP-glycans against DC-SIGN/R-mediated EBOV-GP driven infection of 293T host cells.
* shows the EC50 values for DC-SIGNR.

To reveal multivalency in binding affinity and specificity enhancement, we have constructed polyvalent glycan-nanoparticle probes on a relatively small 5 nm GNP to take the advantages of GNPs' robust gold-thiol surface. Lipoic acid (LA) based glycan ligands containing a terminal α-mannose (Man) or α-mannose-α-1,2-mannose (DiMan) was conjugated onto GNP and resulting GNP-glycans display excellent colloidal stability and show no signs of aggregation in biologically relevant media. As GNP's extinction coefficient scales linearly with its volume, the use of a small 5 nm GNP allows for access to a wide concentration range required for affinity quantitation of weak binders without introducing significant "inner-filter" effects. We have than exploited GNP's fluorescence quenching to quantify multivalent GNP-glycan binding to DC-SIGN and DC-SIGNR. We show that despite they share 80% amino acid sequence identity and overall tetramer structure, DC-SIGN binds to GNP-glycan with higher affinity than DC-SIGNR. By taking advantage of GNP's high-density property, we reveal that DC-SIGN 4 binding sites binds simultaneously to the glycans from same GNP but those in DC-SIGNR binds to glycans from different GNPs to cross-link them to form aggregate. Our dynamic light scattering results show that DC-SIGN can readily assemble onto GNP surface but there is a concentration threshold required to achieve effective DC-SIGNR-GNP assembly. The GNP-lectin binding modes are found to be directly linked to the GNP's ability to block lectin mediated virus infection of host cells: only a GNP-glycan which binds simultaneously to all binding sites of the target lectin can potently and completely block virus infection, but not that showing a cross-linking binding mode. In summary, we report that gold nanoparticles (GNPs) displaying a dense layer of simple glycans are powerful mechanistic probes for multivalent lectin-glycan interactions. They can not only quantify the GNP-glycan-lectin binding affinities via a new fluorescence quenching method, but also reveal drastically different affinity enhancing mechanisms between two closely related tetrameric lectins, DC-SIGN and DC-SIGNR, via a combined hydrodynamic size and electron microscopy analysis. Finally, the GNP-glycans can potently and completely inhibit DC-SIGN-mediated augmentation of Ebola virus glycoprotein-driven cell entry (with IC_{50} values down to 95 pM), but only partially block DC-SIGNR-mediated virus infection. Our results suggest that the ability of a glycoconjugate to simultaneously block all binding sites of a target lectin is key to robust inhibition of viral infection.

Publications

Budhadev D., Poole E., Nehlmeier I., Liu Y.Y., Hooper J., *et al.* (2020) Glycan-gold nanoparticles as multifunctional probes for multivalent lectin-carbohydrate binding: implications for blocking virus infection and nanoparticle assembly. *J Am Chem Soc* **142**:18022-18034.

Funding

This work was funded by the BBSRC, the EU Horizon 2020 *via* a Marie Sklodowska-Curie Fellowship and a School of Food Science and Nutrition Scholarship.

Collaborators

University of Leeds: Nicole Hondow (School of Chemical and Process Engineering)
External: Stefan Pöhlmann, (Infection Biology Unit, German Primate Center—Leibniz Institute for Primate Research and Faculty of Biology and Psychology, University of Göttingen, Göttingen 37073, Germany).

Modelling the active SARS-Cov-2 helicase complex as a basis for structure-based inhibitor design

Sarah Harris

Introduction

Novel drugs are urgently needed to target essential SARS-CoV-2 proteins, such as the RNA helicase (nsp13), for situations where vaccination is unavailable or contraindicated. Here, we have studied nsp13 using molecular dynamics to explore its druggability and to identify potential allosteric binding pockets.

The viral helicase is the molecular machine responsible for separating the viral RNA from proteins and other RNA strands. Here we focus on determining the catalytically active complex structures of the SARS-CoV-2 RNA viral helicase (nsp13). nsp13 performs two essential functions for viral replication making it an ideal drug target. It is thought to perform the first step in the 5'-capping of the viral RNA. Furthermore, its main helicase function is to enable RNA translocation and unwinding in an ATP-dependent mechanism during viral replication. This work therefore provides insight into one of the crucial elements of the viral replication machinery.

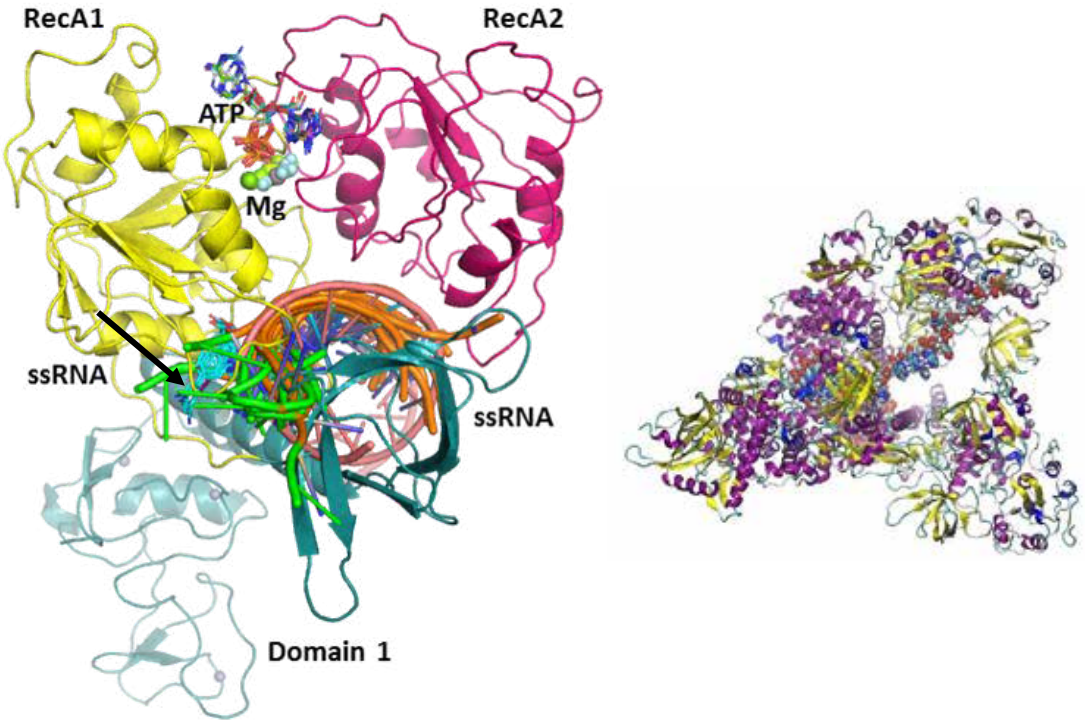

Figure 1: Left: Cartoon representation of the RNA helicase nsp13 of SARS-CoV-2 model. Domains are coloured differently for clarity. ATP analogues along with Mg and single stranded nucleic acids are depicted from aligned homologous structures. The 3' end of the nucleic acids are highlighted in green to show the same orientation in all chains. The binding locations of several known helicase inhibitors are displayed in cyan (arrowed). **Right:** Top (top) and side (bottom) view of the replication and transcription complex, modelled on PDB ID 7CXN. The secondary structure of the protein in the assembly is shown, while the RNA is depicted as van der Waals spheres.

Results and Discussion

We have used homology modelling in conjunction with molecular dynamics simulations to model the catalytically competent structure of nsp13. Our structure is the first to host ATP and a single strand of RNA and provides atomically detailed interactions for the binding modes of the substrates. The analysis of homologous sequences sheds light upon the specificity of the domain structure of the viral helicase yielding no match over 40% (except close relatives from the *coronaviridae* family). The ATP pocket was reconstructed based on the structural

conservation of the most similar crystal structures. Furthermore, we identified the main anchoring points for the ssRNA through the helicase, which are essential to understand the translocation driving the unwinding activity of nsp13.

With molecular dynamics, we have verified the stability of conserved interactions in our model. These structures show good agreement with recent cryo-EM structures published by others. We have assessed the flexibility of the ATP pocket with and without the nucleotide bound detecting a well-maintained cavity. Our structure can be the basis of structure-based compound design and screening, and we have already identified and characterised several promising target sites, including a potential novel allosteric site located close to the N-terminal domain.

We have also combined these models of nsp13 with cryo-EM structures to construct an atomistic structural model of the replication and transcription complex of SARS-Cov-2. These models will enable us to see if including larger subunit assemblies in our docking protocols modifies the hits we obtain. For example, putative target sites might be buried by protein-protein interactions within the larger complex.

Collaborators
External: Edina Rosta, Denes Berta, Thomas Meltzer, Geoff Wells and Magd Badaoui (UCL, UK), Elisa Frezza (Université de Paris, CiTCoM, France, Paris), Nadia Elghobashi-Meinhardt (Technische Universität Berlin, Germany), Andrei Pisliakov (Physics and Computational Biology, Dundee, UK), Mark Sanderson and Andrew Cobb (KCL, UK.), Arvind Ramanathan (Argonne national laboratory/ consortium for advanced science and engineering (CASE), University of Chicago, USA).

Millisecond dynamics of an unlabelled amino acid transporter

George Heath

Introduction

Excitatory amino acid transporters (EAATs) are a family of integral membrane proteins that are essential in the mammalian central nervous system. This family of proteins assures efficient neurotransmission and prevents glutamate-mediated neurotoxic effects by regulating extracellular transmitter levels of neurons and glial cells surrounding synapses. Glt_{Ph} is an archaeal homolog of EAATs from *Pyrococcus horikoshii*. Glt_{Ph} shares ~37% amino acid sequence identity with human EAAT2, and has a high structural similarity with human EAAT1 and with a neutral amino acid transporter ASCT211. Glt_{Ph} is an excellent model system to study EAATs which displays an "elevator" mechanism, whereby the transport domains move ~1.8 nm across the membrane in order to symport three Na^+-ions (down their electrochemical concentration gradient from the extracellular to the intracellular space), and L-aspartate (Asp, against the concentration gradient) across the membrane. The lack of spatiotemporal resolution in previous studies of EAATs has meant that short-lived events and transport sub-states may have escaped observation.

Results and Discussion

Here, we develop and apply High-Speed Atomic Force Microscopy Line Scanning (HS-AFM-LS) on unlabeled molecules and report Glt_{Ph} transport domain movements with unprecedented spatial and temporal resolution. Our results represent the most detailed recordings of individual transport domains under close-to-physiological (at ambient temperature and pressure and in membrane) conditions providing insights into rapid state transitions and transport sub-states. To achieve this, purified Glt_{Ph} was first reconstituted into vesicles of up to 300 nm in size. The proteo-liposomes were then deposited on freshly cleaved mica and imaged in buffer solution. High-resolution HS-AFM imaging of these membranes resolved the Glt_{Ph} trimers and the individual protomers within them. Comparison with Glt_{Ph} X-ray structures showed that the vast majority of transporters exposed the extracellular face, where the protomers stand out of membrane by ~2 nm. In agreement with previous studies, only a minority of the transporters displayed dynamics, whilst the others appeared silent and exposed the transport domains to the extracellular side. The range of the "elevator" movement in this experiment was 1.2 ± 0.3 nm, in good agreement with earlier X-ray and smFRET data.

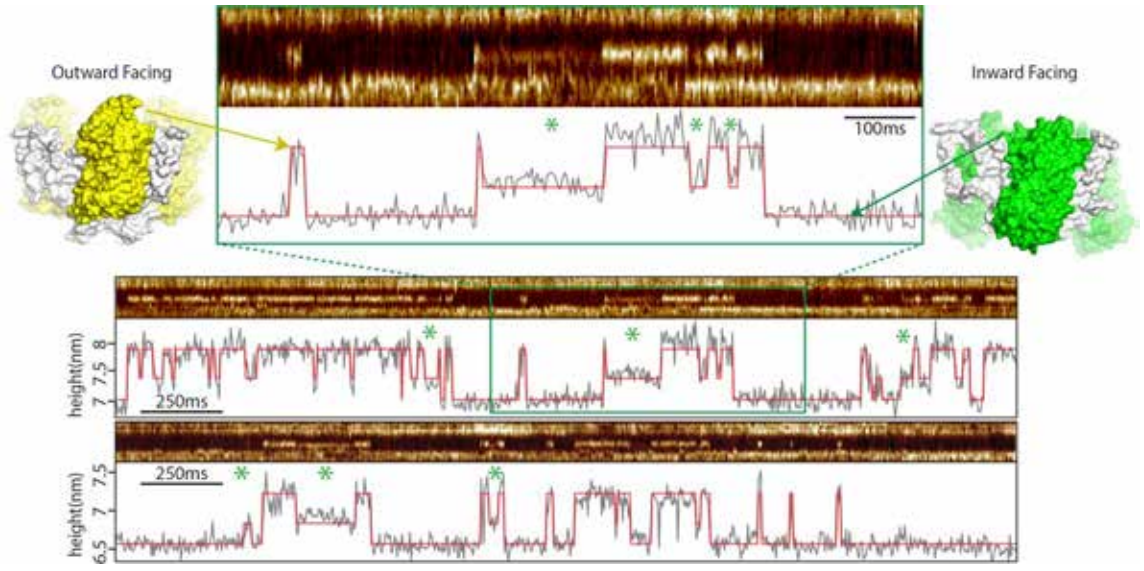

Figure 1: Elevator dynamics of single unlabeled Glt_{Ph} transporter domains: Glt_{Ph} X-ray structures in the outward- (left, PDB 2NWX), and the inward- (right, PDB 3KBC) facing conformational states. The trimerization domain is shown in grey and the transport domains are shown in colour. HS-AFM-LS raw data kymographs and height/time traces recorded in apo conditions. All kymographs were recorded at 3.3 ms line acquisition speed. The height/time traces (grey) report the movements of the protomer in the centre of the kymograph and are overlaid by the state-transition trace (red) of a transport domain visiting three states. Asterisks indicate intermediate state intervals. The full false colour scale of the pixels shown is 1.4 nm.

In HS-AFM-LS, the slow-scan axis (y-direction) is disabled. Therefore, instead of imaging an x/y-area, we scan over one horizontal x-line several hundreds to thousands of times per second, thus reaching millisecond temporal resolution. The topographical readouts of this line are stacked one after another, resulting in kymographs of the dynamical behaviour of the molecules. Through the development of tracking and state assignment approaches, HS-AFM-LS kymographs were transformed into idealized height/time traces that allowed the extraction of dwell-times for transport domain states. In the absence of substrate (apo condition), Glt_{Ph} was visibly more dynamic and underwent shorter-lived excursions, compared to the protein in transport conditions (i.e., in the presence of saturating Na^+ and Asp concentrations). In control experiments with TBOA or saturating Na^+, protomers were found stalled in the outward-facing state. Among the 283 height/time traces of active protomers (apo and transport conditions pooled), the state-assignment algorithm suggested that 40 protomers visited a third state with transporter domain height between the inward- and outward-facing states. Analysis of dwell times showed in apo conditions protomers spent on average a similar amount of time in the outward- (347 ms) and inward- (328 ms) facing states, while the intermediate state was shorter-lived (175 ms). Whereas, in the presence of substrates, the protomers were overall less active and spent longer times in the outward- (510 ms), inward- (341 ms), and intermediate (297 ms) states.

Overall, we find that Glt_{Ph} transporters can operate much faster than previously reported, with state dwell-times down to the 50 ms range and report new kinetics of an intermediate transport state between the outward- and inward-facing states. The HS-AFM-LS approach and analysis methodology are generally applicable to study transporter kinetics at system-relevant temporal resolution.

Publications

Matin T.R., Heath G.R., Huysmans G.H.M., Boudker O. and Scheuring S. (2020) Millisecond dynamics of an unlabeled amino acid transporter. *Nat Commun* **11**, 5016.

Collaborators

External: Simon Scheuring and Olga Boudker (Weill Cornell Medicine, USA).

Targeting enzymes for improved plastic break down

Badri S. Rajagopal, Anna Ah-San Tan, Darren Tomlinson and Glyn R. Hemsworth

Introduction

Plastics are a ubiquitously useful commodity which has seen their use proliferate into all aspects of our lives. These materials however are largely derived from fossil fuel sources and are extremely stable meaning that plastic waste can persist in the environment for years raising considerable concern. There is therefore a lot of interest in finding a more sustainable means for recycling and bioremediating the effects of these materials through biotechnological processes. Recent years have seen the identification of new enzymes that are able to hydrolyse polyethylene terephthalate (PET), a plastic best known for its use in drinks bottles. PETase, the enzyme identified from *Ideonella sakaiensis* that allows it to hydrolyse this plastic and utilise it as a carbon source, has received considerable interest in this regard. That these enzymes act on a solid substrate is relatively unusual. Other well-known enzymes that perform a similar function are those that degrade cellulose, a naturally occurring polymer of glucose. Cellulases often have carbohydrate binding modules within their structures that enhance their interaction with the solid, thereby improving their ability to degrade their substrate. We are interested in developing Affimers to play a similar role in plastic degradation. Affimers are small protein reagents that have been developed in Leeds as antibody alternatives that can bind to any molecule, in principle. We have therefore been seeking to identify Affimers that bind to PET and append them to PETase in a bid to understand the relationship between affinity for the solid substrate and activity in the case of PETase, with the ultimate aim of enhancing PET degradation.

Results and Discussion

We have used a modified phage display method to screen two Affimer libraries (differing in the number of variable binding loops present) for binders of >48% crystallinity PET powder. To ensure that our Affimers were binding to PET we performed negative selection against the polypropylene tubes being used during screening to minimise false positive hits. Approximately 300 hit PET-binding Affimer colonies were obtained during our panning experiments. 96 of these (48 from each library) were sent for sequencing, which returned 66 successfully sequenced clones. The sequences of the constructs were analysed and 20 hit Affimers were taken forward for further study to cover a range of amino acid compositions present in the variable loops. To confirm that these Affimers bind to PET we have used pull-down assays to confirm binding to the substrate (Figure 1A).

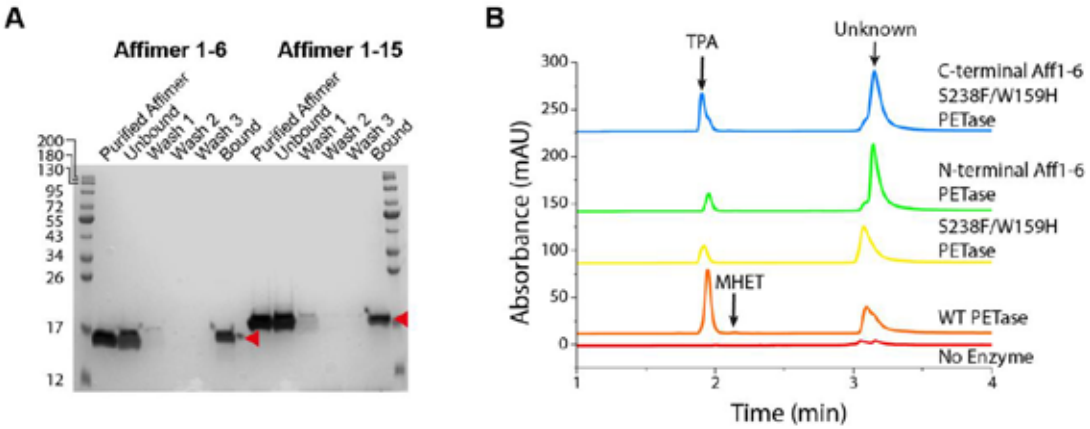

Figure 1: (A) SDS-PAGE gel demonstrating PET binding by two purified Affimers (indicated by red triangles). Bands in the bound lane represent Affimers that have remained bound to the plastic following incubation and washing. **(B)** HPLC data demonstrating the release of Terephthalic acid (TPA) from crystalline PET powder as the principal enzymatic product (traces are offset along the y-axis for clarity).

Ultimately, we hope to use these Affimers to enhance the interaction between PETase and its substrate. We have therefore generated Affimer-PETase fusions using molecular biology such that the Affimer is appended to PETase by a flexible linker at either the N- or C-terminus when expressed in *Escherichia coli*. We have successfully expressed the first two of these constructs and used High Performance Liquid Chromatography to analyse the release of terephthalic acid and the other PETase enzymatic products from the substrate in response to exposure to our initial fusion enzymes (Figure 1B). These results confirm that our assays work and we now plan to expand our study to a broader panel of Affimer-PETase fusions.

To gain further fundamental knowledge on the importance of the interaction between the enzyme and substrate during plastic breakdown, we plan to establish a more robust binding assay that will allow us to more quantitatively measure PET binding. By relating our binding data to activity data across a broad panel of Affimer constructs we aim to establish whether binding interactions mediated in a fashion similar to that of a carbohydrate binding module can be beneficial for plastic degradation.

Funding
G.R.H gratefully acknowledges funding from a BBSRC David Phillips Fellowship and from the University of Leeds.

Investigating the Structure and Function of Murine Norovirus (MNV) VP1 Capsid Protein

Jake Mills, Joseph Snowden, Oluwapelumi Adeyemi,
Nicola Stonehouse and Morgan Herod

Introduction

Human norovirus (HNV) infections are a leading cause of gastroenteritis in people of all ages worldwide. They cause mortality of over 200,000 lives per annum and have an estimated global economic cost of over $40 billion. There is no vaccine or therapy to prevent or treat norovirus and control spread of the disease. Virus-like-particle (VLP) vaccine trials have been disappointing, suggesting that the optimal antigenic structure has yet to be identified. Therefore, in order to develop effective vaccines and/or therapies, further research into the structure and function of the virus is needed. Murine norovirus (MNV) is a commonly used, safe, and appropriate model to study HNV. The MNV capsid is composed of 180 copies of the major viral structural protein, VP1, and a small amount of minor structural protein, VP2. Each copy of VP1 is subdivided into two domains: a shell (S) domain which forms the base of the viral capsid and a protruding (P) domain which projects radially. Our goal, through multiple research strands, is to utilise MNV to improve our understanding of norovirus structure and inform new approaches to disease control. Through genetic manipulation of the virus, we have been able to investigate alternative morphologies of the MNV capsid, study the molecular structure of VP1 and begin to understand virus-receptor interactions.

Results and Discussion

Work published this year demonstrated that precise heat-inactivation of MNV can induce conformational changes to the P domain, rendering the virus non-infectious. In order to further investigate the different conformations VP1 can take, and how these may be dependent on interactions with viral RNA and non-structural (NS) proteins, we have begun to investigate what genetic changes occur in thermally stabilised virions.

First, we generated virus populations stable at 52°C (MNV52) and 54°C (MNV54) (Fig.1A). Both of these populations had the same single thermally stabilising mutation at the consensus level (Snowden et al. 2020). However, next-generation sequencing (NGS) revealed a number of additional VP1 and NS protein point mutations present in these virus populations.

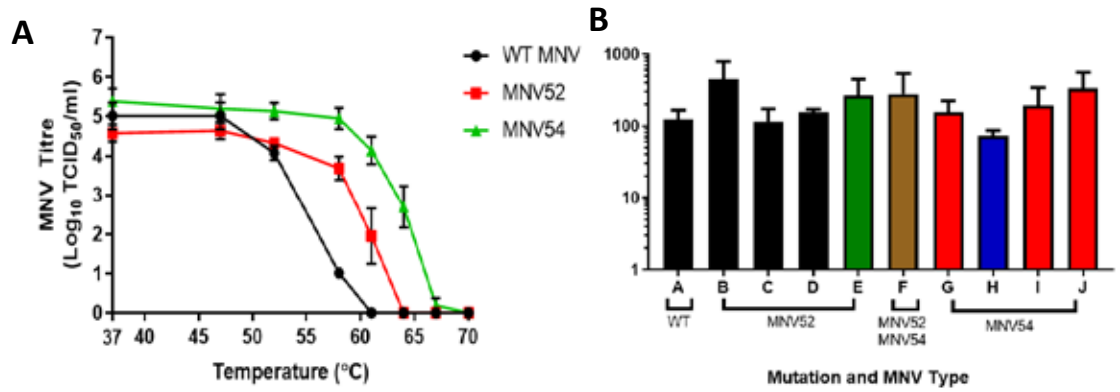

Figure 1: (A) Samples of MNV were heated at 52˚C or 54˚C for 30 min before cooling to 4˚C. The surviving pool of viruses was subsequently passaged for 48 hours at 37˚C on RAW264.7 cells. The pool of virus heated at 52˚C (MNV52), 54˚C (MNV54) and wild type (WT) MNV were heated to a range of temperatures between 37˚C and 70˚C and virus titre determined by $TCID_{50}$ assay on RAW264.7 cells (n = 4 ± SEM). (B) Infectious clones of MNV were generated with the point mutations indicated. Viral titres were measured by $TCID_{50}$ assays performed on BV2 cells and normalised to WT (n = 2 ± SEM). The colour of the bars indicates the position of the mutation in the MNV genome: Black=NS3, Blue=NS4, Green=NS5, Brown=NS7, and Red=VP1.

Infectious clones were generated containing these mutations individually and viral titre was measured following transfection of in vitro transcribed RNA into replication-permissive, receptor-negative, cells (Fig.1B). These initial results helped us to identify single point mutations that may improve viral replication, such as VP1 mutations I and J and NS mutations B, E and F. Importantly, in the thermally selected populations these point mutations occurred together in particular combinations. These preliminary results were combined with the frequency analysis from the NGS, informing the design of population-relevant infectious clones with multiple mutations. Work is ongoing to determine how these mutations contribute to capsid stability, infectivity and replication.

Specific MNV serotypes have an increased prevalence of establishing a persistent infection. For example, MNV-1 induces a non-persistent infection, whereas MNV-3 in particular can establish persistence in the murine host. The primary receptor for MNV is CD300lf, which interacts with the VP1 capsid. Mutations that can change viral receptor interactions have been identified as one of the factors that influences viral persistence. Bioinformatic analysis of the VP1 receptor interface suggested that there is a high degree of genetic variation in a single amino acid position (Fig 2A). We hypothesised that these MNV VP1 variations could influence the ability of viral particles to interact with viral receptor CD300lf and influence how the virus establishes persistence. Natural variation in this amino acid suggested the prevalence of hydrophobic amino acids in persistent strains and the polar amino acids in acute strains.

To begin investigating these variations, we used reverse genetics to generate infectious clones encoding various amino acids at the identified residue, and viral titre was measured by $TCID_{50}$ assays. Interestingly, we identified that some variants improved viral growth specifically in cells grown in suspension. Furthermore, repeat passaging MNV in suspension-grown cells resulted in selection of specific amino acids at this position. This was alongside a >10-fold increase in viral titre (Fig.2B). These data suggest a strong selection pressure at this position for infection in suspension. Preliminary results indicate that infectious clones with mutations at this VP1 position lead to a greater infectivity of BV2 cells when infected in suspension compared to the wildtype (Fig.2C), but is less beneficial when infecting adherent cells. Work is continuing in order to characterise the effect this mutation has on MNV VP1 structure and function.

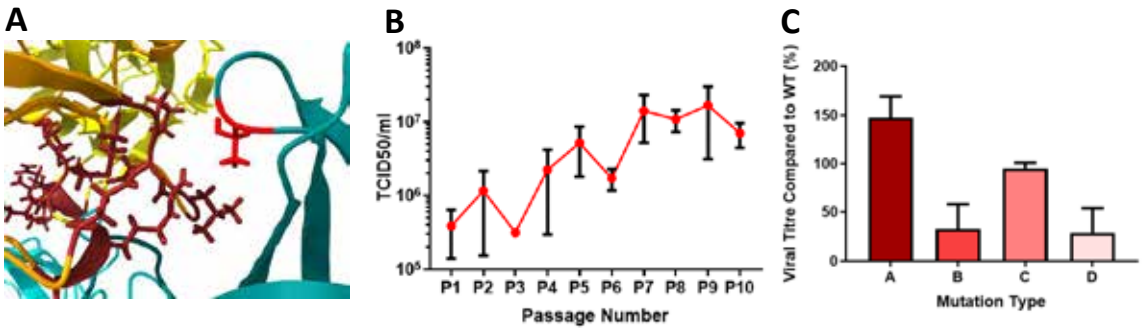

Figure 2: (A) The position of the identified residue in relation to the CD300lf binding site was computationally modelled. Red: Amino Acid, Turquoise: VP1, Yellow: CD300lf, Brown: CD300lf binding pocket. **(B)** WT MNV was passaged in BV2 cells grown in suspension, and viral titre was measured ($TCID_{50}$/mL) through $TCID_{50}$ assays on BV2 adherent cells (n=2). **(C)** An infectious clone with the indicated mutations were created by mutagenesis and T7 RNA was synthesised and transfected in BHK-21 cells. After 48-hours, viral titre was measured ($TCID_{50}$/mL) through $TCID_{50}$ assays on BV2 adherent cells infected in suspension (n=2), and compared to WT.

Publications

Snowden J.S., Hurdiss D.L., Adeyemi O.O., Ranson N.A., Herod M.R.*, et al.* (2020) Dynamics in the murine norovirus capsid revealed by high-resolution cryo-EM. *PLoS Biol* **18:** e3000649.

Adeyemi O.O., Ward J.C., Snowden J.S., Herod M.R., Rowlands D.J.*, et al.* (2020) Functional advantages of triplication of the 3B coding region of the FMDV genome. *FASEB J*. **35**: ee21215.

Funding

This work was funded by the MRC, the Wellcome Trust and BBSRC.

Macromolecular crowding enhances the detection of DNA and proteins by a nanopore

Chalmers Chau, Sheena Radford, Paolo Actis and Eric Hewitt

Introduction

Nanopores are an emerging technology that enable the single-molecule analysis of biological macromolecules. The detection and analysis of single molecules in real time is based on the established Coulter principle used in the Coulter counter. When a molecule passes through a nanopore under the influence of an electric field in a conductive electrolyte, the molecule temporarily blocks the current flow through the nanopore and creates a current blockage event signal (Fig. 1). This signal contains information about the size and the translocation dynamics of the molecule. Furthermore, as each event signal corresponds to the translocation of an individual molecule, the number of molecules can then be quantified. While the detection of DNA is well established, the detection of proteins is very challenging due to their high translocation speed.

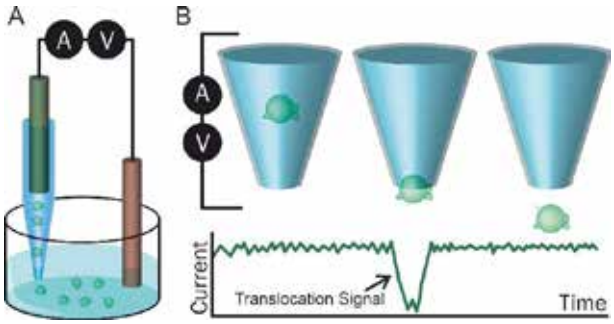

Figure 1. Sensing of molecules by nanopores. (A). Illustration of the single-molecule detection set-up. (B). The molecule temporarily blocks the ion current flow, this generated the translocation signal.

Results and Discussion

We used nanopipettes, a type of solid-state nanopore, that has a nanopore opening of 10 nm at the end of the tip to perform translocation experiments with DNAs and proteins using phosphate buffered saline (PBS) as an electrolyte. We discovered that adding the macromolecular crowder polyethylene glycol (PEG) 8000 to the PBS at high concentration (50% w/v) resulted in a pronounced increase in the sensitivity of the nanopipette for proteins and DNA. We first used the a 3.5 kbp DNA plasmid as the analyte to perform the translocation experiment in PBS. Numerous events were readily detected when a voltage of -700 mV was applied, consistent with the detection of DNA translocation. When PEG 8000 was added at 50% (w/v) to the PBS to generate a macromolecular crowded bath, we observed that the current of each peak was enhanced from under 100 pA to above 500 pA (Fig. 2A). We next investigated whether the detection of proteins can be enhanced, by studying the protein β-galactosidase. Indeed, the detection of β-galactosidase with the nanopipette was enhanced, and the number of detectable translocation signals were increased by almost 1000-fold per minute (Fig. 2B).

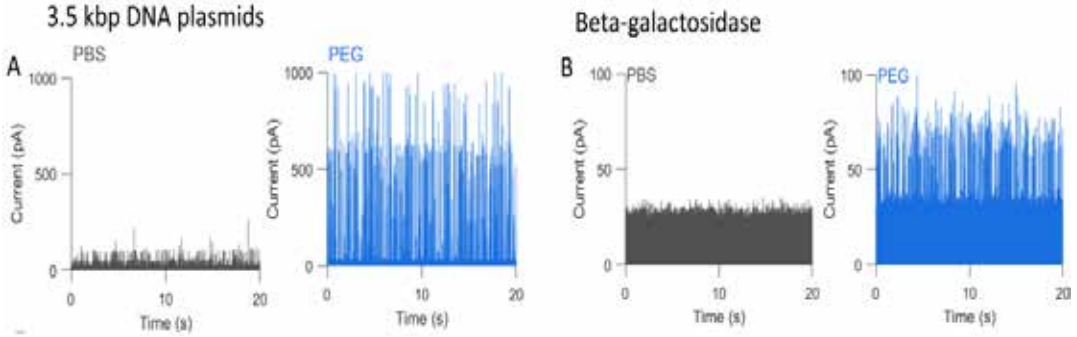

Figure 2; Single-molecule detection of DNA plasmids and β-galactosidase. (A) 3.5 kbp DNA plasmids translocation in PBS (grey; N=122) and PEG 8000 – PBS bath (blue; N=370). (B) β-galactosidase translocation in PBS (grey; N=0) and PEG 8000 – PBS bath (blue; N=316). N is the translocation signal number in 20 seconds.

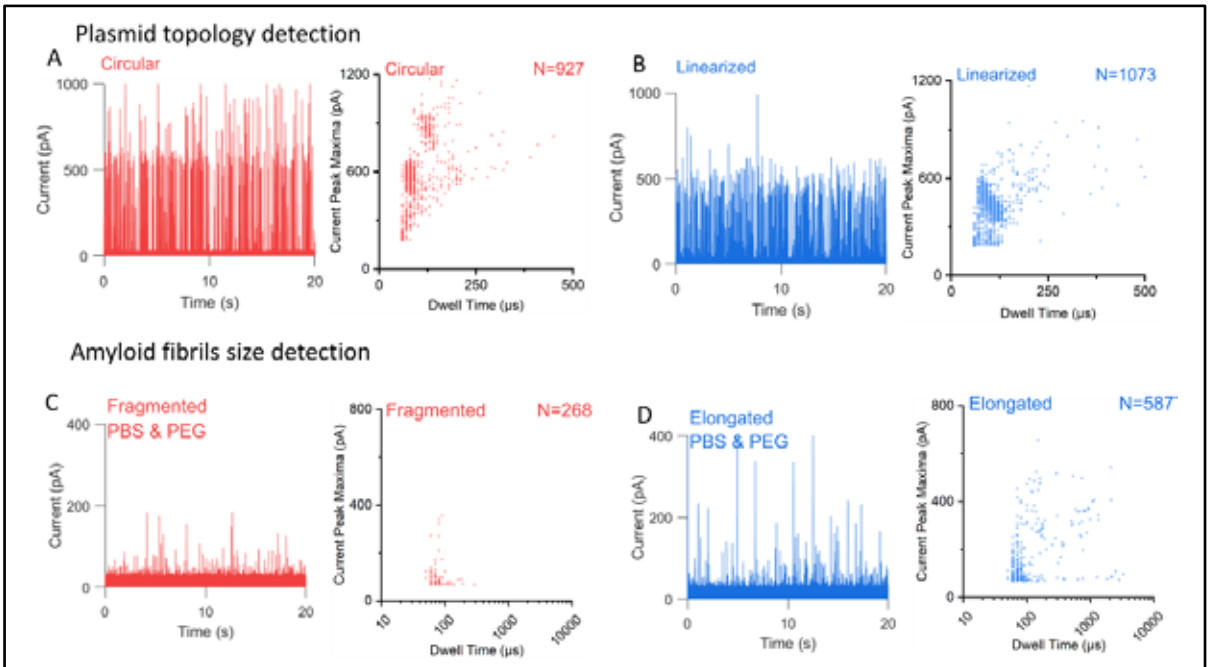

Figure 3: Detection of differences in DNA plasmids topologies and detection of α-synuclein amyloid fibrils of different sizes in PEG 8000 crowded PBS bath. (A) The circular 3.5 kbp DNA plasmids translocation (red) and (B) the linearized 3.5 kbp DNA plasmids in PEG 8000 – PBS bath. The population scatter of the DNA plasmids is altered after linearization. (C) The fragmented and (D) the elongated α-synuclein amyloid fibrils translocation in PEG 8000 – PBS bath. The elongated fibrils have a wider spread as shown in the population scatter.

By using macromolecular crowding to enhance the current amplitude we were also able to distinguish between different populations of DNA. For plasmid circular DNA, we observed that there were at least two populations, one at ~500 pA and a second at ~1000 pA (Fig 3A). Consistent with this, DNA plasmids adopt at least two topologies, namely supercoiled and relaxed. Moreover, when the DNA plasmid was linearised by restriction digestion, the population distribution was altered (Fig 3B). In addition, we analysed α-synuclein amyloid fibrils with different length distributions, fragmented amyloid fibrils (average length ~66 nm) and elongated fibrils (average length ~442 nm). Both the fragmented and the elongated fibrils were analysed using the macromolecular crowded bath; the elongated fibrils showed a broad distribution when compared to the fragmented fibrils (Fig 3C and D), which is consistent with the different length distrubtions of the fibrils.

Publications

Chau C., Actis P. and Hewitt E. (2020) Methods for protein delivery into cells: from current approaches to future perspectives. *Biochem. Soc. Trans.* **48**: 357-365.

Chau C.C., Radford S.E., Hewitt E.W. and Actis P. (2020) Macromolecular crowding enhances the detection of DNA and proteins by a solid-state nanopore. *Nano Letters* **20**: 5553-5561.

Funding

The authors acknowledge funding from the Wellcome Trust, the ERC and the University of Leeds.

Understanding the mechanism of antimicrobials that target electron-transport chain enzymes

Debajyoti Dutta, Stephen P. Muench and Lars Jeuken

Introduction

Microbial enzymes active in the electron-transport chain and oxidative phosphorylation have recently gained interest as antimicrobial targets. A key example is an inhibitor of the F_1F_o ATPase from *Mycobacterium tuberculosis*, bedaquiline, which was approved for clinical use in 2012. Since then, respiratory enzymes such as the type-2 NADH dehydrogenase and cytochrome *bd* have been considered promising targets for specific pathogens such as *Lysteria monocytogenes* and *M. tubercolosis.* Depending on the pathogen, these enzymes are obligatory for infection and they do not have homologues in mitochondria, reducing the likelihood that inhibitors interfere with human bioenergetics. Type-2 NADH:quinone oxidoreductase (NDH-2) is a membrane protein that shares its function with the mitochondrial NDH, complex I. NDH-2 is a 40–70 kDa, peripheral membrane single-domain protein, which unlike complex I does not pump protons across the membrane. This might be advantageous for microbes in the maintenance of a suitable NAD^+/NADH redox balance, independent from a back-pressure from the proton-motive force.

NDH-2 has been targeted in the development of antimicrobials and many compounds have been identified to have moderate activities, e.g., iodonium derivatives, flavones, quinolones, phenothiazines, and nanaomycin A and polymyxin. However, to date, there has been little success in the development of a drug, partly due to a lack of understanding about the mechanism of inhibition. For instance, the molecular inhibition mechanism of a commonly identified compound, phenothiazines, remains unclear despite their inhibitory activity against many NDH-2s. Quinolones are better understood and are quinone homologues and competitive inhibitors of NDH-2. As quinone homologues, they also inhibit electron-transfer chain enzymes in mitochondria and thus are less suitable as antimicrobials.

We have previously developed an electrochemical platform to study quinone-converting respiratory enzymes in native-like lipid membrane environments (Figure 1). Here, we have used this platform to study the activity of a NDH-2 from the food pathogen *L. monocytogenes* and a thermophilic homologue, *Caldalkalibacillus thermarum*. Using this system, the molecular mechanism of quinolones and pheothiazines could further studied.

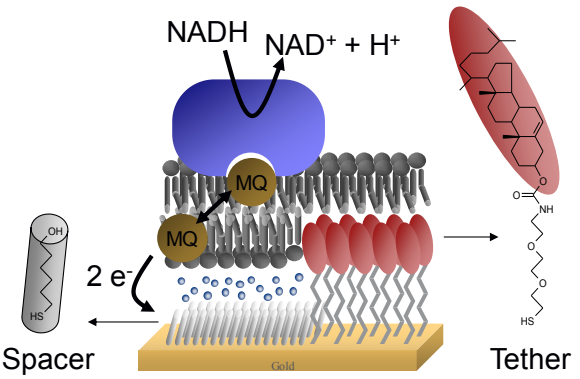

Figure 1: Schematic representation of the electrochemical system used to study the activity of NDH-2 (blue). Not to scale. MQ=menaquinone-7.

Results and Discussion

An electrochemical system was constructed as schematically shown in Figure 1 using NDH-2 from *C. thermarum*. The natural substrate of NDH-2, menaquinone-7 (MQ) was included the in the lipid membrane. The MQ in the membrane can be oxidised and reduced by the gold electrode, which results in reduction and oxidation peaks in the cyclic voltammograms (CVs) at around -0.25 and 0.1 V, respectively (blue traces in Figure 2). In the presence of NADH, an electrochemical wave is observed (red lines in Figure 2), which confirms that NDH-2 oxidises NADH and transfers the electrons to MQ in the membrane. The MQ is subsequently re-oxidised by the electrode and the current at >0.2 V directly reports on NDH-2 turnover (Figure 2). Similar results were obtained with NDH-2 from *L. monocytogenes*. As the latter system was less stable, further experiments were performed with *C. thermarum* NDH-2.

Upon addition of a well-known quinolone which acts as an inhibitor (the MQ analogue N-oxo-2-heptyl-4-Hydroxyquinoline, HQNO), the current and hence the turn-over rate reduces. At high concentrations of HQNO, the CV is identical to the CV in the absence of NADH (compare green with blue trace in Figure 2 top), confirming that NDH-2 is completely inhibited at 100 μM HQNO.

Unexpectedly, when a pheothiazines-type inhibitor, chlorpromazine (CPZ) is added, almost no change in current is observed, indicating that CPZ does not inhibit NADH-MQ oxidoreductase activity by NDH-2. Only at very high concentrations of CPZ (100 μM), a small reduction (~20%) in activity is observed (Figure 2, green curve). Importantly, addition of CPZ causes a shift in the electrochemical wave, which indicates that that kinetics of MQ oxidation by the electrode are affected by CPZ. Additional experiments with liposomes (not shown) revealed that this is due to protonophore activity of CPZ. This raised the question of whether the antimicrobial activity of CPZ is due to a disruption of the proton-motive force rather than inhibition of NADH oxidation activity by NDH-2.

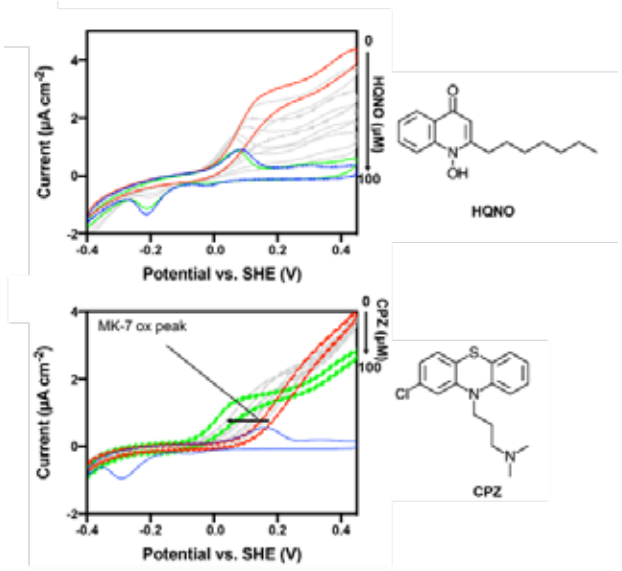

Figure 2: Electrochemical assays showing that HQNO inhibits *C. thermarum* NDH-2 but phenothiazines do not. (Top) Cyclic voltammograms (CVs) recorded in the presence of 0 (red)–100 (green) μM HQNO. Other HQNO concentrations are shown in grey. A baseline CV (blue) in the absence of both NADH and HQNO is also shown. (Bottom) CVs recorded for CPZ experiments. CVs were recorded in the presence of 0 (red)–100 (green) μM CPZ. The MK-7 oxidation peak shift is shown with an arrow. All experiments were performed in the presence of 200 μM NADH.

In summary, we built a novel bioelectrochemical platform to characterise the activity of the respiratory enzyme NDH-2 in a native-like lipid environment. Two NDH-2s from *C. thermarum* and *L. monocytogenes* were successfully characterised. Unexpectedly, we discovered that a class of promising anti-tuberculosis agents, CPZ, does not directly inhibit turn-over by NDH-2. Instead, we discovered a novel effect: CPZ could help to disrupt pH gradients across bacterial membranes. This result might have implications in other biological membrane systems. CPZ is a key medicine in the World Health Organization Model List of Essential Medicines and is used to treat psychotic disorders. CPZ affects a number of receptors in the human nervous system, including dopamine, serotonin, histamine, adrenergic, and muscarinic acetylcholine receptors, but its molecular effects on the nervous system remain largely unknown. Further testing of CPZ is of interest to see if it shows a similar effect against mammalian membranes and the human nervous system.

Publications

Nakatani Y., Shimaki Y., Dutta D., Muench S.P., Ireton K., *et al.* (2020) Unprecedented properties of phenothiazines unraveled by a NDH-2 bioelectrochemical assay platform. *J. Am. Chem. Soc.* **142**: 1311-1320.

Funding

This work was funded by the BBSRC.

Collaborators

External: Yoshio Nakatani, Yosuke Shimaki, Kieth Ireton, Gregory Cook (all University of Otago, Dunedin, New Zealand).

Understanding the structure, dynamics and lipid interactions of the complete T cell receptor using multi-scale simulations

Dheeraj Prakaash, Graham Cook and Antreas Kalli

Introduction

The T cell antigen receptor (TCR) initiates immune responses by recognising a wide variety of foreign peptides presented by Major Histocompatibility Complex (MHC) proteins. It is located in the plasma membrane of T cells. The TCR consists of non-covalently associated TCRαβ, CD3εγ, CD3εδ and ζζ dimers. The CD3δ,γ,ε and ζ subunits contain immunoreceptor tyrosine-based activation motifs (ITAMs) in their cytoplasmic region, with the ζζ subunits containing three on each monomer and the CD3 subunits containing one each. Ligation of the TCRαβ dimer stimulates phosphorylation of the ITAMs in the cytoplasmic region initiating the adaptive immune response.

Work using cryo-electron microscopy (cryo-EM) revealed the structure of most of the human TCR, including its extracellular and transmembrane regions, but lacking the cytoplasmic region. This structural data and other functional studies showed that in their transmembrane region, the CD3 and ζζ dimers maintain critical ionic contacts with TCRαβ. Despite significant knowledge of the TCR structure and topology, lack of information on the arrangement of its cytoplasmic tails limits our understanding of the molecular mechanism of intracellular signal propagation in T cells. Our study provides insights into the TCR's complete structure and dynamics in a bilayer that mimics the TCR membrane activation domain, thus forming the basis to study the molecular mechanism of TCR activation.

Results and Discussion

In this study, we employed molecular modelling to model the entire TCR structure in its resting state using the cryo-EM structure (PDB:6JXR) as a template. Using our model of the complete TCR, we performed multi-scale molecular dynamics simulations in the coarse-grained and atomistic resolutions. Our simulations were performed with the TCR inserted into a lipid bilayer containing the predominant lipids found in the native T cell membrane activation domain. Our results revealed that the cytoplasmic tails of the CD3 and ζ subunits fold into a random coiled conformation during the simulations (Figure 1A). Additionally, they strongly interacted with the inner leaflet of the membrane via cationic stretches whilst some intracellular tyrosine sidechains transiently penetrated the hydrophobic region of the membrane. The intracellular tyrosines constitute the ITAMs which are phosphorylated upon TCR activation. Hence, in the resting state, their sidechains were either hidden within the cytoplasmic region or in the hydrophobic region of the membrane.

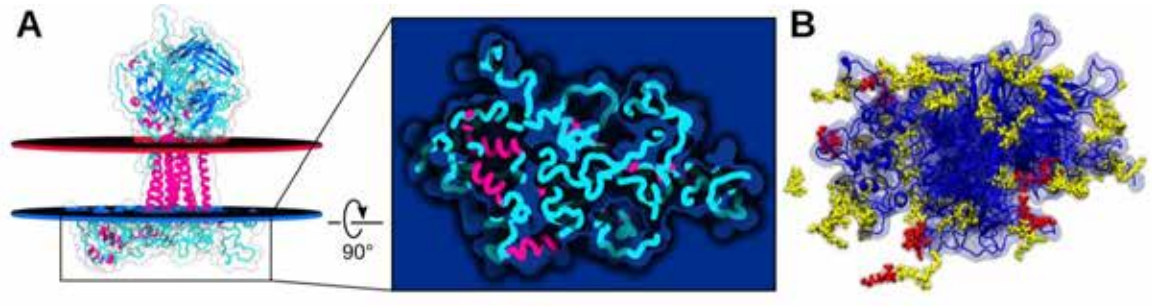

Figure 1: (A) Model of the entire T cell receptor structure (left) highlighting the coiled arrangement of its cytoplasmic tails (right) as viewed from the intracellular region. (B) Intracellular view of the TCR (blue) showing the clustering of PIP2 lipids (yellow) induced by its cytoplasmic tails. PIP3 lipids are also shown (red).

Lipids have been shown to play a key role in TCR activation. Interactions between anionic lipids such as phosphatidylserine (PS) and phosphatidylinositol (PI) molecules, and intracellular signalling proteins that participate in TCR signalling were shown to be critical for their function. Our simulations contain a complex model membrane that enables us to study how the complete TCR interacts with different lipids found in the T cell plasma membrane. Our results suggest that phosphatidylinositol biphosphate and -triphosphate (PIP_2 and PIP_3) lipids formed selective protein-lipid interactions with the TCR creating a local anionic lipid environment around the TCR (Figure 1B). This anionic lipid environment in the inner leaflet of the T cell membrane is potentially critical in recruiting intracellular signalling proteins to the TCR activation site via ionic interactions.

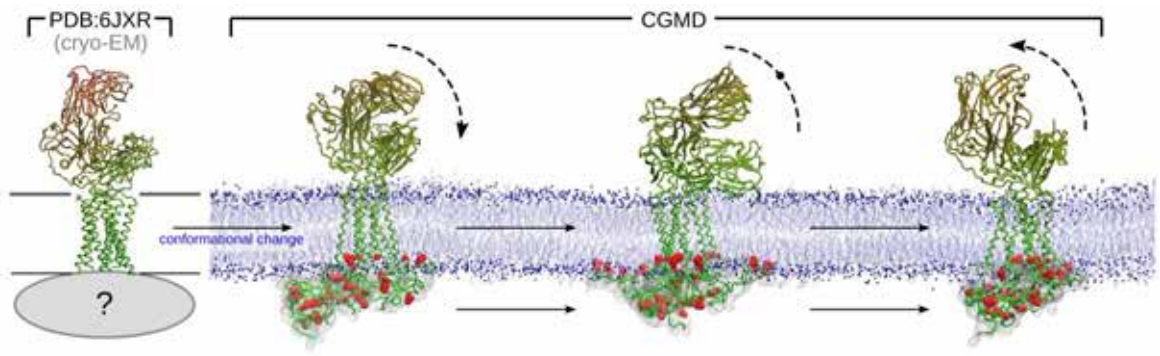

Figure 2: TCR conformational changes observed in our coarse-grained molecular dynamics simulations compared to the cryo-EM structure. The curved arrows indicate the flexibility of the variable domain of the TCR. Lipids and their phosphate groups are shown as blue lines and dark blue spheres respectively. Cytoplasmic tyrosines (red spheres) are observed to be mostly hidden within the TCR cytoplasmic region (transparent surface) or in the hydrophobic region of the membrane.

Our simulations also showed that the entire TCR exhibited different conformational states resulting in a change in protein-protein interactions compared to those observed in the cryo-EM structure (Figure 2). The outermost region of the extracellular domain, called the variable domain, was found to be highly flexible. We also observed some flexibility in the transmembrane region of the TCR. Together, these observations are in agreement with allostery-based TCR activation models. This model proposes that stimulated TCRs undergo conformational changes from the extracellular domain to the cytoplasmic region via the transmembrane region to enable ITAMs' access to intracellular kinase proteins and further initiate signalling.

In summary, our study proposes a molecular model of the complete TCR inserted in a T cell-like plasma membrane, highlighting its lipid interactions and the dynamic conformations of its extracellular, transmembrane and cytoplasmic regions.

Funding
This work was supported by a Springboard Award from the Academy of Medical Sciences and the Wellcome Trust and enabled by ARC3 and ARC4 supercomputers which are part of the High Performance Computing facility at the University of Leeds.

Collaborators
External: Oreste Acuto (University of Oxford).

Insights into Hsp40 mediated proteostasis and anti-aggregation by nuclear magnetic resonance spectroscopy

Theodoros K. Karamanos

Introduction

Molecular chaperones are dynamic molecular machines responsible for the maintenance and regulation of cellular proteins, and thus represent key targets for understanding and preventing a wide range of diseases. The Hsp40-Hsp70 cycle is a key component of this network and an essential player in ensuring cell viability under physiological and stress conditions. However, how Hsp40s (DNAJs) recognise specific substrates and the mechanisms they use to regulate the Hsp70 cycle remained unknown. Dynamic systems such as chaperones, require the application of sensitive biophysical tools that can visualise protein motions across various timescales. Nuclear magnetic resonance (NMR) spectroscopy is a powerful technique that is uniquely capable of studying the structure and dynamics of flexible proteins in solution at atomic resolution. Here, using the DNAJB6b isoform, we highlight our recent NMR results that shed light onto long-standing questions about Hsp40 functions.

Results and Discussion

The J domain of Hsp40s is known to bind to Hsp70 and enhance its ATPase activity. However, the specificity of this interaction arises from the Glycine/Phelynalanine (G/F) linker that connects JD with the C-terminal domain (CTD). Our solution NMR structure of DNAJB6b showed, for the first time, that a short segment in the G/F linker forms a stable helix (helix 5) that completely blocks the binding interface of JD to Hsp70. Based on these and other findings, we proposed the mechanism shown in Figure 1B; In this scheme, helix 5 acts as a switch that shuttles Hsp40s between an active (able to bind Hsp70) and an auto-inhibited (not able to bind Hsp70) form (Figure 1B), effectively controlling the entire Hsp70 cycle. The mechanism of Figure 1B explains a plethora of disease-related mutations in the Hsp40 family and opens the way to an atomic level description of the specificity of the entire chaperone network.

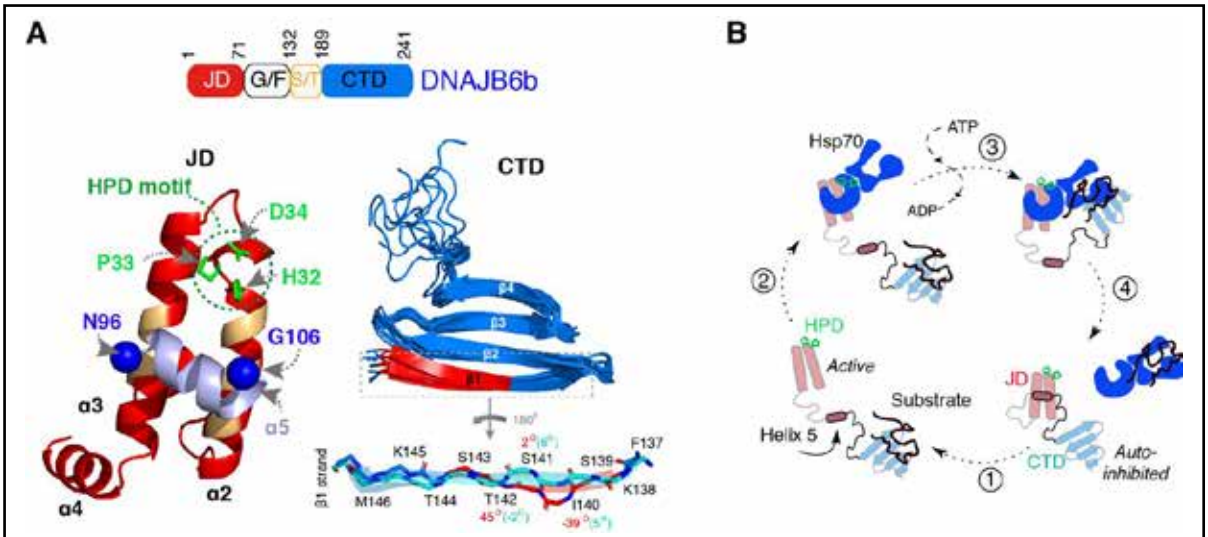

Figure 1: DNAJB6b structure and mechanism of function. (A) Domain architecture (top) and solution structure of DNAJB6b (6U3R, 6U3S, 7JSQ). The J domain is shown in red, helix 5 in light blue and CTD in dark blue. The β1 strand that undergoes twisting and unwinding in the millisecond timescale is shown in a stick representation. (B) Proposed mechanism of regulation of the Hsp70 cycle by helix 5 (see text for details).

DNAJB6b is a unique member of the Hsp40 family, since it cooperates but does not require Hsp70 to achieve its function. The JB6b isoform is a potent inhibitor of protein aggregation *in vivo* and *in vitro* in the absence of Hsp70, with the anti-aggregation function encoded in its C-terminal domains. Using NMR, we were able to show that the CTD exchanges between a monomeric form in which the β1 strand is highly twisted and an oligomeric form with a straight

β1 configuration (Figure 1A). Twisting and unwinding of β1 is at the origin of subunit exchange in native DNAJB6b oligomers that is directly related with anti-aggregation.

Publications

Karamanos T.K., Tugarinov V. and Clore G.M. (2020) An S/T motif controls reversible oligomerization of the Hsp40 chaperone DNAJB6b through subtle reorganization of a beta sheet backbone. *Proc. Natl. Acad. Sci. USA* **117**: 30441-30450.

Karamanos T.K., Tugarinov V., and Clore G.M. (2020) Determining methyl sidechain conformations in a CS-ROSETTA model using methyl 1H-13C residual dipolar couplings. *J. Biomol. NMR* **48**: 1-8.

Tugarinov V, Karamanos TK, Ceccon A, & Clore GM (2020) Optimized NMR Experiments for the Isolation of I=1/2 Manifold Transitions in Methyl Groups of Proteins. *ChemPhysChem* **21**: 13-19.

Tugarinov V, Karamanos TK, & Clore GM (2020) Magic-Angle-Pulse Driven Separation of Degenerate 1H Transitions in Methyl Groups of Proteins: Application to Studies of Methyl Axis Dynamics. *ChemPhysChem*. **21**: 1-6.

Tugarinov V, Karamanos TK, & Clore GM (2020) Optimized selection of slow-relaxing 13C transitions in methyl groups of proteins: application to relaxation dispersion. *J. Biomol. NMR* **74**: 111-118.

Funding

We acknowledge the University of Leeds and the NIH intramural program for financial support of this research.

Collaborators

External: Marius Clore (NIDDK/NIH).

Non-parametric analysis of non-equilibrium simulations

Sergei Krivov

Introduction

One promising strategy towards simulations employing exascale or cloud computing consists of simulating a very large ensemble of short trajectories rather than a singe long trajectory. Adaptive and enhanced sampling approaches can be considered as an extension of this strategy, where one, for example, improves sampling in less sampled parts of configuration space, or parts that produce largest error or controls the exploration/exploitation balance. Such simulations are commonly analyzed by using the Markov state model (MSM) framework. One estimates the transitions probability matrix, which is used to compute many important properties of the equilibrium dynamics. The minimal lag time when a MSM becomes approximately Markovian is a good indicator of the accuracy of the constructed model. The shorter the lag time, the shorter the trajectories that are required to construct the MSM, and the larger the possible speedup over a direct, brute-force simulation. State-of-the-art approaches have lag times in the range of tens of nanoseconds. Recently, we have suggested non-parametric approaches which can determine optimal reaction coordinates that provide diffusive model of dynamics at much shorter lag time of 0.2 ns. These approaches, are restricted to long equilibrium trajectories, however.

Results and Discussion

This year, we have found a way to extend the non-parametric framework to such non-equilibrium ensembles of trajectories. In particular, we showed how one can determine the equilibrium free energy profile as a function of the committor, which can be used to determine exactly such important properties of the dynamics as the equilibrium flux, the mean first passage times, and the mean transition path times between any two points on the committor. We suggest this framework as a general tool, alternative to the Markov state models, for a rigorous and accurate analysis of simulations of large biomolecular systems, as it has the following attractive properties: it is immune to the curse of dimensionality, it does not require system-specific information, it can approximate arbitrary reaction coordinates with high accuracy and it has sensitive and rigorous criteria to test optimality and convergence. The power of the framework was illustrated on a 50-dimensional model system and a realistic protein folding trajectory.

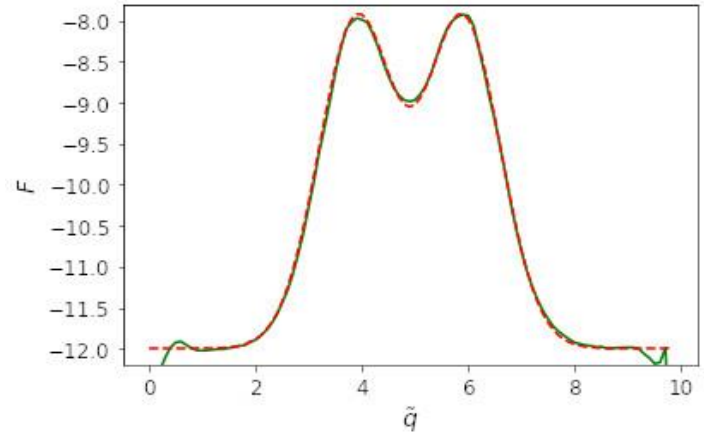

Figure 1: Comparison of the equilibrium free energy profiles of a model 50-dimensional system. Green line shows that obtained from a non-equilibrium ensemble of short trajectories, red line shows the exact analytical results. The agreement is excellent.

Receptor tyrosine kinase signalling in the absence of growth factor stimulation: response to cellular stress

Eleanor Cawthorne, Christopher Jones, Sophie Ketchen, Chi-Chuan Lin, Dovile Milonaityte, Kin Man Suen and John Ladbury

Introduction

Receptor tyrosine kinases (RTKs) expressed on the plasma membrane of cells in normal tissue are rarely exposed to high concentrations of extracellular growth factors. Nonetheless, they express proteins associated with kinase-mediated signalling. We are interested in the signalling associated with these protein that occurs under basal conditions which are close to the conditions experienced by normal tissue. In the absence of extracellular stimulation or genetic mutation, an oncogenic response can be driven by the competitive binding of SH3 domain-containing downstream effector proteins to proline-rich sequences on growth factor receptors. Of the approximately 50 plasma membrane RTKs the majority have proline-rich sequences in their C-termini. These have a propensity to bind to the >300 proteins expressed in human cells which contain SH3 domains. These interactions occur in the absence of any extracellular stimulation (e.g., growth factors, cytokines). Proline-rich sequence binding to SH3 domains are promiscuous and the observed interactions with RTKs are dependent on the relative concentrations of the proteins involved.

We previously established that under non-stimulatory conditions the fibroblast growth factor receptor 2 (FGFR2) recruits the adaptor protein, growth factor receptor binding protein 2 (Grb2) through its C-terminal SH3 domain. In cells depleted of Grb2 other proteins can access the proline-rich motif on FGFR2. One of these proteins, phospholipase C(gamma)1 (Plcγ1) is activated on binding and through turnover of plasma membrane phospholipids to produce second messengers, raises cellular calcium levels which are responsible for increased cell motility and invasive behaviour. In ovarian and lung adenocarcinoma, patients with low levels of Grb2 and increased expression of Plcγ1 have higher incidence of metastasis and this leads to greatly reduced survival outcomes.

The dependence of signalling described above on respective concentrations of RTKs and SH3 domain containing proteins mean that there is no on-off switch for this form of signalling; the outcomes are dictated solely by fluctuations of protein concentrations. As a result, one key driver for this form of signalling is cellular stress. We are working to establish how stresses experienced by tissue (e.g., pH change associated with acid reflux in the oesophagus) can lead to cancer outcomes.

Results and Discussion

We have extended our studies in this area to explore other RTK-SH3 domain-containing protein interactions to establish whether the up-regulation of signal transduction through these interactions is a general phenomenon. This leads to the hypothesis that two tiers of intracellular signalling can be derived from receptors with intrinsic protein kinase activity:
1) Ligand-induced elevation in kinase activity resulting in tyrosylphosphate-mediated effector protein recruitment and committal to a defined cellular outcome (e.g., proliferation).
2) Receptor phosphorylation-independent activation of downstream effectors through SH3 domain/proline-rich sequence interactions, which appear to be required for cell homeostasis/metabolic control.

Hyperactivity of the Tier 1 signalling is a feature of RTK-related cancers arising from genetic mutation. Although the tier 2 signalling mechanism occurs under basal conditions, and is thus likely to be associated with cellular maintenance, we have shown that fluctuations in expression levels of SH3-containing proteins can drive cells into pathological phenotypes including proliferation and metastasis.

We are testing this hypothesis with a range of methods extending from cell-based assays (including fluorescence lifetime imaging microscopy) through to structural and in vitro

biophysical analysis. We are optimising a screening protocol to establish the extent of Tier 2 signalling in a range of cells and conditions. We have identified novel interactions involving well-studied proteins as well as less-understood systems. These are being validated and phenotypic outcomes of knocking down these interactions are being explored to establish the effects of signalling in normal tissue.

We have focused on gastro-intestinal (GI) cancers and we have begun to explore the effects of stress on intracellular protein expression and the outcomes on Tier 2 signalling. We have shown that by mimicking conditions experienced in the GI tract we can affect expression of receptor tyrosine kinases.

In addition to identifying the signalling pathways which are initiated as a result of fluctuations in protein concentrations in cell-based assays, we are exploring the interactions associated with up-regulation of Tier 2 signalling using both biophysical and structural biological methods. High-resolution structural detail on the receptor-ligand interactions are providing invaluable detail on the mode of recruitment of signalling proteins as well as information towards potential inhibition of aberrant pathways that lead to pathogenic outcome.

Publications

Suen K.M., Braukmann F., Butler R., Bensaddek D., Akay A.*, et al.* (2020) DEPS-1 is required for piRNA-dependent silencing and PIWI condensate organisation in *Caenorhabditis elegans*. *Nat. Commun.* **11**: 4242.

Alshawli A.S., Wurdak H., Wood I.C. and Ladbury J.E. (2020) Histone deacetylase inhibitors induce medulloblastoma cell death independent of HDACs recruited in REST repression complexes. *Mol. Genet. Genomic. Med.* **8**: ee1429.

Ketchen S., Rohwedder A., Knipp S., Esteves F., Struve N.*, et al.* (2020) A novel workflow for three-dimensional analysis of tumour cell migration. *Interface Focus* **10**: 20190070.

Funding

This work is funded by Cancer Research UK.

Collaborators

University of Leeds: Phillip Quirke, Susan Short, Alex. Breeze and Darren Tomlinson.
External: Zamal Ahmed (University of Texas, MD Anderson Cancer Center, USA), Mien-Chie Hung (University of Texas MD Anderson Cancer Center, USA), Swathi Arur (University of Texas MD Anderson Cancer Center, USA), Mikhail Bogdanov (University of Texas, USA), Richard Grose (Barts Cancer Institute, London).

Cellular re-wiring: Understanding how oncogenic viruses transform their host cells

Molly Patterson, James Scarth, Ethan Morgan, Diego Barba-Moreno, Yigen Li, Corinna Brockhaus, Eleni-Anna Loundras, Miao Wang and Andrew Macdonald

Introduction

Despite available vaccines, persistent infection with high-risk human papillomaviruses (HPV) remains a major health problem. HPV is the cause of ~5% of the global cancer burden (~630,000 cancers per year), including most cervical carcinomas and an increasing proportion of oropharyngeal and other anogenital cancers. Cervical cancer is the fourth most common cause of cancer death in women. This HPV disease burden disproportionately impacts low- and middle-income countries, where the death rate is 18 times higher than in developed nations. Collectively, these developing nations are expected to account for more than 95% of HPV-mediated deaths by 2030. Limited vaccine availability in developing countries, hesitancy in developed countries and the lag between infection and disease ensures that the burden of HPV-associated malignancies remains high. HPV-encoded oncoproteins co-opt cell signalling machinery to dysregulate host gene expression within the infected epithelia in order to create an environment that favours virus replication and persistence, predisposing infected cells to transformation. The focus of our work is to identify host factors essential for cancer initiation during HPV infection. This knowledge could underpin new therapeutic strategies to treat virus-induced cancer.

Results and Discussion

Non-coding RNA molecules play essential roles in controlling cellular homeostasis. We identified that the oncogenic microRNA (OncomIR) mIR18a is over-expressed in cervical cancers and is crucial for enforcing cell survival signals within the cells. A key mIR18a target identified was the Hippo kinase STK4. This tumour suppressor is tasked with ensuring that the YAP transcription factor is not hyperactivated. Thus, our work revealed a new signalling network in cervical cancer cells. Encouragingly, inhibition of mIR18a reduced cervical cancer cell growth and activated cell death. Going forward, we wish to identify whether additional mIR18a targets exist in cervical cancer cells and understand their contribution to cell growth and survival (Figure. 1).

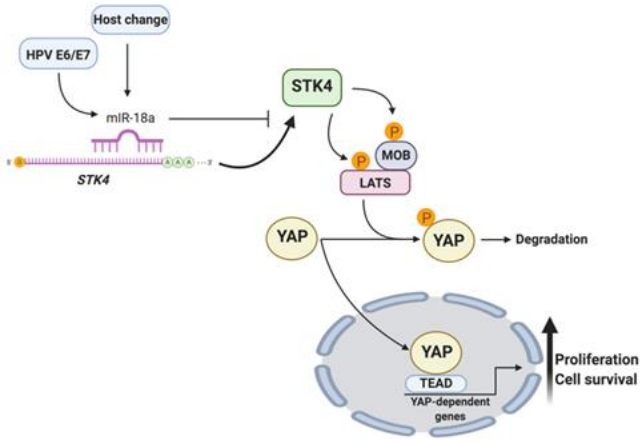

Figure 1: An oncogenic microRNA targets the Hippo pathway in HPV-positive cervical cancer. Driven by the HPV encoded oncoproteins E6 and E7, levels of mIR18a increase from low levels in normal keratinocytes to high levels in cervical cancers. Targeting of the STK4 mRNA by mIR18 reduces STK4 protein expression and impairs the Hippo pathway. This tumour suppressor pathway can no longer hold YAP in check, which translocates to the nucleus to drive expression of genes necessary for growth and survival.

We have focussed on how HPV successfully modifies the phosphorylation of host proteins to alter the cellular signalling landscape. In a new, exciting project, we reveal that another post-translational modification – ubiquitination – is modified in HPV-driven diseases. We focussed on a class of enzymes called deubiquitinases (DUB) which remove ubiquitin from target proteins, and found that expression of the DUB USP13 was significantly increased in cervical cancers. We identified that a target of USP13 called Mcl-1 was essential for the growth and survival of HPV-positive cervical cancers. Mcl-1 is a member of the Bcl2 family of anti-apoptotic proteins. It is implicated in the resistance of cervical cancer cells to certain anti-cancer drugs. Our fundamental studies on USP13 may therefore shed light on new targets for therapy in HPV-associated cancers (Morgan *et al*., Oncogene in press).

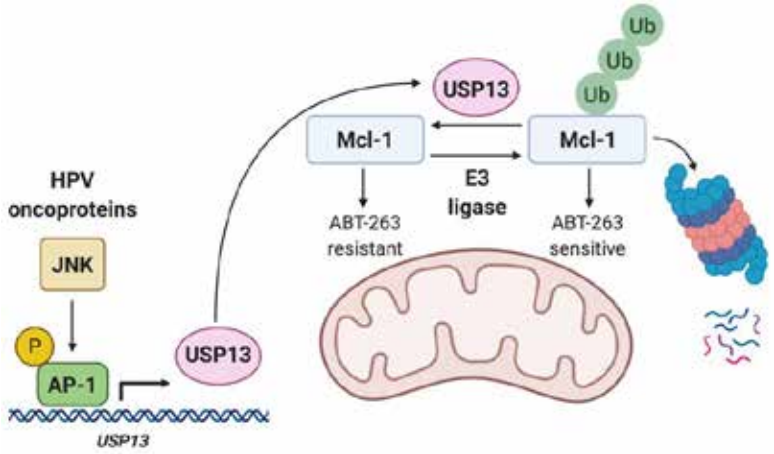

Figure 2: HPV oncoproteins increase USP13 expression which subsequently removes ubiquitin from target proteins including Mcl-1. This stabilises Mcl-1 levels, allowing cervical cancer cells to survive insults from therapeutic agents. Blockade of Mcl-1 sensitises cervical cancer cells to therapies. USP13 targets beyond Mcl-1 are not known in cervical cancers.

Publications

Morgan E.L. and Macdonald A. (2020) Manipulation of JAK/STAT signalling by high-risk HPVs: potential therapeutic targets for HPV-associated malignancies. *Viruses* **12**: 977.

Morgan E.L., Patterson M.R., Ryder E.L., Lee S.Y., Wasson C.W.*, et al.* (2020) MicroRNA-18a targeting of the STK4/MST1 tumour suppressor is necessary for transformation in HPV positive cervical cancer. *PLoS Pathog.* **16**: e1008624.

Morgan E.L., Scarth J.A., Patterson M.R., Wasson C.W., Hemingway G.C.*, et al.* (2020) E6-mediated activation of JNK drives EGFR signalling to promote proliferation and viral oncoprotein expression in cervical cancer. *Cell Death and Differ*. doi: 10.1038/s41418-020-00693-9.

James C.D., Das D., Morgan E.L., Otoa R., Macdonald A.*, et al.* (2020) Werner Syndrome protein (WRN) regulates cell proliferation and the human papillomavirus 16 life cycle during epithelial differentiation. *mSphere* **5**: e00858-20.

Funding

This work was funded by the MRC, BBSRC and Wellcome Trust.

Collaborators

University of Leeds: Neil Ranson, Adel Samson, Stephen Griffin and Adrian Whitehouse
External: Sally Roberts (University of Birmingham, UK), Iain Morgan (Virginia Commonwealth University, USA).

TMEM16A/ANO1 calcium-activated chloride channel as a novel target for the treatment of human respiratory syncytial virus infection

Hayley Pearson, Eleanor Todd, Samantha Hover, Martin Stacey, Jonathan Lippiat, Adrian Whitehouse, John Barr and Jamel Mankouri

Introduction

Human respiratory syncytial virus (HRSV) is a common cause of respiratory tract infections (RTIs) globally and is one of the most fatal infectious diseases for infants in developing countries. Of those infected, 25%-40% aged ≤1 year develop severe lower RTIs leading to pneumonia and bronchiolitis, with ~10% requiring hospitalisation. Evidence also suggests that HRSV infection early in life is a major cause of adult asthma. There is no HRSV vaccine, and the only clinically approved treatment is immunoprophylaxis that is expensive and only moderately effective. New anti-HRSV therapeutic strategies are therefore urgently required.

Results and Discussion

It is now established that viruses require cellular ion channel functionality to infect cells. Here, we infected human lung epithelial cell lines and *ex vivo* human lung slices with HRSV in the presence of a defined panel of chloride (Cl^-) channel modulators to investigate their role during the HRSV life-cycle. We demonstrate the requirement for TMEM16A, a calcium-activated Cl^- channel, for HRSV infection. Time-of-addition assays revealed that the TMEM16A blockers inhibit HRSV at a post-entry stage of the virus life-cycle, showing activity as a post-exposure prophylaxis. Another important negative-sense RNA respiratory pathogen influenza virus was also inhibited by the TMEM16A-specific inhibitor T16Ainh-A01. These findings reveal TMEM16A as an exciting target for future host-directed antiviral therapeutics.

Publications

Charlton F.W., Pearson H.M., Hover S., Lippiat J.D., Fontana J., *et al.* (2020) Ion channels as therapeutic targets for viral infections: further dscoveries and future perspectives. *Viruses* **12**: 844.

Dobson S.J., Anene A., Boyne J.R., Mankouri J., Macdonald A., *et al.* (2020) Merkel cell polyomavirus small tumour antigen activates the p38 MAPK pathway to enhance cellular motility. *Biochem. J.* **477**: 2721-2733.

Davies K.A., Chadwick B., Hewson R., Fontana J., Mankouri J., *et al.* (2020) The RNA replication site of Tula Orthohantavirus resides within a remodelled Golgi network. *Cells* **9**: 1569

Mega D.F., Fuller J., Alvarez-Rodriguez B., Mankouri J., Hewson R., *et al.* (2020) Mutagenic analysis of hazara nairovirus nontranslated regions during single- and multistep growth identifies both attenuating and functionally critical sequences for virus replication. *J. Virol.* **94**: e00357-20.

Panou M.M., Antoni M., Morgan E.L., Loundras E.A., Wasson C.W., *et al.* (2020) Glibenclamide inhibits BK polyomavirus infection in kidney cells through CFTR blockade. *Antiviral Res.* **178:** 104778.

Dobson S.J., Mankouri J. and Whitehouse A. (2020) Identification of potassium and calcium channel inhibitors as modulators of polyomavirus endosomal trafficking. *Antiviral Research* **179**: 104819.

Funding

This work was funded by the Royal Society, the British Lung Foundation and the University of Leeds.

Collaborators
External: Alan Kohl (MRC-University of Glasgow Centre for Virus Research), Steve Goldstein (Loyola University Chicago), Stefan Finke (Friedrich Loeffler Institute), Christina Hesse (Fraunhofer Institute for Toxicology and Experimental Medicine, Hanover)

Electron microscopy of membrane proteins to underpin structure guided inhibitor design

David Klebl, Rebecca Thompson, Frank Sobott and Stephen Muench

Introduction

Recent developments in electron microscopy (EM) have led to a step-change in our ability to solve the "high resolution" structure of previously intractable proteins. Moreover, this has had a significant impact in the membrane protein field, with a number of previously intractable systems now having their structures solved. Despite these significant steps forward there are still a number of areas that would benefit from further development, not least sample preparation. My group are focused on methods development in two broad areas. The first is the development of a new grid making technology that can rapidly freeze grids and trap changes in structure in the low-millisecond timeframe (>6 ms). The second is in the use of new methodologies for stabilizing membrane proteins, for example, styrene maleic acid co-polymer lipoproteins (SMALPs) and amphipols.

Results and Discussion

In collaboration with Prof Howard White, the group have being developing the use of time-resolved EM whereby a sample can be mixed to trigger a reaction and different states can be obtained with a time delay of >7 ms. This device can mix two or three samples (substrate and reactant) after which they are sprayed onto a fast-moving EM grid which is subsequently vitrified in liquid ethane. We have used this setup to study systems such as virus assembly, membrane disruption and motor proteins (Figure 1A). Moreover, the rapid speed of grid making has also allowed us to investigate the role of the air-water-interface on the behavior of the sample within cryo-EM. Comparing grids made in the conventional way (~10 s) with those made rapidly (~10 ms and 50 ms) has shown that there are multiple interactions of the protein sample with the air-water-interface which can result in preferred orientation and protein damage. Making grids in the low ms time-frame can reduce some of the negative impacts of the air-water-interface such as the degree of preferred orientation. Moreover, studies with the ribosome have shown that damage can occur within the traditionally blotted sample which is reduced when making the grids rapidly that may be reflective of the reduced time at the air-water-interface. The group have been using an EM approach to inform on small-molecule binding and have recently shown that Pico145 binds to TRPC5 by exchanging for a lipid in the channel. We have also shown how a large protease complex (H-gal-GP) is conserved across roundworm parasites and that this acts as a potent vaccine adjuvant through its role in substrate transport over the parasite gut membrane (Figure 1B). Working with industrial partners through a joint BBSRC grant, (GlaxoSmithKline and UCB pharma) we are studying a

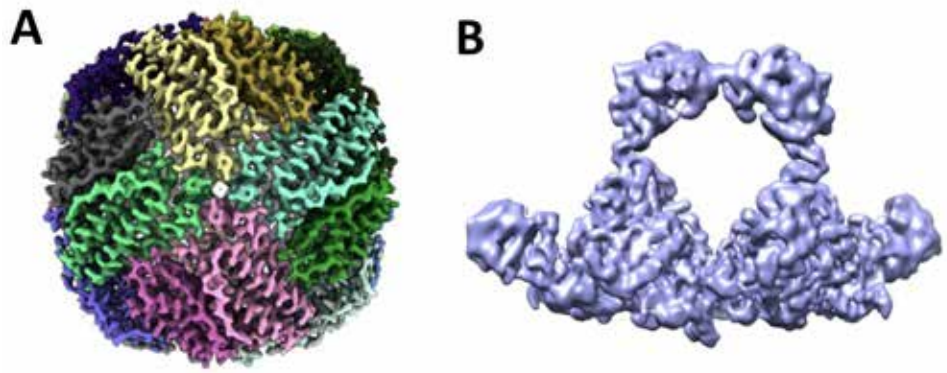

Figure 1: (**A**) 3.5 Å single particle cryoEM reconstruction of equine apoferritin from a grid prepared in 36 ms between spraying and vitrification. (**B**) CryoEM structure of the H-gal-GP complex from the *Haemonchus contortus* gut membrane.

range of systems to optimize pipelines for EM. This includes the use of new ways to extract and isolate membrane proteins in more "native" environments through the use of styrene

maleic acid (SMA) co-polymers and more recently adapted amphipol polymers which allows for downstream analysis by mass spectrometry and electron microscopy.

Publications

Klebl D.P., Gravett M.S.C., Kontziampasis D., Wright D.J., Bon R.S.*, et al.* (2020) Need for speed: examining protein behavior during CryoEM grid preparation at different timescales. *Structure* **28**: 1238-1248.

Klebl D.P., Monteiro D.C.F., Kontziampasis D., Kopf F., Sobott F.*, et al.* (2020) Sample deposition onto cryo-EM grids: from sprays to jets and back. *Acta Crystallogr. D, Struct. Biol.* **76**: 340-349.

Hesketh S.J., Klebl D.P., Higgins A.J., Thomsen M., Pickles I.B.*, et al.* (2020) Styrene maleic-acid lipid particles (SMALPs) into detergent or amphipols: An exchange protocol for membrane protein characterisation. *Biochim. Biophys. Acta, Biomembr.* **1862**: 183192.

Wright D.J., Simmons K.J., Johnson R.M., Beech D.J., Muench S.P.*, et al.* (2020) Human TRPC5 structures reveal interaction of a xanthine-based TRPC1/4/5 inhibitor with a conserved lipid binding site. *Commun. Biol.* **3**: 704.

Johnson R.M., Fais C., Parmar M., Cheruvara H., Marshall R.L.*, et al.* (2020) Cryo-EM structure and molecular dynamics analysis of the fluoroquinolone resistant mutant of the AcrB transporter from *Salmonella*. *Microorganisms* **8**: 943.

Scarff C.A., Carrington G., Casas-Mao D., Chalovich J.M., Knight P.J.*, et al.* (2020) Structure of the shutdown state of myosin-2. *Nature* **588**: 515-520.

Funding

This work was supported by the BBSRC and Wellcome Trust.

Collaborators

University of Leeds: Robin Bon, Rebecca Thompson, Frank Sobott and Colin Fishwick.
External: Howard White (Eastern Virgina Medical School), Martin Trebbin (State University of New York), Samar Hasnain & Dr Svetlana Antonyuk (University of Liverpool), Dr Chun-wa Chung (GlaxoSmithKline) and Dr Tom Ceska (UCB Pharma).

Activity-Directed Synthesis of Bioactive Small Molecules

Shiao Chow, Justin Clarke, Adam Green, Fruzsina Hobor, Abbie Leggott, Alex O'Neill, Stuart Warriner, Andrew Wilson and Adam Nelson

Introduction

The discovery of biologically-active small molecules is an enduring theme in chemical biology and medicinal chemistry. However, the historical exploration of chemical space has been highly uneven and unsystematic: a sixth of known cyclic organic compounds are based on just 30 (of 2.5 million) known molecular scaffolds! This uneven exploration stems, in large part, from the narrow toolkit of reliable reactions that currently underpins molecular discovery. We have an ongoing and vibrant research programme that is focused on the realisation of new chemical approaches that can underpin the discovery of structurally-distinctive, bioactive small molecules.

We have developed activity-directed synthesis as a structure-blind, function driven approach for the discovery of functional molecules. Here, arrays of (typically hundreds of) reactions are performed on a microscale in which the components (usually, substrates, co-substrates and catalysts) are widely varied. Crucially, we deliberately harness reactions that have the potential to yield many different products, and which are outside of the standard reaction toolkit that underpins molecular discovery. After minimal purification, the crude products of these reactions are screened for biological function. The identified hit reactions are then scaled up, typically by around 50-fold, and the products are purified, structurally elucidated for the first time and characterized. Here, we describe the application of activity-directed synthesis in the discovery of both protein-protein interaction inhibitors and antibacterial compounds.

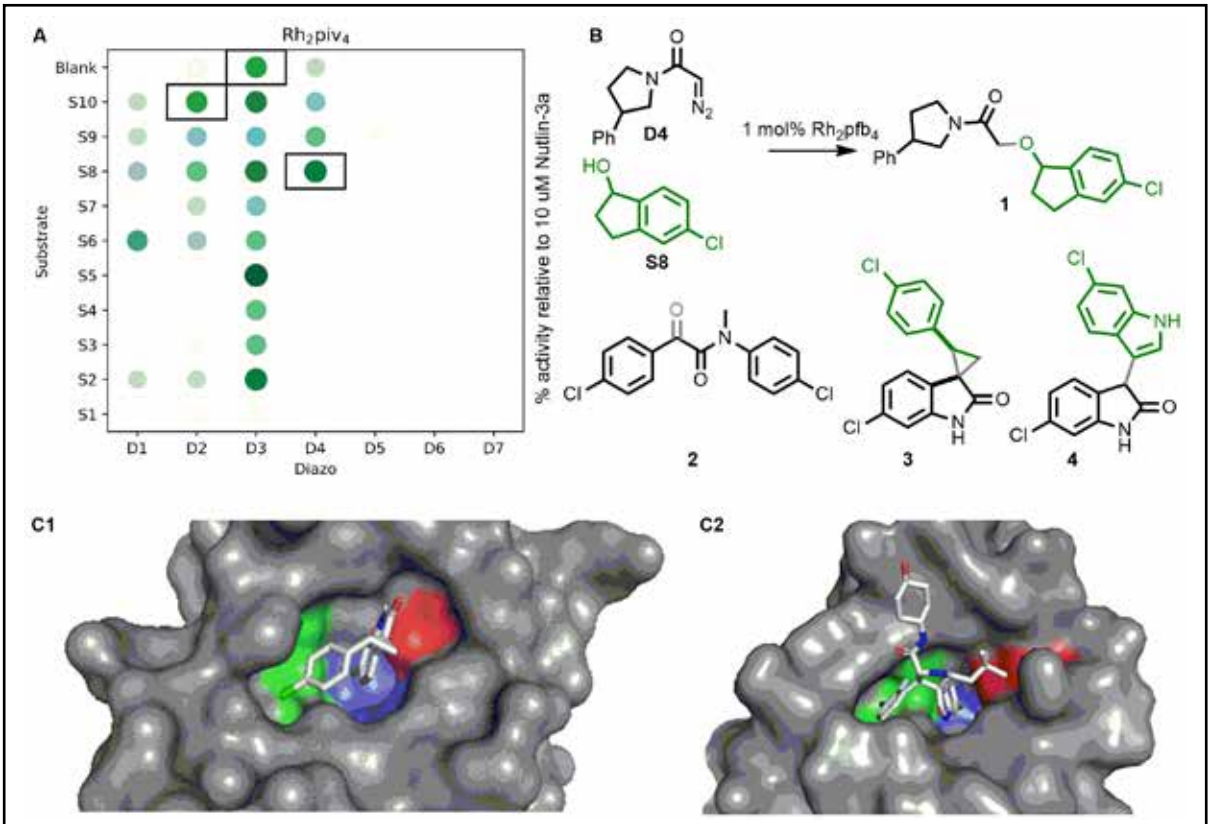

Figure 1: Discovery of multiple series of inhibitors of p53/*h*DM2 protein-protein interaction inhibitors. Panel A: Identification of reactions that yield bioactive molecules. Panel B: Example of a hit reaction and other bioactive molecules discovered. Panel C: Docked exemplar molecules to *h*DM2: compound **3** (C1) and the known inhibitor M1-77301 (C2).

Results and Discussion

We investigated the potential of activity-directed synthesis to yield structurally-distinctive inhibitors of the p53/*h*DM2 protein-protein interaction (Figure 1). It had been previously shown that nutlin analogues were only able to bind *h*DM2 if they mimicked at least two of the three hotspot residues in the p53 peptide. An array of 196 rhodium-catalysed reactions was performed in which different combinations of diazo substrates, co-substrates and catalyzed were investigated. Many of the substrates and co-substrates were chosen to bear substituents with the potential to mimic hotspot residues. Hit reactions were identified on the basis of the ability of the crude reaction products to inhibit the interaction between *h*DM2 and a fluorescently-labelled p53 peptide (Figure 1, Panel A). The hit reactions then informed the design of the substates and co-substrates for a second reaction array. Hit reactions from both rounds were scaled up, and the products were purified, structurally elucidated and characterized (Figure 1, Panel B). Remarkably, it was shown that activity-directed synthesis had enabled the discovery of four distinct series of p53/*h*DM2 interaction inhibitors. In each case, biophysical characterization and docking studies suggested that a pair of p53 hotspot residues was mimicked (Figure 1, Panel C). Crucially, the ligand efficiencies of these compounds compared very favourably with those of deconstructed nutlin analogues.

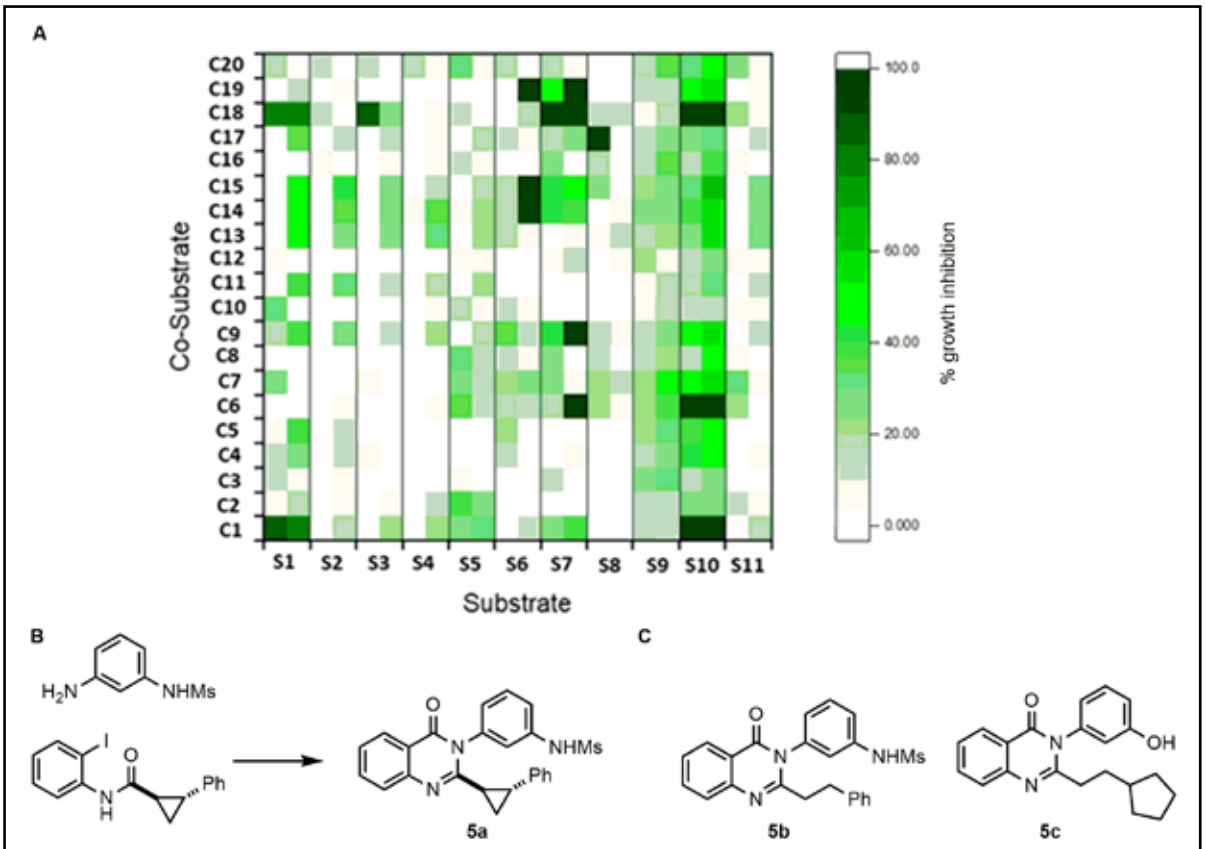

Figure 2: Expansion of a series of antibacterial quinazolinones **5**. Panel A: Identification of reactions that yield bioactive molecules. Panel B: Example of a hit reaction and its bioactive product. Panel C: Examples of other molecules also identified.

We harnessed activity-directed synthesis to expand a series of antibacterial quinazolinones that target penicillin-binding proteins (Figure 2). An array of 220 palladium-catalysed carbonylation reactions was performed in which substrates (*o*-iodo anilides) were combined with co-substrates (nitrogen nucleophiles). The underpinning chemistry was chosen on the basis of its ability to yield compounds based on alternative scaffolds including quinazolinones. The crude reaction mixtures were screened in duplicate against *S. aureus* ATCC29213 (Figure 2, Panel A). The products of six hit reactions displayed antibacterial activity against both replicate cultures. The hit reactions were scaled up, and the purified products were all found to be quinazolinones that displayed significant antibacterial activity (Figure 2, Panel B). Overall, the approach enabled identification of the structural features that are critical for activity.

We have shown that activity-directed synthesis can support a range of alternative medicinal chemistry strategies. In the work presented here, we demonstrated that activity-directed synthesis could both expand series of bioactive small molecules, and enable the parallel discovery of new bioactive chemotypes. Publications from all programmes of our programmes that focus on the discovery of novel bioactive molecules are listed below. Further details of research within the Nelson group may be found at www.asn.leeds.ac.uk.

Publications

Lowe R.A., Taylor D., Chibale K., Nelson A. and Marsden S.P. (2020) Synthesis and evaluation of the performance of a small molecule library based on diverse tropane-related scaffolds. *Bioorg. Med. Chem.* **28:** 115442.

Green A.I., Hobor F., Tinworth C.P., Warriner S., Wilson A.J.*, et al.* (2020) Activity-directed synthesis of inhibitors of the p53/hDM2 protein-protein interaction. *Chemistry* **26**: 10682-10689.

Leggott A., Clarke J.E., Chow S., Warriner S.L., O'Neill A.J.*, et al.* (2020) Activity-directed expansion of a series of antibacterial agents. *Chem. Commun.* **56**: 8047-8050.

Trindade A.F., Faulkner E.L., Leach A.G., Nelson A. and Marsden S.P. (2020) Fragment-oriented synthesis: beta-elaboration of cyclic amine fragments using enecarbamates as platform intermediates. *Chem. Commun.* **56**: 8802-8805.

Karageorgis G., Liver S. and Nelson A. (2020) Activity-directed synthesis: a flexible approach for lead generation. *ChemMedChem* **15**: 1776-1782.

Francis D., Nelson A. and Marsden S.P. (2020) Synthesis of beta-diamine building blocks by photocatalytic hydroamination of enecarbamates with amines, ammonia and N-H heterocycles. *Chemistry* **26**: 14861-14865.

Funding

We thank EPSRC and GSK for funding.

Collaborators

External: Christopher Tinworth (GSK). We also acknowledge other scientific collaborators who have also contributed strongly to other aspects of our on-going research programme.

Breaking symmetry of the centriole

Takashi Ochi

Introduction

Symmetry breaking is a fundamental phenomenon in biology. For instance, establishing left-right asymmetry is one of the most dramatic events during our body development. Symmetry breaking is not exceptional at the macromolecular level. This happens in one of the largest protein complexes in eukaryotic cells: the centriole.

The centriole is an organelle which is crucial for organising centrosomes and generating cilia. The core of the centriole is comprised of nine parallel blades of microtubule triples that are inter-connected by protein linkers (Figure 1). This makes a 9-fold rotational symmetry. In multiciliated cells, this symmetry is broken by accessory structures of centrioles (Figure 1). The asymmetric addition of the accessory structures are observed not only in multicellular organisms but also in unicellular organisms, indicating that the symmetry breaking of centrioles is evolutionarily conserved. An outstanding question is how accessory structures are added asymmetrically to the symmetric centriole. A key to answer this question is Coiled-coil domain-containing protein 61 (CCDC61).

CCDC61 (also known as VFL3) is known to be crucial for correctly generating accessory structures of centrioles of motile cilia in uni- and multi-cellular organisms. CCDC61-deficient cells display abnormal numbers of cilia/flagella and locomotion because of abnormal accessory structures. In centrosomes, CCDC61 is important for the correct formation of spindle poles by interacting with a component of accessory structures. These results suggest that CCDC61 is important for accessory structure generation. However, how CCDC61 plays these roles is unknown.

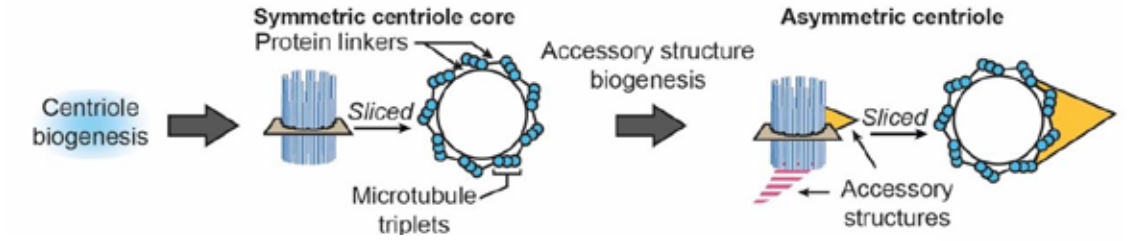

Figure 1: Symmetry and asymmetry of centrioles

Results and Discussion

Computational analyses of the amino acid sequence of CCDC61 indicated that it consists of an N-terminal globular domain followed by a coiled-coil domain and low complexity region (Figure 2A). A further analysis suggested that CCDC61 is a putative paralogue of a key centriolar protein, Spindle assembly abnormal protein 6 (SAS6). The crystal structure of the N-terminal and the beginning of the coiled-coil domains of CCDC61 indeed showed that it has a similar fold to SAS6 (Figure 2A). SAS6 has two homodimer interfaces in its head and coiled-coil domains. Using these two interfaces, SAS-6 self-assembles into a 9-fold ring structure, which is the basis of the 9-fold rotational symmetry of the centriole. The crystal structure of CCDC61 showed that it also has similar two homodimer interfaces to those of SAS-6 (Figure 2B). However, instead of a ring, the crystal structure showed that CCDC61 forms a linear helical filament with a 3-fold screw axis. The helical rise of the CCDC61 filament is about 80 Å, which is close to the dimensions of the tubulin dimer. Strikingly, we found that CCDC61 interacts with microtubules via its coiled-coil domain (Figure 2C and D). This interaction is mediated by conserved positively-charged residues of CCDC61 and the acidic C-terminal tail of tubulin. These results prompted us to think that the CCDC61 filament binds to microtubules and provides a platform for protein-protein interactions.

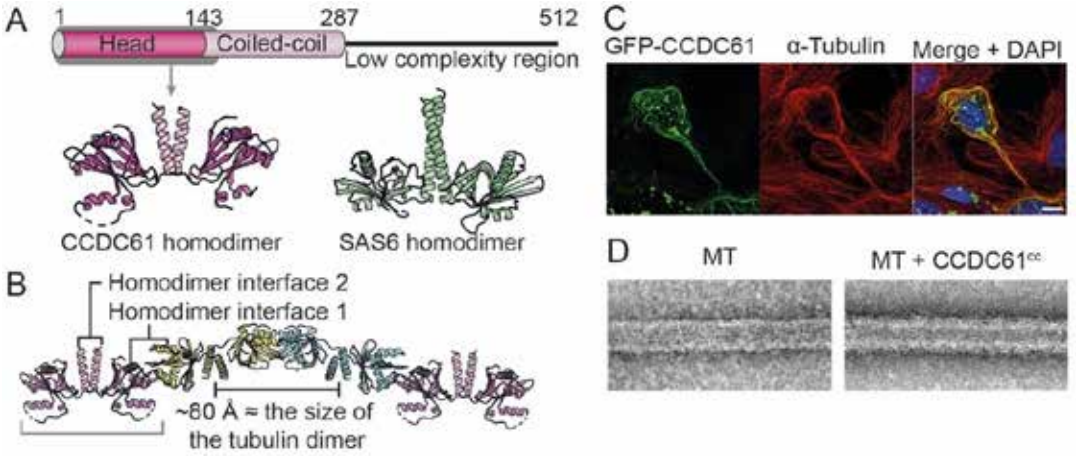

Figure 2: CCDC61 forms filaments and binds to microtubules. (A) Structure of CCDC61 homodimer. The crystal structure of zebrafish CCDC61 (PDB code: 6HXT) is shown below a schematic domain diagram of human CCDC61. The crystal structure of zebrafish SAS6 (PDB code: 2Y3W) is also shown next to the structure of CCDC61. (B) CCDC61 filament. A filament model of CCDC61 was generated using the crystal structure of zebrafish CCDC61 homodimer. Symmetrically-equivalent CCDC61 dimers are displayed with the same colours. Two homodimerisation interfaces are labelled as 1 and 2. (C) CCDC61 binds to microtubules. Immunofluorescent images show that GFP-CCDC61 (green) colocalises with microtubules (red). Scale bar, 10 μm. (D) The coiled-coil domain of CCDC61 (CCDC61^{cc}) binds to a microtubule (MT). Negative stain EM images show the MT and MT in-complex with CCDC61^{cc}.

We next wanted to test significance of those *in vitro* observations *in vivo*. To this end, in collaboration with Prof. Susan Dutcher group, we tested a CCDC61 mutation that does not form filaments (FD mutant) and a CCDC61 mutation that does not bind to microtubules (5E mutant) in *Chlamydomonas*, which is an excellent model organism to study centrioles and motile cilia and in which CCDC61 was first identified. We examined whether these mutants rescued the phenotype of abnormal flagella numbers that was displayed by a CCDC61-deficient *Chlamydomonas* strain. The results showed that the FD mutant partially rescued the phenotype whereas the 5E mutant was indistinguishable from the CCDC61-deficient strain, suggesting that the microtubule-binding of CCDC61 is essential for its function.

Our studies raised several new questions. Is the interaction between CCDC61 and microtubules regulated by post-translational modifications on the tubulin tail? What does CCDC61 recruit to centrioles? How do these functions of CCDC61 affect the asymmetric addition of accessory structures of centrioles? Further structural and functional studies of CCDC61 and its interactors will answer these questions.

Publications

Ochi T., Quarantotti V., Lin H.W., Jullien J., Silva I.R.E.*, et al.* (2020) CCDC61/VFL3 is a paralog of SAS6 and promotes ciliary functions. *Structure* **28**: 674-689.

Funding

The Ochi lab is supported by the BBSRC and the startup fund of the University Academic Fellowship scheme in the University of Leeds.

Collaborations

External: Tom L. Blundell (University of Cambridge, UK), Mark van Breugel (MRC Laboratory of Molecular Biology, UK), Fanni Gergely (CRUK Cambridge Institute, UK), Susan K. Dutcher (Washington University School of Medicine, USA), Jerome Jullien (Gurdon Institute, UK), Stephen P. Jackson (Gurdon Institute, UK), Raymond E. Goldstein (University of Cambridge, UK), Yuu Kimata (ShanghaiTech University, China), Andrew N. Blackford (University of Oxford, UK).

Tissue-specific tools to identify regulators of transcellular chaperone signalling

Jay Miles, David Westhead and Patricija van Oosten-Hawle

Introduction

In metazoans, tissues experiencing proteotoxic stress induce “transcellular chaperone signalling” (TCS), that activates molecular chaperones, such as *hsp-90*, in distal tissues. Thus, conserved stress responses such as the heat shock response initiate inter-cellular communication that allows protective chaperone expression to be signalled and spread from one tissue to another, a process known as transcellular chaperone signalling (TCS). One key observation of TCS is that an imbalance of proteostasis in only one tissue (e.g., neurons) through altered expression of the major chaperone *hsp-90*, can lead to an upregulated *hsp-90* chaperone response in receiving tissues that is spread throughout the organism[1,2]. How this form of inter-tissue communication is mediated to upregulate systemic chaperone expression is an open question to date.

Results and Discussion

Using *C. elegans* as model system, we have previously identified transcellular chaperone signalling (TCS) as one such cell-non-autonomous stress response mechanism that mediates the activation of protective chaperone expression from one tissue to another. TCS can be induced by tissue-specific knockdown of the major molecular chaperone Hsp90 in the gut. This creates mild stress in the gut which then “signals” to the muscle and other tissues to upregulate Hsp70 expression (Fig. 1A and 1B).

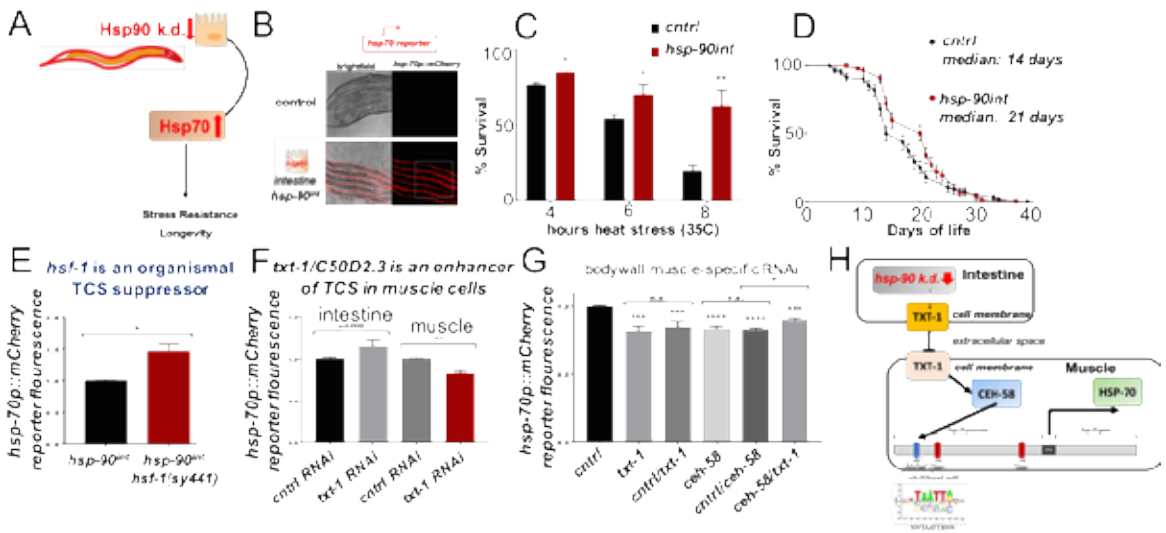

Figure 1: Intestine-specific Hsp90 knockdown results in cell-non-autonomous upregulation of *hsp-70* expression and increases organismal stress resistance and lifespan. A) Schematic of transcellular chaperone signaling induced by gut-specific knockdown of Hsp90. B) *hsp-90* hairpin RNAi in the intestine induces *hsp-70* red fluorescent protein (RFP) reporter expression in the muscle. C) Heat-stress survival of *hsp-90*^{int} animals exposed to a 10-hour heat shock at 35 °C is increased. D) Lifespan of *hsp-90*^{int} is enhanced (median lifespan 21 days) compared to control animals (median lifespan 14 days). E) *hsf-1* acts as a suppressor of TCS. F) Muscle-specific but not intestine-specific *txt-1* RNAi reduces TCS. G) Double RNAi of *ceh-58* and *txt-1* in muscle cells does not further modify TCS-induced *hsp-70* expression, indicating that both components function in the same pathways. H) Model of the regulation of TCS signaling components from the gut to the muscle. *hsp-90* knockdown in the intestine leads to activation of membrane-associated TXT-1 in the intestine, where it suppresses *hsp-70* induction. This leads to activation of TXT-1 and the transcription factor CEH-58 in the muscle (by an unknown signal) where they function as facilitators of TCS-induced *hsp-70* expression. The *hsp-70* promoter contains a CEH-58 binding motif (blue), in addition to the two heat shock elements recognized by HSF-1 (red).

TCS-induced Hsp70 upregulation is sustained throughout aging and protective for the entire organism, as it increases heat stress resistance and extends lifespan (Fig. 1C and D).

Surprisingly, TCS-induced *hsp-70* expression does not require the master regulator of the cytosolic heat shock response (HSR), heat shock transcription factor HSF-1. In fact, using an *hsf-1* mutant shows that HSF1 acts as a suppressor of TCS (Fig. 1E). Using a combinatorial approach of whole-animal transcriptome analysis, forward genetic screening and tissue-specific RNAi, we have identified the conserved PDZ domain protein C50D2.3, an orthologue of the human membrane associated guanylate cyclase MAGI1, that we named *txt-1* (tcs-(x)cross-tissue); and the homeobox transcription factor *ceh-58* as important mediators of TCS from the gut to the muscle (Fig.1F-1H). Our data show that activation of TCS in the gut requires *txt-1* and *ceh-58* to interact in the muscle in order to upregulate *hsp-70* expression in the same tissue (Fig. 1G). Indeed, *hsp-70* contains a CEH-58 binding motif in its promoter that potentially facilitates CEH-58 driven upregulation of *hsp-70* in the muscle (Fig 1H). Interestingly, *txt-1* functions as a suppressor of TCS in the intestine and as an enhancer in the muscle (Fig. 1F), suggesting that *txt-1* is differentially regulated dependent on tissue-type context (i.e., muscle versus gut). We are currently investigating how TXT-1 receives its input in the muscle to activate CEH-58 as a downstream effector to promote enhanced survival and lifespan.

Publications

Miles J. and van Oosten-Hawle P. (2020) Tissue-specific RNAi tools to identify components for systemic stress signaling. *J Vis Exp* **e6**:1357

Funding

We are grateful for support from the NC3Rs, and a BBSRC and MRC doctoral studentship.

Collaborators

University of Leeds: David Westhead.

The Shutdown State of Smooth Muscle Myosin and other stories

Charlotte Scarff, Glenn Carrington, David Casas-Mao, Neil Ranson, Peter Knight, Alistair Curd, Brendan Rogers, Ruth Hughes, Christian Tiede, Chi Trinh and Michelle Peckham

Introduction

Myosin is a molecular motor that moves along and re-organises the actin cytoskeleton, using ATP as an energy source. In muscle, the main form of myosin (class 2) is hexameric, consisting of two heavy chains and four light chains (two essential and two regulatory). The heavy chain forms the motor domain, which binds nucleotide and actin; the lever, which binds essential and regulatory light chains; and a coiled-coil tail, which binds to other myosin molecules to form thick filaments. In skeletal and cardiac muscle, almost all the myosin is assembled into thick filaments. When the muscle is activated, the motor domain interacts with actin in the adjacent thin filaments to contract the muscle. Between contractions, most of the motor domains are folded back along the filament, such that the two heads interact (interacting head motif), and energy consumption is low. In smooth muscle and non-muscle cells, formation and remodelling of thick filaments is more frequent. Isolated myosin molecules (not in the filament) adopt a shutdown state in which not only do the two heads interact, but in addition, the coiled-coil tail wraps around the motor domains. The energy consumption of these molecules is very low. Phosphorylation of the regulatory light chain activates the myosin, releasing it from its shutdown state and allowing it to form filaments and interact with actin.

Although previous work using negative stain electron microscopy generated a low-resolution structure that showed the overall conformation of the shutdown state of smooth muscle myosin, we did not know how phosphorylation of the regulatory light chain activated it. To address this question, we used Cryo-EM, image analysis and molecular modelling to solve the structure of the shutdown state and reveal how phosphorylation activates the molecule.

Results and Discussion

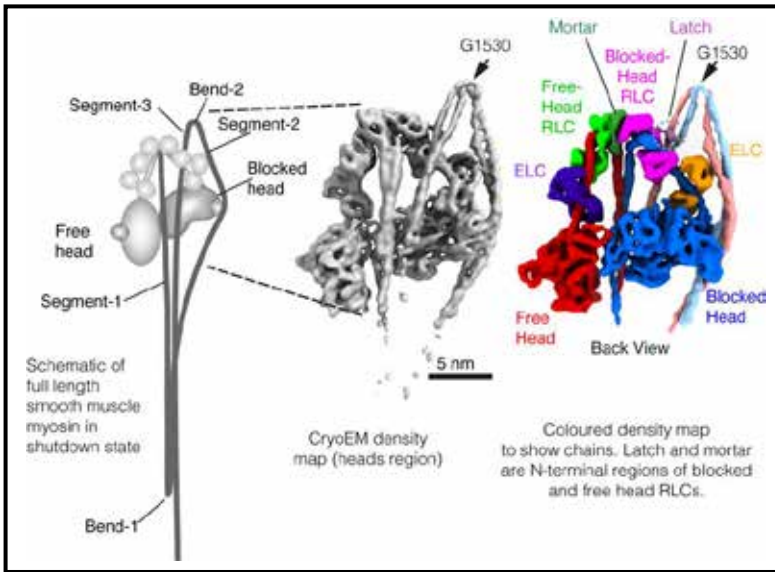

Figure 1: The coiled-coil tail of smooth muscle myosin wraps around the free and blocked heads as shown in the schematic. The cryo-EM density map reveals the detail of interactions between the coiled coil and the heads. Density for the N-terminal region of the blocked head regulatory light chain (RLC) (latch, coloured dark purple) and free head RLC (mortar, coloured dark green)) reveals their positions in the shutdown state.

We used CryoEM, image processing and molecular modelling to obtain a structure of the shutdown smooth muscle myosin, with a resolution of 6Å in the region of the heads (Figure 1). The N-terminal region of the regulatory light chains contains the phosphorylatable serine (S19), phosphorylation of which activates the myosin. The structure of this region had not been seen. Density attributable to the N-terminal region of the blocked head (latch) and free head (mortar) RLC is seen in our structure. The latch interacts with segment-3 of the coiled coil (Fig. 1). The mortar lies between the two RLCs, sandwiching them together. Phosphorylation likely ablates these interactions through charge repulsion revealing how phosphorylation releases the molecule from its shutdown state.

The new structure also reveals how interactions between the coiled-coil tail and the blocked head, and between the two heads, stabilize the shutdown state. We also found that the levers retain their structure in the shutdown state, which means the two heads are ready to generate force as soon as the molecule is activated. The structure of the shutdown state is common to other class 2 myosins and provides additional new insight into the effects of disease mutations.

In other work, we have continued our work on super-resolution imaging, and developed novel software that uncovers patterns of molecular organization using super-resolution datasets. We used this new software to show the pattern of organization of nuclear pore proteins and DNA origami structures (Figure 2), as well as the arrangement of α-actinin in the Z-disc of cardiac muscle cells. This new approach will be invaluable in uncovering the molecular organization of proteins using super-resolution imaging.

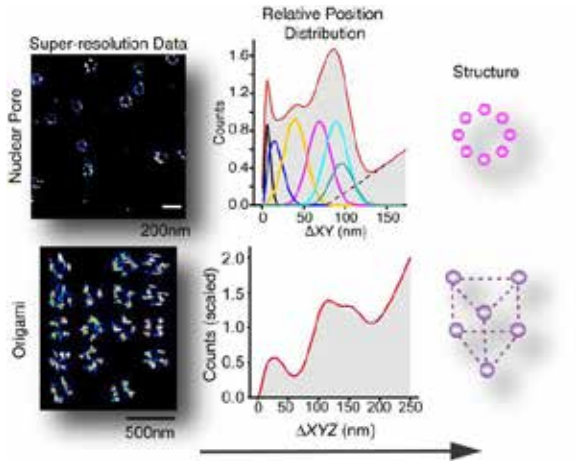

Figure 2: Finding patterns in super-resolution imaging data. dSTORM datasets for Nup107 in the nuclear pore, or for DNA origami were analysed to find the underlying structure.

Publications

Scarff C.A., Carrington G., Casas-Mao D., Chalovich J.M., Knight P.J., *et al.* (2020) Structure of the shutdown state of myosin-2. *Nature* **588**:515-520.

Parker F., and Peckham M. (2020) Disease mutations in striated muscle myosins. *Biophys Rev* **12**, 887-894

Parker F., Baboolal T.G. and Peckham M. (2020) Actin mutations and their role in disease. *Int J Mol Sci* **21**:3371.

Ketchen S., Rohwedder A., Knipp S., Esteves F., Struve N., *et al.* (2020) A novel workflow for three-dimensional analysis of tumour cell migration. *Interface Focus* **10**:20190070.

Cuvertino S., Hartill V., Colyer A., Garner T., Nair N., *et al.* (2020) A restricted spectrum of missense KMT2D variants cause a multiple malformations disorder distinct from Kabuki syndrome. *Genet Med* **22**:867-877.

Funding

This work was funded by BBSRC, MRC and the Wellcome Trust.

Collaborators

University of Leeds: Joanna Leng (Computing), Colin Johnson (FMH)
External: Hari Shroff & Yashuharu Takagi (NIH, USA), Thomas Schlichthaerle & Ralph Jungmann (MPI, Munich, Germany), Christian Sieben & Suliana Manley, (EPFL, Switzerland), Jonas Ries (EMBL, Germany), Anke Brunning-Richardson (Huddersfield), Joe Chalovich (East Carolina University, USA)

Interrogating structural dynamics of mechanosensitive membrane proteins by pulsed EPR spectroscopy

Benjamin J. Lane, Yue Ma, Andrew M. Hartley, Bolin Wang, James Ault, Frank Sobott, Antonio N. Calabrese, Antreas Kalli and Christos Pliotas

Introduction

Pulsed EPR methods such as Pulsed Electron–Electron Double Resonance (PELDOR, or DEER) and Electron Spin Echo Envelope Modulation (ESEEM) have emerged as powerful tools in the study of membrane proteins (Table 1). PELDOR spectroscopy can measure distances (2 –16 nm) between unpaired electrons introduced to selected sites of proteins allowing an assessment of protein conformation, folding, oligomerisation and dynamics. ESEEM spectroscopy can be used to measure solvent (deuterium) and lipid (phosphorus) accessibility at the single residue level, allowing structural biologists to probe the secondary structure and the local environment of proteins. Both methodologies can be performed in an unsurpassed variety of conditions, including a range of lipids and solubilizing agents.

Table 1: Membrane proteins studied by PELDOR, adopted from [1]

Protein family	Protein	Ref.	Protein
ABC transporters	TAP	21	TM287/288
	TAPL	22	MsbA
	MalE-FGK$_2$	31-34	BtuCD-F
	MccJD	23	
Multidrug transporters	P-glycoprotein	48-51	LmrP
	EmrE	40	BmrCD
	NorM	43,44	MdfA
	LmrA	46	
Secondary transporters	TmrAB	211	Glt$_{Ph}$
	SLC26	69,213	FeoB
	LeuT	62-65	OxlT
	NhaA	215	PutP
	PepT$_{So}$	216	BetP
	PepT$_{St}$	216	vSGLT
	Mhp1	217	CaiT
	ExbB	126	LacY
	ExbD	126	ClC-ec1
	TonB	121,127,220	
GPCRs	Rhodopsin	72-74,77,78	Bacterio-rhodopsin
	Rhodopsin-arrestin	75,76	Sensory rhodopsin
	Gloeobacter rhodopsin	79	Proteo-rhodopsin
	Channel-rhodopsin 2	82	AT1R
	β2-adrenergic receptor	70	
Ion channels	KcsA	83-87	CorA
	GLIC	223,224	ELIC
	mVDAC1	109	VDAC2
	Na$_v$Sp1	88	BacNa$_v$
	KvAP	90	HCN2
	KCNE1	91,92	M2
	MscL	11,14,94,97	MscS
Photosynthetic proteins	LHCII	98-102	Photosystem II
	Photosystem I	104	Photosynthetic reaction centre
Mitochondrial proteins	Bax	111-113	Bak
	V-ATPase	107	Complex I
	F0-F1 ATP synthase	108	*Hs*DHODH
Outer membrane proteins	Omp85	118	FecA
	OmpA	117	BtuB
	Wza	116	FhuA
Peptides	Colicin A	231,232	Gramicidin A
	Melittin	236-238	Alamethicin
	Sticholysin I	243	Zervamicin
	α-synuclein	245,246	K and E peptides
	WALP peptides	249-251	β-peptides
Receptors	SRII/HtrII	253	GluN1-GluN2B (NMDA)
	GluA2 (AMPA)	132	EGFR
	TCRα (peptide)	193	
Others	HIV-1 gp41	134	YgaP
	Sec translocon	135	GlpG

The crystal structure of the MscL channel from M. *tuberculosis* (Tb) is used as a structural model for interpreting experimental observations in other MscL orthologs, including *E. coli* (Ec) MscL (Fig 1). Although the structural architecture is expected to be very similar, TbMscL and EcMscL display significant functional differences. Experimental observations and studies of the transmembrane domains of these channels, were rationalized using the TbMscL structure in computationally derived homology models based on sequence alignments. Hydrophobic pockets have previously been identified between transmembrane helices in MscL. These pockets are sensitive to lipids moving in and out and play an important role in the gating mechanism of MscL. It was hypothesized that observed functional differences were associated with structural difference localized to this region. The pockets of EcMscL and TbMscL were modified and PELDOR and ESEEM were employed to investigate channel structure within lipid environment. Structural comparisons suggest EcMscL adopts a more compact structure due to a TM helix rotation. This has implications for the extrapolation between MscL orthologues and provides a possible explanation for observed functional differences.

Eukaryotic mechanosensitive channels are multimodal and regulated both by tension changes in the membrane and molecular triggers. However, it is not understood whether tension and molecular activation present mechanistic similarities, and whether such mechanisms have evolved *via* converged structural plasticity. Disruption of lipid access *via* modification of tension-sensitive pockets in MscL has previously been shown to cause a structural and functional response. However, it is unknown whether there is a structural correlation between tension mediated and molecular activation in MscL. We hypothesized that there is a structural

correlation between the physiologically relevant tension activated MscL state, and the molecularly stabilized one. A molecular activated state was stabilized *via* modification of the MscL pockets and a tension-activated state was generated by molecular dynamic simulations. We then combined untargeted (HDX-MS) and single-residue (3pESEEM) solvent accessibility measurements to interrogate whether there is a mechanistic link between the two states. We found these states to be structurally analogous, suggesting an intimate relationship between the two activation mechanisms.

Results and Discussion

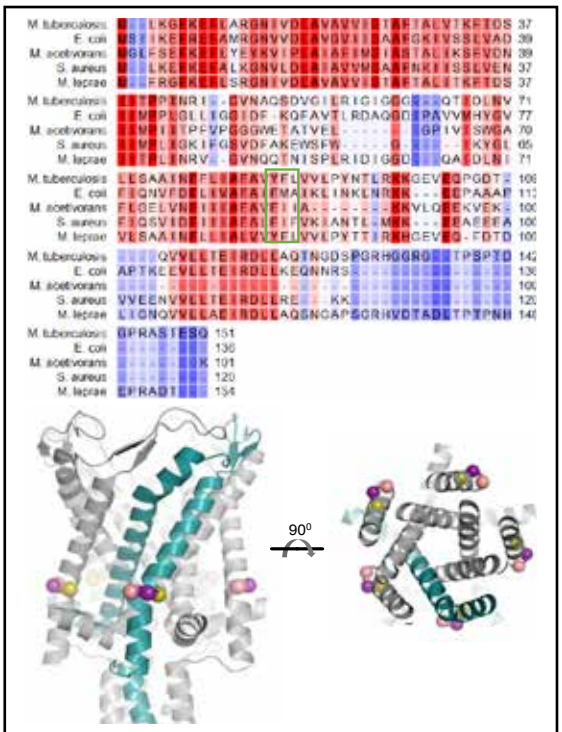

Figure1: Protein sequence alignment of MscL orthologs. TbMscL monomer is shown in cyan, Y87 in olive, F88 in purple, and L89 in salmon spheres.

EcMscL F93C and M94C were generated and the equivalent by sequence alignment transmembrane residues in TbMscL were identified, EcM94 corresponds to TbF88 and EcF93 to TbY87. In-lipid (NDs) PELDOR distance distributions showed that EcF93 structurally agrees with TbF88 and EcM94 with TbL89. ESEEM was then used to investigate solvent exposure. Following reconstitution into NDs, deuterium accessibility increased for TbMscL and reduced for EcMscL mutants. These measurements allowed a structural alignment of these two orthologous MscL channels within their critical, and sensitive to tension, pocket domains. The data is consistent with a helical rotation of TM2 in EcMscL relative to TbMscL. This has implications for the analysis of studies using models based on the sequence alignment of these variants and could provide an explanation for the differences in their functional behaviour.

An expanded sub-conducting state of MscL was stabilized by a modification at the entrance of the pockets (molecular trigger). Regions of MscL undergoing major structural rearrangements were highlighted using HDX-MS. Differences in deuterium uptake allowed us to identify regions to investigate at a higher resolution using ESEEM. Cysteine mutations were paired with the L89W to allow solvent accessibility measurements at the single-residue level. Solvent accessibility increased within the vapour lock residue V21, consistent with a pore hydration, while consecutive residues 70-73 showed changes in accessibility, consistent with a TM2 rotation. In order to mimic the tension-activation of MscL, we applied tension to lipid bilayers by MD. The channel underwent large conformational changes reaching an overall RMSD of ~14 Å compared to the initial closed structure accompanied by pore hydration. Comparison of the tension-activated and molecularly stabilized state showed they were structurally analogous, suggesting a similar gating mechanism.

Publications

Kapsalis C., Ma Y., Bode B.E. and Pliotas C. (2020) In-lipid structure of pressure-sensitive domains hints mechanosensitive channel functional diversity. *Biophys J* **119**:448-459.

Funding

This work was funded by the BBSRC, the Wellcome Trust and the University of Leeds

Collaborators

C Kapsalis, H El Mkami, BE Bode (University of St Andrews)

A Master Regulator for Function and Toxicity in Alpha-Synuclein

Sabine Ulamec, Ciaran Doherty, Roberto Maya-Martinez, Sarah Good, Patricija van Oosten-Hawle, Nasir Khan, David Brockwell and Sheena Radford

Introduction

The protein alpha-synuclein (αSyn) is associated with neurodegenerative disorders such as Parkinson's disease, affecting more than 10 million people worldwide. The function of αSyn is not fully understood, but it has been shown to interact with membranes and to be involved in vesicle binding and remodelling. The aggregation of αSyn into oligomers and/or amyloidogenic fibrils, can be toxic for dopaminergic neurons resulting in cell death and disease. How and why αSyn aggregates on a molecular basis is not clarified.

αSyn is a 140-residue, intrinsically disordered protein that can be divided into three distinct regions: the N-terminal region (involved in lipid binding), the NAC region (highly aggregation prone, forming the fibril core of all solved fibril structures to date) and the C-terminal region which is highly acidic and responsible for intramolecular interactions that protect αSyn from aggregation (Fig. 1). Although the NAC region is known to be important in amyloid formation, recent studies have highlighted a crucial role of other regions for aggregation. In order to better understand the effect of the αSyn protein sequence on aggregation and function, we have engineered αSyn variants which lack amino acids in two segments of the N-terminal region that we predicted to be important in aggregation based on their sequence properties. *In vitro* and *in vivo* experiments indicate that these regions indeed play a significant role in modulating fibril formation, as well as being crucial for functional membrane remodelling.

Results and Discussion

In silico aggregation and hydrophobicity calculators were used to identify aggregation-prone regions within the αSyn sequence (Fig. 1, top left). Besides the NAC region, three motifs in the N-terminal region were found to be aggregation prone (residues ^{1}MDVFMKGL^{7}, ^{36}GVLYVGS^{42} (named P1) and ^{45}KEGVVHGVATVAE^{57} (named P2)). Whilst the N-terminal segment already has been analysed in detail, little was known about the P1 and P2 regions. αSyn deletion variants, lacking P1 (ΔP1), P2 (ΔP2) or both motifs (ΔΔ) were engineered and characterised to understand the role of these segments in αSyn aggregation and in its function in membrane remodelling in more detail.

An *in vitro* aggregation assay (Thioflavin T assay) clearly demonstrated that deletion of the P1 or P1P2 regions drastically inhibits aggregation (Fig. 1, top right). While the WT protein forms fibrils after 11 h (pH 4.5) or 60 h (pH 7.5), the deletion of both P1 and P2 abolishes aggregation for at least 100 h. ΔP1 shows a strong pH dependence with a lag-time of 20 h at pH 4.5 and no aggregation at pH 7.5. The inhibitory effect of the αSyn variants was also confirmed *in vivo* using the model organism *C. elegans* expressing αSyn C-terminally attached to YFP (Fig.1, bottom left). Whilst nematodes expressing αSyn WT form puncta/insoluble aggregates, show a higher mortality and phenotypic effects after three days, nematodes expressing ΔP1 or ΔΔ show little aggregation and the organisms remain healthy for up to 13 days.

Paramagnetic relaxation experiments (PRE) using NMR were performed to gain insight on the transient interactions of αSyn *in vitro* that might contribute to fibril formation (Fig. 1, middle). The WT protein forms intra- and inter-molecular interactions with the P1 and P2 regions. These interactions are absent in the ΔΔ variant, while other interactions are preserved. This indicates that transient contacts with P1 and P2 are crucial for aggregation. Finally, the role of the P1 and P2 motifs for the physiological function of αSyn was tested *in vitro* using DMPS liposomes. While aggregation of αSyn WT is more rapid in the presence of these liposomes, the ΔΔ variant only shows little fibril formation under these conditions. Further, as shown by transmission electron microscopy and previously described in the literature, in the presence of an excess of liposomes, WT αSyn remodels the DMPS liposomes forming lipid tubes. Interestingly, the deletion of P1P2 abolished this functional activity, instead, smaller, pre-fibrillar aggregates were formed.

In summary, the studies have shown that the P1 and P2 motifs in the N-terminal region of αSyn are 'master regulators' of its aggregation and function. This fine balance between toxicity and function might explain why P1 and P2 have not been removed through evolution. Future experiments will focus on which residues play significant roles in controlling aggregation and in modulating function, with a view to deriving new strategies to combat Parkinson's disease.

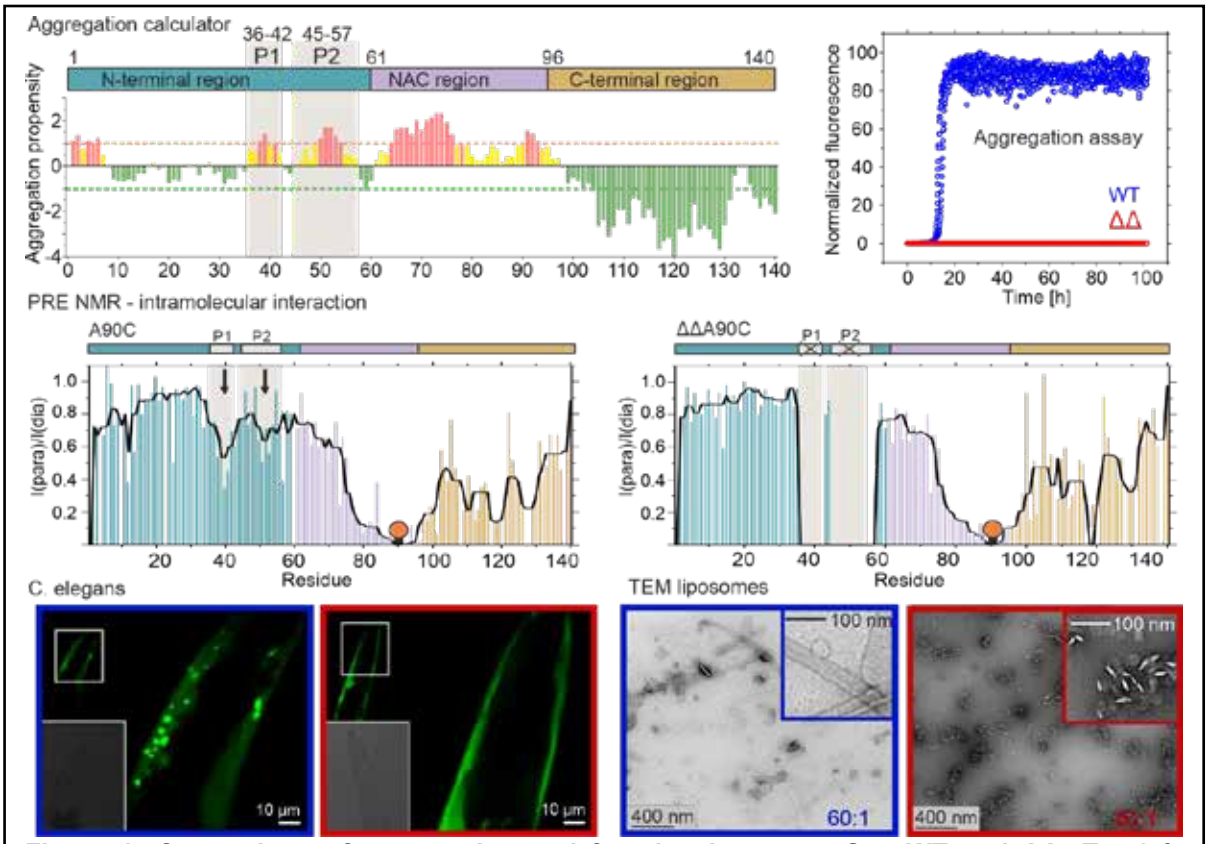

Figure 1: Comparison of aggregation and function between αSyn WT and ΔΔ. Top left: Zyggregator score to identify aggregation-prone regions within αSyn sequence. Top right: Thioflavin T assay to detect *in vitro* aggregation at pH 4.5. Middle: PRE NMR measurements with spin label at position A90C (orange circle) at pH 4.5 to identify intramolecular long-range interactions in WT αSyn and ΔΔ. Bottom left: *In vivo* aggregation in *C. elegans* at day 11. Puncta can be observed in nematodes expressing αSyn WT (blue outline) but not in ΔΔ (red outline). Bottom right: TEM images of αSyn WT (blue outline) and ΔΔ (red outline) after incubation with DMPS liposomes for 100 h in a 60:1 (lipid: protein) molar ratio. Tube formation is observed for WT αSyn, but not for ΔΔ.

Publications

Doherty C.P.A., Ulamec S.M., Maya-Martinez R., Good S.C., Makepeace J., *et al.* (2020) A short motif in the N-terminal region of alpha-synuclein is critical for both aggregation and function. *Nat Struct Mol Biol* **27**:249-259.

Ulamec S.M., Brockwell D.J. and Radford S.E. (2020) Looking beyond the core: The role of flanking regions in the aggregation of amyloidogenic peptides and proteins. *Front Neurosci* **14**:611285.

Funding

European Research Council, Wellcome Trust, BBSRC and N3CR.

Investigating the mechanism of SusCD-like TonB-dependent transporters using cryo-electron microscopy

Joshua White, Shaun Rawson and Neil Ranson

Introduction

The Gram-negative Bacteroidetes are abundant members of the human microbiota. Primarily occupying niches devoid of small, easily accessible nutrients, these bacteria must import larger, more complex substrates for survival. Translocation of these molecules across the bacterial outer membrane is an energy-dependent process which, in Bacteroidetes, is facilitated by an outer membrane protein complex comprising a TonB-dependent transporter (TBDT) and a substrate binding lipoprotein. X-ray crystal structures of these transport complexes, often referred to as SusCD-like systems, after the archetypal starch utilisation system, have revealed a dimeric arrangement in which two TonB-dependent transporter components are tightly capped by their associated lipoprotein subunits; trapping substrate in a solvent excluded cavity. However, the mechanistic details of substrate capture remained unclear.

Our recent work has focussed on the RagAB complex, a SusCD-like transporter from the asaccharolytic Bacteroidete, *Porphyromonas gingivalis.* RagAB acts as an importer for protease-generated peptides which are required for growth. Given that *P. gingivalis* is a keystone pathogen with a critical role in the development of periodontitis, understanding the molecular basis of nutrient acquisition that allows it to thrive below the gum line is an important goal.

Results and Discussion

Using single-particle cryo-EM our group has investigated the structure of the RagAB complex. Three distinct conformational states were reconstructed from the data (Figure 1). A closed-closed state, consistent with a previously determined RagAB crystal structure, and two novel states in which either one or both RagB subunits occupy an open position, flipped up and away from the barrel of its corresponding TBDT subunit.

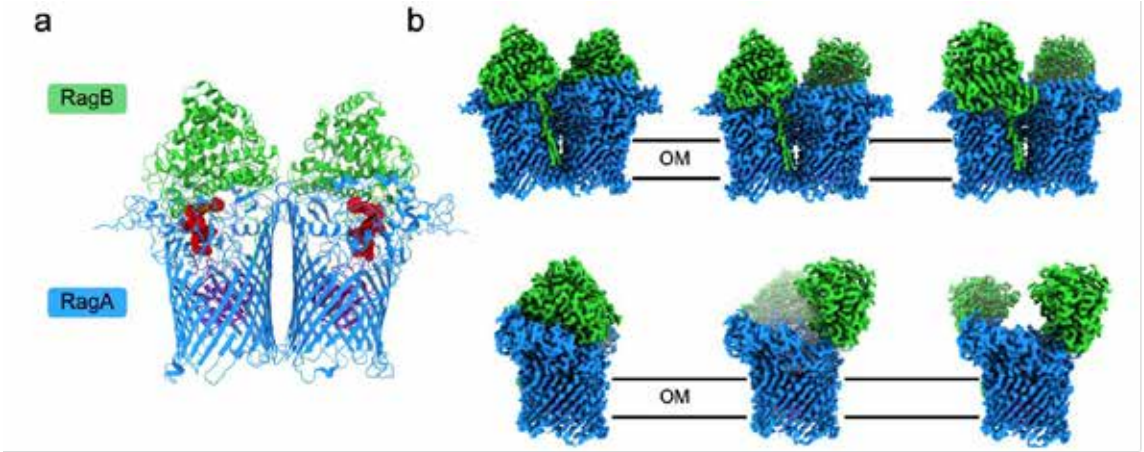

Figure 1: Different conformations of the RagAB transporter revealed by cryoEM. **a,** X-ray crystal structure of the RagAB complex. RagA possesses a plugged barrel architecture characteristic of all TBDTs. The peptide substrate (red) is trapped between the RagB lid (green) and the plug domain of RagA (purple). **b,** cryo-EM maps of RagAB revealing three unique conformational states of the complex: closed-closed (left), open-closed (middle) and open-open (right). These maps were resolved to 3.3 Å, 3.3 Å and 3.4 Å repectively.

Translocation of substrate through TBDTs requires disruption of the plug domain that occludes the barrel lumen. This is achieved through interaction with TonB, a member of the TonB subcomplex located in the inner membrane. This complex functions to transduce energy in the form of the proton motive force to power TonB-dependent transport at the outer

membrane. Current models for TonB-dependent transport propose that substrate binding at the extracellular face of the transporter induces a conformational change that is propagated through the plug domain and results in disordering of a TonB box region at the periplasmic face of the transporter. The disordered TonB box region is responsible for interaction with TonB and can therefore be considered a signal, ensuring that only substrate-loaded transporters form productive complexes with TonB, avoiding futile transport cycles.Assuming lid closure is an essential step in the translocation process, the open-closed structure allows us to compare two conformational snapshots of the translocation cycle.

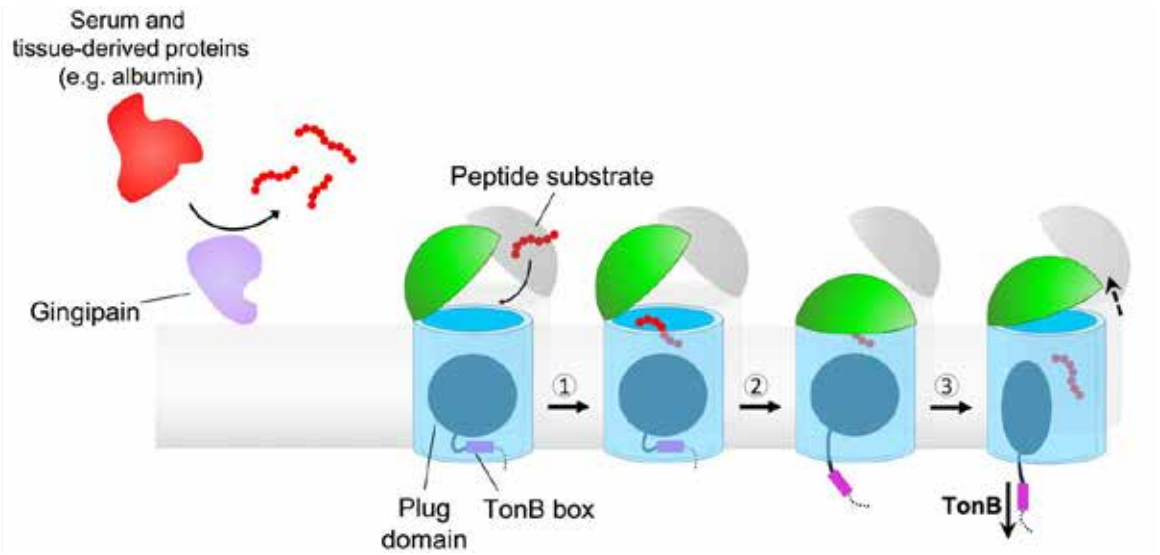

Figure 2: A proposed pedal-bin mechanism for substrate capture and translocation by RagAB. Peptide ligands to be imported by the RagAB system are predominantly generated by the action of gingipains (cysteine endoproteases) on serum and tissue-derived proteins. **1.** A lid-open state of RagAB permits peptide binding. **2.** Contributions from both RagA and RagB to peptide binding elicits closure of the lid, forming the transport competent state of the complex. This is signalled across the OM by perturbation of the TonB box region on the periplasmic side of the plug domain, making it accessible to TonB. **3.** According to the literature consensus, TonB-mediated disruption of the plug permits substrate translocation and a return to the open state of RagAB.

Alignment of the plug domains from the open and closed subunits revealed that the overall architecture of the plug is not grossly affected by lid closure. However, the TonB box region is visible only in the open state where it is positioned well within the barrel, apparently inaccessible to TonB. This region is not visible in the closed state and is assumed to be disordered, more mobile and, as a result, accessible to TonB. Taken together, this work provides direct structural evidence for a 'pedal-bin' mechanism of nutrient uptake by the SusCD-like family of transporters (Figure 2).

Publications

Madej M., White J.B.R., Nowakowska Z., Rawson S., Scavenius C., *et al.* (2020) Structural and functional insights into oligopeptide acquisition by the RagAB transporter from *Porphyromonas gingivalis*. *Nat Microbiol* **5**:1016-1025.

Funding

This work was supported by a Wellcome Trust 4 year PhD studentship and a Wellcome Trust equipment grant

Collaborators

External: Marius Madej, Bert van den Berg, Jan Potempa.

Basis for surface-templated amyloid growth revealed by the structures of Type-2 Diabetes amyloid IAPP and its early-onset variant S20G

Rodrigo Gallardo, Matthew Iadanza, Yong Xu, George Heath, Richard Foster, Sheena Radford and Neil Ranson

Introduction

Amyloid aggregation is the histopathological hallmark of more than 50 human diseases, most of which have no medical treatment. Type 2 Diabetes (T2D) is one such disease, affecting >400 million people across the world. In T2D the peptide hormone Islet Amyloid PolyPeptide (IAPP) aggregates generating long, insoluble amyloid fibrils that accumulate in the Islets of Langerhans, which leads to death of insulin-secreting β-cells. The mechanistic link between IAPP aggregation and deposition, β-cell death and T2D is not clear. However, the discoveries that the S20G mutation in IAPP is associated with an early-onset phenotype of T2D, and that this variant aggregates more rapidly than the wild-type hormone *in vitro* support a role for amyloidogenic aggregation in the pathophysiology of T2D. Understanding the structure that amyloid fibrils acquire explains the intrinsic properties and interactions that stabilise these pathological agents, but also reveals which surfaces and moieties are available for deleterious interactions with cellular and extracellular components that characterise the disease. Moreover, a direct comparison with the structure of a disease-related mutation might explain the role of sequence variation in accelerating the disease.

Results and Discussion

In this work we used Transmission Electron Microscopy (TEM), Atomic Force Microscopy (AFM), and cryogenic-Electron Microscopy (cryo-EM) to determine the structures of amyloid fibrils formed by IAPP and its variant S20G. The peptide hormones were synthesised in house by FMOC-SPSS tailored for aggregating peptides, and purified to homogeneity by HPLC. The mass and oxidation state of the peptides was confirmed by HPLC MS-MS analysis. Peptides were subjected to amyloidogenic aggregation *in vitro* and the macromolecular characteristics of the fibrils formed where determined by TEM. This analysis indicated that the majority of wild-type fibrils in the preparation were similar, with a 25 nm cross-over length, while the S20G fibril preparation was more heterogeneous, with several fibril morphologies observed of which a predominant polymorph was characterised by a 50 nm cross-over length. Analysis of the samples by AFM confirmed these observations and allowed us to unambiguously determine the fibrils for both wild-type and S20G to be left-handed. Aliquots of each sample were vitrified on cryo-EM grids and cryo-EM data sets were collected for each sample using the Titan Krios microscopes available at the Astbury Biostructure Laboratory. In agreement with TEM and AFM, the raw data from cryo-EM shows predominant morphology for the wild-type fibrils (80% abundance relative to the all wild-type fibrils imaged by cryo-EM) and at least four different morphologies for the S20G sample (the most abundant polymorph represents 60% of all fibrils imaged by cryo-EM).

Cryo-EM data processing and helical reconstruction was performed using the High-Performance Computing infrastructure available at University of Leeds (ARC4). We solved the structure of the most abundant wild-type fibril at 3.6-Å resolution, which we found to be composed of two protofilaments each built from IAPP monomers adopting an S-shape fold (Figure 1, left). The data for the most abundant polymorph of the S20G variant actually corresponded to two different fibril structures, both of which have the same cross-over length of 50 nm. We solved each of these structures, at 3.9-Å and 4.0-Å resolution, and showed that they share a common two-protofilament core that is distinct from the wild-type structure (Figure 1, right). Remarkably, one of these polymorphs is a novel asymmetric three-protofilament fibril in which the monomers on the third protofilament adopt a distinct cross-β fold to the two core protofilaments. To our knowledge this is the first example of an amyloid fibril where protofilaments of the same fibril adopt different backbone folds. The possibility to adopt different backbone conformations within the same fibril may explain the increased aggregation propensity of S20G and illustrates a potential structural basis for surface-templated fibril assembly.

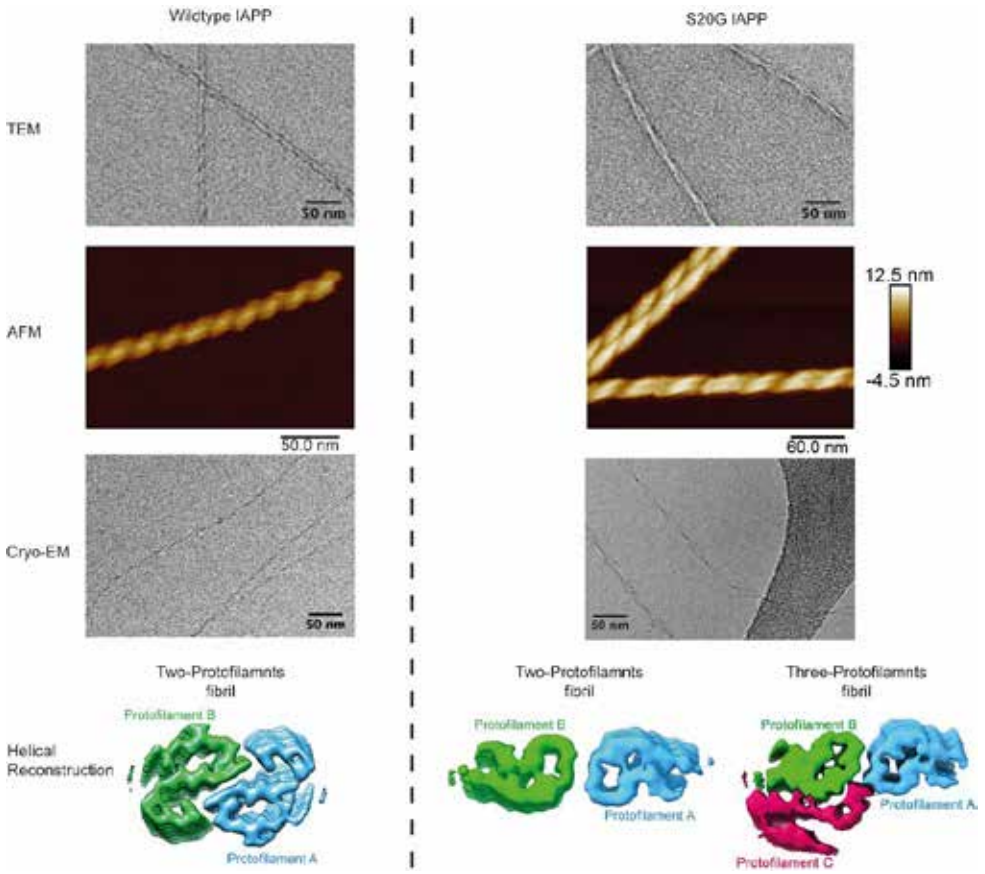

Figure 1

Publications

Gallardo R., Iadanza M.G., Xu Y., Heath G.R., Foster R., *et al.* (2020) Fibril structures of diabetes-related amylin variants reveal a basis for surface-templated assembly. *Nat Struct Mol Biol* **27**:1048-1056.

Gallardo R., Ranson N.A. and Radford S.E. (2020) Amyloid structures: much more than just a cross-beta fold. *Curr Opin Struct Biol* **60**:7-16.

Funding

This work was funded by the Wellcome Trust.

Collaborators

University of Leeds: Andrew Wilson, Frank Sobott and Alex Breeze

A Method to Quantify Molecular Diffusion within Thin Solvated Polymer Films

Rickard Frost, Saikat Jana, Fouzia Bano and Ralf Richter

Introduction

Solvated polymer coatings measuring tens to hundreds of nanometers in thickness find applications in a variety of areas like reconstituted biomolecular films, biomaterials, biosensors, nanomedicine, lubricants, antifouling coatings and separation membranes. Quantifying the molecular transport and interaction processes within these coatings is crucial not only for a deeper understanding, but also for developing the ability to manipulate the functionality of such coatings. Common optical microscopy platforms offer large detection volumes when compared to the thickness of a nanometric film and capture bulk diffusion in the solvent which make them unsuitable for measuring in-film processes (Figure 1A). We overcome this problem by confining polymer films between two surfaces, one planar and the other hemispherical. The plane-sphere contact creates a well-defined nanoscale gap and a region of high signal where molecular diffusion/interaction can be resolved (Figure 1B).

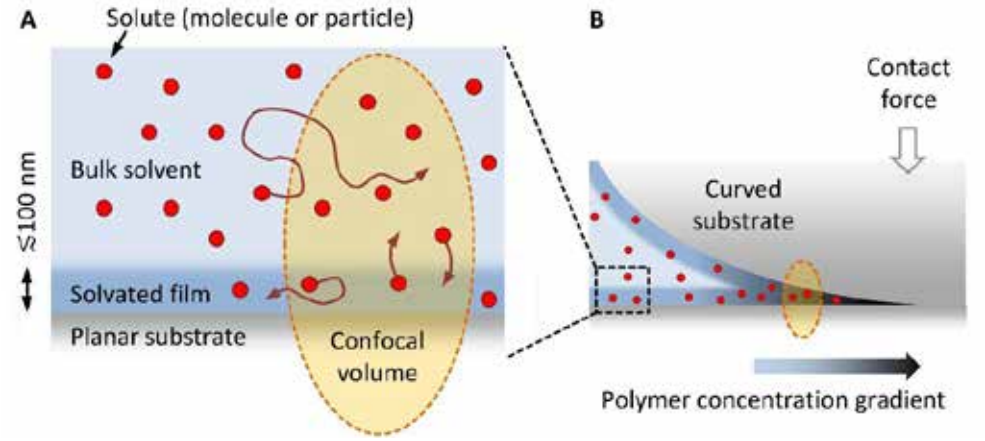

Figure 1: Schematic representation of the problem at hand and the experimental approach. (**A**) Probe solutes (red dots) partition between the bulk solution and a thin, solvated polymer film. They diffuse in these phases with rates D_{bulk} and D_{film}, respectively. The objective is to quantify D_{film}. Because the probe molecules continuously move between the two phases and the polymer film thickness is below the optical resolution limit, it is challenging to separate D_{film} from D_{bulk}. (**B**) By confining the polymer coating(s) between a planar and a curved surface, the bulk solution is excluded in the region surrounding the contact between the two surfaces. This enables optical microscopy to probe diffusion within the polymer film(s), and to quantify the partitioning of probe molecules between the bulk and polymer phases. The gradual compression of the polymer film(s) near the contact point entails a polymer concentration gradient that can be exploited to measure the diffusion and partitioning of probe molecules as a function of polymer film compression and concentration.

Results and Discussion

To demonstrate the use of the technique, which we term plane-sphere confinement microscopy (PSCM), we have studied the mechanisms of protein transport within ultrathin films of FG nucleoporins (FG Nups; Figure 2A). These films serve as a model system of the nuclear pore permeability barrier, a meshwork of intrinsically disordered proteins that fills the central channel of nuclear pore complexes and controls the transport of proteins and nucleic acids across the nuclear envelope of eukaryotic cells.

Nuclear transport receptors (NTRs) are soluble proteins that help shuttle cargo proteins and nucleic acids across the nuclear pore complex. Using a mutant of green fluorescent protein designed to gain NTR-like properties (GFP^{NTR}) as a model transporter, we demonstrate direct quantitation of diffusion coefficients within the FG Nup film by fluorescence recovery after photobleaching (lineFRAP). *Via* fluorescence intensity analysis, we additionally quantify the level of GFP^{NTR} binding into the FG Nup film (Figure 2B). We find that whilst the FG Nup concentration affects diffusion only moderately, it sensitively affects protein uptake.

These data suggest that FG Nups balance their cohesive interactions (and thus their concentration in the nuclear pore) to maximise the selectivity of NTR transport over other

cytosolic proteins. They also open up avenues for further investigations to better understand the physical mechanism underpinning the exquisite permeation selectivity of nuclear pores.

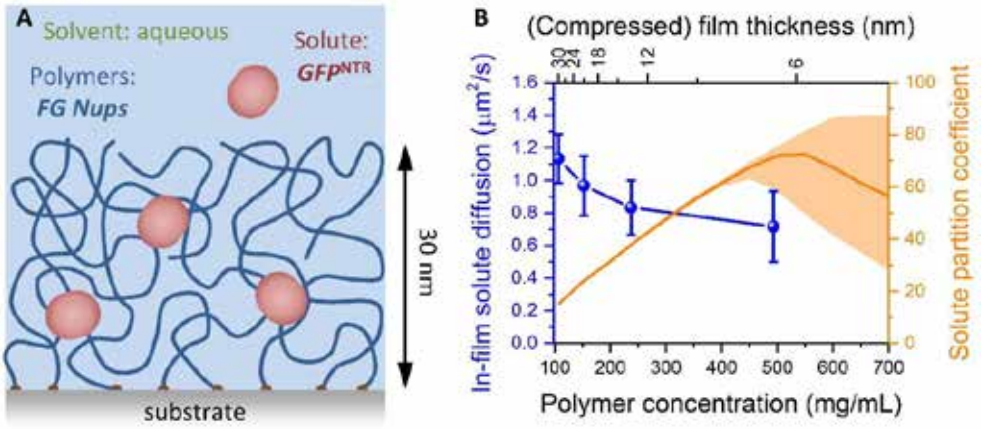

Figure 2: Application example of plane-sphere confinement microscopy (PSCM). (**A**) Ultrathin films of one-end grafted FG nucleoporin domains reproduce the supramolecular organisation (*i.e.* molecular anchorage, density and thickness) of these intrinsically disordered proteins in the central channel of the nuclear pore complex; an NTR-like GFP variant is here used as a model solute. (**B**) PSCM provides the in-film solute diffusion constant and the solute partition coefficient as a function of polymer concentrations, where the latter is spatially controlled by defined compression of the film under plane-sphere confinement.

More generally, PSCM has the potential to catalyse new investigations in the area of thin films and functional coatings; for example, in quantifying the release of active compounds from polyelectrolyte polymer coatings or understanding the diffusivity of viruses through extracellular matrices.

Publications

Frost R., Debarre D., Jana S., Bano F., Schiinemann J., *et al.* (2020) A method to quantify molecular diffusion within thin solvated polymer films: a case study on films of natively unfolded nucleoporins. *ACS Nano* **14**:9938-9952.

Funding

This work was funded by the European Union (European Research Council Starting Grant and Proof of Concept Grant) and the BBSRC.

Collaborators

External: Delphine Débarre (University Grenoble Alpes & CNRS, France), Jürgen Schünemann and Dirk Görlich (Max Planck Institute for Biophysical Chemistry).

Regulation of antimycin biosynthesis is controlled by the ClpXP protease

Bohdan Bilyk, Asif Fazal and Ryan Seipke

Introduction

The survival of any microbe relies on its ability to respond to environmental change. Use of extracytoplasmic function (ECF) RNA polymerase sigma (σ) factors is a major strategy enabling dynamic responses to extracellular signals. *Streptomyces* species harbour a large number of ECF factors, nearly all of which are uncharacterised, but those that have been characterized generally regulate genes required for morphological differentiation and/or response to environmental stress, except for σ^{AntA}, which regulates starter-unit biosynthesis in the production of antimycin, an anticancer compound. Unlike a canonical ECF factor, whose activity is regulated by a cognate anti-σ factor, σ^{AntA} is an orphan, raising intriguing questions about how its activity may be controlled.

Results and Discussion

Here, we used quantitative Western blotting to demonstrate that the abundance of σ^{AntA} *in vivo* was enhanced by changing of the C-terminal Ala-Ala ClpXP recognition sequence to Asp-Asp. We also found that the abundance of σ^{AntA} was elevated in the absence of genes encoding the primary peptidase, ClpP, and its unfoldase, ClpX. We reconstituted *in vitro* ClpXP proteolysis of σ^{AntA} and showed that a variant lacking the C-terminal di-alanine recognition sequence was resistant to degradation, unambiguously establishing that σ^{AntA} is substrate for the ClpXP protease. Figure 1 incorporates these new findings into our existing understanding for the regulation of antimycin biosynthesis.

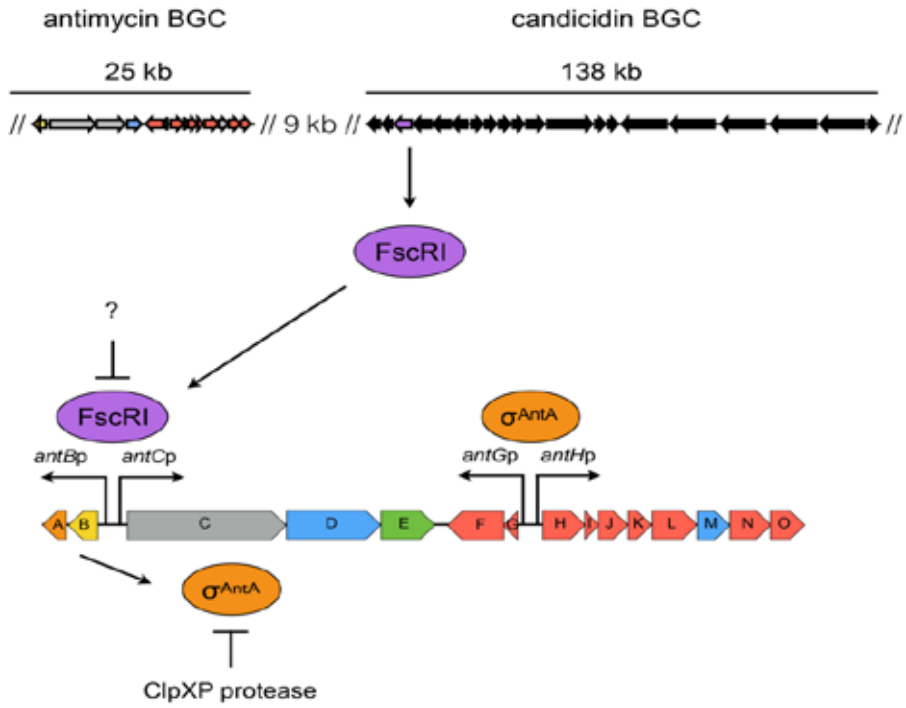

Figure 1: Model for the regulation of antimycin biosynthesis. The upper panel displays the relative locations of the antimycin and candicidin biosynthetic gene clusters (BGCs) in the *S. albidoflavus* chromosome. As shown in the lower panel, FscRI, a LuxR-family regulator, from the candicidin BGC, activates expression of *antBA* and *antCDE*. This in turn enables direct activation of the 3-formamidosalicylate biosynthetic operons (*antGF* and *antHIJKLMNO*) by σ^{AntA}. The cellular level of σ^{AntA} is antagonised by the ClpXP-protease system, for which it is a direct target and ultimately responsible for clearing residual σ^{AntA} when FscRI is inactivated following the onset of differentiation.

Overall, we have a poor understanding of how microbial secondary metabolism is regulated. This is a major roadblock that prevents exploitation of natural product biosynthetic pathways for drug discovery. Our findings thus provide a new lens through which to examine microbial signal transduction and the regulation of secondary metabolism in *Streptomyces* species. Understanding the diversity of regulatory strategies controlling the expression of these pathways is critical for the development of new tools for exploiting the 'silent majority' of biosynthetic pathways harboured by these organisms.

Publications

Bilyk B., Kim S., Fazal A., Baker T.A. and Seipke R.F. (2020) Regulation of antimycin biosynthesis is controlled by the ClpXP protease. *Msphere* **5**:e00144-20.

Funding

This work was funded by the BBSRC.

Collaborators

External: Sora Kim and Tania Baker (Massachusetts Institute of Technology)

Aptamer-ligand recognition studied by native ion mobility-mass spectrometry

Elise Daems, Debbie Dewaele, Konstantin Barylyuk, Karolien De Wael and Frank Sobott

Introduction

Aptamers are oligonucleotide sequences that occur naturally as the sensing part of riboswitches, which are regulatory segments of messenger RNA involved in gene expression. These short single-stranded molecules approximately 20-80 nucleotides long with a molecular mass of 6-30 kDa possess specific 3D conformations which enables high-specificity and high-affinity recognition of targets. Aptamers have been designed to target small molecules, peptides, proteins, nucleic acids, and even cells. Their high affinity and specificity render them an attractive alternative to monoclonal antibodies, and there is great interest in their application in diverse fields of biomedicine and analytical science.

The use of aptamers as therapeutic agents has several advantages. First, aptamers can have a superior selectivity, specificity and binding affinity to their targets. Second, aptamers are produced in vitro with high reproducibility and purity, which reduces the production costs. Furthermore, aptamer sequences are generally not targeted by the immune system and are therefore not immunogenic. Finally, aptamers are relatively small, chemically stable, and easy to modify. Thanks to their unique characteristics and multiple advantages, aptamers have seen a recent resurgence as drug targets and biopharmaceutical agents, but they are also used for the detection of environmentally important compounds in sensors.

We have developed a comprehensive analytical toolset based on electrospray ionization coupled with native mass spectrometry (MS) and ion mobility (IM) for the characterization of aptamer structure, stability, ligand affinity and conformational response to ligand binding (Figure 1). We use a set of closely related DNA-based cocaine-binding aptamers, with different known ligand binding affinities, as model compounds for the comparative analysis. Four cocaine-binding aptamers were chosen: MN19, MNS-7.9, MN4 and 38-GC, as well as a randomized sequence (Figure 2). Their structure contains three stems built around a three-way junction, which is the proposed binding pocket. The second stem contains only Watson-Crick base pairs, whereas stems 1 and 3 contain non-canonical base pairs. When aligned, the sequences only differ in their terminal parts and at position 24 of the consensus sequence.

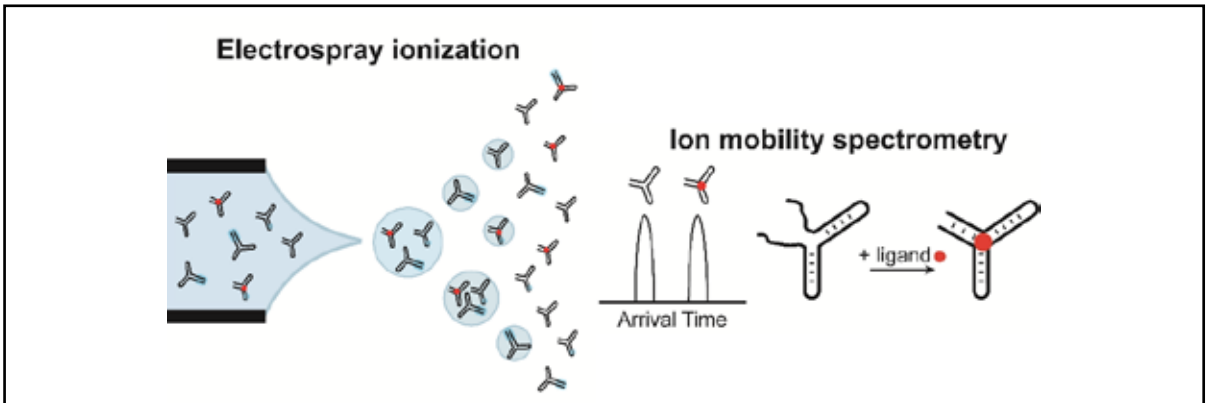

Figure 1: Schematic of the native electrospray ionization - mass spectrometry - ion mobility analysis of aptamer-ligand interactions. Ion mobility measures arrival times which represent the collision cross section of the molecules, i.e. the rotationally averaged size of the aptamer in comparison with the aptamer-ligand complex, thus highlighting conformational change upon binding.

Results and Discussion

In order to investigate ligand binding to the cocaine-binding aptamers, the ligand quinine was chosen because of its higher affinity than cocaine. A 300 mmol/L ammonium acetate buffer solution was selected here for the IM-MS experiments, since an ionic strength of at least 100 mmol/L was found to be necessary to preserve the folded structure. The addition of quinine to

the different oligonucleotide sequences at 1:1 molar ratio resulted in the formation of ligand-aptamer complexes, next to remaining unbound aptamer (Figure 3A). Relative binding affinities can be derived from the peak intensities in native MS, and they are found to follow the trend of K_d values determined by ITC measurements.

Ion mobility measurements indicate conformational changes upon ligand binding, with different percentage increases in arrival time (i.e. overall size) reported (Figure 3B). With increasing length of stem 1 from MN19 to MN4 and 38-GC, the arrival time differences upon complexation showed a downward trend from 6.4 % to 3.9 %, while at the same time binding affinity increased (lower K_d). We propose that the more preformed, "rigid" binding e.g. seen in MN4 requires less structural rearrangement upon complexation (as evidenced by the smaller arrival time changes) accompanied by a higher binding affinity, whereas the adaptive binding suggested for MN19 comes with some structural reorganization and also a lower ligand affinity, possibly due to an entropic penalty. The results obtained with IM-MS are broadly consistent with data in literature obtained with NMR and small-angle X-ray scattering.

In summary, native IM-MS captures trends in ligand affinity and conformational dynamics of increasingly more rigid cocaine-binding aptamers, and highlights the structural reorganization required for the adaptive binding mechanism displayed by short-stem, low-affinity aptamers.

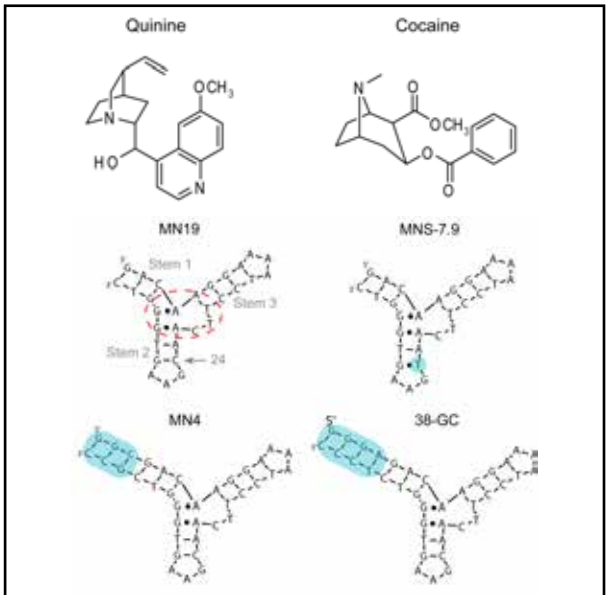

Figure 2: Structures of the cocaine-binding aptamers and quinine and cocaine ligands. Watson-Crick base pairs are indicated with dashes and non-Watson-Crick base pairs with dots. The ligand binding site is indicated with a red circle. Differences in aptamer sequence compared to the MN19 reference aptamer are indicated with a blue background

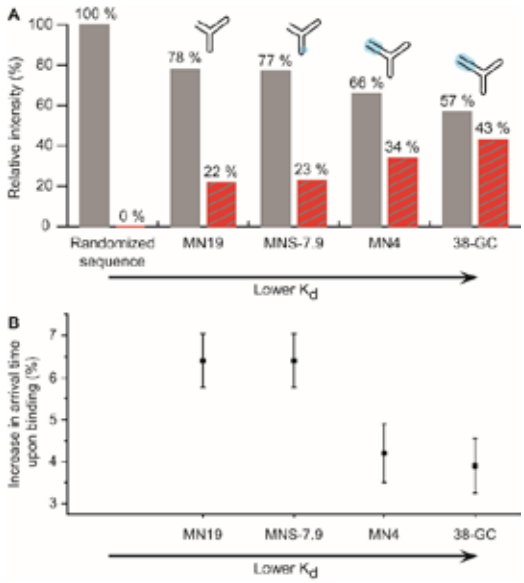

Figure 3: A) Native MS of aptamers MN19, MNS-7.9, MN4, 38-GC and a randomized sequence incubated with quinine at 1:1 molar ratio show the abundance of the apo form (grey) vs. the complex (red).
B) Ion mobility highlights the conformational effects of quinine binding, as the corresponding percentage increase in arrival time

Funding
We thank the FWO - Research Foundation Flanders for funding.

Structural insight into *Pichia pastoris* fatty acid synthase

Joseph Snowden, Jehad Alzahrani, Lee Sherry, Martin Stacey, David Rowlands, Neil Ranson and Nicola Stonehouse

Introduction

Type I fatty acid synthases (FASs) are critical metabolic enzyme complexes that catalyse the synthesis of long-chain fatty acids through iterative cycles of chain elongation. In yeast, FAS is a 2.6 MDa hetero-dodecameric barrel. The growing fatty acid chain is tethered to a mobile acyl carrier protein (ACP) domain, which transfers it between different enzymatic domains that form the walls of the complex. Aside from their physiological role, FASs are also a common focus of bioengineering approaches to generate short-chain fatty acids with industrial importance. To ensure the best chance of success with these approaches, a comprehensive structural and functional understanding of different FAS systems is key.

Serendipitously, we identified FAS as a contaminant in a cryoEM dataset of virus-like particles (VLPs) purified from the yeast *P. pastoris*. To date, no structures have been reported for *P. pastoris* FAS, despite the major practical advantages this strain presents over other yeast strains like *S. cerevisiae*. For example, *P. pastoris* produces relatively little ethanol, making it more tractable to maintain high cell density cultures in fermenters.

Results and Discussion

Through a variety of image processing approaches, we determined the structure of *P. pastoris* FAS to 3.1 Å resolution from this 'contaminant' cryoEM data. The complex had a domain organisation typical of yeast FASs, displaying D3 symmetry with an asymmetric unit comprising one α and one β subunit (Figure1A). Though density for most enzymatic domains was clear, density for the ACP domain was weak and poorly resolved. This was unsurprising, given the mobile nature of the ACP domain. Since cryoEM single particle analysis relies on averaging many particle images, if ACP domains are not held in a fixed position relative to the rest of the complex, density becomes 'blurred' and high-resolution information is lost.

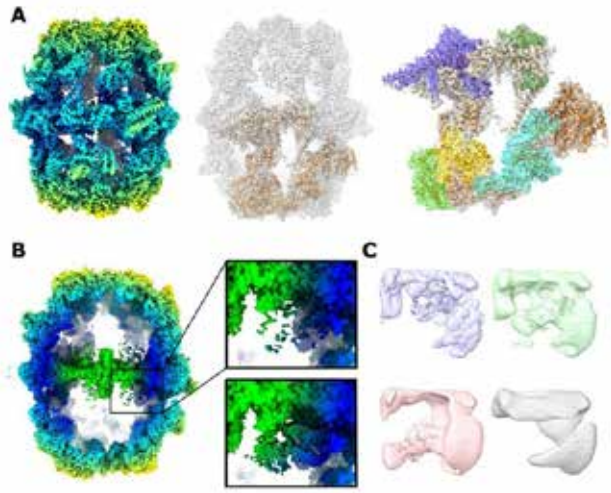

Figure 1: The molecular structure of *P. pastoris* FAS. (A) Cryo-EM structure of *P. pastoris* FAS at 3.1 Å resolution (left). The atomic model for an asymmetric unit is shown fitted to density (centre & right), with density coloured according to enzymatic domain (dark green – ketoacyl reductase, dark blue – ketoacyl synthase, light green – acetyl transferase, yellow – enoyl reductase, light blue – dehydratase, brown – malonyl/palmitoyl transferase). (B) Change in density quality of the ACP domain before (upper inset) and after (lower inset) focussed 3D classification. (C) Representative 3D classes showing putative ACP domain density in different positions.

To overcome this, we employed a focussed 3D classification approach. A mask was applied around the expected position of the ACP domain within the interior of the complex, and all particles in each symmetrically redundant orientation were classified according to the contents of the masked region. We used particles from the best resolved class for asymmetric reconstruction and sharpening, leading to a striking improvement in ACP domain density (Figure 1B). We also identified classes containing putative low-resolution ACP domain density in alternative positions within the complex interior (Figure 1C).

The quality of the density was sufficient for us to build an atomic model for *P. pastoris* FAS. We compared this model with the 'prototypical' yeast FAS structure from the strain *S. cerevisiae* (PDB: 6TA1), and identified numerous differences throughout the complex (Figure 2A). As well as minor changes in non-enzymatic regions of the structure, an additional linker was resolved in *P. pastoris* FAS subunit β between the enoyl reductase and dehydratase domains (Figure 2B,C). We also identified different rotamers for critical active site residues in the acetyl transferase (Q171) and enoyl reductase (H749) domains (Figure 2D). Interestingly, the rotamer displayed by *P. pastoris* FAS for H749 was much better aligned with that seen in a crystal structure of a homologous bacterial enzyme, FabK, in its active state (PDB 2Z6I). While the functional significance of these changes is unclear, this structure should prove a useful resource for future attempts to engineer yeast FAS.

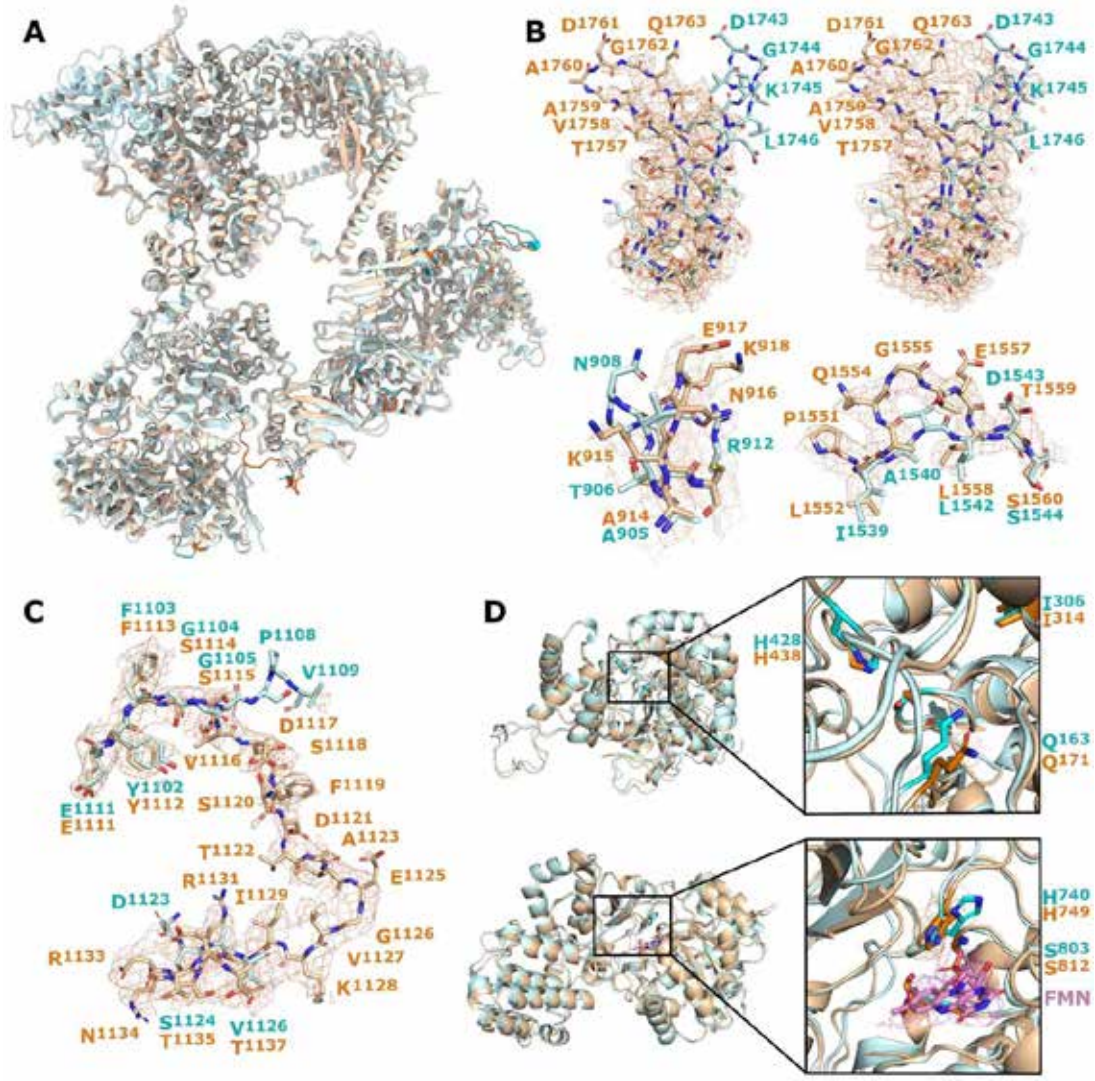

Figure 2: Unique structural features of *P. pastoris* FAS**. (A)** Overlay of *P. pastoris* FAS (orange) and *S. cerevisiae* FAS (blue, PDB: 6TA1). **(B)** Representative structural differences identified between the two FAS atomic models, with density for *P. pastoris* FAS overlaid. Two different density thresholds are shown side-by-side for loop 1753-1768 (upper). **(C)** Additional linker region resolved in the *P. pastoris* FAS structure. **(D)** Rotameric differences for key active site residues in the acetyl transferase (upper) and enoyl reductase (lower) domains.

Funding

This work was funded by the Wellcome Trust, the Saudi Ministry of Education, and the WHO.

A Case Study of Eukaryogenesis: the Evolution of Photoreception by Photolyase / Cryptochrome Proteins

Jennifer Miles and Paul Taylor

Introduction

It is widely accepted that eukaryogenesis involved an endosymbiosis between at least one archaeon, probably from the Asgard lineage, and at least one bacterium, most likely an ancestral α-proteobacterium. More controversial and less well understood is the possibility of further symbioses or other significant gene flows from bacteria to ancestral eukaryotes. Both the order in which these key evolutionary events occurred and their timeline are unclear. Characterising the emergence of animals from this ancient mix is of particular interest and offers a useful perspective from which to explore the major transitions.

Results and Discussion

We show how a detailed all-kingdom phylogenetic analysis overlaid with a map of key biochemical features can provide valuable clues. The photolyase / cryptochrome family of proteins are well known to repair DNA in response to potentially harmful effects of sunlight and to entrain circadian rhythms. Phylogenetic analysis of photolyase / cryptochrome protein sequences from a wide range of prokaryotes and eukaryotes points to a number of horizontal gene transfer (HGT) events between ancestral bacteria and ancestral eukaryotes (Figure 1). Previous experimental research has characterised patterns of tryptophan residues in these proteins that are important for photoreception, specifically a tryptophan dyad, a canonical tryptophan triad, an alternative tryptophan triad, a tryptophan tetrad and an alternative tetrad. Our analysis suggests that bacteria have contributed significantly and repeatedly to the evolution of photolyases and cryptochromes across all kingdoms of life, including in animals, by putative horizontal gene transfer. These apparent gene transfer events seem to be linked to the acquisition of additional and/or different tryptophan residues that contribute to increased stability of the diradical intermediate that is so crucial to the mechanism of photoreception. We show that incongruent nodes in this gene tree align with fundamental distinctions in the biochemistry of different groups of photolyase / cryptochrome proteins, which invites further investigation. Indeed, case studies such as the complex phylogeny of the photolyase / cryptochrome superfamily could

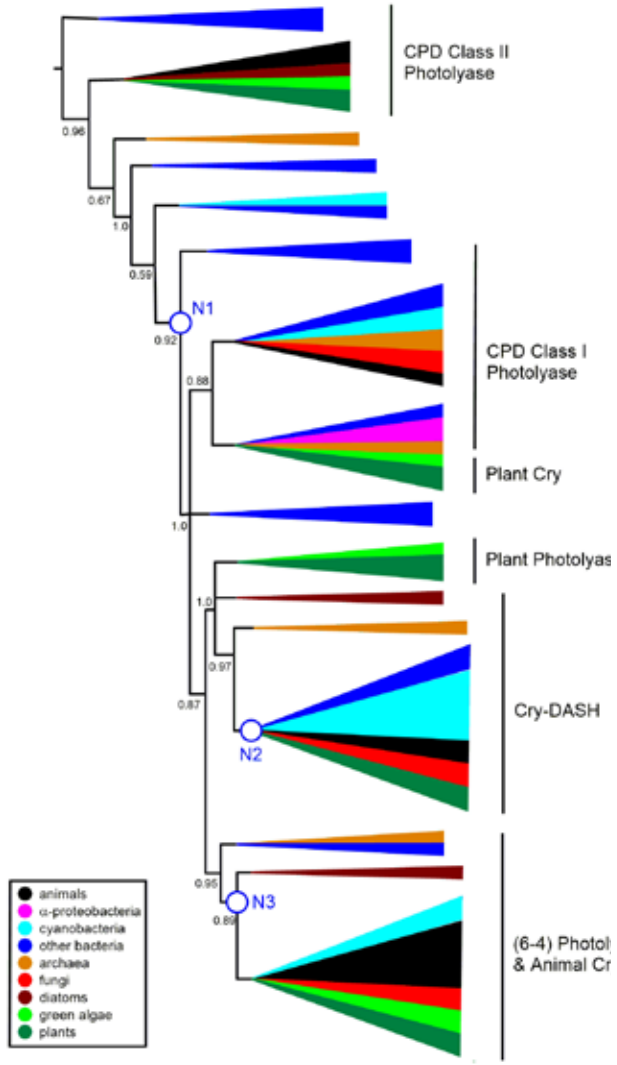

Figure 1: Schematic phylogenetic tree from MUSCLE alignment. N1-N3 indicate nodes that are incongruent with respect to standard trees of life. The Figure highlights the positions of animal sequences (in black) relative to α-proteobacterial sequences (in magenta) and cyanobacterial sequences (in cyan). Also colour coded are sequences from other bacteria (blue), archaea (orange), fungi (red), diatoms (brown), green algae (light green) and plants (dark green).

contribute valuable insight to emerging models of eukaryogenesis that acknowledge a rich bacterial heritage.

Publications

Miles J.A., Davies T.A., Hayman R.D., Lorenzen G., Taylor J.*, et al.* (2020) A case study of eukaryogenesis: the evolution of photoreception by photolyase/cryptochrome proteins. *J Mol Evol* **88**:662-673.

Funding

This work was funded by the University of Leeds.

DNA origami nanostructures for biological and biomedical applications

Ashley Stammers and Neil Thomson

Introduction

DNA structural nanotechnology is now a rapidly developing field in biomaterials, based on the natural self-assembly of rationally designed single-stranded DNA sequences into double helices. DNA origami is a specific subset of this potentially underpinning technology that utilises synthetic short DNA oligomers or “staples” to “fold” a longer single-stranded DNA template (typically a viral ssDNA) into complex 2D and 3D patterns and shapes with maximum dimensions on the order of 100nm. A long-term goal of this field is to develop nanoscale molecular devices with high efficiency to carry out tasks such as energy harvesting, computation and therapeutic delivery for healthcare applications. Our group is studying the structure and dynamics of single layer DNA origami nanotiles using atomic force microscopy (AFM) in aqueous liquid conditions. AFM is an ideal high-resolution microscopy to study these 2D DNA nanosheets down to the double-helix length scale. Understanding in greater detail how to control origami assembly and structure is key for designing and developing new materials applications based on DNA nanotechnology.

The solution structure of single layer origami (SLO) is determined by the inter-linked pattern of DNA staples throughout the 2D structure. The staple strands act as bridges, linking adjacent double-helices together at cross-over sites, whose spacing along the DNA axes can affect the nanotile curvature. These bridges where two staples next to each other cross between double-helices are analogous to Holliday junctions, with single-strand nicks between abutting staples on the same dsDNA strand. SLOs will tend to hold intrinsic curvature due to the non-integer helical repeat of base-pairs along the axis in B-form DNA, meaning that sequential cross-overs cannot be restricted to a single plane. The ability to understand and control origami curvature is important for scaling up and implementation of origami devices. This may include fabrication of self-assembled 2D arrays and 3D functional stacks. Controlling origami orientation on surfaces will be important for surface supported sensors, scaffolds and devices.

Results and Discussion

We utilised a notched rectangle SLO to impart an asymmetry, allowing for discrimination of the adsorption orientation (Fig 1). When the SLO are deposited on a mica surface counting the ratio between origami bound facing “up” or “down” in the AFM images tells us whether the SLO is more or less curved. We investigated three designs with different average cross-over spacings around the “ideal” 10.5 base-pairs per turn (bppt) for B-form DNA. We studied these three designs and how their curvature was affected by both ionic strength and species in the surrounding solution. These data, along with control experiments on UV-irradiated SLOs, demonstrated that curvature is influenced by a number of factors, including not only the design and topology of the SLOs but also electrostatic interactions between neighbouring DNA double-helices within the nanotiles. The AFM data were compared to modelling from both CanDo software and the coarse-grained model OxDNA (in collaboration with J. Doye, Oxford) which gave quite different predictions on the SLO curvature. In general, OxDNA correlated very well with the AFM results, while the simple mechanical model of DNA that CanDo invokes, did not predict the curvature accurately, specifically where the implemented spacings were not of the “ideal” case. The results demonstrate that the curvature of SLO can be determined from AFM imaging with the aid of an asymmetric design. More importantly, the curvature of DNA origami can be modulated to a large degree by altering the local solution environment as well as the folding pattern design.

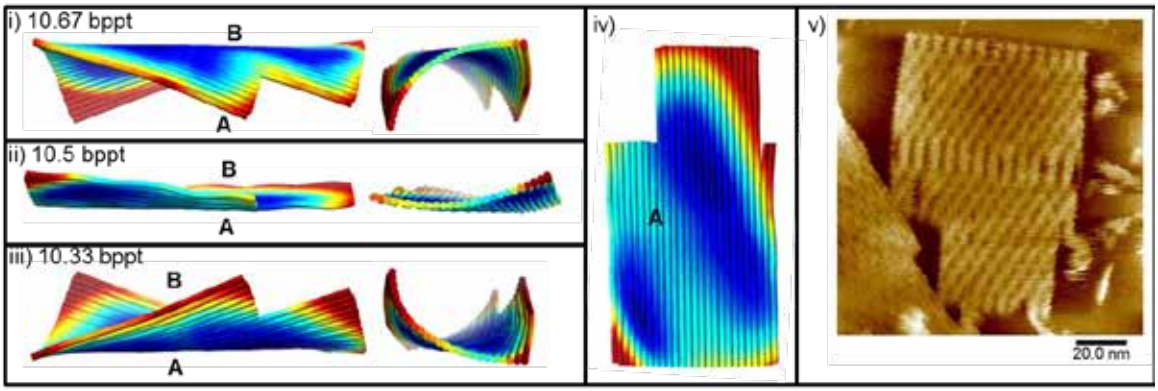

Figure 1: The three notched rectangle SLOs with different cross-over spacings showing their expected curvature in CanDo models. A and B denote the two faces of the nanotiles. The convex face preferentially binds to the mica surface, so by counting the A/B ratio in AFM images determines if the SLOs bind majority face-up or face-down. **i-iii**) Side and end views of the CanDo models of the three SLOs with different average cross-over spacings (bppt), denoting the A/B face of each. **iv**) Top-down view of CanDo model of the 10.5 bppt nanotile A-face as observed in AFM images. **v**) High magnification AFM image of the 10.5 bppt nanotile B-face, showing the DNA double-helical strands. The internal diamond pattern is caused by electrostatic repulsion between neighbouring DNA helices between cross-over junctions.

Funding
This work was funded by the EPSRC "*Molecular Scale Engineering"* Centre for Doctoral Training, a Wellcome Trust Equipment Grant and Bruker Nano Surfaces Division.

Collaborators
University of Leeds: Christoph Walti (Electrical and Electronic Engineering), Matteo Castronovo (Food Science).
External: Jonathan Doye (University of Oxford).

Lamellar structure of bacterial photosynthetic antennae

Rebecca Thompson, Neil Ranson and Roman Tuma

Introduction

Green photosynthetic bacteria employ large light-harvesting antennae called chlorosomes, which are ellipsoidal particles composed mostly of bacteriochlorophyll (BChl c, d or e). Proteins constitute only a minor fraction and are located on the surface. The interior is occupied by thousands of self-assembled bacteriochlorophyll molecules arranged into layers of stacked chlorin macro rings with the hydrophobic esterifying alcohols protruding into the interstitial space. Two principal arrangements have been proposed: (1) A rod model, in which the layers are arranged into concentric cylinders; (2) a lamellar model in which BChl layers arrange in parallel sheets. At the present, both models are compatible with projection images obtained by electron cryo-microscopy (cEM) while X-ray scattering favours the lamellar arrangement. Given the considerable disorder of pigments within chlorosomes it has been difficult to directly visualize details of the interior and use common electron density enhancement techniques, such as sub-tomogram averaging. Using chlorosomes isolated from *Chloroflexus aurantiacus* we attempted to visualize single chlorosomes interior by electron cryo-tomography.

Results and Discussion

Chlorosomes were purified by density gradient centrifugation, rapidly dialysed against water and mixed 1:1 with 10 nm Au nanoparticles (Aurion). Three microliters of the mix were placed on a negatively charged Quantifoil (R2/1) grid, blotted and vitrified in Vitrobot Mark IV. Selected areas with chlorosomes in thin ice were subjected to low-dose data collection on a Titan Krios microscope (Astbury Biostructure Laboratory) controlled by SerialEM software and equipped with an energy filtered camera Gatan K2 summit. Electron tomograms were aligned and reconstructed in Etomo software package using SIRT and CTF corrected (Figure 1A). Sub-volumes exhibiting striations corresponding to bacteriochlorophyll electron density were

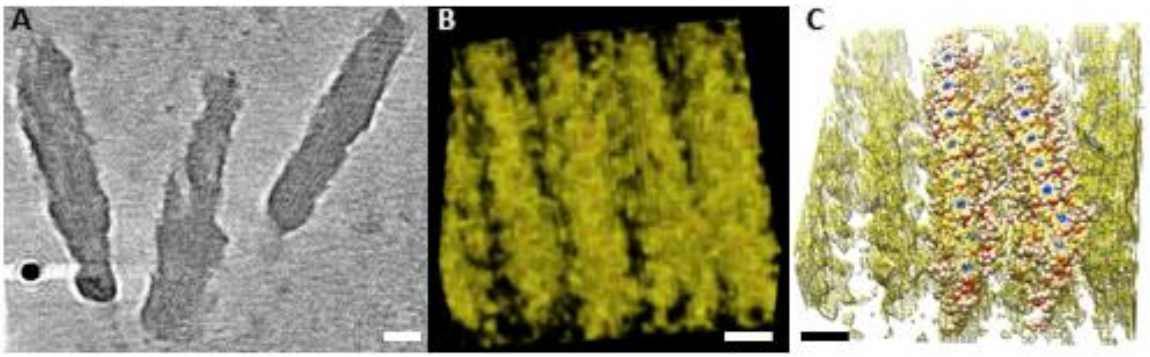

Figure 1: (**A**) A middle section from cEM tomographic reconstruction. A nanogold fiduciary marker is located on the left. Scale bar 20 nm. (**B**) 3D sub-volume example (solid representation). Bar 2 nm. (**C**) Plausible arrangement of bacteriochlorophyll layers (spacefill, central Mg atoms in blue, oxygen in red) within the lamellar density (yellow mesh). Scale bar 2 nm.

picked manually (representative volume shown in Figure 1B). The lamellar system shows minimal curvature incompatible with the rod model. Figure 1C shows tentative fit of pigment layers into the lamellar density with average inter-layer distance 2.7 nm, consistent with previous X-ray diffraction and cEM projections.

Funding

This work was funded by EU ERDF.

Collaborators

University of Leeds: Rebecca Thompson and Neil Ranson.
External: Tomas Bily, David Kaftan, David Reha (University of South Bohemia), Jakub Psencik (Charles University Prague).

Arbovirus replication and host cell interactions

Andrew Tuplin

Introduction

Arthropod-borne viruses (arboviruses) are important human pathogens for which there are no specific antiviral medicines. The abundance of genetically distinct arbovirus species, coupled with the unpredictable nature of their outbreaks, has made the development of virus-specific treatments challenging. Instead, we have defined and targeted a key aspect of the host innate immune response to virus at the arthropod bite that is common to all arbovirus infections, potentially circumventing the need for virus-specific therapies. Using mouse models and human skin explants, we identify innate immune responses by dermal macrophages in the skin as a key determinant of disease severity. Post-exposure treatment of the inoculation site by a topical TLR7 agonist suppressed both the local and subsequent systemic course of infection with a variety of arboviruses from the *Alphavirus*, *Flavivirus*, and *Orthobunyavirus* genera. Clinical outcome was improved in mice after infection with a model alphavirus. In the absence of treatment, antiviral interferon expression to virus in the skin was restricted to dermal dendritic cells. In contrast, stimulating the more populous skin-resident macrophages with a TLR7 agonist elicited protective responses in key cellular targets of virus that otherwise proficiently replicated virus. By defining and targeting a key aspect of the innate immune response to virus at the mosquito bite site, we have identified a putative new strategy for limiting disease after infection with a variety of genetically distinct arboviruses.

Publications

Lello L.S., Utt A., Bartholomeeusen K., Wang S.N., Rausalu K.*, et al.* (2020) Cross-utilisation of template RNAs by alphavirus replicases. *PLoS Pathog* **16:**e1008825.

Sharma N., Prosser O., Kumar P., Tuplin A. and Giri R. (2020) Small molecule inhibitors possibly targeting the rearrangement of Zika virus envelope protein. *Antiviral Res* **182:**104876

Rombi F., Bayliss R., Tuplin A. and Yeoh S. (2020) The journey of Zika to the developing brain. *Mol Biol Rep* **47**:3097-3115.

Bryden S.R., Pingen M., Lefteri D.A., Miltenburg J., Delang L.*, et al.* (2020) Pan-viral protection against arboviruses by activating skin macrophages at the inoculation site. *Sci Transl Med* **12**: eaax2421.

Collaborators

University of Leeds: Prof. M. Harris, Dr. A. Zhuravleva, Prof Nic Stonehouse and Dr J. Mankouri

External: Dr. Alain Kohl (MRC Centre for Virus Research, UK), Dr Andrew Davidson (University of Bristol, UK) and Prof Andres Merits (University of Tartu, Estonia).

Investigating the limits of sortase-catalysed protein labelling

Holly Morgan, Zoe Arnott, Kristian Hollingsworth, Yixin Li, Jonathan Dolan, Tomasz Kaminski, Charlie Stevenson, Bruce Turnbull and Michael Webb

Introduction

Selective protein labelling remains an essential tool both for academic research and the production of biopharmaceuticals. One attractive approach to protein labelling is to use enzymatic methods to modify particular recognition sequences within a protein. Over the last few years, we have focussed our efforts on the development of strategies to optimise protein labelling using sortases. These proteins are used by Gram-positive bacteria to link proteins to the bacterial cell wall and catalyse cross-linking of LPXTGX sorting sequences in proteins to polyglycine linkers in the bacterial cell wall. We have previously developed approaches for quantitative N-terminal labelling of proteins and are now focussed on optimising C-terminal labelling as well as multiple, orthogonal N-terminal labelling reactions as described below.

Results and Discussion

A fundamental challenge with sortases as with all enzymes is that they catalyse a reversible reaction. Fundamentally, transpeptidation leads to equilibrium mixtures and we have therefore investigated a range of strategies to perturb the equilibrium reaction position including mechanical separation of by-products, on-column isolation of enzyme-bound intermediates and, most successfully, depsipeptide substrates to make *N*-terminal labelling irreversible. In this project, we sought to extend this principle to selectively label the *N*-termini of proteins in heteromeric complexes using orthogonal sortases with differential substrate specificity. A number of such orthogonal sortases have been reported in the literature with altered substrate specificity including LPXSGS, FPXTGX and LAXTGX. We generated enzymes and depsipeptide substrates corresponding to each of these and evaluated their activity compared

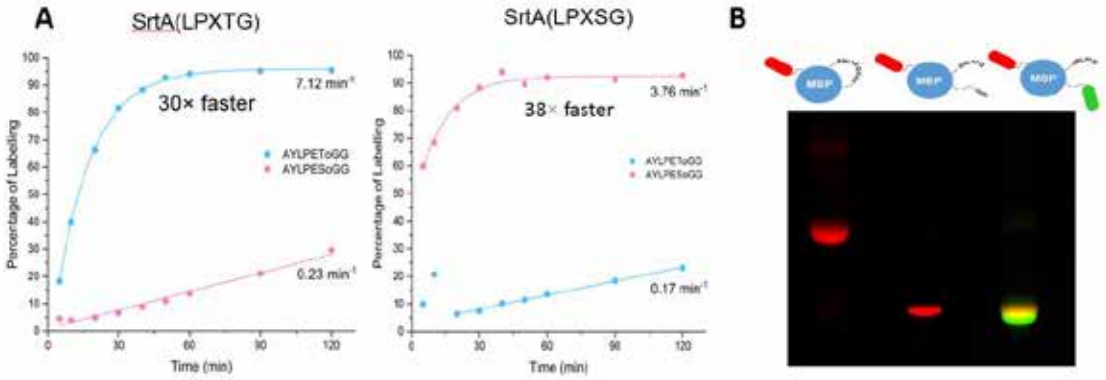

Figure 1: A MS analysis of orthogonal sortases reveals >30-fold selectively for cognate over mis-matched depsipeptide substrates. **B** Double fluorescence labelling of an exemplar protein using an artificially generated N-terminus following proteolysis.

to our existing labelling system as well as the degree of orthogonality. Only one pair of sortases using a LPXSGX and the wild-type LPXTGX sequence showed sufficient orthogonality for application with a 40-fold preference for the matched substrate over the unmatched substrate in both cases. We exemplified the orthogonality of labelling using a model protein substrate, maltose binding protein. We can quantitatively label the N-terminus of this monomeric protein before using a protease to cleave an internal loop in the protein to generate a second N-terminus which can then be labelled with the orthogonal sortase.This example is just one of several complementary approaches to protein labelling we are currently investigating in the group. Ultimately the objective is to develop approaches to quantitatively label and ligate proteins in a controlled fashion using minimal quantities of reagents.

Funding

This work was funded by the BBSRC.

Collaborators
External: Dani Ungar (University of York).

Virus-host cell interactions required for oncogenic virus replication and transformation

Oliver Manners, James Murphy, Sam Dobson, Sophie Schumann, Tim Mottram, Amy Barker, Becky Foster, Zoe Jackson, Holli Carden, Katie Harper, Ellie Harrington, Freddy Weaver and Ade Whitehouse

Introduction

Infection is a major cause of cancer worldwide. Viruses are associated with ~15% of human cancers, which approximates to about 2 million new cases every year in the world. We have utilised a range of cutting-edge transcriptomic and quantitative proteomic approaches to globally identify how the oncogenic viruses, Kaposi's sarcoma-associated herpesvirus (KSHV) and Merkel cell polyomavirus (MCPyV), affect the cellular environment to enhance their own replication and drive tumourigenesis.

Results and Discussion

1.Merkel cell polyomavirus (MCPyV) small tumour antigen (sT) is considered to be the main viral transforming factor, however potential mechanisms linking sT expression to the highly metastatic nature of Merkel cell carcinoma are yet to be fully elucidated. We have determined that MCPyV sT affects multiple stages of the metastatic cascade.

(i) Previously, we have shown that MCPyV sT can induce the migratory and invasive phenotype of MCC cells through the transcriptional activation of the Sheddase molecule, ADAM 10 (A disintegrin and metalloprotease domain-containing protein 10). We have now shown that MCPyV sT protein stimulates differential expression of epithelial–mesenchymal transition (EMT) associated genes, including MMP-9 and Snail. This effect is dependent on the presence of the large T stabilization domain (LSD), which is known to be responsible for cell transformation through targeting of promiscuous E3 ligases, including FBW7, a known MMP-9 and Snail regulator. Chemical treatments of MMP-9 markedly inhibited sT-induced cell migration and invasion. These results suggest that MCV sT contributes to the activation of MMP-9 as a result of FBW7 targeting, and increases the invasive potential of cells, which can be used for targeted therapeutic intervention.

(ii) Our recent findings have also implicated MCPyV sT expression in the highly metastatic nature of MCC by promoting cell motility and migration, through differential expression of cellular proteins that lead to microtubule destabilisation, filopodium formation and breakdown of cell-cell junctions. However, the molecular mechanisms which dysregulate these cellular processes are yet to be fully elucidated. We have now demonstrated that MCPyV sT expression activates p38 MAPK signalling to drive cell migration and motility. Notably, MCPyV sT-mediated p38 MAPK signalling occurs through MKK4, as opposed to the canonical MKK3/6 signalling pathway. In addition, our results indicate that an interaction between MCPyV sT and the cellular phospatase subunit PP4C is essential for its effect on p38 MAPK signalling. These results provide novel opportunities for the treatment of metastatic MCC given the intense interest in p38 MAPK inhibitors as therapeutic agents.

(iii) Using broad spectrum blockers of both K^+ and Ca^{2+} channels to specifically target host cell ion channel functionality, we show that MCPyV, but not SV40, can be inhibited by K^+ channel modulators, whilst both viruses are restricted by the broad spectrum Ca^{2+} channel inhibitor verapamil. Using a panel of more specific Ca^{2+} blockers, we show that both MCPyV and SV40 are dependent on the activity of two-pore Ca^{2+} channels (TPCs), as the TPC-specific blocker tetrandrine could prevent the capsid disassembly and nuclear transport required for virus entry. We therefore reveal a novel target to restrict the entry of polyomaviruses, which given the known role of TPCs during endolysosomal-ER fusion, is likely to be applicable to other viruses that transit this pathway.

2. Kaposi's sarcoma-associated herpesvirus (KSHV) is a gammaherpesvirus associated with development of the human diseases Kaposi's sarcoma, Primary Effusion Lymphoma and

Multicentric Castleman's Disease. KSHV establishes a chronic latent infection in hosts, with periods of viral lytic replication, where both latent and lytic virus cycles contribute to malignancy, most often in the immunodeficient host. We demonstrate that lytic KSHV replication and latent infection is regulated by cell stress and functionality of KSHV proteins relies on folding and conformational stabilization which is mediated by host chaperone systems, including Hsp90, Hsp70 and the endoplasmic reticulum stress response, as well as chaperone-mediated host signalling pathways. Dependence on the host cell chaperone systems means that inhibitors targeting host cell chaperone activity represent a possible avenue for effective therapeutic intervention in the future.

Publications

Kirigin. E., Ruck, D.K., Jackson, Z., Murphy, J., McDonnell, E., Okpara, M.O., Whitehouse, A. and Edkins, A.L. (2020). Regulation of Kaposi's sarcoma-associated herpesvirus biology by host molecular chaperones. In: Asea A.A.A., Kaur P. (eds) Heat Shock Proteins in Human Diseases. Heat Shock Proteins, vol 21. *Springer Cham* http://doi.org/10.1007/7515_2020_18.

Dobson S.J., Anene A., Boyne J.R., Mankouri J., Macdonald A.*, et al.* (2020) Merkel cell polyomavirus small tumour antigen activates the p38 MAPK pathway to enhance cellular motility. *Biochem J* **477**:2721-2733.

Dobson S.J., Mankouri J. and Whitehouse A. (2020) Identification of potassium and calcium channel inhibitors as modulators of polyomavirus endosomal trafficking. *Antiviral Research* **179**:104819.

Morgan E.L., Patterson M.R., Ryder E.L., Lee S.Y., Wasson C.W.*, et al.* (2020) MicroRNA-18a targeting of the STK4/MST1 tumour suppressor is necessary for transformation in HPV positive cervical cancer. *PLoS Pathog* **16**:e1008624.

Nwogu N., Ortiz L.E., Whitehouse A. and Kwun H.J. (2020) Merkel cell polyomavirus small tumor antigen activates matrix metallopeptidase-9 gene expression for cell migration and invasion. *J Virol* **94**:e00786-20.

Funding

This work was funded by the BBSRC, MRC, Rosetrees Trust, Royal Society and Wellcome Trust.

Collaborators

University of Leeds: Andrew Macdonald, Jamel Mankouri, John Lippiat, Eric Blair
External: James Boyne (University of Bradford), David Hughes (University of St Andrews), David Blackbourn (University of Surrey), Hyun Jin Kwun (University of Penn State, USA), Adrienne Edkins (University of Rhodes, South Africa).

Modulation of Protein-Protein Interactions Using Chemical Biology Approaches

Emma E. Cawood, Sergi Celis, Jessica S. Ebo, Nicholas Guthertz, Zsófia Hegedüs, Kristina Hetherington, Fruzsina Hóbor, Sonja Srdanovic, Martin Walko, Chi Trinh, Thomas. A. Edwards, Theo K. Karamanos, Adam Nelson, Sheena E. Radford and Andrew J. Wilson

Introduction

Small molecules and peptides are powerful tools for inhibiting or stabilizing protein-protein interactions (PPIs). However, both classes of compounds have challenges which must be overcome when developing tools for modulating PPIs. Understanding how such compounds can be developed and optimised is crucial for expanding the toolkit of PPI-modulating compounds. Here, we highlight our ongoing work developing distinct strategies for inhibiting or stabilizing PPIs.

Results and Discussion

PPI interfaces are often shallow and large compared with typical small molecule binding sites, making it difficult to identify molecules which bind with sufficient affinity and specificity to be effective modulators. The use of a covalent tether to stabilise a non-covalent protein-ligand interaction can improve the binding properties of such compounds, making covalent ligands powerful tools for modulating PPIs, even when the size of the ligand is small. Using a disulfide-based fragment screening platform ("disulfide tethering"), we identified a series of covalent ligands for an amyloidogenic variant of β_2-microglobulin (ΔN6). These ligands were capable of stabilising a non-amyloidogenic, tetrameric form of this protein, an oligomer which is normally only transiently populated and thus not amenable to high-resolution structural studies. In the presence of a covalent ligand, we successfully obtained a crystal structure of this oligomer, showing that these PPI interfaces can be stabilised by small molecules which

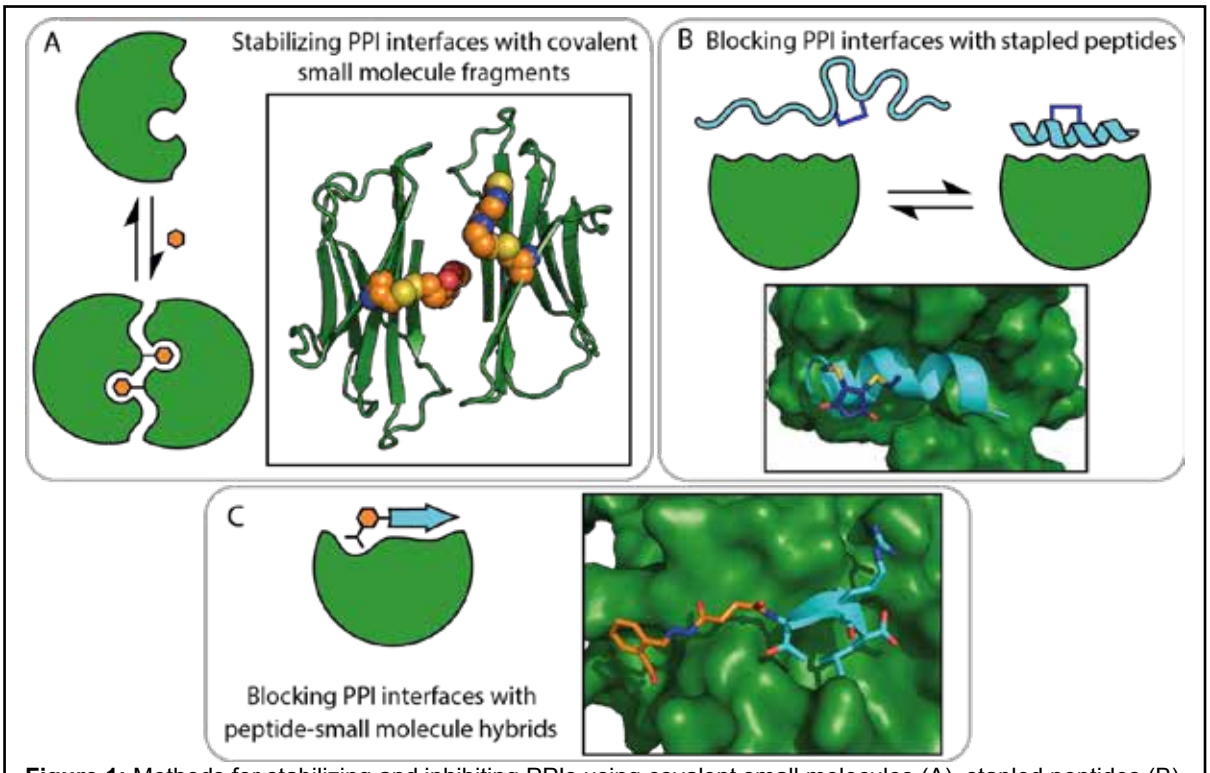

Figure 1: Methods for stabilizing and inhibiting PPIs using covalent small molecules (A), stapled peptides (B), or peptide-small molecule hybrids (C). In all cases, proteins are shown in green, peptides in cyan, and small molecules in orange. A) Covalent small molecule fragments are capable of stabilizing a tetramer of the ΔN6 variant of β_2-microglobulin – the dimer asymmetric unit of this structure is shown in the inset (PDB 7AFV). B) Stapled peptides (based on a HIF-1α sequence) improve the interaction affinity of this moiety for p300 due to stabilisation of the bound, α-helical conformation. C) Peptide-small molecule hybrids represent a novel class of compounds which combine advantages associated with both small molecule and peptide-based compounds.

act as “molecular glue” between adjacent protein subunits, and which stabilise conformations of the protein that promote the formation of specific interaction surfaces (Figure 1A).
Peptide-based modulators of PPIs can cover larger surface areas than small molecules but often suffer from poor cellular uptake and stability, as well as exhibiting a high entropic cost for binding. Such liabilities can be overcome by the introduction of covalent constraints (“staples”) within the peptide. However the precise role of such constraints in improving the binding and/or pharmacokinetic properties of peptides can be both constraint- and peptide-dependent. We have investigated how dibromomaleimide and disulfide constraints between *i* and *i+4* residues in a peptide inhibitor of the HIF-1α/p300 interaction can improve binding potency. We have found that rather than increasing the propensity of the peptide inhibitor to adopt its bound conformation, as was initially expected, these staples stabilise the bound protein-peptide complex (Figure 1B). These findings expand our understandings of the mechanisms by which covalent staples can modulate peptide-based modulators of PPIs, which will impact the use of these tools in the future development of PPI inhibitors and stabilisers.

Peptides can also be used as a scaffold/ligand to identify non-covalent small molecule binders at PPI interfaces. We developed a dynamic hydrazone screening assay to identify peptide-small molecule combinations/ligations capable of inhibiting a PPI of interest: in this case, the binding of GKAP to SHANK1-PDZ. The resulting peptide-fragment hybrids have the potential to be developed further as protease-resistant peptide-small molecule inhibitors or to be used as leads for the development of high affinity small molecule binders and chemical probes (Figure 1C). Most importantly, this “dynamic ligation” screening approach represents a high-throughput, site-directed method for exploring ligandable binding pockets at and around PPI interfaces.

Publications
Cawood E.E., Guthertz N., Ebo J.S., Karamanos T.K., Radford S.E.*, et al.* (2020) Modulation of amyloidogenic protein self-assembly using tethered small molecules. *J Am Chem Soc* **142**:20845-20854.

Hetherington K., Hegedus Z., Edwards T.A., Sessions R.B., Nelson A.*, et al.* (2020) Stapled peptides as HIF-1 alpha/p300 inhibitors: helicity enhancement in the bound state increases inhibitory potency. *Chemistry* **26**:7638-7646

Wolter M., de Vink P., Neves J. F., Srdanovic S., Higuchi Y., Kato N., Wilson A. J., Landrieu I., Brunsveld L., Ottmann C. (2020) Selectivity via Cooperativity: Preferential Stabilization of the p65/14-3-3 interaction with Semi-Synthetic Natural Products, J*. Am. Chem. Soc.*, **142**, 11772–11783.

Lindsey-Crosthwait A., Rodriguez-Lema D., Walko M., Pask C.M. and Wilson A.J. Structural optimization of reversible dibromomaleimide peptide stapling. *Pept Sci*. **113**:e24157.

Wood C.W., Ibarra A.A., Bartlett G.J., Wilson A.J., Woolfson D.N.*, et al.* (2020) BAlaS: fast, interactive and accessible computational alanine-scanning using BudeAlaScan. *Bioinformatics* **36**:2917-2919.

Funding
We acknowledge The University of Leeds, The Wellcome Trust, EPSRC, EU-H2020, The Royal Society and The Leverhulme Trust for financial support of this research.

Collaborators
External: Richard Sessions, Deborah Shoemark and Dek Woolfson (University of Bristol), Luc Brunsveld and Christian Ottmann (Eindhoven University of Technology), AstraZeneca, Domainex, Northern Institute of Cancer Research.

Defining the structural mechanisms for human DNA damage response and repair in cancer cells

William Wilson and Qian Wu

Introduction

DNA double-strand breaks (DSBs) are highly toxic DNA lesions for cells, causing cell death or chromosomal translocation. Ionizing radiation (IR) from radiotherapy and chemical crosslinking agents from chemotherapy work by introducing many DSBs with the aim of killing cancer cells, which are under high replication stress. Radiotherapy and chemotherapy are used to treat around two thirds of cancer patients in the UK each year. DNA damage response (DDR) and repair play critical roles in influencing the efficiency and sensitivity of these cancer treatments. At the same time, synthetic lethality approaches taking advantage of mutations in key DDR proteins have already yielded impressive results and launched a new class of targeted anti-cancer drugs called PARP (poly ADP ribose polymerase) inhibitors (PARPi). However, intrinsic or acquired resistance to these drugs occurs in many patients, causing a lack of response or tumour regrowth. We therefore need to understand the basic mechanisms of DNA repair in cancer cells that underpin disease outcomes to predict and improve efficacy of existing drugs and to aid in the design of new and effective cancer treatments and selective tumour cell inhibitors. Non-homologous end joining (NHEJ) and homologous recombination (HR) are the two major pathways for repairing DSBs, which are promoted by 53BP1 or BRCA1 signalling pathways respectively. We aim to understand the DNA repair pathway choice between NHEJ and HR in molecular detail.

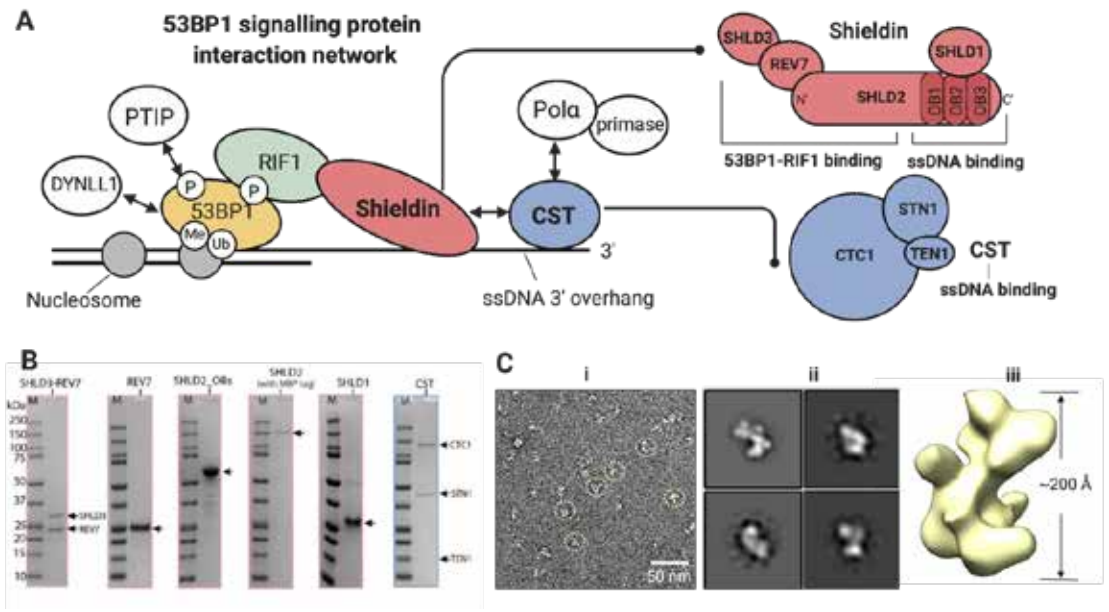

Figure 1: Structural study of Shieldin-CST complex. **A**) Shieldin among 53BP1 signalling protein interaction network. Arrows indicate direct interaction. Post-translational modifications are also indicated: P (phosphorylation), Me (methylation) and Ub (ubiquitination). Protein components for Shieldin and CST complex are indicated. SHLD2 contains three tandem oligosaccharide/oligonucleotide binding (OB) folds. **B**) SDS-PAGE of purified protein components of the Shieldin and CST complexes. Within Shieldin, the size for REV7, SHLD1, SHLD2 and SHLD3 are 24.3 kDa, 23 kDa, 93.7 kDa and 28.8 kDa respectively. Within CST, the size for CTC1, STN1 and TEN1 are 134.6 kDa, 42.1 kDa and 13.9 kDa respectively. Gels showing Shieldin components are boxed in red, the one for CST is boxed in blue. M indicated the protein molecular weight marker. **C**) Negative staining EM of CST. (i) Representative Micrographs of CST complex. Typical particles are shown in yellow dashed circles. (ii) Representative 2D classes of CST complex. (iii) Low resolution (~29 Å) 3D model of CST suggests a "croissant"-shaped complex and longest dimension of ~200 Å.

Results and Discussion
We study Shieldin-CST complex that binds DNA ends through 53BP1 signalling cascade. The Shieldin complex (SHLD1, SHLD2, SHLD3 and Rev7) was recently identified through whole genome CRISPR-Cas9 screening in BRCA1-deficient breast cancer cells treated with PARP inhibitors. It binds to DSB sites with 3' overhang ssDNA, preventing further DNA end resection and therefore promotes DNA repair through NHEJ. The structural mechanism of how Shieldin-CST complex function at the DNA ends is largely unknown. We are in the process of purifying, characterizing and determining the structures of individual domain and large Shieldin-CST complex with DNA using both cryo-EM and X-ray crystallography methods (Figure 1B,C). Our preliminary data for CST complex shows a 'croissant-shaped' complex with a longest dimension of ~200 Å and shows that the CST complex alone is likely to be monomeric.

Publications
Wu Q. (2020) Guardians of the genome: DNA damage and repair. *Essays Biochem*; **64** (5): 683–685.

Funding
Qian Wu's lab is currently supported by University Academic Fellowship (University of Leeds) and Springboard Award (Academy of Medical Sciences (AMS), the Wellcome Trust, the Government Department of Business, Energy and Industrial Strategy (BEIS) and the British Heart Foundation).

Collaborators
University of Leeds: Dr Darren Tomlinson, Prof Frank Sobott
External: Prof Stephen Jackson (University of Cambridge), Prof Patrick Sung (University of Texas Health Science Centre at San Antonio).

Assembly, activation and function of BRCC36 deubiquitylating complexes

Lisa Campbell, Francesca Chandler, Martina Foglizzo, Linda Makhlouf, Laura Marr, Miriam Walden and Elton Zeqiraj

Introduction

Ubiquitylation of proteins serves as a post-translational signal to regulate virtually all cellular processes through the precise spatial and temporal control of protein stability, activity and/or localisation. Enzymes involved in the ubiquitin system are frequently dysregulated in cancer, neurodegeneration, autoimmunity and other human diseases. Ubiquitylation is a versatile post-translational modification aptly suited for a cellular communication system similar to other post-translational modifications (e.g. phosphorylation).

Ubiquitin (Ub) processing enzymes (E1, E2 and E3) write the Ub signalling code by adding Ub to substrates. A single Ub can be conjugated to lysine residues on the surface of substrate proteins (known as mono-ubiquitylation), or conjugated further to lysine residues on the surface of Ub itself, leading to poly-Ub chains with different topologies and unique signalling properties. Ub and poly-Ub chains can be “read out” by ubiquitin binding domains (UBDs), which allow signal decoding and transmission. Ubiquitylation is a reversible process and Ub is removed by deubiquitylating (DUB) enzymes. DUB actions produce monomeric Ub, recycle Ub from chains and reverse signalling events resulting from ubiquitylation.

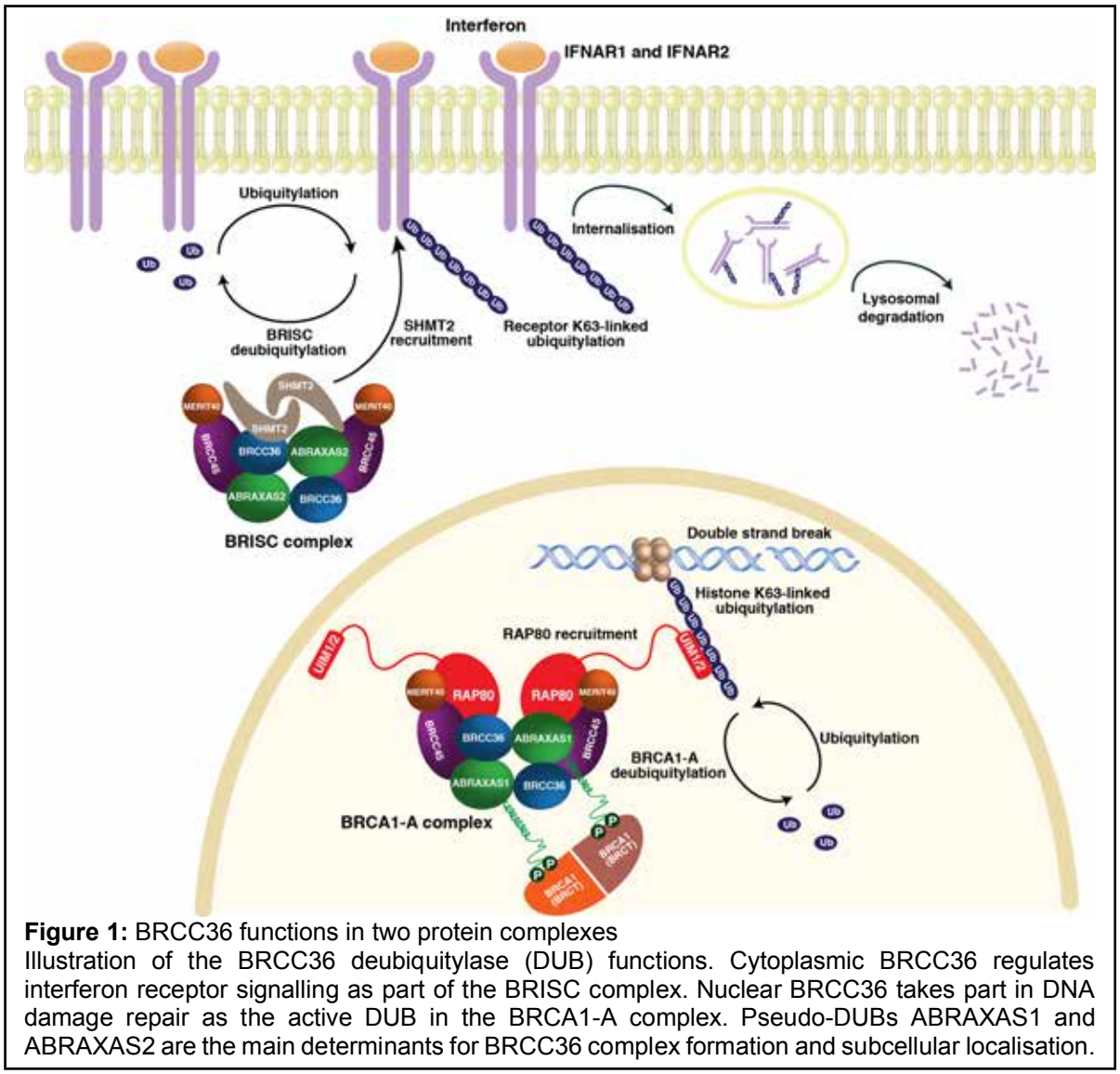

Figure 1: BRCC36 functions in two protein complexes
Illustration of the BRCC36 deubiquitylase (DUB) functions. Cytoplasmic BRCC36 regulates interferon receptor signalling as part of the BRISC complex. Nuclear BRCC36 takes part in DNA damage repair as the active DUB in the BRCA1-A complex. Pseudo-DUBs ABRAXAS1 and ABRAXAS2 are the main determinants for BRCC36 complex formation and subcellular localisation.

The active DUB BRCC36 is found in two macromolecular complexes (Fig. 1), depending on which inactive MPN– pseudo-DUB it interacts with (ABRAXAS1 or ABRAXAS2). The BRCC36-ABRAXAS1 complex translocates to the nucleus and forms the BRCA1-A complex. BRCA1-A localises to sites of DNA double strand breaks through RAP80 anchoring to K63-linked poly-Ub chains (Fig. 1). The BRCA1-A complex plays at least two roles in DNA damage repair: (1) binding and cleaving K63-linked poly-Ub chains and (2) recruitment of BRCA1 to sites of DNA damage.

In the cytoplasm, BRCC36 interacts with ABRAXAS2 and is part of a larger complex called BRISC-SHMT2 (Fig. 1). This cytoplasmic DUB complex interacts with and deubiquitylates interferon receptors 1 and 2 (IFANR1/2) and prevents their premature endocytosis and degradation through the lysosomal degradation pathway. Thus, the BRISC-SHMT2 complex regulates interferon-dependent immune responses by stabilising interferon receptors and ensuring their availability at the membrane. BRISC deficiency in mice results in reduced IFN signalling and improved survival when treated with bacterial lipopolysaccharide raising the possibility that BRISC inhibitors may have clinical utility against diseases stemming from elevated inflammatory cytokine signals.

Results

BRCC36 resides in the BRISC-SHMT2 and BRCA1-A complexes and regulates different aspects of cell biology (Fig. 1). How do the different subunit compositions affect BRCC36 catalytic function, substrate recognition and regulation? How is each holoenzyme structurally organized? Is it possible to develop tool compounds that discriminate between complexes to selectively influence different arms of BRCC36 biology?

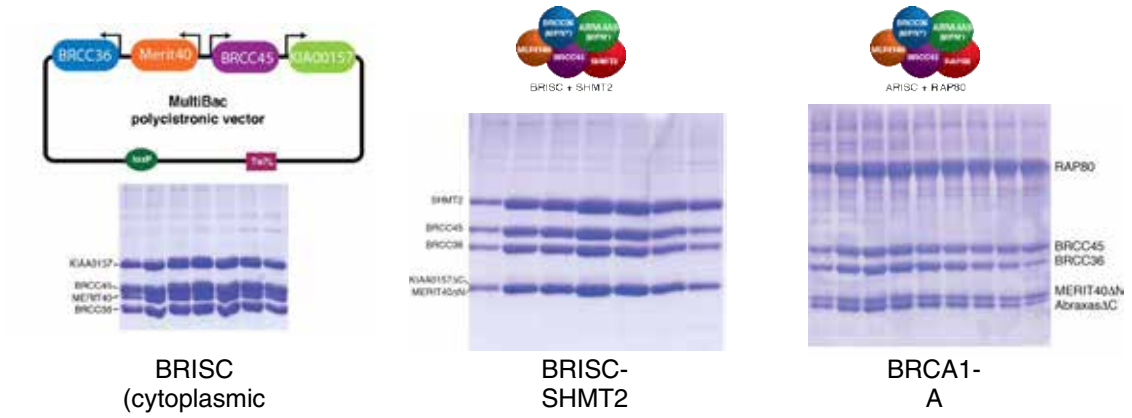

BRISC (cytoplasmic | BRISC-SHMT2 | BRCA1-A

Figure 2: Large scale production of BRCC36-containing DUB complexes
Schematic of a polycistronic vector for co-expression of the BRISC complex in insect cells (left panel). Coomassie-stained gels of 5-subunit complexes (middle and right panels).

To probe these questions at a biochemical and structural level, we have developed preparative expression systems for each multi-protein complex using the MultiBac insect cell/baculovirus system (Fig. 2). We recently solved the cryo-EM structure of BRISC-SHMT2 (Walden et al, 2019, Nature) and we are performing additional cryo-EM studies of these preparations to better understand complex assembly and BRCC36 mechanism of action. We are also taking an active approach to develop JAMM domain DUB inhibitors as tool compounds and as potential starting points for therapeutics.

Funding

This work is funded by the Wellcome Trust, The Royal Society and MRC-UKRI.

Collaborators

University of Leeds: Emma Hesketh, Neil Ranson, Francesco Del Galdo.
External: Roger Greenberg (Unviversity of Pennsylvania).

Photon induced quantum yield regeneration of cap-exchanged CdSe/CdS quantum rods for ratiometric biosensing and cellular imaging

Weili Wang, Yifei Kong, U.S. Akshath, Christian Tiede, Yuan Guo and Dejian Zhou

Introduction

Quantum rods (QRs) are elongated semiconductor nanoscrystals which display unique, size and shape-dependent strong fluorescence. Compared to the spherical quantum dot (QD), it has even higher single particle brightness and gives higher energy transfer efficiency, making it a powerful fluorescence probe for broad biomedical applications. However, most high quality QRs are prepared via the organometallic precursors and are capped with hydrophobic ligands, making them insoluble in aqueous media and thus incompatible with biological systems. They must be cap-exchanged with hydrophilic ligands and transferred into the aqueous media prior to use in bio-related applications. Unfortunately, cap-exchange of a hydrophobic CdSe/CdS core/shell QR using a dihydrolipoic acid zwitterion (DHLA-ZW) ligand has resulted in almost complete quench of the QR fluorescence, making it effectively useless in fluorescence applications. Fortunately, we have discovered that the QR fluorescence could be reinstalled by exposure to light in the near ultra-violate to blue region of the spectrum (*e.g.* 300-450 nm). These light activated QRs are compact, bright, stable, and resist non-specific adsorption, making them powerful fluorescence probes in biomedical applications. The QRs can be easily conjugated with Affimers for sensitive detection of target proteins *via* a Förster resonance energy transfer (FRET) readout strategy. They can also be functionalised with biotin for targeted fluorescence imaging of cancer cells.

Results and Discussion

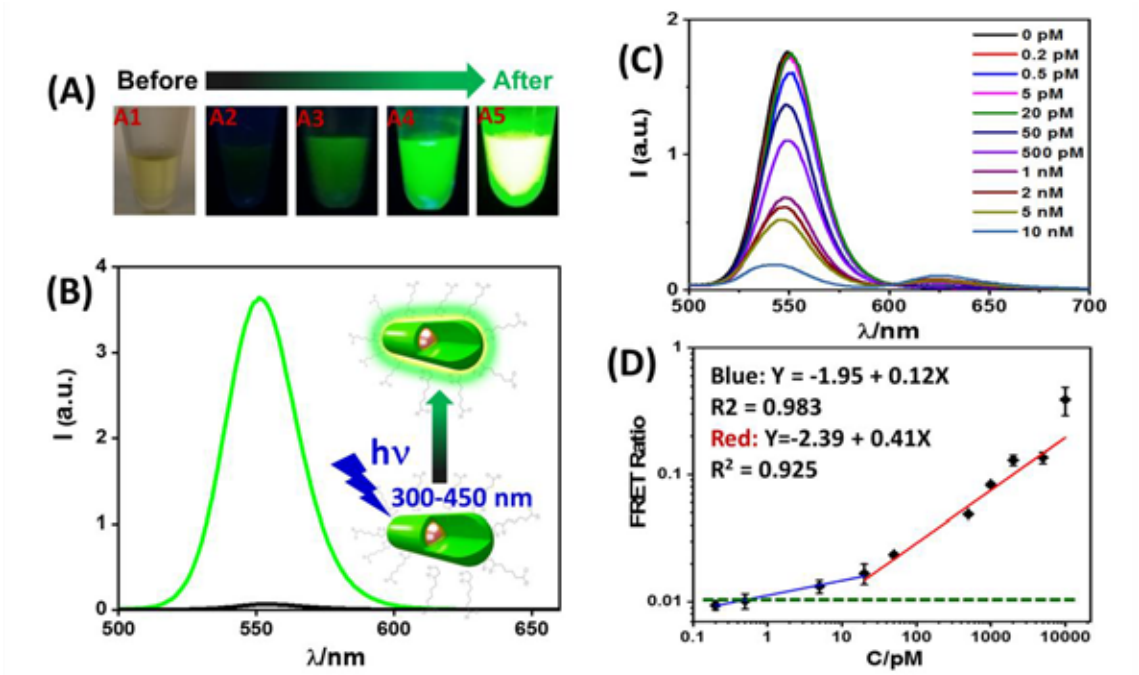

Figure 1: (A) Photos of a cap-exchanged QR (λ_{EM} ~550 nm) in water before (A1, under ambient light) and during the photo-activation (A2-A5, under a 365 nm UV light). (B) Fluorescence spectra of the QR before (black line) and after (green) photo-activation; inset: schematic of the photo-activation. (C) Fluorescence spectra of a QR-Affimer conjugate after mixing with different amount of target protein (Atto-594 labelled). (D) A log-log plot of the FRET ratio (I_{625}/I_{550}) *v.s.* concentration fitted by two stage linear relationship, giving a detection limit (marked by the green line) of 5 pM.

Using the ultra-efficient cap-exchange protocol recently developed in our group, a commercial hydrophobic CdSe/CdS core/shell QR (~3.6 x 24 nm) can be completely dispersed in H_2O as a compact, uniform dispersion with a hydrodynamic diameter of ~13.5±2.6 nm at a ligand:QR

ratio of 1000, consistent to that expected for isolated single QR particles. However, the cap-exchange has resulted in almost complete quench of the QR fluorescence, making the QR apparently non-fluorescent under UV-light excitation (Figure 1A), greatly hampering its use as a fluorescence probe. Fortunately, we find that the QR fluorescence can be slowly recovered upon exposure to ambient room light over 1 month. This process is greatly accelerated using a 365 nm UV-lamp, where a 4 h exposure can regenerate >75% of its original fluorescence (Figure 1A). The photo-regenerated QR is >50-fold brighter than that before at the same concentration (Figure 1B). It also retains a compact hydrodynamic size (D_h <20 nm), making it well-suited for FRET based ratiometric sensing. We have further conjugated his-tagged anti-SUMO affimers onto the QR and used them for sensitive detection of SUMO protein (Atto-594 labelled). Figure 1C shows that with increasing SUMO concentration, the QR fluorescence at ~550 nm is greatly quenched while the Atto-594 FRET signal at ~625 nm is enhanced concurrently. A log-log plot of the apparent FRET ratio (I_{625}/I_{550}) *v.s*. SUMO concentration gives an interesting two stage linear relationship, and detection limit of ~5 pM, placing it among the most sensitive FRET based protein sensors. Moreover, the QR-Affimer conjugate can be further exploited for detection of unlabelled protein target down to the sub-nM level *via* a FRET competition assay using the 1:1 mixed QD-Affimer and labelled SUMO as the FRET reporter.

Notably, the QR can be biotinylated directly using mixed DHLA-ZW and DHLA-PEG-biotin ligands to perform cap-exchange. After photo-activation as above, the resulting biotinylated QR can be employed for sensitive quantification of Atto-594 labelled neutravidin with excellent specificity and sensitivity (LOD ~0.2 nM). Moreover, the biotinylated QR can be employed for targeted, high specific fluorescence imaging of the model 4T1 breast cancer cells by exploiting their surface over-expressed biotin receptors, demonstrating the potential broad ranges of biomedical applications of such photo-regenerated QRs.

In summary, we have successfully water-dispersed hydrophobic CdSe/CdS QRs *via* a highly efficient cap-exchange method to produce compact, but almost completely quenched QRs. We find that the resulting QR fluorescence can be effectively regenerated *via* a novel photon activation method. Such regenerated QRs are readily bioconjugated with his-tagged Affimers for sensitive detection of 5 pM of a target protein. Water soluble, biotinylated QRs are also prepared via one step cap-exchange which are useful for ratiometric detection of pM levels of neutravidin and also for specific imaging of cancer cells. The high brightness and compact structures of such photo-regenerated QRs prepared via our cap-exchange method make them attractive fluorescence probes in broad biosensing and imaging applications, especially those relying on the FRET-based readout strategies.

Publications

Wang W.L., Kong Y.F., Jiang J., Tian X., Li S.*, et al.* (2020) Photon induced quantum yield regeneration of cap-exchanged CdSe/CdS quantum rods for ratiometric biosensing and cellular imaging. *Nanoscale* **12**:8647-8655.

Lapitan L.D.S. and Zhou D.J. (2020). A simple magnetic nanoparticle-poly-enzyme nanobead sandwich assay for direct, ultrasensitive DNA detection. *Methods Enzymol* **630:** 453-480.

Funding

This work was funded by the BBSRC and the EU Horizon 2020 *via* a Marie Sklodowska-Curie Fellowship.

Collaborators

University of Leeds: Nicole Hondow, School of Chemical and Process Engineering, University of Leeds.
External: Anchi Yu, Department of Chemistry, Remin University of China, Beijing, China.

Astbury Publications

Abou-Saleh R.H., Delaney A., Ingram N., Batchelor D.V.B., Johnson B.R.G., *et al.* (2020) Freeze-dried therapeutic microbubbles: stability and gas exchange. *ACS Appl Bio Mater* **3**:7840-7848.

Adamson H. and Jeuken L.J.C. (2020) Engineering protein switches for rapid diagnostic tests. *ACS Sens* **5**:3001-3012.

Adeyemi O.O., Ward J.C., Snowden J.S., Herod M.R., Rowlands D.J., *et al.* Functional advantages of triplication of the 3B coding region of the FMDV genome. *FASEB J*. 35:ee21215.

Allison T.M., Barran P., Benesch J.L.P., Cianferani S., Degiacomi M.T., *et al.* (2020) Software requirements for the analysis and interpretation of native Ion Mobility Mass Spectrometry data. *Anal Chem* **92**:10881-10890.

Allison T.M., Barran P., Cianferani S., Degiacomi M.T., Gabelica V., *et al.* (2020) Computational strategies and challenges for using native Ion Mobility Mass Spectrometry in biophysics and structural biology. *Anal Chem* **92**:10872-10880.

Alshawli A.S., Wurdak H., Wood I.C. and Ladbury J.E. (2020) Histone deacetylase inhibitors induce medulloblastoma cell death independent of HDACs recruited in REST repression complexes. *Mol Genet Genomic Med* **8**:ee1429.

Alvarez-Rodriguez B., Tiede C., Hoste A.C.R., Surtees R.A., Trinh C., *et al.* (2020) Characterization and applications of a Crimean-Congo hemorrhagic fever virus nucleoprotein-specific Affimer: Inhibitory effects in viral replication and development of colorimetric diagnostic tests. *PLoS Negl Trop Dis* **14**:e0008364.

Armistead F.J., De Pablo J.G., Gadelha H., Peyman S.A. and Evans S.D. (2020) Physical biomarkers of disease progression: on-chip monitoring of changes in mechanobiology of colorectal cancer cells. *Sci Rep* **10**:3254.

Aufderhorst-Roberts A., Hughes M.D.G., Hare A., Head D.A., Kapur N., *et al.* (2020) Reaction rate governs the viscoelasticity and nanostructure of folded protein hydrogels. *Biomacromolecules* **21**:4253-4260.

Bar L., Dejeu J., Lartia R., Bano F., Richter R.P., *et al.* (2020) Impact of antigen density on recognition by monoclonal antibodies. *Anal Chem* **92**:5396-5403.

Bartoli F., Bailey M.A., Rode B., Mateo P., Antigny F., *et al.* (2020) Orai1 channel inhibition preserves left ventricular systolic function and normal Ca^{2+} handling after pressure overload. *Circulation* **141**:199-216.

Batchelor D.V.B., Abou-Saleh R.H., Coletta P.L., McLaughlan J.R., Peyman S.A., *et al.* (2020) Nested nanobubbles for ultrasound-triggered drug release. *ACS Appl Mater Interfaces* **12**:29085-29093.

Batchelor M., Papachristos K., Stofella M., Yew Z. and Paci E. (2020) Protein mechanics probed using simple molecular models. *Biochim Biophys Acta Gen Subj* **1864**:129613.

Bauer C.C, Minard A.M., Pickles I.B., Simmons K.J., Chuntharpursat-Bon E., Burnham M.P., Kapur N., Beech D.J., Muench S.P., Wright M.H., Warriner S.L. and Bon R.S. (2020) Xanthine-based photoaffinity probes allow assessment of ligand engagement by TRPC5 channels. *RSC Chem. Biol.* **1:** 436-448.

Bell A.S., Yu Z.Y., Hutton J.A., Wright M.H., Brannigan J.A., *et al.* (2020) Novel thienopyrimidine inhibitors of Leishmania N-myristoyltransferase with on-target activity in intracellular amastigotes. *J Med Chem* **63**:7740-7765.

Berdiell I.C., Kulmaczewski R., Warriner S.L., Cespedes O. and Halcrow M.A. (2020) Iron and silver complexes of 4-(Imidazol-1-yl)-2,6-di(pyrazol-1-yl)-pyridine (L), including a $Fe_3(\mu\text{-}F)_2F_6L_8^+$ Assembly. *Eur J Inorg Chem* **2020**:4334-4340.

Bilyk B., Kim S., Fazal A., Baker T.A. and Seipke R.F. (2020) Regulation of antimycin biosynthesis is controlled by the ClpXP protease. *Msphere* **5**:e00144-20.

Boissinot M., King H., Adams M., Higgins J., Shaw G., *et al.* (2020) Profiling cytotoxic microRNAs in pediatric and adult glioblastoma cells by high-content screening, identification, and validation of miR-1300. *Oncogene* **39**:5292-5306.

Bottari F., Daems E., de Vries A.M., Van Wielendaele P., Trashin S., *et al.* (2020) Do aptamers always bind? The need for a multifaceted analytical approach when demonstrating binding affinity between aptamer and low molecular weight compounds. *J Am Chem Soc* **142**:19622-19630.

Bourn M.D., Batchelor D.V.B., Ingram N., McLaughlan J.R., Coletta P.L., *et al.* (2020) High-throughput microfluidics for evaluating microbubble enhanced delivery of cancer therapeutics in spheroid cultures. *J Control Release* **326**:13-24.

Brabham R.L., Keenan T., Husken A., Bilsborrow J., McBerney R., *et al.* (2020) Rapid sodium periodate cleavage of an unnatural amino acid enables unmasking of a highly reactive alpha-oxo aldehyde for protein bioconjugation. *Org Biomol Chem* **18**:4000-4003.

Brown M.R., Radford S.E. and Hewitt E.W. (2020) Modulation of beta-amyloid fibril formation in Alzheimer's disease by microglia and infection. *Front Mol Neurosci* **13**:609073.

Bryden S.R., Pingen M., Lefteri D.A., Miltenburg J., Delang L., *et al.* (2020) Pan-viral protection against arboviruses by activating skin macrophages at the inoculation site. *Sci Transl Med* **12**: eaax2421.

Budhadev D., Poole E., Nehlmeier I., Liu Y.Y., Hooper J., *et al.* (2020) Glycan-gold nanoparticles as multifunctional probes for multivalent lectin-carbohydrate binding: implications for blocking virus infection and nanoparticle assembly. *J Am Chem Soc* **142**:18022-18034.

Bunce S.J., Wang Y.M., Radford S.E., Wilson A.J. and Hall C.K. Structural insights into peptide self-assembly using photo-induced crosslinking experiments and discontinuous molecular dynamics. *AIChE J* e17101.

Burke M.J., Stockley P.G. and Boyes J. (2020) Broadly neutralizing bovine antibodies: highly effective new tools against evasive pathogens? *Viruses-Basel* **12**:473.

Byrne M.J., Nasir N., Basmadjian C., Bhatia C., Cunnison R.F., *et al.* (2020) Nek7 conformational flexibility and inhibitor binding probed through protein engineering of the R-spine. *Biochem J* **477**:1525-1539.

Calabrese A.N., Schiffrin B., Watson M., Karamanos T.K., Walko M., *et al.* (2020) Inter-domain dynamics in the chaperone SurA and multi-site binding to its outer membrane protein clients. *Nat Commun* **11**:2155.

Cawood E.E., Guthertz N., Ebo J.S., Karamanos T.K., Radford S.E., *et al.* (2020) Modulation of amyloidogenic protein self-assembly using tethered small molecules. *J Am Chem Soc*

142:20845-20854.

Ceasar S.A., Ramakrishnan M., Vinod K.K., Roch G.V., Upadhyaya H.D.*, et al.* (2020) Phenotypic responses of foxtail millet (*Setaria italica*) genotypes to phosphate supply under greenhouse and natural field conditions. *PLoS One* **15**:e0233896.

Chandler-Bostock R., Mata C.P., Bingham R.J., Dykeman E.C., Meng B.*, et al.* (2020) Assembly of infectious enteroviruses depends on multiple, conserved genomic RNA-coat protein contacts. *PLoS Pathog* **16**:e1009146.

Charlton F.W., Pearson H.M., Hover S., Lippiat J.D., Fontana J.*, et al.* (2020) Ion channels as therapeutic targets for viral infections: further dscoveries and future perspectives. *Viruses-Basel* **12**:844.

Chau C., Actis P. and Hewitt E. (2020) Methods for protein delivery into cells: from current approaches to future perspectives. *Biochem Soc Trans* **48**:357-365.

Chau C.C., Radford S.E., Hewitt E.W. and Actis P. (2020) Macromolecular crowding enhances the detection of DNA and proteins by a solid-state nanopore. *Nano Letters* **20**:5553-5561.

Cheetham M.R., Griffiths J., de Nijs B., Heath G.R., Evans S.D.*, et al.* (2020) Out-of-Plane nanoscale reorganization of lipid molecules and nanoparticles revealed by plasmonic spectroscopy. *J Phys Chem Lett* **11**:2875-2882.

Chow S., Green A.I., Arter C., Liver S., Leggott A.*, et al.* (2020) efficient approaches for the synthesis of diverse alpha-diazo amides. *Synthesis (Stuttg)* **52**:1695-1706.

Chung J.Y., Brittin C.A., Evans S.D., Cohen N. and Shim J.U. (2020) Rotatable microfluidic device for simultaneous study of bilateral chemosensory neurons in *Caenorhabditis elegans*. *Microfluid and Nanofluidics* **24**:56.

Ciano L., Paradisi A., Hemsworth G.R., Tovborg M., Davies G.J.*, et al.* (2020) Insights from semi-oriented EPR spectroscopy studies into the interaction of lytic polysaccharide monooxygenases with cellulose. *Dalton Trans* **49**:3413-3422.

Cole B.A., Johnson R.M., Dejakaisaya H., Pilati N., Fishwick C.W.G.*, et al.* (2020) structure-based identification and characterization of inhibitors of the epilepsy-associated $K_{Na}1.1$ (KCNT1) potassium channel. *Iscience* **23:**101100.

Coubrough H.M., Balonova B., Pask C.M., Blight B.A. and Wilson A.J. (2020) A pH-switchable triple hydrogen-bonding motif. *Chemistryopen* **9**:40-44.

Coubrough H.M., Reynolds M., Goodchild J.A., Connell S.D.A., Mattsson J.*, et al.* (2020) Assembly of miscible supramolecular network blends using DDA·AAD hydrogen-bonding interactions of pendent side-chains. *Polym Chem* **11**:3593-3604.

Cuvertino S., Hartill V., Colyer A., Garner T., Nair N.*, et al.* A restricted spectrum of missense KMT2D variants cause a multiple malformations disorder distinct from Kabuki syndrome. *Genet Med* 22:867-877.

Davies K.A., Chadwick B., Hewson R., Fontana J., Mankouri J.*, et al.* (2020) The RNA replication site of Tula Orthohantavirus resides within a remodelled Golgi network. *Cells* **9**:1569.

de Oliveira D.M., Santos I.D., Martins D.O.S., Goncalves Y.G., Cardoso-Sousa L.*, et al.* (2020) Organometallic complex strongly impairs Chikungunya virus entry to the host cells.

Front Microbiol, **11:**608924.

de Pablo J.G., Chisholm D.R., Ambler C.A., Peyman S.A., Whiting A.*, et al.* (2020) Detection and time-tracking activation of a photosensitiser on live single colorectal cancer cells using Raman spectroscopy. *Analyst* **145**:5878-5888.

Dobson S.J., Anene A., Boyne J.R., Mankouri J., Macdonald A.*, et al.* (2020) Merkel cell polyomavirus small tumour antigen activates the p38 MAPK pathway to enhance cellular motility. *Biochem J* **477**:2721-2733.

Dobson S.J., Mankouri J. and Whitehouse A. (2020) Identification of potassium and calcium channel inhibitors as modulators of polyomavirus endosomal trafficking. *Antiviral Research* **179**:104819.

Doherty C.P.A., Ulamec S.M., Maya-Martinez R., Good S.C., Makepeace J.*, et al.* (2020) A short motif in the N-terminal region of alpha-synuclein is critical for both aggregation and function. *Nat Struct Mol Biol* **27**:249-259.

Dutoit R., Brandt N., Van Gompel T., Van Elder D., Van Dyck J.*, et al.* (2020) M42 aminopeptidase catalytic site: the structural and functional role of a strictly conserved aspartate residue. *Proteins: Struct Funct Bioinform* **88**:1639-1647.

Ebo J.S., Guthertz N., Radford S.E. and Brockwell D.J. (2020) Using protein engineering to understand and modulate aggregation. *Curr Opin Struct Biol* **60**:157-166.

Ebo J.S., Saunders J.C., Devine P.W.A., Gordon A.M., Warwick A.S.*, et al.* (2020) An *in vivo* platform to select and evolve aggregation-resistant proteins. *Nat Commun* **11**:1816.

Evans E.L., Povstyan O.V., De Vecchis D., Macrae F., Lichtenstein L.*, et al.* (2020) RBCs prevent rapid PIEZO1 inactivation and expose slow deactivation as a mechanism of dehydrated hereditary stomatocytosis. *Blood* **136**:140-144.

Fazal A., Webb M.E. and Seipke R.F. (2020) The Desotamide family of antibiotics. *Antibiotics (Basel)* **9**:452.

Foster H., Wilson C., Philippou H. and Foster R. (2020) Progress toward a Glycoprotein VI modulator for the treatment of thrombosis. *J Med Chem* **63**:12213-12242.

Foyer C.H., Baker A., Wright M., Sparkes I.A., Mhamdi A.*, et al.* (2020) On the move: redox-dependent protein relocation in plants. *J Exp Bot* **71**:620-631.

Francis D., Nelson A. and Marsden S.P. (2020) Synthesis of beta-diamine building blocks by photocatalytic hydroamination of enecarbamates with amines, ammonia and N-H heterocycles. *Chemistry* **26**:14861-14865.

Frost R., Debarre D., Jana S., Bano F., Schiinemann J.*, et al.* (2020) A method to quantify molecular diffusion within thin solvated polymer films: a case study on films of natively unfolded nucleoporins. *ACS Nano* **14**:9938-9952.

Fuller J., Alvarez-Rodriguez B., Todd E., Mankouri J., Hewson R.*, et al.* (2020) Hazara Nairovirus requires COPI components in both Arf1-dependent and Arf1-independent stages of its replication cycle. *J Virol* **94**:e00766-20.

Gallagher L.A., Shears R.K., Fingleton C., Alvarez L., Waters E.M.*, et al.* (2020) Impaired Alanine Transport or Exposure to D-Cycloserine Increases the Susceptibility of MRSA to beta-lactam Antibiotics. *Journal of Infectious Diseases* **221**:1006-1016.

Gallardo R., Iadanza M.G., Xu Y., Heath G.R., Foster R.*, et al.* (2020) Fibril structures of diabetes-related amylin variants reveal a basis for surface-templated assembly. *Nat Struct Mol Biol* **27**:1048-1056.

Gallardo R., Ranson N.A. and Radford S.E. (2020) Amyloid structures: much more than just a cross-beta fold. *Curr Opin Struct Biol* **60**:7-16.

Gantner M., Laftsoglou T., Rong H.L., Postis V.L.G. and Jeuken L.J.C. (2020) Electrophysiology measurements of metal transport by MntH2 from *Enterococcus faecalis*. *Membranes* **10**:255.

Gomm A. and Nelson A. (2020) A radical approach to diverse meroterpenoids. *Nat Chem* **12**:109-111.

Goonawardane N., Yin C.H. and Harris M. (2020) Phenotypic analysis of mutations at residue 146 provides insights into the relationship between NS5A hyperphosphorylation and hepatitis C virus genome replication. *J Gen Virol* **101**:252-264.

Green A.I., Hobor F., Tinworth C.P., Warriner S., Wilson A.J.*, et al.* (2020) Activity-directed synthesis of inhibitors of the p53/hDM2 protein-protein interaction. *Chemistry* **26**:10682-10689.

Groves K., Cryar A., Cowen S., Ashcroft A.E. and Quaglia M. (2020) Mass spectrometry characterization of higher order structural changes associated with the fc-glycan structure of the nistmab reference material, RM 8761. *J Am Soc Mass Spectrom* **31**:553-564.

Haigh J.L., Williamson D.J., Poole E., Guo Y., Zhou D.J.*, et al.* (2020) A versatile cholera toxin conjugate for neuronal targeting and tracing. *Chem Commun* **56**:6098-6101.

Hanson B.S. and Dougan L. (2020) Network growth and structural characteristics of globular protein hydrogels. *Macromolecules* **53**:7335-7345.

Harris M. (2020) Microbiology Society online workshop on SARS-CoV-2 and COVID-19, Wednesday 29 July 2020. *Journal of General Virology* **101**:1227-1228.

Haza K., Martin H., Tiede C., Tipping K., Trinh C.*, et al.* (2020) Development of small-molecule RAS inhibitors using affimer reagents. *Mol Cancer Res* **18**:64-65.

Hesketh S.J., Klebl D.P., Higgins A.J., Thomsen M., Pickles I.B.*, et al.* (2020) Styrene maleic-acid lipid particles (SMALPs) into detergent or amphipols: An exchange protocol for membrane protein characterisation. *Biochim Biophys Acta Biomembr* **1862**:183192.

Hetherington K., Hegedus Z., Edwards T.A., Sessions R.B., Nelson A.*, et al.* (2020) Stapled peptides as HIF-1 alpha/p300 inhibitors: helicity enhancement in the bound state increases inhibitory potency. *Chemistry* **26**:7638-7646.

Horne J.E., Brockwell D.J. and Radford S.E. (2020) Role of the lipid bilayer in outer membrane protein folding in Gram-negative bacteria. *J Biol Chem* **295**:10340-10367.

Hoskisson P.A. and Seipke R.F. (2020) Cryptic or Silent? The known unknowns, unknown knowns, and unknown unknowns of secondary metabolism. *Mbio* **11**:e02642-20.

Hoste A.C.R., Ruiz T., Fernandez-Pacheco P., Jimenez-Clavero M.A., Djadjovski I.*, et al.* Development of a multiplex assay for antibody detection in serum against pathogens affecting ruminants. *Transbound Emerg Dis*. **00**:1–11.

Huang K., Marchesi A., Hollingsworth K., Both P., Mattey A.P.*, et al.* (2020) Biochemical

characterisation of an alpha 1,4 galactosyltransferase from *Neisseria weaveri* for the synthesis of alpha 1,4-linked galactosides. *Org Biomol Chem* **18**:3142-3148.

Hughes M.D.G., Cussons S., Mahmoudi N., Brockwell D.J. and Dougan L. (2020) Single molecule protein stabilisation translates to macromolecular mechanics of a protein network. *Soft Matter* **16**:6389-6399.

Hunter L., de Pablo J.G., Stammers A.C., Thomson N.H., Evans S.D.*, et al.* (2020) On-chip pressure measurements and channel deformation after oil absorption. *SN Appl Sci* **2**:1501.

Iadanza M.G., Schiffrin B., White P., Watson M.A., Horne J.E.*, et al.* (2020) Distortion of the bilayer and dynamics of the BAM complex in lipid nanodiscs. *Commun Biol* **3**:766.

Ingram N., McVeigh L.E., Abou-Saleh R.H., Maynard J., Peyman S.A.*, et al.* (2020) Ultrasound-triggered therapeutic microbubbles enhance the efficacy of cytotoxic drugs by increasing circulation and tumor drug accumulation and limiting bioavailability and toxicity in normal tissues. *Theranostics* **10**:10973-10992.

Jamali M.A.M., Gopalasingam C.C., Johnson R.M., Tosha T., Muramoto K.*, et al.* (2020) The active form of quinol-dependent nitric oxide reductase from *Neisseria meningitidis* is a dimer. *IUCrJ* **7**:404-415.

James C.D., Das D., Morgan E.L., Otoa R., Macdonald A.*, et al.* (2020) Werner Syndrome protein (WRN) regulates cell proliferation and the human papillomavirus 16 life cycle during epithelial differentiation. *Msphere* **5**:e00858-20.

Jeuken L.J.C., Hards K. and Nakatani Y. (2020) Extracellular electron transfer: respiratory or nutrient homeostasis? *J Bacteriol* **202**:e00029-20.

Johansson N.G., Turku A., Vidilaseris K., Dreano L., Khattab A.*, et al.* (2020) Discovery of membrane-bound pyrophosphatase inhibitors derived from an isoxazole fragment. *ACS Med Chem Lett* **11**:605-610.

Johnson R.M., Fais C., Parmar M., Cheruvara H., Marshall R.L.*, et al.* (2020) Cryo-EM structure and molecular dynamics analysis of the fluoroquinolone resistant mutant of the AcrB transporter from Salmonella. *Microorganisms* **8**:943.

Kapsalis C., Ma Y., Bode B.E. and Pliotas C. (2020) In-lipid structure of pressure-sensitive domains hints mechanosensitive channel functional diversity. *Biophys J* **119**:448-459.

Karageorgis G., Liver S. and Nelson A. (2020) Activity-directed synthesis: a flexible approach for lead generation. *ChemMedChem* **15**:1776-1782.

Karamanos T.K., Tugarinov V. and Clore G.M. (2020) An S/T motif controls reversible oligomerization of the Hsp40 chaperone DNAJB6b through subtle reorganization of a beta sheet backbone. *Proc Natl Acad Sci USA* **117**:30441-30450.

Karamanos T.K., Tugarinov V., and Clore G.M. (2020) Determining methyl sidechain conformations in a CS-ROSETTA model using methyl 1H-13C residual dipolar couplings. *J. Biomol. NMR* **48**: 1-8.

Ketchen S., Rohwedder A., Knipp S., Esteves F., Struve N.*, et al.* (2020) A novel workflow for three-dimensional analysis of tumour cell migration. *Interface Focus* **10**:20190070.

Khan S., McCabe J., Hill K. and Beales P.A. (2020) Biodegradable hybrid block copolymer - lipid vesicles as potential drug delivery systems. *Journal Colloid Interface Sci* **562**:418-428.

Kirigin. E., Ruck, D.K., Jackson, Z., Murphy, J., McDonnell, E., Okpara, M.O., Whitehouse, A. and Edkins, A.L. (2020). Regulation of Kaposi's sarcoma-associated herpesvirus biology by host molecular chaperones. In: Asea A.A.A., Kaur P. (eds) Heat Shock Proteins in Human Diseases. Heat Shock Proteins, vol 21. *Springer Cham* http://doi.org/10.1007/7515_2020_18.

Klebl D.P., Gravett M.S.C., Kontziampasis D., Wright D.J., Bon R.S., *et al.* (2020) Need for speed: examining protein behavior during CryoEM grid preparation at different timescales. *Structure* **28**:1238-1248.

Klebl D.P., Monteiro D.C.F., Kontziampasis D., Kopf F., Sobott F., *et al.* (2020) Sample deposition onto cryo-EM grids: from sprays to jets and back. *Acta Crystallogr D Struct Biol* **76**:340-349.

Komikawa T., Tanaka M., Tamang A., Evans S.D., Critchley K., *et al.* (2020) Peptide-functionalized quantum dots for rapid label-free sensing of 2,4,6-trinitrotoluene. *Bioconjug Chem* **31**:1400-1407.

Komikawa T., Tanaka M., Yanai K., Johnson B.R.G., Critchley K., *et al.* (2020) A bioinspired peptide matrix for the detection of 2,4,6-trinitrotoluene (TNT). *Biosens & Bioelectron* **153**: 112030

Koo C.Z., Harrison N., Noy P.J., Szyroka J., Matthews A.L., *et al.* (2020) The tetraspanin Tspan15 is an essential subunit of an ADAM10 scissor complex. *J Biol Chem* **295**:12822-12839.

Kumar A., Gopalswamy M., Wolf A., Brockwell D.J., Hatzfeld M., *et al.* (2018) Phosphorylation-induced unfolding regulates p19(INK4d) during the human cell cycle. *Proc Natl Acad Sci USA* **115**:3344-3349.

Lang P.A., Parkova A., Leissing T.M., Calvopina K., Cain R., *et al.* (2020) Bicyclic boronates as potent inhibitors of AmpC, the class C beta-Lactamase from *Escherichia coli*. *Biomolecules* **10**:899.

Lapitan L.D.S. and Zhou D.J. (2020). A simple magnetic nanoparticle-poly-enzyme nanobead sandwich assay for direct, ultrasensitive DNA detection. *Methods Enzymol* **630:** 453-480.

Laurent H., Baker D.L., Soper A.K., Ries M.E. and Dougan L. (2020) Solute specific perturbations to water structure and dynamics in tertiary aqueous solution. *J Phys Chem B* **124**:10983-10993.

Laurent H., Soper A.K. and Dougan L. (2020) Trimethylamine N-oxide (TMAO) resists the compression of water structure by magnesium perchlorate: terrestrial kosmotrope vs. Martian chaotrope. *Phys Chem Chem Phys* **22**:4924-4937.

Lauwers E., Lalli G., Brandner S., Collinge J., Compernolle V., *et al.* (2020) Potential human transmission of amyloid beta pathology: surveillance and risks. *Lancet Neurol* **19**:872-878.

Leggott A., Clarke J.E., Chow S., Warriner S.L., O'Neill A.J., *et al.* (2020) Activity-directed expansion of a series of antibacterial agents. *Chem Commun* **56**:8047-8050.

Leitner A., Bonvin A., Borchers C.H., Chalkley R.J., Chamot-Rooke J., *et al.* (2020) Toward increased reliability, transparency, and accessibility in cross-linking mass spectrometry. *Structure* **28**:1259-1268.

Lello L.S., Utt A., Bartholomeeusen K., Wang S.N., Rausalu K., *et al.* (2020) Cross-utilisation of template RNAs by alphavirus replicases. *PLoS Pathog* **16:**e1008825.

Liamas E., Connell S.D., Ramakrishna S.N. and Sarkar A. (2020) Probing the frictional properties of soft materials at the nanoscale. *Nanoscale* **12**:2292-2308.

Liao L.E., Carruthers J., Smither S.J., Weller S.A., Williamson D.*, et al.* (2020) Quantification of Ebola virus replication kinetics in vitro. *PLoS Comput Biol* **16:**e1008375.

Lindsey-Crosthwait A., Rodriguez-Lema D., Walko M., Pask C.M. and Wilson A.J. Structural optimization of reversible dibromomaleimide peptide stapling. *Pept Sci*. **113**:e24157.

Lowe R.A., Taylor D., Chibale K., Nelson A. and Marsden S.P. (2020) Synthesis and evaluation of the performance of a small molecule library based on diverse tropane-related scaffolds. *Bioorg Med Chem* **28:**115442.

Madej M., White J.B.R., Nowakowska Z., Rawson S., Scavenius C.*, et al.* (2020) Structural and functional insights into oligopeptide acquisition by the RagAB transporter from *Porphyromonas gingivalis*. *Nat Microbiol* **5**:1016-1025.

Martir D.R., Delforce L., Cordes D.B., Slawin A.M.Z., Warriner S.L.*, et al.* (2020) A Pd_3L_6 supramolecular cage incorporating photoactive [2.2] paracyclophane units. *Inorg Chem Front* **7**:232-238.

Matin T.R., Heath G.R., Huysmans G.H.M., Boudker O. and Scheuring S. (2020) Millisecond dynamics of an unlabeled amino acid transporter. *Nat Commun* **11**, 5016.

Matheson C.J., Coxon C.R., Bayliss R., Boxall K., Carbain B.*, et al.* (2020) 2-Arylamino-6-ethynylpurines are cysteine-targeting irreversible inhibitors of Nek2 kinase. *RSC Med Chem* **11**:707-731.

McDermott K., Lee M.R.F., McDowall K.J. and Greathead H.M.R. (2020) Cross inoculation of rumen fluid to improve dry matter disappearance and its effect on bacterial composition using an *in vitro* batch culture model. *Front Microbiol,* **11:**531404.

McPhillie M.J., Zhou Y., Hickman M.R., Gordon J.A., Weber C.R.*, et al.* (2020) Potent tetrahydroquinolone eliminates apicomplexan parasites. *Front Cell Infect Microbiol* **10**:203.

Mega D.F., Fuller J., Alvarez-Rodriguez B., Mankouri J., Hewson R.*, et al.* (2020) Mutagenic analysis of hazara nairovirus nontranslated regions during single- and multistep growth identifies both attenuating and functionally critical sequences for virus replication. *J Virol* **94**: e00357-20.

Miles J.A., Davies T.A., Hayman R.D., Lorenzen G., Taylor J.*, et al.* (2020) A case study of eukaryogenesis: the evolution of photoreception by photolyase/cryptochrome proteins. *J Mol Evol* **88**:662-673.

Miles J. and van Oosten-Hawle P. (2020) Tissue-specific RNAi tools to identify components for systemic stress signaling. *J Vis Exp* **e6**:1357

Moons R., Konijnenberg A., Mensch C., Van Elzen R., Johannessen C.*, et al.* (2020) Metal ions shape alpha-synuclein. *Sci Rep* **10**:16293.

Moons R., van der Wekken-de Bruijne R., Maudsley S., Lemiere F., Lambeir A.M.*, et al.* (2020) Effects of detergent on alpha-synuclein structure: a native ms-ion mobility study. *Int J Mol Sci* **21**:7884.

Moorcroft S.C.T., Roach L., Jayne D.G., Ong Z.Y. and Evans S.D. (2020) Nanoparticle-loaded hydrogel for the light-activated release and photothermal enhancement of

antimicrobial peptides. *ACS Appl Mater Interfaces* **12**:24544-24554.

Morgan E.L. and Macdonald A. (2020) Manipulation of JAK/STAT signalling by high-risk HPVs: potential therapeutic targets for HPV-associated malignancies. *Viruses-Basel* **12**:977.

Morgan E.L., Patterson M.R., Ryder E.L., Lee S.Y., Wasson C.W.*, et al.* (2020) MicroRNA-18a targeting of the STK4/MST1 tumour suppressor is necessary for transformation in HPV positive cervical cancer. *PLoS Pathog* **16**:e1008624.

Morgan E.L., Scarth J.A., Patterson M.R., Wasson C.W., Hemingway G.C.*, et al.* (2020) E6-mediated activation of JNK drives EGFR signalling to promote proliferation and viral oncoprotein expression in cervical cancer. *Cell Death and Differ*.

Nakatani Y., Shimaki Y., Dutta D., Muench S.P., Ireton K.*, et al.* (2020) Unprecedented properties of phenothiazines unraveled by a NDH-2 bioelectrochemical assay platform. *J Am Chem Soc* **142**:1311-1320.

Newton R., Waszkowycz B., Seewooruthun C., Burschowsky D., Richards M.*, et al.* (2020) Discovery and optimization of wt-RET/KDR-selective inhibitors of RETV804M kinase. *ACS Med Chem Lett* **11**:497-505.

Nicholson D., Edwards T.A., O'Neill A.J. and Ranson N.A. (2020) Structure of the 70S ribosome from the human pathogen *Acinetobacter baumannii* in complex with clinically relevant antibiotics. *Structure* **28**:1087-1100.

Nwogu N., Ortiz L.E., Whitehouse A. and Kwun H.J. (2020) Merkel cell polyomavirus small tumor antigen activates matrix metallopeptidase-9 gene expression for cell migration and invasion. *J Virol* **94**:e00786-20.

Ochi T., Quarantotti V., Lin H.W., Jullien J., Silva I.R.E.*, et al.* (2020) CCDC61/VFL3 Is a paralog of SAS6 and promotes ciliary functions. *Structure* **28**:674-689.

Okrugin B.M., Richter R.P., Leermakers F.A.M., Neelov I.M., Zhulina E.B.*, et al.* (2020) Electroresponsive polyelectrolyte brushes studied by self-consistent field theory. *Polymers* **12**:898.

O'Regan L., Barone G., Adib R., Woo C.G., Jeong H.J.*, et al.* (2020) EML4-ALK V3 oncogenic fusion proteins promote microtubule stabilization and accelerated migration through NEK9 and NEK7. *J Cell Sci* **133:**jcs241505.

Panou M.M., Antoni M., Morgan E.L., Loundras E.A., Wasson C.W.*, et al.* (2020) Glibenclamide inhibits BK polyomavirus infection in kidney cells through CFTR blockade. *Antiviral Res* **178:**104778.

Parker F., Baboolal T.G. and Peckham M. (2020) Actin mutations and their role in disease. *Int J Mol Sci* **21**:3371.

Paterson D.A., Bao P., Abou-Saleh R.H., Peyman S.A., Jones J.C.*, et al.* (2020) Control of director fields in phospholipid-coated liquid crystal droplets. *Langmuir* **36**:6436-6446.

Paterson J.B., Camargo-Valero M.A. and Baker A. (2020) Uncoupling growth from phosphorus uptake in Lemna: Implications for use of duckweed in wastewater remediation and P recovery in temperate climates. *Food Energy Secur* **9:**e244.

Pietsch F., O'Neill A.J., Ivask A., Jenssen H., Inkinen J.*, et al.* (2020) Selection of resistance by antimicrobial coatings in the healthcare setting. *J Hosp Infect* **106**:115-125.

Poon E., Liang T., Jamin Y., Walz S., Kwok C.*, et al.* (2020) Orally bioavailable CDK9/2 inhibitor shows mechanism-based therapeutic potential in MYCN-driven neuroblastoma. *J Clin Invest* **130**:5875-5892.

Poulter J.A., Gravett M.S.C., Taylor R.L., Fujinami K., De Zaeytijd J.*, et al.* New variants and *in silico* analyses in GRK1 associated Oguchi disease. *Human Mutation*. **42**:164-176.

Rao A., Haza K., Trinh C., Edwards T. and Tomlinson D. (2020) Using Affimer to aid small-molecule drug development against KRAS. *Mol Cancer Res* **18**:69-69.

Richardson R.A., Hanson B.S., Read D.J., Harlen O.G. and Harris S.A. (2020) Exploring the dynamics of flagellar dynein within the axoneme with Fluctuating Finite Element Analysis. *Q Rev Biophys* **53**:e9.

Rodriguez-Alonso R., Letoquart J., Nguyen V.S., Louis G., Calabrese A.N.*, et al.* (2020) Structural insight into the formation of lipoprotein-beta-barrel complexes. *Nat Chem Biol* **16**:1019-1025.

Rombi F., Bayliss R., Tuplin A. and Yeoh S. (2020) The journey of Zika to the developing brain. *Mol Biol Rep* **47**:3097-3115.

Rottet S., Iqbal S., Beales P.A., Lin A.R., Lee J.*, et al.* (2020) Characterisation of hybrid polymersome vesicles containing the efflux pumps NaAtm1 or P-Glycoprotein. *Polymers* **12**:1049.

Saunders S.E., Tiede C., Edwards T., Breeze A. and Tomlinson D. (2020) Inhibition of Ras signalling by targeting Son of Sevenless with affimers. *Mol Cancer Res* **18**:57-58.

Scarff C.A., Carrington G., Casas-Mao D., Chalovich J.M., Knight P.J.*, et al.* (2020) Structure of the shutdown state of myosin-2. *Nature* **588**:515-520.

Scarff C.A., Thompson R.F., Newlands G.F.J., Jamson A.H., Kennaway C.*, et al.* (2020) Structure of the protective nematode protease complex H-gal-GP and its conservation across roundworm parasites. *PLoS Pathog* **16:**e1008465.

Schiffrin B., Radford S.E., Brockwell D.J. and Calabrese A.N. (2020) PyXlinkViewer: A flexible tool for visualization of protein chemical crosslinking data within the PyMOL molecular graphics system. *Protein Sci* **29**:1851-1857.

Scott C., Kankanala J., Foster T.L., Goldhill D.H., Bao P.*, et al.* (2020) Site-directed M2 proton channel inhibitors enable synergistic combination therapy for rimantadine-resistant pandemic influenza. *Plos Pathog* **16:**e1008716.

Seneviratne R., Jeuken L.J.C., Rappolt M. and Beales P.A. (2020) Hybrid vesicle stability under sterilisation and preservation processes used in the manufacture of medicinal formulations. *Polymers* **12**:914.

Shaik F., Cuthbert G.A., Homer-Vanniasinkam S., Muench S.P., Ponnambalam S.*, et al.* (2020) Structural basis for vascular endothelial growth factor receptor activation and implications for disease therapy. *Biomolecules* **10**:1673.

Sharma N., Prosser O., Kumar P., Tuplin A. and Giri R. (2020) Small molecule inhibitors possibly targeting the rearrangement of Zika virus envelope protein. *Antiviral Res* **182:**104876.

Shaw J., Gosain R., Kalita M.M., Foster T.L., Kankanala J.*, et al.* (2020) Rationally derived inhibitors of hepatitis C virus (HCV) p7 channel activity reveal prospect for bimodal antiviral

therapy. *Elife* **9:**e52555.

Sherry L., Grehan K., Snowden J.S., Knight M.L., Adeyemi O.O.*, et al.* (2020) Comparative molecular biology approaches for the production of poliovirus virus-like particles using *Pichia pastoris*. *Msphere* **5:**e00838-19.

Shi J., Hyman A.J., De Vecchis D., Chong J.H., Lichtenstein L.*, et al.* (2020) Sphingomyelinase disables inactivation in endogenous PIEZO1 channels. *Cell Rep* **33**:108225.

Shimizu J.F., Martins D.O.S., McPhillie M.J., Roberts G.C., Zothner C.*, et al.* (2020) Is the ADP ribose site of the Chikungunya virus NSP3 Macro domain a target for antiviral approaches? *Acta Tropica* **207**:105490.

Slocombe S.P., Zuniga-Burgos T., Chu L.L., Wood N.J., Camargo-Valero M.A.*, et al.* (2020) Fixing the broken phosphorus cycle: wastewater remediation by microalgal polyphosphates. *Front Plant Sci* **11**:982.

Smith C.E.L., Whitehouse L.L.E., Poulter J.A., Wilkinson Hewitt L., Nadat F.*, et al.* (2020) A missense variant in specificity protein 6 (SP6) is associated with amelogenesis imperfecta. *Hum Mol Genet* **29**:1417-1425.

Smith H.I., Guthertz N., Cawood E.E., Maya-Martinez R., Breeze A.L.*, et al.* (2020) The role of the I-T-state in D76N β2-microglobulin amyloid assembly: A crucial intermediate or an innocuous bystander? *J Biol Chem* **295**:12474-12484.

Snowden J.S., Hurdiss D.L., Adeyemi O.O., Ranson N.A., Herod M.R.*, et al.* (2020) Dynamics in the murine norovirus capsid revealed by high-resolution cryo-EM. *PLoS Biol* **18:**e3000649.

Srzentic K., Fornelli L., Tsybin Y.O., Loo J.A., Seckler H.*, et al.* (2020) Interlaboratory study for characterizing monoclonal antibodies by top-Down and middle-down mass spectrometry. *J Am Soc Mass Spectrom* **31**:1783-1802.

Stephens A.D., Zacharopoulou M., Moons R., Fusco G., Seetaloo N.*, et al.* (2020) Extent of N-terminus exposure of monomeric alpha-synuclein determines its aggregation propensity. *Nat Commun* **11**:2820.

Suen K.M., Braukmann F., Butler R., Bensaddek D., Akay A.*, et al.* (2020) DEPS-1 is required for piRNA-dependent silencing and PIWI condensate organisation in *Caenorhabditis elegans*. *Nat Commun* **11**:4242.

Surtees R., Stern D., Ahrens K., Kromarek N., Lander A.*, et al.* (2020) Development of a multiplex microsphere immunoassay for the detection of antibodies against highly pathogenic viruses in human and animal serum samples. *PLoS Negl Trop Dis* **14:**e0008699.

Suwatthanarak T., Tanaka M., Minamide T., Harvie A.J., Tamang A.*, et al.* (2020) Screening and characterisation of CdTe/CdS quantum dot-binding peptides for material surface functionalisation. *RSC Adv* **10**:8218-8223.

Trindade A.F., Faulkner E.L., Leach A.G., Nelson A. and Marsden S.P. (2020) Fragment-oriented synthesis: beta-elaboration of cyclic amine fragments using enecarbamates as platform intermediates. *Chem Commun* **56**:8802-8805.

Tsuchiya Y., Byrne D.P., Burgess S.G., Bormann J., Bakovic J.*, et al.* (2020) Covalent Aurora A regulation by the metabolic integrator coenzyme A. *Redox Biol* **28**:101318.

Tugarinov V, Karamanos TK, Ceccon A, & Clore GM (2020) Optimized NMR Experiments for the Isolation of I=1/2 Manifold Transitions in Methyl Groups of Proteins. *ChemPhysChem* **21**: 13-19.

Tugarinov V, Karamanos TK, & Clore GM (2020) Magic-Angle-Pulse Driven Separation of Degenerate 1H Transitions in Methyl Groups of Proteins: Application to Studies of Methyl Axis Dynamics. *ChemPhysChem*. **21**: 1-6.

Tugarinov V, Karamanos TK, & Clore GM (2020) Optimized selection of slow-relaxing 13C transitions in methyl groups of proteins: application to relaxation dispersion. *J. Biomol. NMR* **74**: 111-118.

Ulamec S.M., Brockwell D.J. and Radford S.E. (2020) Looking beyond the core: The role of flanking regions in the aggregation of amyloidogenic peptides and proteins. *Front Neurosci* **14**:611285.

Ulamec S.M. and Radford S.E. (2020) Spot the Difference: function versus toxicity in amyloid fibrils. *Trends Biochem Sci* **45**:635-636.

Valverde P., Vendeville J.B., Hollingsworth K., Mattey A.P., Keenan T.*, et al.* (2020) Chemoenzymatic synthesis of 3-deoxy-3-fluoro-l-fucose and its enzymatic incorporation into glycoconjugates. *Chem Commun* **56**:6408-6411.

van der Heijden T.W.G., Read D.J., Harlen O.G., van der Schoot P., Harris S.A.*, et al.* (2020) Combined force-torque spectroscopy of proteins by means of multiscale molecular simulation. *Biophys J* **119**:2240-2250.

Wang W.L., Kong Y.F., Jiang J., Tian X., Li S.*, et al.* (2020) Photon induced quantum yield regeneration of cap-exchanged CdSe/CdS quantum rods for ratiometric biosensing and cellular imaging. *Nanoscale* **12**:8647-8655.

Ward J.C., Bowyer S., Chen S.C., Campos G.R.F., Ramirez S.*, et al.* (2020) Insights into the unique characteristics of hepatitis C virus genotype 3 revealed by development of a robust sub-genomic DBN3a replicon. *J Gen Virol* **101**:1182-1190.

Welch R., Harris S.A., Harlen O.G. and Read D.J. (2020) KOBRA: a fluctuating elastic rod model for slender biological macromolecules. *Soft Matter* **16**:7544-7555.

Willis L.F., Kumar A., Jain T., Caffry I., Xu Y., Radford S.E., Kapur N., Vásquez M., and Brockwell D.J. (2020) The uniqueness of flow in probing the aggregation behavior of clinically relevant antibodies. *Engin. Rep.* **2**:e12147.

Wilson D.N., Hauryliuk V., Atkinson G.C. and O'Neill A.J. (2020) Target protection as a key antibiotic resistance mechanism. *Nat Rev Microbiol* **18**:637-648.

Wood C.W., Ibarra A.A., Bartlett G.J., Wilson A.J., Woolfson D.N.*, et al.* (2020) BAlaS: fast, interactive and accessible computational alanine-scanning using BudeAlaScan. *Bioinformatics* **36**:2917-2919.

Wood N.J., Baker A., Quinnell R.J. and Camargo-Valero M.A. (2020) A simple and non-destructive method for chlorophyll quantification of chlamydomonas cultures using digital image analysis. *Front Bioeng Biotechnol* **8**:746.

Wright D.J., Simmons K.J., Johnson R.M., Beech D.J., Muench S.P.*, et al.* (2020) Human TRPC5 structures reveal interaction of a xanthine-based TRPC1/4/5 inhibitor with a conserved lipid binding site. *Commun Biol* **3**:704.

Wroblewska-Wolna A.M., Harvie A.J., Rowe S.F., Critchley K., Butt J.N.*, et al.* (2020) Quantum dot interactions with and toxicity to *Shewanella oneidensis* MR-1. *Nanotechnology* **31**.

Wu Q. (2020) Guardians of the genome: DNA damage and repair. *Essays Biochem*; **64** (5): 683–685.

Yamamoto E., Domanski J., Naughton F.B., Best R.B., Kalli A.C.*, et al.* (2020) Multiple lipid binding sites determine the affinity of PH domains for phosphoinositide-containing membranes. *Sci Adv* **6:**eaay5736.

Yang D., Klebl D.P., Zeng S., Sobott F., Prevost M.*, et al.* (2020) Interplays between copper and *Mycobacterium tuberculosis* GroEL1. *Metallomics* **12**:1267-1277.

Ye S.J., Azad A.A., Chambers J.E., Beckett A.J., Roach L.*, et al.* (2020) Exploring high aspect ratio gold nanotubes as cytosolic agents: structural engineering and uptake into mesothelioma cells. *Small* **16**:2003793.

Ye S.J., Connell S.D., McLaughlan J.R., Roach L., Aslam Z.*, et al.* (2020) One-step preparation of biocompatible gold nanoplates with controlled thickness and adjustable optical properties for plasmon-based applications. *Adv Funct Mater* **30:**2003512.

Zhang H.J., Catania R. and Jeuken L.J.C. (2020) Membrane protein modified electrodes in bioelectrocatalysis. *Catalysts* **10**:1427.

The Astbury Centre for
Structural Molecular Biology
University of Leeds
Leeds
LS2 9JT
Tel: 0113 343 3086
astbury@leeds.ac.uk
www.astbury.leeds.ac.uk

UNIVERSITY OF LEEDS
University of Leeds
Leeds, United Kingdom
LS2 9JT
Tel: 0113 243 1751
www.leeds.ac.uk